DOE/SF/10816-T6
(DE84006253)

Energy

SOLAR

INSTRUMENTATION SELECTION, INSTALLATION, VERIFICATION AND CALIBRATION AT THE PASSIVE COOLING EXPERIMENTAL FACILITY FOR A HOT/ARID CLIMATE

By
John F. Peck

August 1983

Work Performed Under Contract No. AC03-80SF10816

The University of Arizona
Environmental Research Laboratory
Tucson, Arizona

Technical Information Center
Office of Scientific and Technical Information
United States Department of Energy

DISCLAIMER

Available from the National Technical Information Service, U. S. Department of Commerce, Springfield, Virginia 22161.

Price: Printed Copy A09
Microfiche A01

Codes are used for pricing all publications. The code is determined by the number of pages in the publication. Information pertaining to the pricing codes can be found in the current issues of the following publications, which are generally available in most libraries: *Energy Research Abstracts (ERA); Government Reports Announcements* and Index (*GRA* and I); *Scientific and Technical Abstract Reports (STAR);* and publication NTIS-PR-360 available from NTIS at the above address.

Printed in the United States of America
USDOE Technical Information Center, Oak Ridge, Tennessee

DOE/SF/10816-T6
(DE84006253)
Distribution Category UC-59a

Passive Cooling Experimental Facility
Hot/Arid Zone
Contract No. DE-AC03-80SF-10816

DOE/SF/10816--T6

DE84 006253

INSTRUMENTATION
SELECTION, INSTALLATION, VERIFICATION and CALIBRATION
at the
PASSIVE COOLING EXPERIMENTAL FACILITY
for a
HOT/ARID CLIMATE

Principal Investigator: John F. Peck

Participants:

Barry Anthis
Kevin Duffy
John E. Groh
Helen J. Kessler
Paul Kinyicky
Gregory Lansdon
George V. Mignon
Leon Szabunia
T. Lewis Thompson

Report written by:

George V. Mignon

Editing and graphics by:

Helen J. Kessler

Prepared for the U.S. Department of Energy

August, 1983

THE UNIVERSITY OF ARIZONA
Environmental Research Laboratory
Tucson International Airport
Tucson, Arizona 85706

TABLE OF CONTENTS

TABLE OF CONTENTS (cont'd)

LIST OF ILLUSTRATIONS

I. INTRODUCTION

The purpose of the Passive Cooling Experimental Facility is to acquire data and perform experiments regarding different passive cooling techniques and strategies. In order to adequately explain the cooling techniques employed, sufficient instrumentation and data logging equipment was installed.

Sensors were selected based on their accuracy, cost effectiveness, and ability to calibrate consistently and with ease. This section decribes the sensors and instrumentation and the basis for their selection, installation, verification and calibration.

Installation and calibration details are provided for certain selected critical sensors, i.e. heat flux meters, pyrgeometers, etc.

The following list summarizes the critical sensors and instruments selected and installed:

Heat Flux: Hy-Cal Engineering BI-7 thermoelectric sensors.

Temperature (wet and dry bulb): Copper-constantine thermocouples, Hewlett Packard reference junction.

Pyranometers: Eppley PSP, LICOR photovoltaic pyranometers and Eppley Shadow Band 8-48 pyranometer.

Infrared Radiometer: Eppley PIR pyrgeometer.

Ambient Wind Velocity: Gill Propeller Vane Anemometer by R. M. Young

Air Flow: EII Air Flow Meters

Infiltration: SF_6 gas chromatography

II. SENSOR AND INSTRUMENT SELECTION

A. Dry Bulb Temperature

1. Utilization

Temperature sensors are utilized to measure the thermal performance of the structures. They are distributed throughout the structures. Temperature measurements are used in the heat balance calculations and to measure the relative effectiveness of the passive systems. Temperature sensor locations can be seen in section VI (a separate document).

2. Accuracy Requirements

The primary purpose of the temperature sensors is to determine how effective the passive features are and to help verify performance models. The accuracy required would only need to be ± 1 to 2°F. The order of magnitude of the heat flux due to temperature differences is about 10 BTU/hr. sq. ft. and thus a 1 or 2°F error would only yield an absolute error of less than 10%.

3. Selected Sensors

Electric thermometers are adapted to automatic recording. Basically there are two main types of electrical transducers, self-generating and non-self-generating. The self-generating transducers produce an electric current as a function of temperature. The non-self-generating transducers require the application of an external signal in order to detect a change in property. Thermocouples are examples of the former, while resistance elements, thermistors and RTD's are examples of the latter.

Three types of sensors fall within this accuracy range: Thermistors, Resistance Temperature Devices (RTD) and Thermocouples. Since there are about 500 (including backups) temperature sensor locations, cost was the driving element in this decision.

a. Thermistors are semiconductors of ceramic materials made from sintering mixtures of oxides of manganese, nickle, cobalt, copper, iron, and uranium. Thermistors have very large negative temperature coefficients; each temperature increase of 1°C will increase the resistance 5%. Thermistor resistance change with temperature is much larger than for resistance thermometers, however the change is quite nonlinear. Thermistors can be calibrated to measure temperature to within ± 0.1°F, and can, with suitable bridge networks, yield outputs of 0-5 volts, thus eliminating the need for instrumentation with microvolt resolution. The self-heating errors in a thermistor can be quite large because of the large temperature coefficient. Thus they require frequent calibration. Thermistors are relatively expensive in comparison to thermocouples.

b. RTD's are resistance temperature devices which change resistance with temperature. The electrical resistance of most materials varies with temperature. This characteristic is utilized to measure temperatures with resistance thermometers made from a variety of materials. Given a known resistance-temperature relationship and

appropriate recording equipment, temperatures can be determined to a high degree of precision. These devices exhibit good long-term stability and linear output; however, they are expensive and fragile.

c. Thermocouples have won a permanent role as temperature sensors for numerous industrial applications. Their favorable characteristics include acceptable accuracy, suitabilty over a wide range of temperatures, adequate thermal response, ruggedness, high reliabilty, low cost, ease of installation and compatibilty with most measuring and recording systems.

Based upon cost and desired accuracy thermocouples were chosen for the temperature transducers for this project. The required accuracy of $\pm$ 1 to 2^{o}F falls well within the error of type T copper constantan thermocouples. In order to avoid detailed and time consuming calibration of each sensor, enough wire was acquired from the same lot number to assure consistency of the calibration.

B. Wet Bulb Temperature

1. Utilization

In order to measure the humidity, and in turn to calculate the Fanger PMV comfort index, the wet bulb temperatures need to be measured. The temperature transducers to be utilized are the same as for dry bulb temperature measurements.

The temperature transducer (thermocouple) is enclosed in a capillary sock and then placed in an aspirated and shielded device of ERL design.

Calculations are then made to determine the humidity and other psychrometric properties.

2. Accuracy Requirements

The accuracy required for this sensor is the same as for the dry bulb temperature sensors.

3. Selected Sensors

Considerations for selection of sensors is the same as for the dry bulb temperature sensors.

C. Radiant Temperature

1. Utilization

In order to calculate the Fanger PMV comfort index, the Mean Radiant Temperature needs to be measured. The temperature

transducers to be utilized are the same as for the measurement of dry bulb temperatures. The Mean Radiant Temperature is derived from the Globe Temperature (the device utilized to measure the radiant temperature).

The temperature transducer (thermocouple) is enclosed in a six inch copper sphere that is painted flat black (Dupont Nextel flat black paint) with absorptivity and emissivity of about .95, nearly a black body receiver.

2. Accuracy Requirements

The accuracy required of this sensor is the same as for the dry bulb temperature sensors.

3. Selected Sensors

Consideration for selection of sensors is the same as for the dry bulb sensors.

D. Heat Flux Meters

1. Utilization

The heat flux meters are utilized to measure the heat flow in and out of the structures. They are used in conjunction with the temperature and insolation sensors to arrive at a general heat balance for each structure.

2. Accuracy Requirements

The accuracy required from this instrument is similar to the accuracy required of the pyrgeometer and pyranometers. The accuracy should be about 1 to 2% full scale, with a range of 0 to 10 BTU/hr. sq. ft.

3. Selected Sensor

All heat flux meters utilize a thermopile type arrangement. The differences arise in the accuracy, consistency of calibration, size and cost. Two manufacturer's devices were considered: HY-CAL Engineering BI series, and International Thermal Instrument Company.

a. HY-CAL BI series Heat Flux Meters have a $\pm$ 2% accuracy, and exhibit fairly consistent calibration. They are factory calibrated prior to delivery. The BI series is a very sensitive instrument and is suitable for low temperatures (-50 to 200^{o}F). In addition, the devices measure heat flow uniformly in both directions. They cost about $220.

b. International Thermal Instrument Company (ITI) devices are not as accurate (± 3%) and cost about $150.

Based upon the cost, desired accuracy and consistency of calibration, the HY-CAL BI series heat flux meter was chosen.

E. Pyranometer

1. Utilization

The pyranometers will be utilized to measure solar insolation incident upon horizontal and vertical surfaces. These measurements will aid in determining the heat gains due to fenestration for each structure. Several instruments are required in order to fully assess the solar heat gains to the structures.

2. Accuracy Requirements

The primary purpose of the project is to determine how well certain passive features work. When dealing with solar insolation, the flux is on the order of 300 BTU/hr. sq. ft. maximum, and thus an error of 1% is about 3 BTU/hr. sq. ft. The order of magnitude of heat flux due to passive design features is about 10 BTU/hr. sq. ft., thus an instrument with only 1% accuracy is marginally acceptable, and in practice, unachievable. The most that can be expected is about 3%. This would yield an error of about 9 BTU/hr. sq. ft. Thus, better than 50% of the heat gain/loss could be due to instrument error.

3. Selected Sensors

Two different types of pyranometers were considered, thermopile and photovoltaic.

a. The Eppley Precision Spectral Pyranometer is of the thermopile type and utilizes a multijunction copper-constantan plated thermopile. The thermal transducer is blackened with optical black lacquer and is shielded from the weather with two removable concentric hemispheres. The instrument has a sensitivity of 9 micro volts/watt.

This instrument is a very accurate and stable commercially-available sensor. The calibration of this instrument can be maintained at about 1%. Cost is $1200.

Another Eppley thermopile pyranometer considered was the Eppley Black and White pyranometer Model 8-48. This

pyranometer is a development of the well-known Eppley 10 and 50 junction 180° pyreheliometer. The detector is a differential thermopile with the hot-junction receivers blackened and the cold junction receivers whitened. The linearity, cosine response, response time and spectral response are not quite as good as that of the Eppley PSP, but they are adequate for the measurements required. The cost of the Eppley Black and White is about $850.

b. The LICOR Photovoltaic pyranometer is not nearly as accurate as the Eppley PSP pyranometer; however, it is considerably less expensive. This type of sensor utilizes a photodiode. The response of the silicon photodiode does not cause serious errors provided it is used only for solar radiation and not under conditions of altered spectral distribution. The relative spectral response of the silicon photodiode does not extend uniformly over the full solar radiation range. The changes in the spectral distribution of the incident light, coupled with the non-uniform spectral response, can cause errors in the photodiode output.

The LICOR LI-200SB pyranometer has been calibrated against an Eppley Precision Pyranometer. Under full sun conditions at solar noon, the uncertainty of the calibration was 5%. When the error of the PSP is taken into account, the absolute error of the LICOR sensor is about 6%. While this is an extremely high error in relation to the desired accuracy, it is acceptable for the measurements required. The cost of these sensors is about $165, considerably less than the Eppley PSP.

Based upon cost and accuracy, the Eppley PSP was chosen to measure the site horizontal insolation and the LICOR's were chosen to measure the insolation of specific surfaces (i.e. windows) of each structure. In addition to these instruments, the Eppley Model 8-48 Black and White Pyranometer was chosen for use with the Eppley Shadow Band Stand Model SBS to measure diffuse insolation.

F. Infrared Radiometer

1. Utilization

This sensor is utilized for continuous measurement of net radiative heat exchange between the sky and surface. In particular, the radiation exchange between the radiative roof and the night sky are measured in order to determine the heat exchange ability of the radiative roof.

2. Accuracy Requirements

The net radiation errors should be small in comparison to typical nocturnal radiative heat fluxes and other heat transfer rates. This goal is exceedingly difficult to attain because typical radiative heat transfer rates are of the order of 100 BTU/hr. sq. ft. from a roof surface. An error of 1% in the irradience would give a 1 BTU/hr. sq. ft. error and would result in a 10% error in the net radiation rate.

Most sensors surveyed had a greater than 1% error. Even those with 1% error could only achieve this accuracy under ideal conditions and at radiation rates in excess of 10 BTU/hr. sq. ft.

3. Selected Sensor

There were two basic types of instruments to select from:

a. Funk type radiometers utilize thermopiles which contain about 250 thermal junctions bonded with two blackened plates. Hemispherically formed windshields made from polyethylene are used on both sides to reduce the thermal convection term. This type of sensor, when operated with both windows, yields a net radiation. When operated with only one window, it gives the sky irradience. This type of instrument is very accurate, but requires careful maintenance. In addition, the polyethylene windows degrade with ultraviolet light and thus the calibration is not very stable. Cost is about $1300.

b. The Eppley pyrgeometer also utilizes a thermopile. The thermopile is protected by a silicon dome with an interference filter and a temperature compensation circuit. The output voltage is proportional to the irradiance incident from the sky, not the net radiation. These instruments in practice are generally accurate to within 2% of the received irradience, however they are not accurate in daylight due to heating of the silicon dome. Cost is about $1300.

Based on cost, accuracy, calibration and ease of maintenance, the Eppley PIR was selected.

G. Wind Velocity

1. Utilization

The wind velocity is required in order to determine convective heat transfer losses and gains to the structure and also to determine infiltration rates.

2. Accuracy Requirements

A sensitivity analysis indicates that a wind speed accuracy of 1 m/s is required in order to verify any heat transfer algorithms. In addition, the Fanger PMV comfort index requires the air velocity. Several comfort stations are to be monitored. The PMV correlation falls apart at air velocities greater than 5 m/s.

3. Selected Sensors

Two types of wind sensors were considered, hot wire/film and tachometer type. The following sensors were evaluated:

a. Tachometer type drives are rugged and reliable units that require little maintenance and are easily calibrated. The Gill Propeller Vane anemometer by R. M. Young has an azimuth range of 0-540° and a threshold sensitivity of 0.1 to 0.2 m/s, well within the accuracy required. The output signal from the generator is analog. The signal is linearized by the power supply translator. Cost including translator is about $2500.

b. The hot film type anemometers are more sensitive than the tachometer drive units and have lower ranges. The Environmental Instruments, Inc. (EII) 300 series hot film anemometer was evaluated. This sensor utilizes a temperature compensated hot film probe. The accuracy is about 2% full scale. These sensors are only wind speed sensors and do not yield the velocity direction vector.

The 0-5 m/s scale is accurate to within $\pm$ 0.1 m/s. The cost of the EII sensors including power supplies and electronics is about $750.

It was decided to place two wind velocity stations at opposite corners of the site in order to account for disturbance to the wind patterns by the individual test buildings.

Additionally, where lower air flow measurements and greater accuracy are required, the EII meters were chosen. These sensors were placed at selected comfort stations to measure the air velocity for use in the Fanger PMV calculations. Two instruments were installed (see Section III and Appendix L on sensor location).

H. Infiltration Method

1. Utilization

Air infiltration measurements are necessary in order to arrive at a thermal balance for the structures and also to assess the effectivenes of different building techniques.

Due to the continuing experiments in progress the method of measurement should have as little impact as possible. It is hoped that the infiltration measurements will be as accurate as the other measurements; however, allowing for the variance in weather conditions, it would not be practical to assume the measurements will be.

There are two general means of determining infiltration, pressure differential and tracer gas. It was decided to utilize the SF_6 tracer gas technique to determine the quasi-static infiltration rate for each structure, and to use the Sherman and Grimsrud Method in conjunction with the computerized data acquisition system.

2. Tracer Gas Method

The tracer gas technique has reasonably well-defined limits of error. This method was chosen due to the availability of a gas chromatograph here at the Environmental Research Lab. See Appendix H.

3. Pressure Differential Method

This method, as implemented, would utilize the Sherman and Grimsrud methodology. The data required for this is collected on an hourly basis by the data system. See Appendix I.

III. SENSOR AND INSTRUMENT CHANNEL VERIFICATION

All channels were verified as to their proper location and termination at the Data Acquisition System (DAS). The following procedures were employed for each building.

A. Thermocouples

1. The DAS was programmed to acquire each instrument in sequence with operator command and to continue to read the instrument until interrupted by the operator.

2. The verification team consisted of two members, each equipped with two-way radios.

3. The correct location of the thermocouples was verified by increasing the temperature of the junctions by external means (i.e. skin contact). When a temperature rise was read by the DAS, the channel was verified. Those junctions not readily accessible (embedded in the walls and ground) were verified by tracing their wires to the nearest terminal interconnect. At that point, a test thermocouple was installed. The following procedure was utilized:

a. Thermocouple Rakes: The inner and outer probe leads were disconnected and the lead wires were connected together and heated. It was assumed that if the inner and outer probes were correct that the middle ones would also be correct due to the design of the rake.

b. Earth Temperature Arrays: Due to the inaccessibility of the thermocouple junctions, these probes were indirectly verified by comparing the daily temperature profiles for given levels and dates to test site data previously collected at a nearby location. This verified the channels.

c. Globe Thermometer: In order to verify that the globe thermometers were properly connected, the globes were heated in a manner similar to the thermocouples.

B. Heat Flux Meters

The heat flux meters were verified in a similar manner to the thermocouples. In addition to verifying location, polarity was also verified (i.e. direction of heat flow).

C. Pyranometers

The pyranometers were verified by first reading the instrument exposed to light and then reading it shaded.

D. Pyrgeometer

The Eppley PIR Pyrgeometer was verified by tracing the wires to the DAS.

E. Wind Speed and Direction

The Gill Propeller Vane Anemometer was verified by tracing the wires and by inspection.

IV. SENSOR AND INSTRUMENT CALIBRATION

Once the structures and sensors were installed, an in-situ calibration program was initiated. The following types of sensors were calibrated: thermocouples, heat flux meters, pyranometers, pyrgeometers, and wind velocity. Not all instruments were calibrated in place.

A. Thermocouples

Test thermocouples were installed in an ice bath and calibrated. The HP-3497 Multiplexer DVM has an electronic ice point reference. Once the set of test thermocouples had been calibrated these were then utilized to calibrate inaccessible junctions.

1. Thermocouples that were installed and inaccessible were calibrated by referencing them to the test thermocouples. Since all the thermocouple wire came off the same spool of wire, it can be safely assumed that each thermocouple was the same.

2. Thermocouples that were easily accessible were calibrated by using a portable ice bath.

3. Irregularities in the wire or junctions in the cables running from the thermocouples to the Data Building were checked and verified. One of the pre-calibrated test thermocouples was attached and placed in an ice bath.

4. The following thermocouple calibration statistics were compiled:

Test thermocouples:	Ice bath (32°F) 53 readings (10 min intervals) Mean: -0.039 Std Deviation: 0.1165
Installed thermocouples:	Ice bath (32°F) 24 readings (1 hr interval) Mean: -0.22596 Std Deviation: 0.422

Based upon the preceding statistics, it was determined that the thermocouple calibration was well within the predicted and desirable accuracy range. Not all thermocouples were calibrated, however a sufficient sample from each structure was calibrated to assure that the calibrations were correct.

B. Heat Flux Meters

The heat flux meter calibration was conducted by M.I.T. We were unable to consistently calibrate each meter. As it turns out, the M.I.T. lab was also unable to repeat its calibrations. The heat flux meters, while providing useful information, are very troublesome, and their accuracy is suspect. Appendix A contains the calibration constants for each meter.

C. Pyranometers

ERL does not possess the equipment necessary to calibrate the precision pyranometers. Thus, they were sent to a certified lab for calibration. Appendix B contains the factory calibration procedures and specifications and the calibration sheets for the Eppley PSP pyranometer. The other pyranometers were calibrated by reference to the PSP.

1. The output from the shadow band pyranometer (Eppley model 8-48), located adjacent to the Eppley PSP, was compared to the output from the PSP.

2. The LICOR pyranometers were referenced to a portable, calibrated Eppley Model 8-48 Black and White pyranometer. The Eppley Black and White pyranometer was placed adjacent to each installed LICOR sensor and the two outputs were monitored by the computer over an 8-hour period.

D. Pyrgeometer

The Eppley PIR pyrgeometer is calibrated by Eppley labs once a year. In addition to calibration, a battery check is made regularly to assure the instrument is functioning properly. A battery adjustment is made when necessary, utilizing the procedure detailed in Appendix C.

E. Wind Velocity

The wind velocity and/or air flow instruments were calibrated utilizing the following factory procedures:

1. Gill Propeller Vane Anemometer: This instrument was calibrated utilizing a calibration unit from R. M. Young. The unit is a constant, regulated 1800 RPM drive motor. The tachometer is driven by this unit and the electronics adjusted to yield the desired response. The procedures for this calibration are in Appendix D.

2. EII 300 Series Air Flow Sensor: This unit was calibrated in a calibrated wind tunnel utilizing the orifice method. Measurements were made at different temperatures and pressures. Calibration data are in Appendix E.

V. INSTRUMENTATION PHOTOGRAPHS

Figure 1. HP 85 data acquisition computer and digital volt meter

Figure 2. HP 9845 computer for data analysis

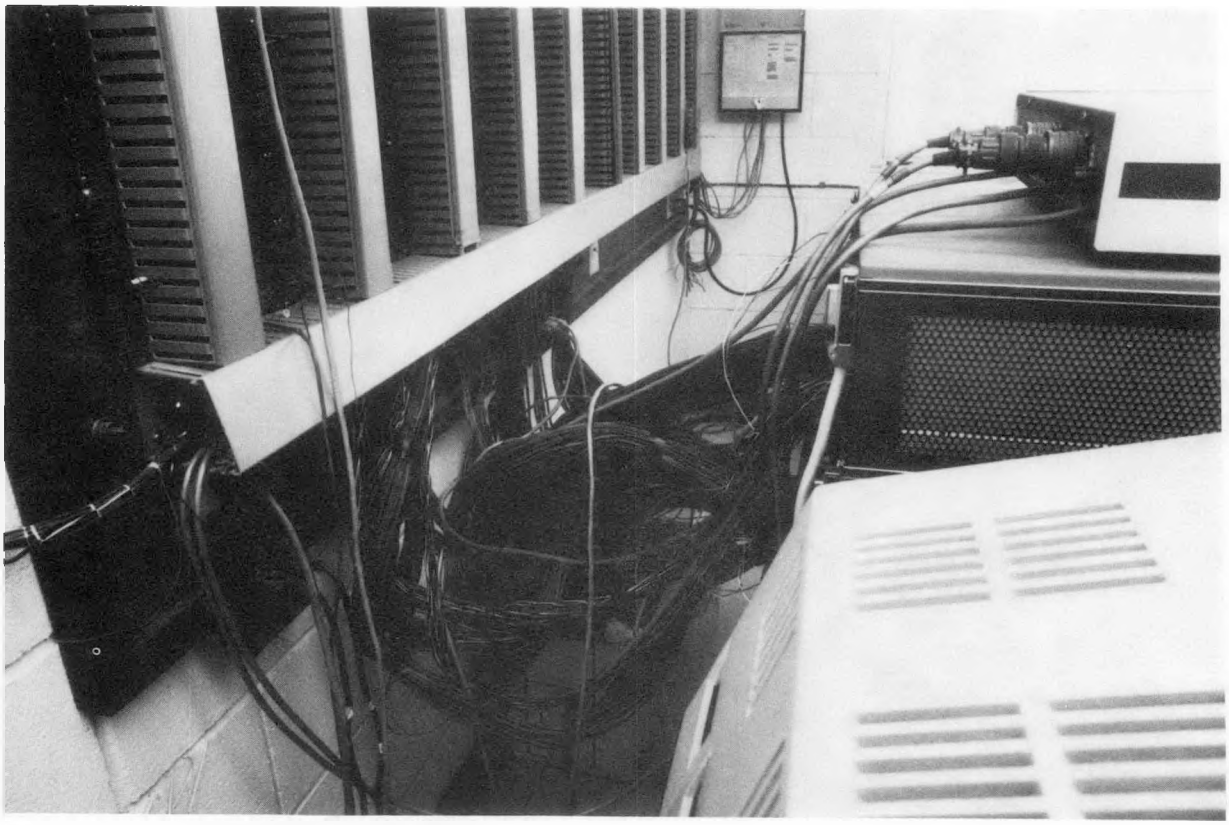

Figure 3. Thermocouple wires and sensor cables entering digital volt meter from circuit board

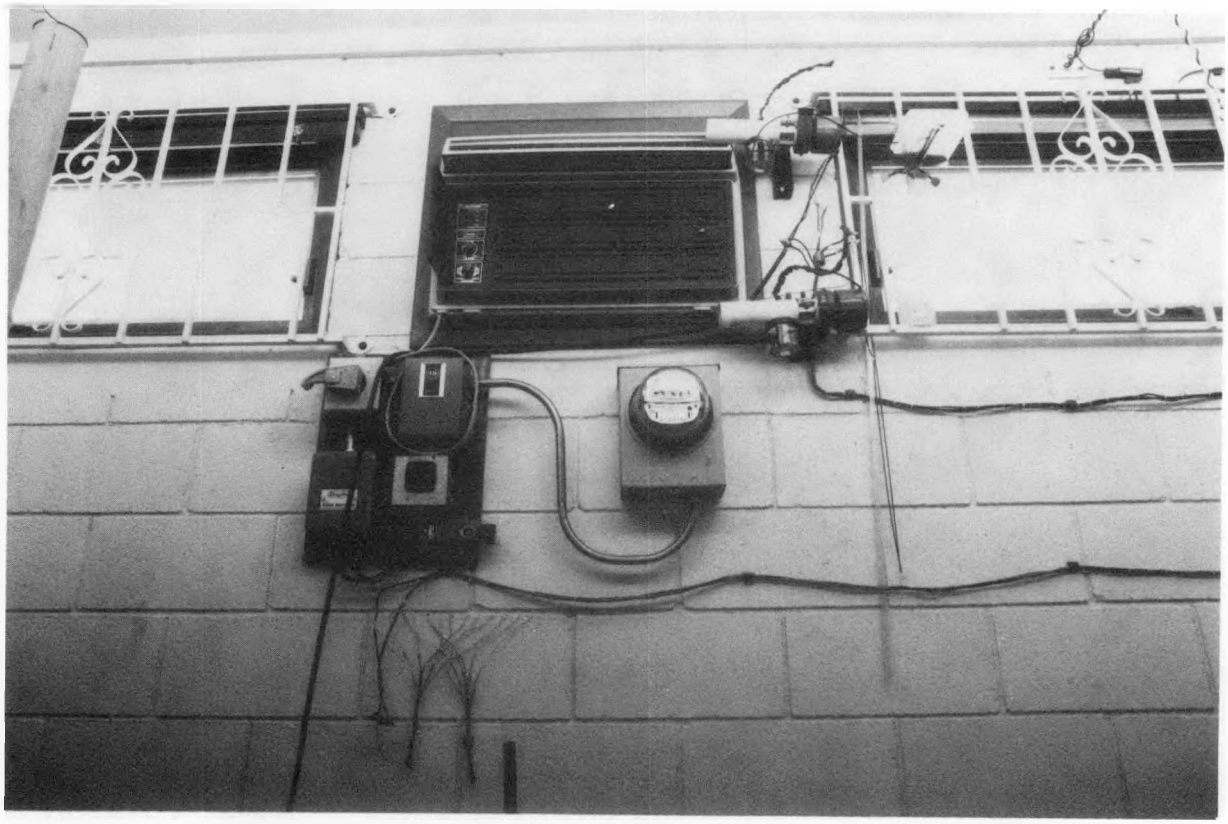

Figure 4. Air conditioner and controls, wet-bulb and dry-bulb temperature sensors

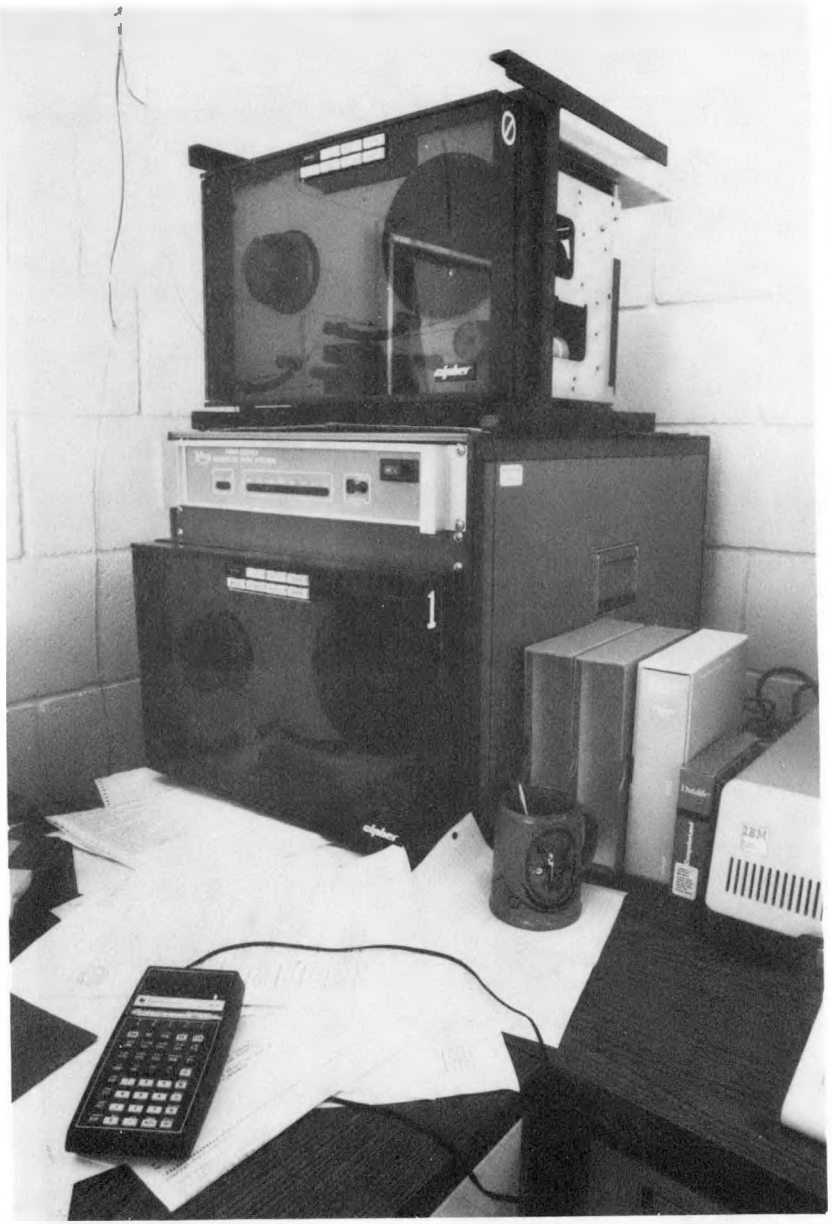

Figure 5. Two nine-track tape drives

Figure 6. Gill Propeller Vane wind sensor

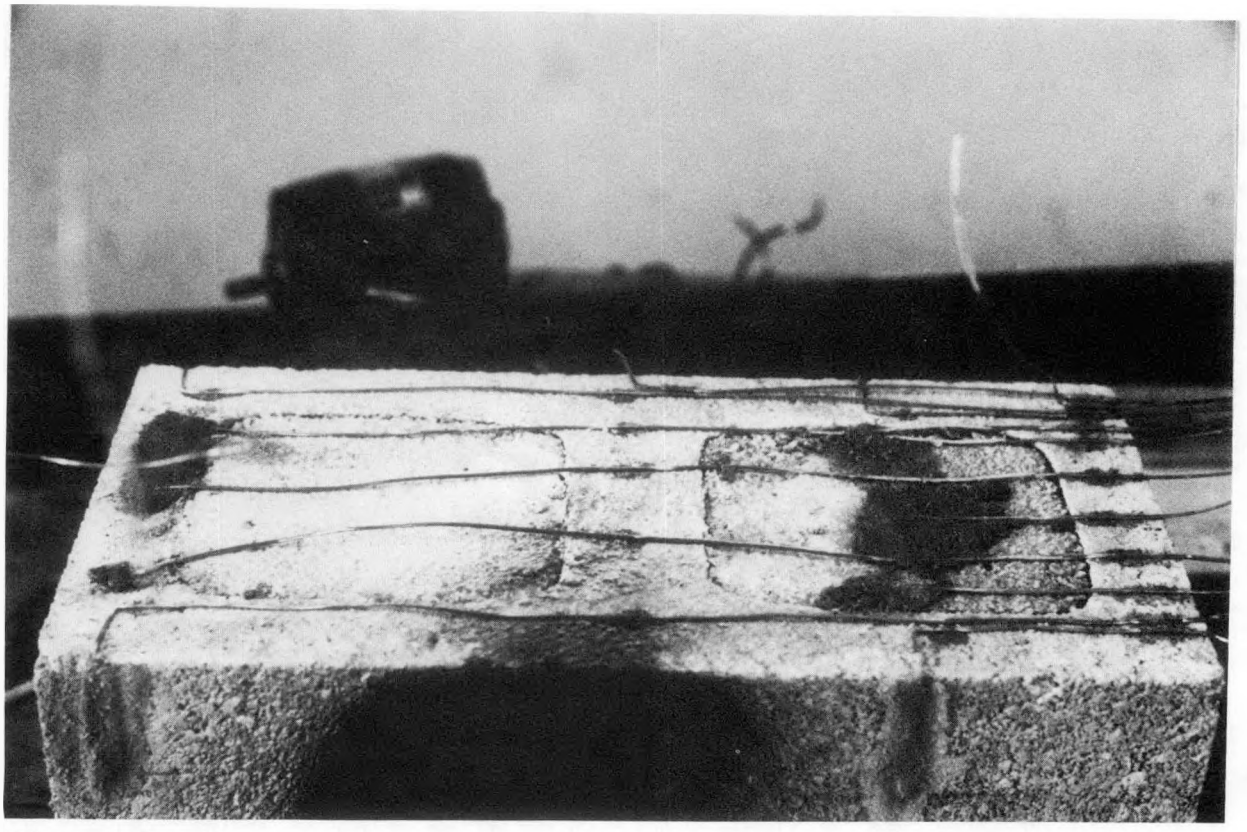

Figure 7. Thermocouples embedded in concrete block, ready to be installed in structure two

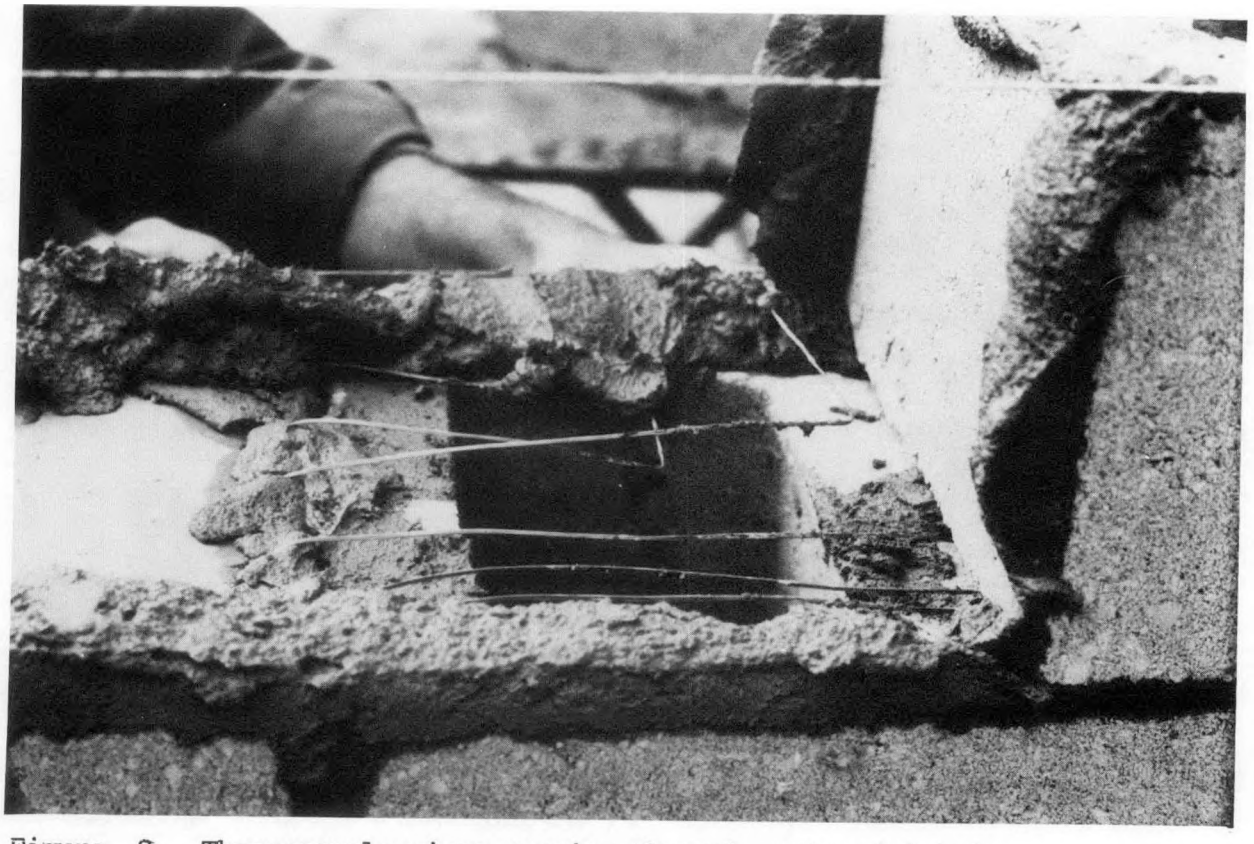

Figure 8. Thermocouple wires running through mortar joint in structure two

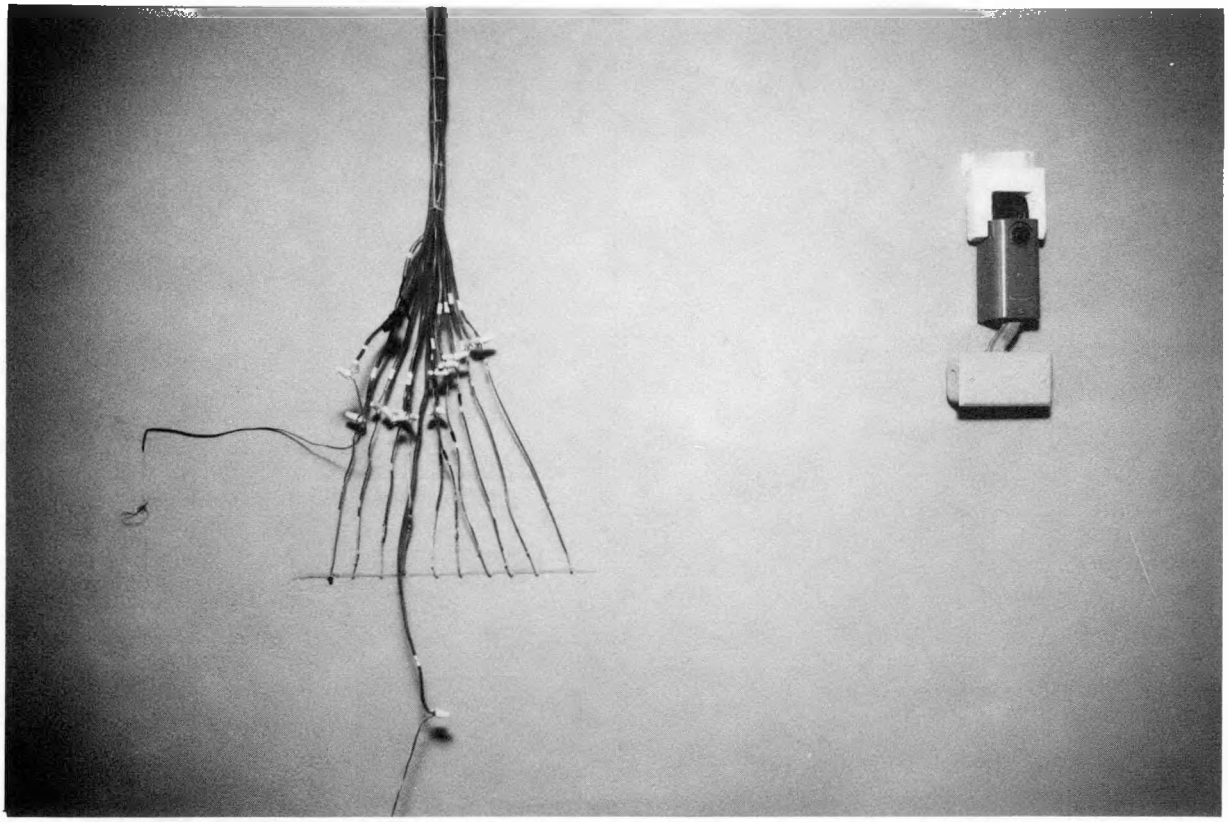

Figure 9. Thermocouple wires in adobe wall

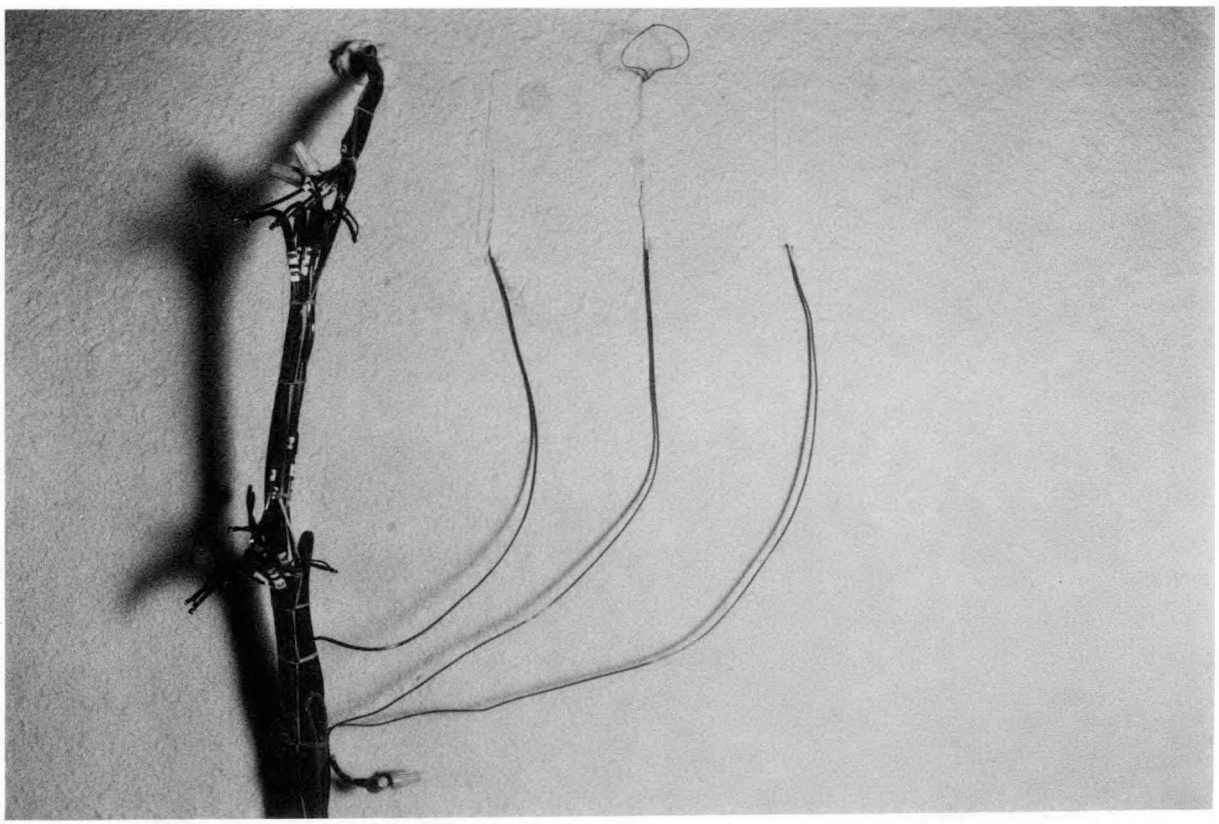

Figure 10. Thermocouple wires attached to wall surface and in air

Figure 11. Pyranometers on solar/screen porch of structure one

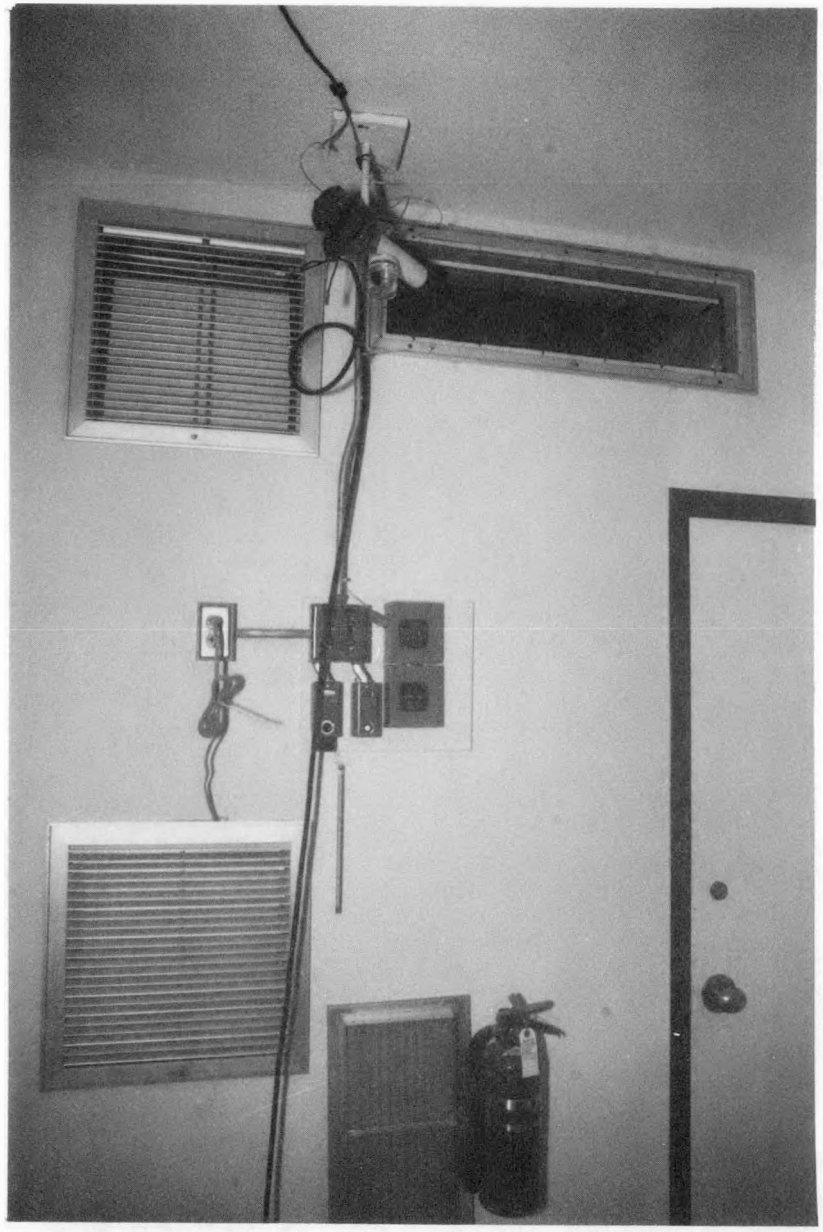

Figure 12. Controls and vents for attic solar collector system; open vent at top is for evaporative cooler

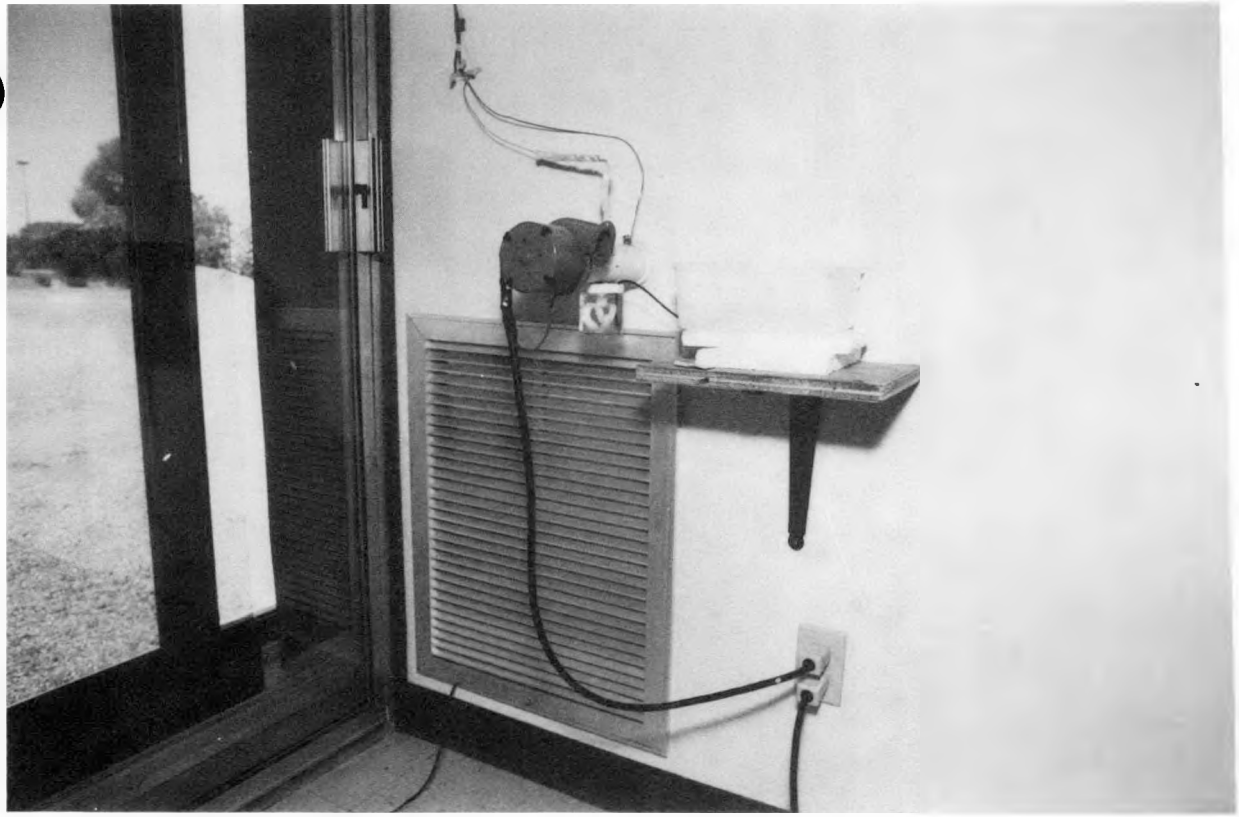

Figure 13. Dry-bulb/wet-bulb measurement device on rockbed plenum vent

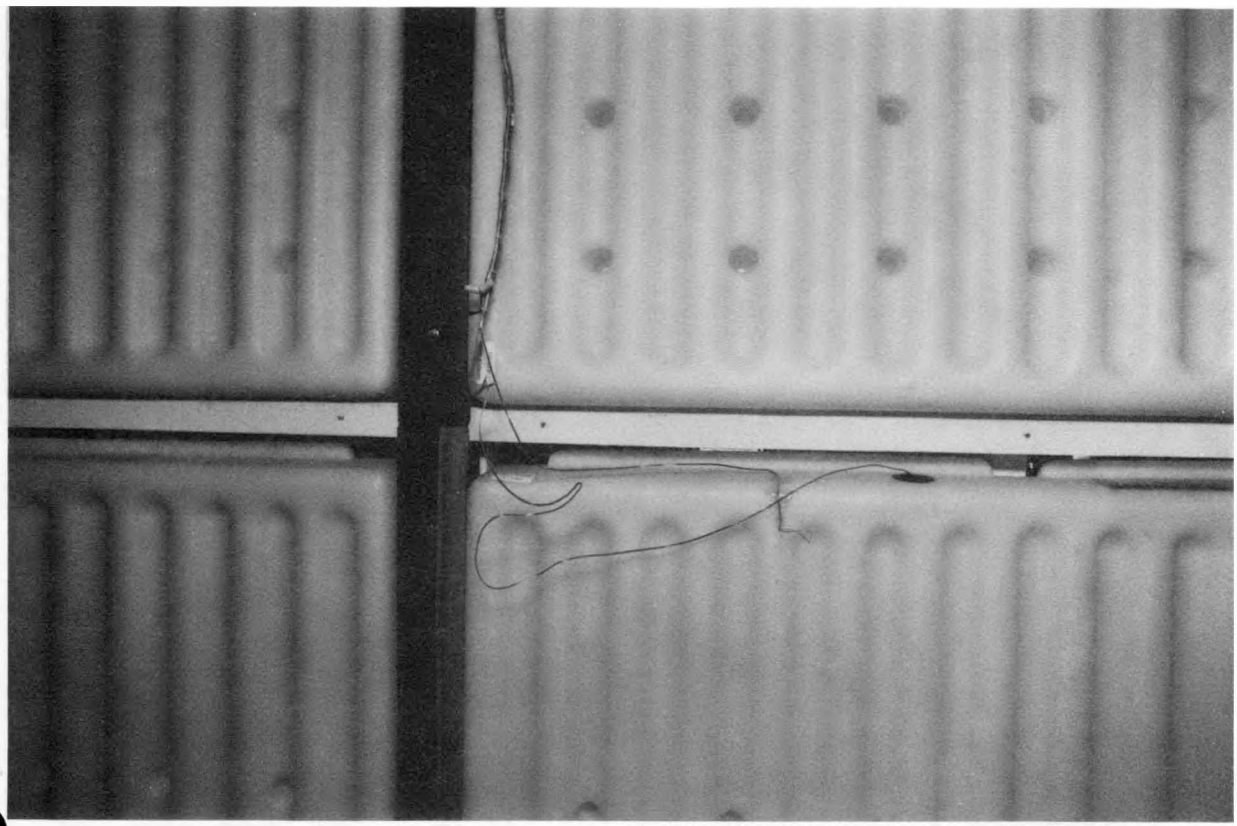

Figure 14. Thermocouple wires in water wall

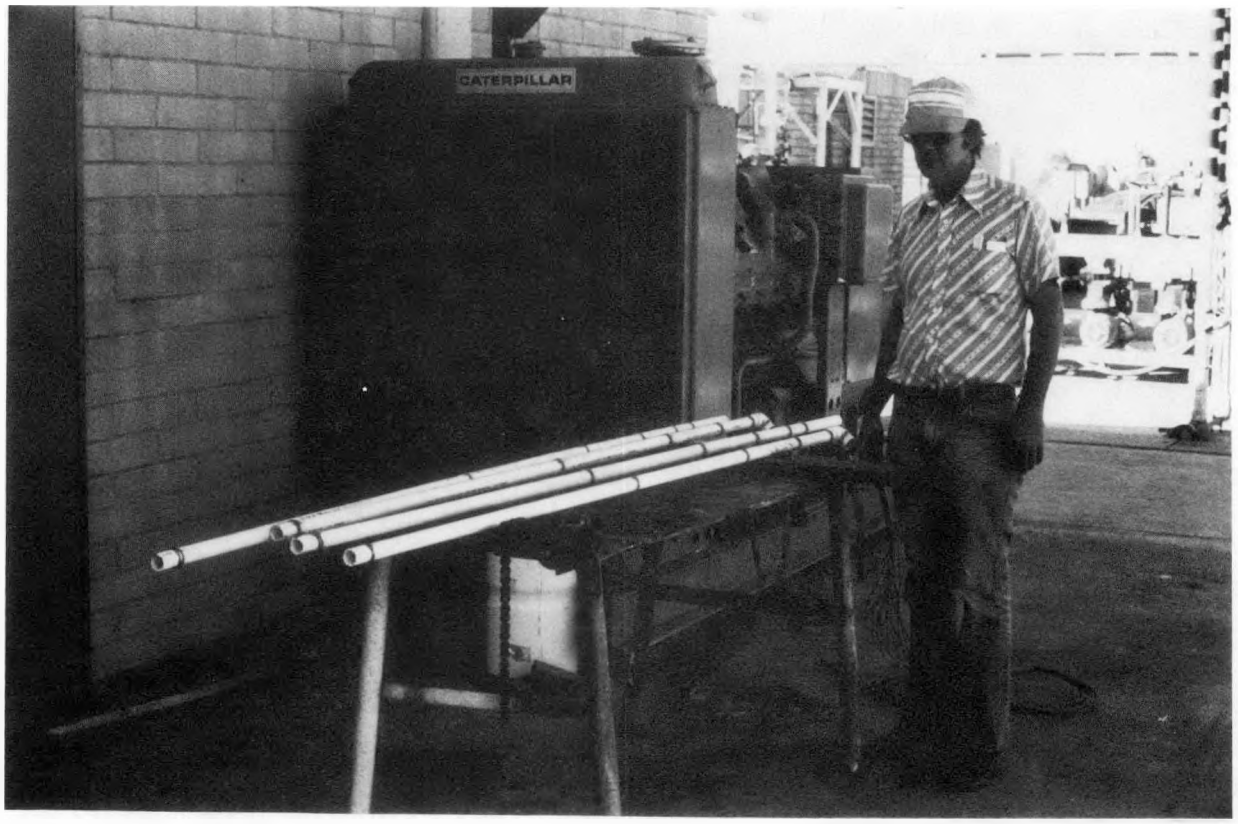

Figure 15. Earth temperature arrays ready for installation

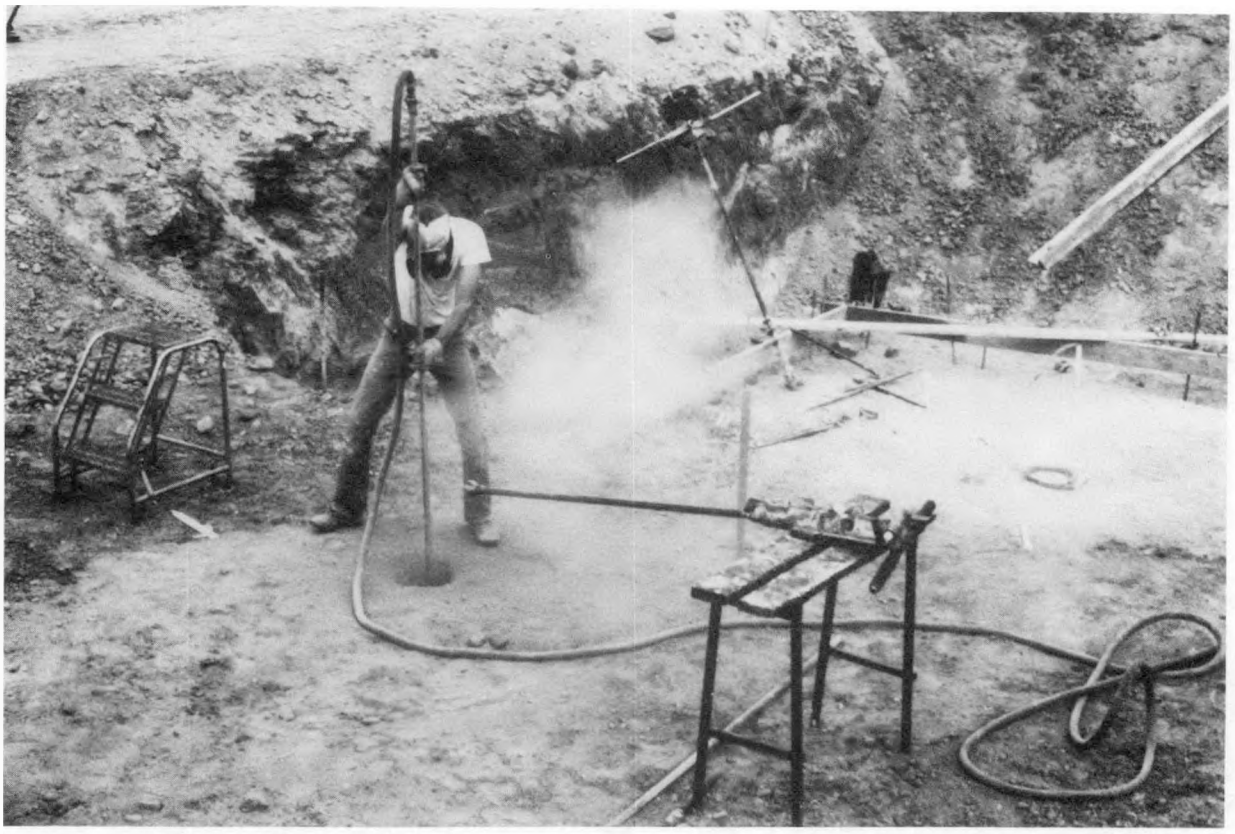

Figure 16. Digging hole for earth temperature array

Figure 17. Thermocouple wire cases for ground arrays before footings and floors installed

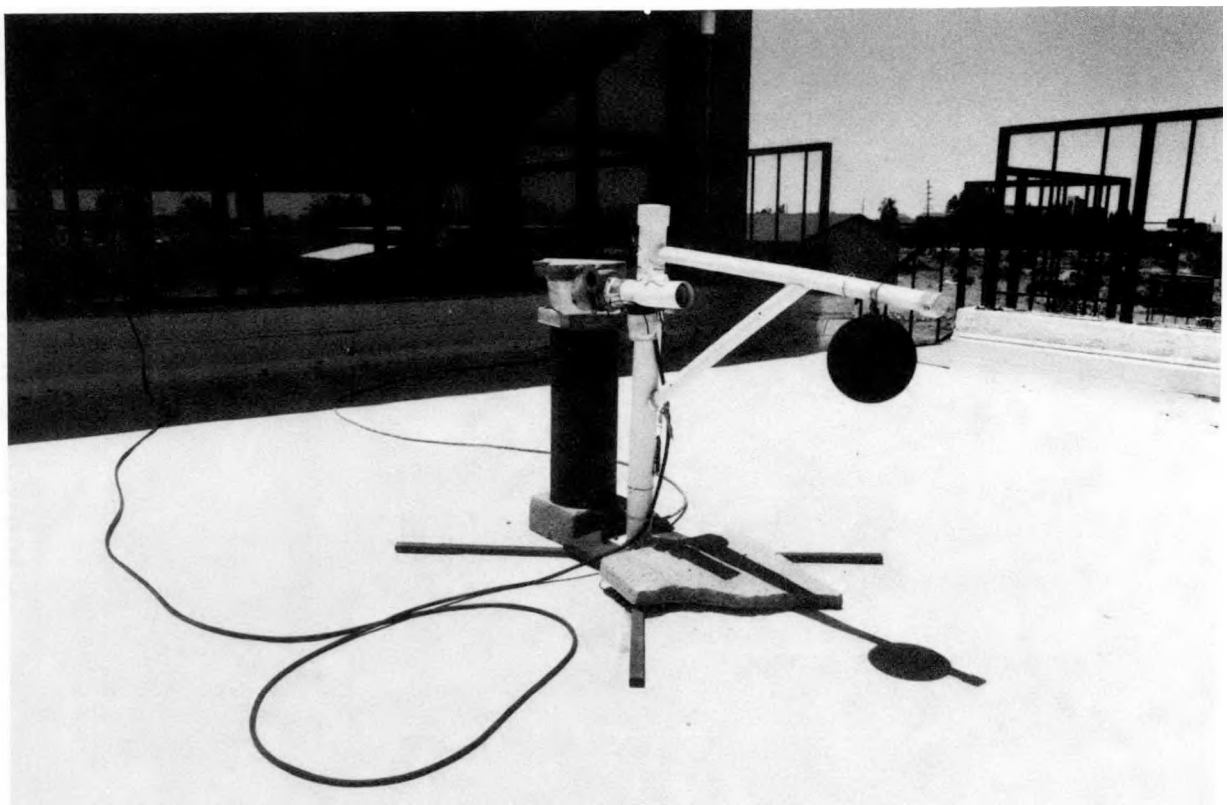

Figure 18. Comfort sensing station (DB, WB, Globe) on roof deck of structure two

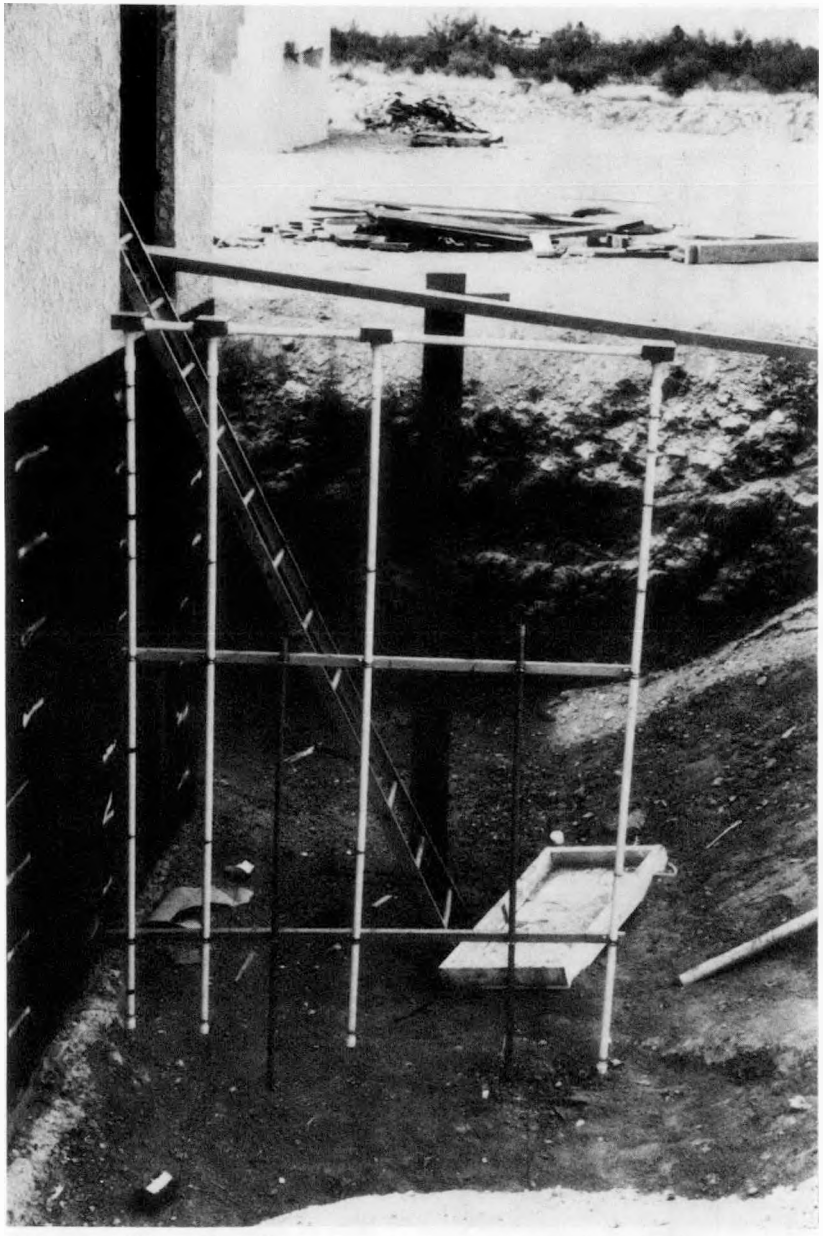

Figure 19. Earth array before backfilling, outside basement of structure two

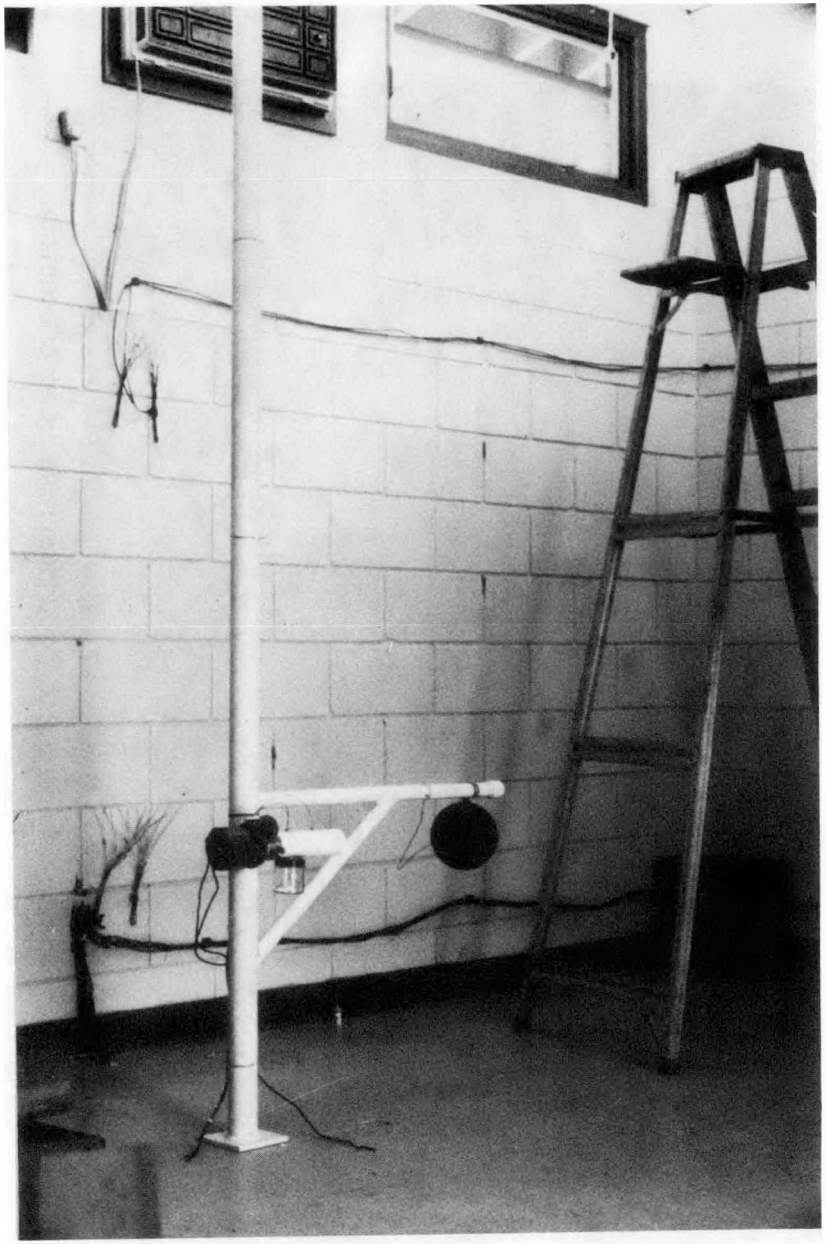

Figure 20. Full height comfort sensing station (DB, WB, Globe and naturally aspirated TC's)

Appendix A

Hy-Cal Heat Flow Sensors

SENSABLE®

HEAT FLOW SENSORS

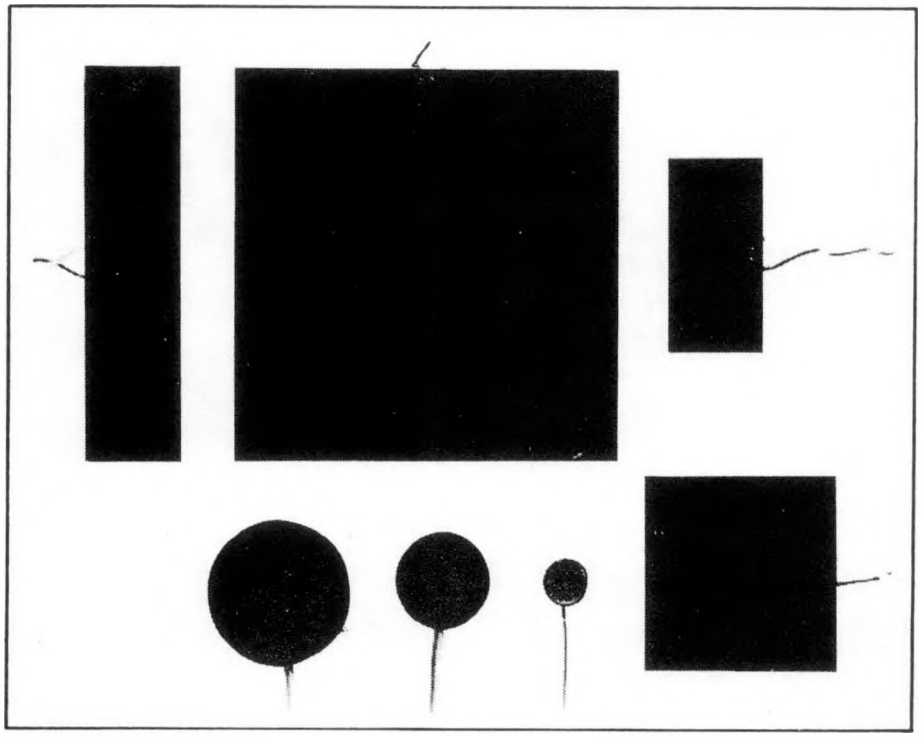

PERFORMANCE FEATURES

- Δ Rugged Construction
- Δ Measures Heat Flow To and From A Surface
- Δ Unaffected by Vacuum
- Δ Reads Out in Millivolts
- Δ Simple to Install
- Δ Sensitive to Both Radiation and Convection
- Δ Self Generating Output

MEASURE MOVING HEAT

The SENSABLE® is able to sense heat flow to or from pipes, tanks, walls, equipment, and solar surfaces. It can be used to measure and/or control. Uses are found in every industry: refineries, steel mills, insulation, air conditioning, chemical, medical, aerospace, automotive, aircraft, laboratories, and food processing, to name a few.

These transducers are self-generating and are compatible with any high impedance recorder, strip chart, millivolt meter, or any potentiometric readout device. They are wafer thin, available in seven configurations and three series to meet any of your requirements. All SENSABLE®s are calibrated, and a sensitivity is marked on the part.

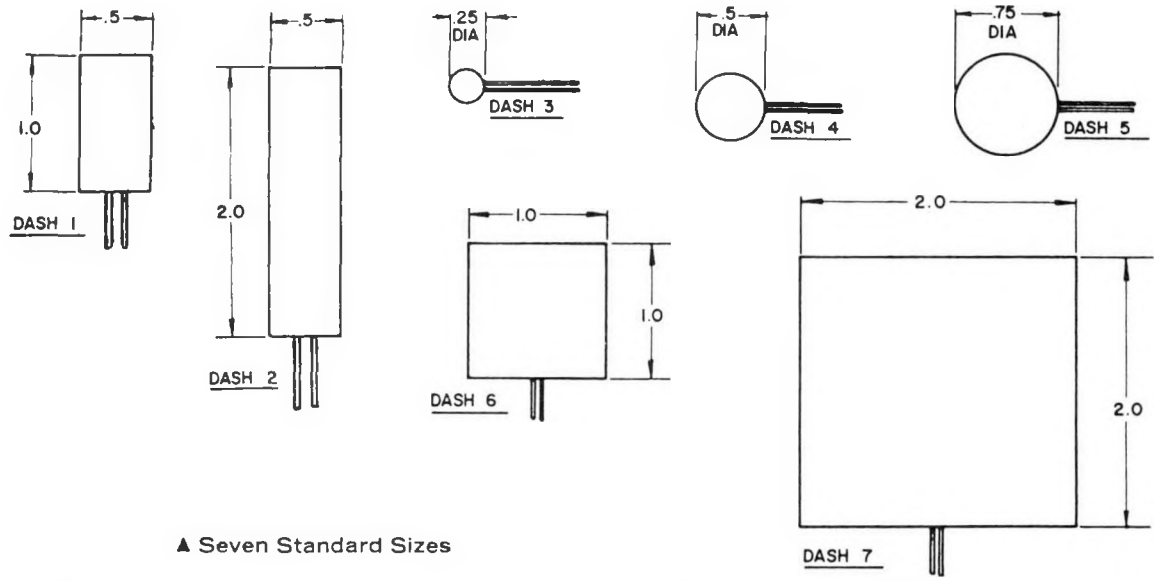

▲ Seven Standard Sizes

SENSABLE® HEAT FLOW TRANSDUCER SPECIFICATIONS			
Series	LO	HI	BI
Operating Temperature Range	0° To 200°F	* -50° To 400°F	* -50° To 200°F
Response Time	6 sec.	6 sec.	6 sec.
Linearity	± 2%	± 2%	± 2%
Repeatability	0.5%	0.5%	0.5%
Resolution	Inf.	Inf.	Inf.
Body	0.1" thick anodized aluminum		
Lead Wire	10' of #28 AWG Copper/Copper Conductors		
Construction	Solid State		
Power Requirement	None - self-generating device with an output in millivolts which is proportional to the heat flow		
Mounting	Pressure sensitive Tape; epoxy adhesives		
Quality Control	Exacting standards of manufacture and quality assurance are employed throughout all phases of fabrication and assembly.		
Calibration	Each part calibrated and marked with sensitivity constant		

*If used below -50°F, special calibration required.

For specs of Sensitivity (MV. vs. BTU/Ft^2-Hr) and Impedance, see GA-3127

Two of the SENSIMETER® Indicators built by Hy-Cal are recommended for use as readout instruments for the SENSABLE® gages (as well as other linear transducers). Write for PD-523 telling of the BTU SENSIMETER®, and PD-524 describing the Universal SENSIMETER®. When used with the SENSABLE® gage, you get a readout directly in BTU/Ft^2-hr. (or other calibration if desired). This gives you a portable system for use in the lab or in the field.

Various Technical Briefs describing how to use the SENSABLE® gage in many applications are available from the factory. Describe your application and we will forward the brief to you.

THREE SERIES TO FIT YOUR APPLICATION

LO Series: These SENSABLE® gages are used where temperatures are below 250°F (recommended level is 200°F) and where high sensitivity is required. Normally they are selected for applications in the ambient to 200°F range where the heat flow is to be measured in one direction only.

HI Series: The higher temperature levels, up to 450°F, require the use of a HI model. Sensitivity is about eight times less than the LO Series, so it is best to order a -2, -6, or -7, which are higher output.

BI Series: This is a very sensitive gage and is recommended for low temperature ranges where there will not be much heat flow, and consequently, the higher output is needed. They are used where heat flow is to be measured in both directions; in applications where it is important for each side of the sensor to have the same nominal sensitivity. In applications where the sensor will be immersed in liquid, a special BI Model is recommended. This would be made from different materials, and the leads sealed so as to not cause shorting or change in calibration. The BI Series are calibrated to assure both sides have the same nominal output.

Special Models: For some applications it is necessary to combine some of the construction techniques of the HI and BI Series. These are then designated BIH.

Non-standard sizes or output signals are required many times, and these can be supplied at relatively the same cost as a standard model. They would take a longer delivery, however, since they are not stocked.

When temperature measurements are desired in conjunction with the heat flow, a thermocouple can be added as an integral part of the sensor.

ORDERING INFORMATION

Nomenclature: SENSABLE® Heat Flow Transducer

Model LO-* SENSABLE®
HI-* SENSABLE®
BI-* SENSABLE®

* Indicate dash number desired (-1, -2, -3, -4, -5, -6, -7)
If longer lead lengths required, please specify

FOB: Our plant, Santa Fe Springs, California
Delivery: Stock Item
Terms: Net, 30 days

HY-CAL ENGINEERING
12105 Los Nietos Rd. • Santa Fe Springs, Ca. 90670 • (213) 698-7785 • Telex 67-

SENSABLE® HEAT FLOW GAGE

SENSITIVITY AT 500 BTU/ft² hr.

Type	Ideal Output	Minimum Output	Size	Maximum Impedance (Ohms)
LO SERIES				
LO-1	30 mV 16.6	22.5 mV	1/2" x 1"	500
LO-2	60 mV	45.0 mV	1/2" x 2"	1.5 K
LO-3	3 mV 166.6	2.2 mV	1/4" dia.	100
LO-4	10 mV	7.5 mV	1/2" dia.	300
LO-5	15 mV	11.2 mV	3/4" dia.	300
LO-6	50 mV	37.5 mV	1" x 1"	900
LO-7	200 mV 2.5	150.0 mV	2" x 2"	4 K
HI SERIES				
HI-1	4 mV 125	3.0 mV	1/2" x 1"	500
HI-2	7 mV	5.2 mV	1/2" x 2"	1 K
HI-3	0.5 mV 1000	.3 mV	1/4" dia.	75
HI-4	2 mV	1.5 mV	1/2" dia.	200
HI-5	2.5 mV	1.8 mV	3/4" dia.	400
HI-6	7 mV	5.2 mV	1" x 1"	1 K
HI-7	30 mV 16.6	22.5 mV	2" x 2"	4.4 K
BI SERIES				
BI-1	50 mV 10.0	37.5 mV	1/2" x 1"	2.5 K
BI-2	120 mV 4.16	90.0 mV	1/2" x 2"	6 K
BI-3	7 mV 71	5.2 mV	1/4" dia.	600
BI-4	18 mV 27.7	13.5 mV	1/2" dia.	1.2 K
BI-5	75 mV 6.66	56.2 mV	3/4" dia.	5 K
BI-6	100 mV 5	75.0 mV	1" x 1"	5.5 K
BI-7*	450 mV = 1.1 BTU/hr ft² mV	337.5 mV	2" x 2"	23 K
BIH SERIES				
BIH-1	4 mV	3.0 mV	1/2" x 1"	500
BIH-2	7 mV	5.2 mV	1/2" x 2"	1 K
BIH-3	0.5 mV	.3 mV	1/4" dia.	75
BIH-4	2 mV	1.5 mV	1/2" dia.	200
BIH-5	2.5 mV	1.8 mV	3/4" dia.	400
BIH-6	7 mV	5.2 mV	1" x 1"	1 K
BIH-7	30 mV	22.5 mV	2" x 2"	4.4 K

*For extra high sensitivity, 1000 mV nominal, 46K ohms; add 'X' after model number.

SENSABLE®

HEAT FLOW TRANSDUCERS

LO, HI and BI Series

MODEL	SHAPE/SIZE	Temperature Range	Nominal Output mV/500 BTU/ft^2-hr.	Max. Impedance ohms	Unit Price
LO-1	1/2" × 1"	0° to +200°F	30 mV	500	$ 73.00
HI -1		-50°F to +400°F	4 mV	500	$ 88.00
BI -1		-50°F to +200°F	50 mV	2.5K	$ 115.00
BIH-1		-50°F to +400°F	4 mV	500	$ 130.00
LO-2	1/2" × 2"	0° to +200°F	60 mV	1.5K	$ 85.00
HI -2		-50°F to +400°F	7 mV	1.0K	$ 100.00
BI -2		-50°F to +200°F	120 mV	6.0K	$ 125.00
BIH-2		-50°F to +400°F	7 mV	1.0K	$ 140.00
LO-3	1/4" dia.	0° to +200°F	3 mV	100	$ 85.00
HI -3		-50°F to +400°F	0.5 mV	75	$ 110.00
BI -3		-50°F to +200°F	7 mV	600	$
LO-4	1/2" dia.	0° to +200°F	10 mV	300	$ 85.00
HI -4		-50°F to +400°F	2 mV	200	$ 110.00
BI -4		-50°F to +200°F	18 mV	1.2K	$
LO-5	3/4" dia.	0° to +200°F	15 mV	300	$ 85.00
HI -5		-50°F to +400°F	2.5 mV	400	$ 110.00
BI -5		-50°F to +200°F	75 mV	5.0K	$ 135.00
LO-6	1" × 1"	0° to +200°F	50 mV	900	$ 95.00
HI -6		-50°F to +400°F	7 mV	1.0K	$ 110.00
BI -6		-50°F to +200°F	100 mV	5.5K	$ 135.00
BIH-6		-50°F to +400°F	7 mV	1.0K	$ 150.00
LO-7	2" × 2"	0° to +200°F	200 mV	4.0K	$ 140.00
HI -7		-50°F to +400°F	30 mV	4.4K	$ 170.00
BI -7		-50°F to +200°F	450 mV	23.0K	$ 215.00
BIH-7					$ 235.00

CODE	LEADWIRE LENGTH AND DESCRIPTION	ADD
	Standard leadwire length - 10 Ft.; #28 AWG Copper/Copper Conductors	$0.25/ft. over 10'

CODE	OPTIONS	ADD
WP	Epoxy coated overall for moisture proofing.	$ 10.00
	Integral thermocouple. Specify thermocouple type: J K T E Provided with 10 ft. leads.	$ 25.00

TOTAL $

Reference: PD-515
Note: Price includes calibration at 500 BTU/ft.^{2}-hr.

200 mV / 500 BTU/ft²-hr = 2½ BTU/ft²-hr / mV
= 1:11 BTU/mV
50/500 = 16.66 BTU/mV

HY-CAL ENGINEERING PRICE LIST
12105 Los Nietos Rd • Santa Fe Springs Ca 90670 • (213) 698-7785 • Telex 67-4494

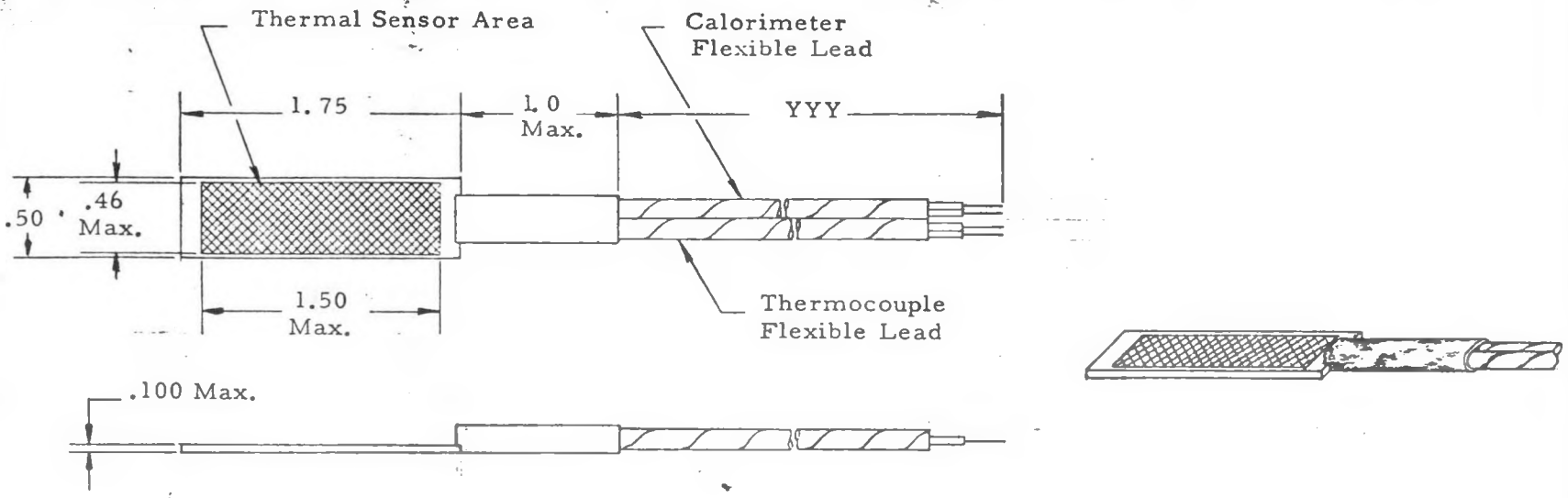

NOTES:

1. Model dash numbers designated as follows:
   - * - Last digit of corresponding N. A. A. dash number.
   - SS - Heating rate in solar constants (1 SS = 7.37 Btu/ft^2-min.)
   - YYY - Flexible extension wire length in inches.
2. Flexible extension wire for calorimeter: #24 gage silver coated copper conductors with Teflon insulation over each conductor; silver coated copper braid overall; Teflon overall; Black wire - negative; White wire - positive. Braid floated.
3. Flexible extension wire for thermocouple: #24 gage copper-constantan thermocouple wires with Teflon insulation over each conductor; nickel coated copper braid overall, Teflon overall. Color code per I. S. A.
4. Temperature range: -250 to + 250°F.
5. Sensing Surface prepared to accept customer specified coatings.
6. Response time less than 1 second.
7. All thermal and electrical junctions metallurgically bonded to assure non-variance from the normal EMF curve, as applicable.
8. Output: 10 ± .50 m. v. at 8 Btu/ft^2-min. (i. e. 9.2 m. v. per solar constant nominal)
9. Heating rate ranges: 0 to 10 solar constants.

REVISIONS		
NO.	DATE	BY
1	12-1-66	
2		
3		
4		
5		

ALL DIMENSIONS IN INCHES WITH FOLLOWING TOLERANCES UNLESS OTHERWISE NOTED:

DECIMALS	FRACTIONS	ANGLES
.X ± .15	±	±
.XX ± .03	1/32	1/2°
.XXX ± .01		

Hy-Cal Engineering
SANTA FE SPRINGS CALIFORNIA

BI-DIRECTIONAL CALORIMETER
MODEL: C-7006-E*-SS-YYY

DATE 1-6-66
SCALE Full
DRAWN WS.
APP'D

MATERIAL -----

DRAWING NO. A-3479

	MIT. NO.	ARIZ. NO	SERIAL NO	FACTORY CALIB /w/m^2 – V	M.I.T. CALIB /w/m^2 – V	* ERROR/%
2HF018	42	32	86769	2.99	2.70	-9.7
2HF014	43	33	70	2.46	2.29	-6.9
2HF015	44	34	71	2.80	2.42	-13.6
2HF016	45	35	72	2.36	2.11	-10.6
2HF011	46	36	73	2.83	2.28	-19.4
	47	37	74	2.69	2.20	-18.2
2HF017	48	40	75	4.59	3.62	-21.1
	49	80	76	2.98	2.48	-16.8
2HF012	50	81	77	3.43	2.89	-15.7
	51	82	78	2.39	2.13	-10.9
* 3HF025	52	83	79	2.46	2.22	-9.8
2HF013	53	93	80	2.93	2.48	-15.4
	55	21	91807	2.76	2.23	-19.2
	56	22	06	2.67	2.42	-9.4
	57	23	05	2.62	2.33	-11.1
	58	24	03	2.44	2.15	-11.9
	59	25	01	2.59	2.35	-9.3
	60	26	04	2.62	2.21	-15.6
	61	27	02	2.71	2.32	-14.4
	62	28	86765	3.14	2.63	-16.2
	63	29	66	3.32	3.06	-7.8
	64	30	67	3.14	2.85	-9.2
	65	31	68	2.44	2.22	-9.0
	66	38	75	3.47	2.82	-18.7

* ERROR = $\frac{\text{M.I.T.} - \text{FACTORY}}{\text{FACTORY}} \times 100\%$

N.B THESE VALUES SUPERCEDE THE EARLIER ONES

* 3HF025 Replaced 3HF027 ON 11/02/82 15:00

The meters were calibrated in a series of 11 tests, with 4 meters being calibrated each test. In all 37 individual tests were performed on your meters. Each meter has been tested at least twice, to check the repeatability of the tests. Meter #47 was arbitrarily chosen as a reference and was included in every test.

The calibration factor for meter #47 should have been the same for all the tests, but it showed a variation from test to test, probably caused by condensation in the styrofoam which would change its conductivity.

Six M.I.T. meters were also tested, four of which have been calibrated before at M.I.T. One has also been tested by an outside agency. All the present tests gave calibration factors 12% higher than those found previously. I have not corrected at all for this discrepency as at present I cannot explain it or account for it.

This discrepency also explains why I have had your meters for so long as I ran a comprehensive series of tests on the M.I.T. meters trying to either explain or eliminate this error.

The tests show a mean random error of 0.9%, although errors up to 5% were found.

I have kept 2 meters - M.I.T. Numbers 47 and 52 - for further testing and I may have to send you a post-correction on all the meters when I discover why my results do not agree with the original ones.

My calibration factors agree with the factory ones to within 5% on 9 of the meters, and within 10% on all of them.

If there's anything else I can do to help, don't hesitate to call or write.

Duncan Apthp

DUNCAN APTHORP
Room 3-470, M.I.T.
(617) -253 -5095

MIT NO.	ARIZONA NO	SERIAL NO.	FACTORY CALIB (w/cm²mV)	M.I.T CALIB (w/cm²mV)	DIFFERENCE * %
42	32	86769	2.99	3.13	4.7
43	33	86770	2.46	2.67	8.5
44	34	86771	2.80	2.81	0.4
45	35	86772	2.36	2.45	3.8
46	36	86773	2.83	2.65	-6.4
47	37	86774	2.69	2.56	-4.8
48	40	86775	4.59	4.21	-8.3
49	80	86776	2.98	2.88	-3.4
50	81	86777	3.43	3.36	-2.0
51	82	86778	2.39	2.48	3.8
52	83	86779	2.46	2.58	4.9
53	93	86780	2.96	2.88	-2.7

$$* \text{ Difference} = \frac{\text{M.I.T.} - \text{FACTORY}}{\text{FACTORY}} \times 100\%$$

MIT NO.	TEST NO.	CF 1 [1]	UNCORRECTED CALIB. (W/m²mV)	CORRECTED (W/m²mV)	ERROR [2] %
42	3	1.011	3.1	3.14	.4
	10	1.019	3.06	3.12	-.4
43	~~4~~ 5	.991	2.63	2.61	-2.3
	8	1.03	2.65	2.73	2.3
44	4	.98	2.86	2.80	-.3
	4A	.98	2.87	2.82	0.3
45	3	1.01	2.44	2.47	0.6
	6	0.99	2.47	2.44	-0.6
46	5	0.99	2.66	2.64	-0.4
	10	1.02	2.61	2.65	0.4
47	PRESENT IN ALL TESTS				
48	4	0.98	4.28	4.20	-0.3
	4A	0.98	4.30	4.22	+0.3
49	5	0.99	2.89	2.86	-0.5
	10	1.02	2.84	2.89	0.5
50	3	~~1~~ 1.01	3.26	3.30	-1.8
	8	1.03	3.32	3.42	1.8
51	1	.96	2.50	2.40	-3.0
	2A	.98	2.64	2.58	4.1
	6	.99	2.47	2.43	-1.8
	9	1.03	2.43	2.49	0.7
52	1	.96	2.68	2.58	0
	2	1.02	2.57	2.62	1.9
	2A	0.98	2.61	2.55	-1.0
	9	1.03	2.49	2.56	-0.8
53	4	0.98	2.95	2.89	0.2
	4A	0.98	2.93	2.88	-0.2

1 : CF, is a correction factor equal to the ratio of the mean calibration factor for meter #47 to the calibration factor for meter #47 in that test.

2 : ERROR = $\frac{\text{CORRECTED CALIBRATION} - \text{MEAN CORRECTED CALIB.}}{\text{MEAN CORRECTED CALIBRATION}} \times 100$

Appendix B

Pyranometer Calibration - Eppley PSP

Standardization of Eppley Precision Pyranometer
and Black and White Pyranometer

Certificate of Calibration - Li-Cor Pyranometer Sensor

Instrumentation Manual - LI-200SB Pyranometer Sensor

DSET
LABORATORIES, INC.

Box 1850
Black Canyon Stage I
Phoenix, Arizona 85029

Telephone: 602-465-7356
TWX: 910-950-4681 DSET PHX

CERTIFICATE
OF
PYRANOMETER CALIBRATION

PYRANOMETER: EPPLEY MODEL PSP, SN 20474F3

Client: University of Arizona
Environmental Research Laboratory

Date of Calibration: 04-28-82 and 04-30-82
Tilt: Horizontal
Latitude: 33° 50'
Time: 09:04:30 to 13:02:30; 09:00 to 13:13 AST
Scale: Absolute
Ambient Temperature: 33°C ± 2°

INSTRUMENT CONSTANT: 9.85×10^{-6} volts/watt meter^{-2}
6.87 millivolts/cal cm^{-2} min^{-1}

Traceability: Calibrated in 525 instantaneous increments to DSET's working standard pyranometer, an Eppley PSP, SN 19129 F3, which is itself calibrated by the shading disk technique to DSET's Model H-F Absolute Cavity Self-Calibrating Pyrheliometer (SN 17142). Primary intercomparisons of the Eppley H-F Absolute Cavity have been against similar instruments in four intercomparisons -- the Second, Third and Fourth New River Intercomparisons of Absolute Cavity Pyrheliometers, held May 1-4 and November 5-9, 1979, and November 17-19, 1980, and the International Pyrheliometric Conference IPC V held in Davos, Switzerland in October 1980.

DSET Laboratories, Inc. uses reasonable diligence in the manner of performing the services required, but no warranties are given and none may be implied directly or indirectly relating to DSET services or facilities or to the tests or calibrations by DSET upon Buyer's equipment. In no event shall DSET be liable for collateral, special or consequential damage. See reverse for additional information.

DSET LABORATORIES, INC.

Gene A. Zerlaut, President

5-17-82
Date

Please note that the instrument constant provided on the Certificate represents calibration performed at a specific temperature. You will have a specific Eppley Temperature compensation plot for your pyrheliometer or pyranometer. Should you use the instrument at, for example, 25°C, you may compensate the calibration factor by ratioing the sensitivity of your instrument at 25°C to that at the calibration temperature.

Further, your instrument was calibrated at a specific tilt (to the horizontal) and the calibration may change slightly when it is operated at other tilts.

Should you have any questions about this procedure, please telephone either J. Maybee or G. Zerlaut.

(401) 847-1020

EPLAB

THE EPPLEY LABORATORY, INC.
SCIENTIFIC INSTRUMENTS
NEWPORT, R.I. 02840 U.S.A.

STANDARDIZATION
OF
EPPLEY PRECISION PYRANOMETER

(horizontal surface receiver-180° twin hemisphere)

Model PSP Serial Number 20474F3 Resistance 656 ohm at 21 °C

Temperature Compensation

Range -20 to +40 °C

This radiometer has been compared with the Eppley group of reference standards. under radiation intensities of about 700 watts meter^{-2} (roughly one-half a solar constant), the adopted calibration temperature is 25 °C.

As a result of a series of comparisons, it has been found to develop an emf of:

10.32 x10^{-6} volts/watt meter^{-2}

7.20 millivolts/cal cm^{-2} min^{-1}

The calculation of this constant is based on the fact that the relationship between radiation intensity and emf is rectilinear to intensities of 1400 watts meter^{-2}. This pyranometer is linear to within ± 0.5 percent up to this intensity.

The calibration was made with both hemispheres of Schott WG295 (clear) glass. This value should be *increased* for other Schott hemispheres as follows: GG400 = 0.0 %, OG530 = 0.5%, RG610 = 1.5% and RG695 = 2.0%.

The calibration of this instrument is traceable to standard self-calibrating cavity pyrheliometers in terms of the Systems Internationale des Unites (SI units), which participated in the Fourth International Pyrheliometric Comparisons (IPCIV) at Davos, Switzerland in October 1975.*

Useful conversion facts: 1 cal-cm^{-2} min^{-1} = 697.3 watts/meter^2
1 BTU/ft^2-hr^{-1} = 3.153 watts/meter^2

Date of Test: December 23, 1980

IN CHARGE OF TEST
Richard H. Hatch

The Eppley Laboratory, Inc.

By: [signature]

S. O. 40569

Newport, R. I.

Date January 9, 1981

Shipped to: University of Arizona
Tucson, Arizona

Remarks:

* *See Reverse For Explanation*

EPPLEY PRECISION SPECTRAL PYRANOMETER - MODEL PSP - INSTRUMENT NO. 20474 F3

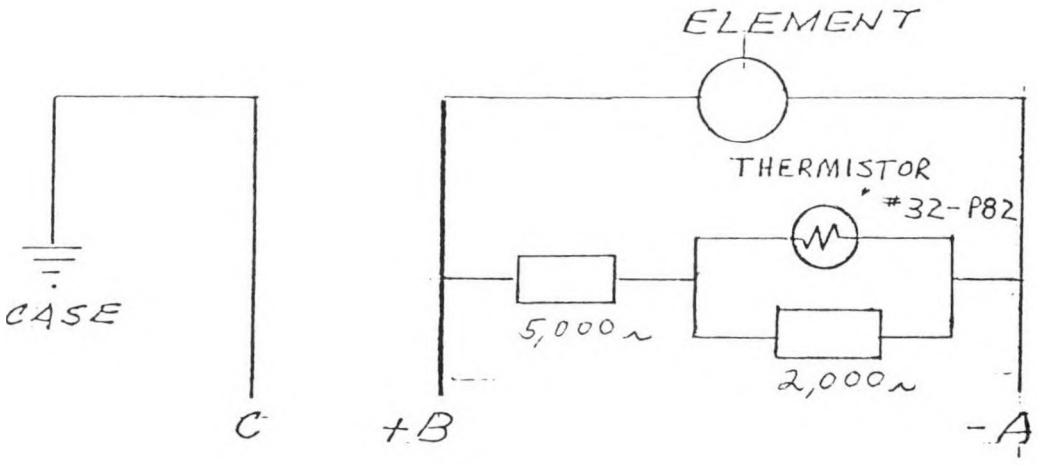

INTERNAL WIRING

TEMPERATURE DEPENDENCE

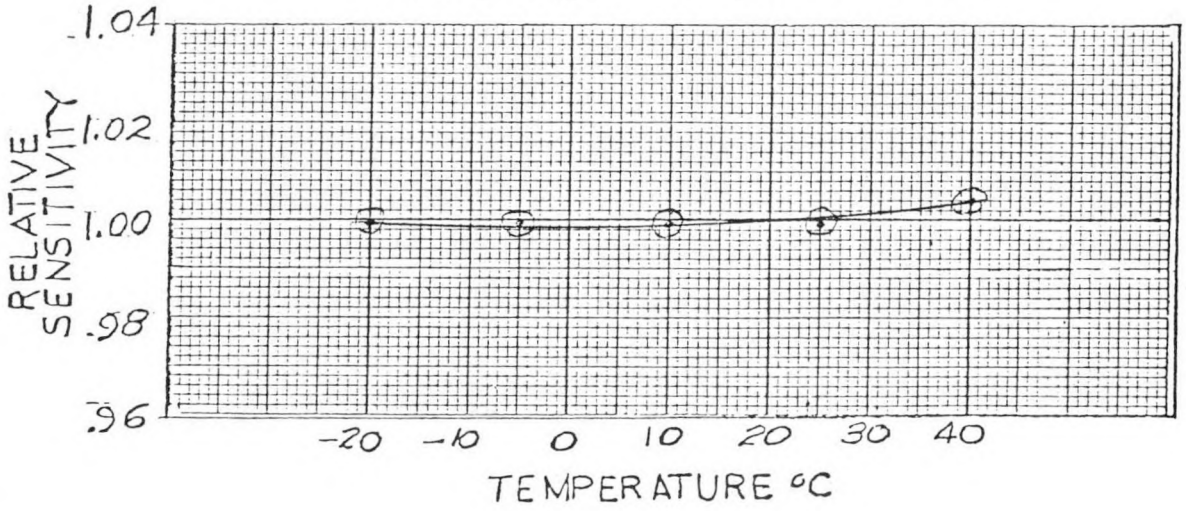

TESTED BY R. Hatch

DATE Dec. 8, 1980

(401) 847-1020

EPLAB

THE EPPLEY LABORATORY, INC.
SCIENTIFIC INSTRUMENTS
NEWPORT, R.I. 02840 U.S.A.

STANDARDIZATION
OF
EPPLEY BLACK AND WHITE PYRANOMETER

(horizontal surface receiver - 180°)

Model 8-48 Serial Number 16426 Resistance 350 ohm at 26 °C

Temperature Compensation

Range -20 to + 40 °C

This radiometer has been compared with the Eppley group of reference standards, under radiation intensities of about 700 watts meter^{-2} (roughly one-half a solar constant), the adopted calibration temperature is 25 °C.

As a result of a series of comparisons, it has been found to develop an emf of:

11.06 x10^{-6} volts/watt meter^{-2}

7.71 millivolts/cal cm^{-2} min^{-1}

The calculation of this constant is based on the fact that the relationship between radiation intensity and emf is rectilinear to intensities of 1400 watts meter^{-2}. This pyranometer is linear to within ± 1.0 percent up to this intensity.

The calibration of this instrument is traceable to standard self-calibrating cavity pyrheliometers in terms of the Systems Internationale des Unites (SI units), which participated in the Fourth International Pyrheliometric Comparisons (IPCIV) at Davos, Switzerland in October 1975.*

Useful conversion facts: 1 cal-cm^{-2} min^{-1} = 697.3 watts/meter^2

1 BTU/ft^2-hr^{-1} = 3.153 watts/meter^2

Date of Test: October 17, 1977 IN CHARGE OF TEST W. J. Scholes

The Eppley Laboratory, Inc.

By: Randall S. Osborne S. O. 35406

Newport, R. I. Date November 2, 1977

Shipped to: University of Arizona
Tucson, Arizona

Remarks:

* See Reverse For Explanation

EPPLEY BLACK AND WHITE PYRANOMETER

MODEL 8-48 INSTRUMENT NO. 16426

INTERNAL WIRING

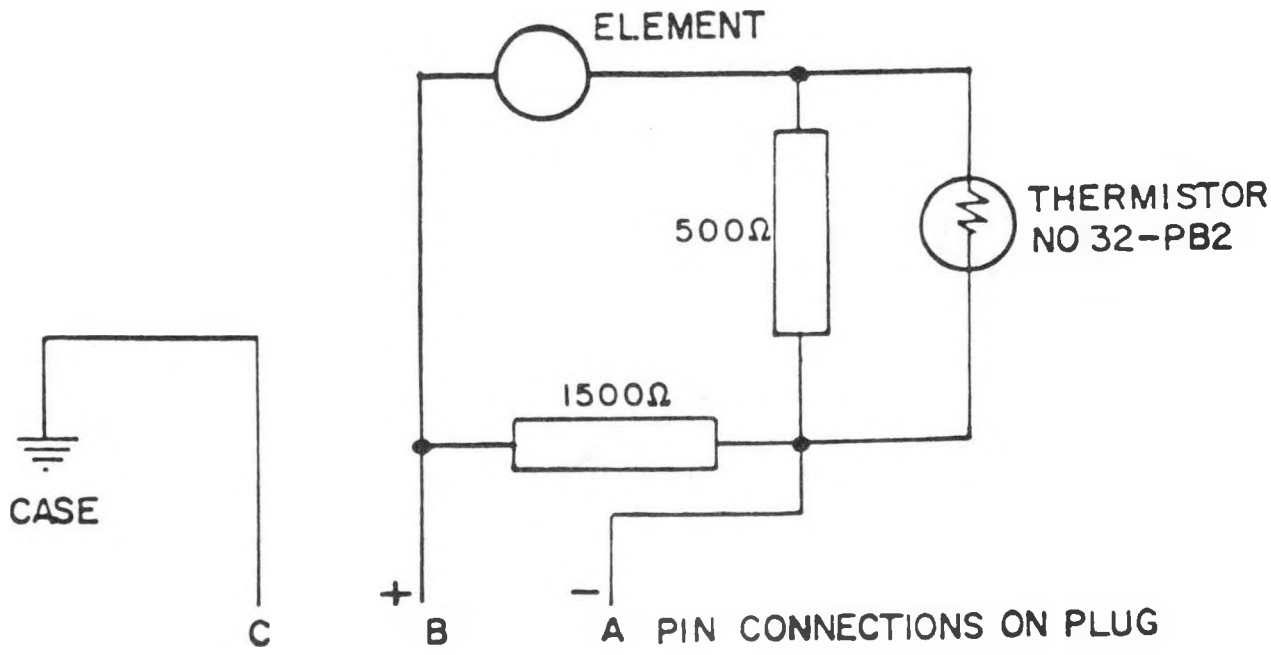

TEMPERATURE DEPENDENCE

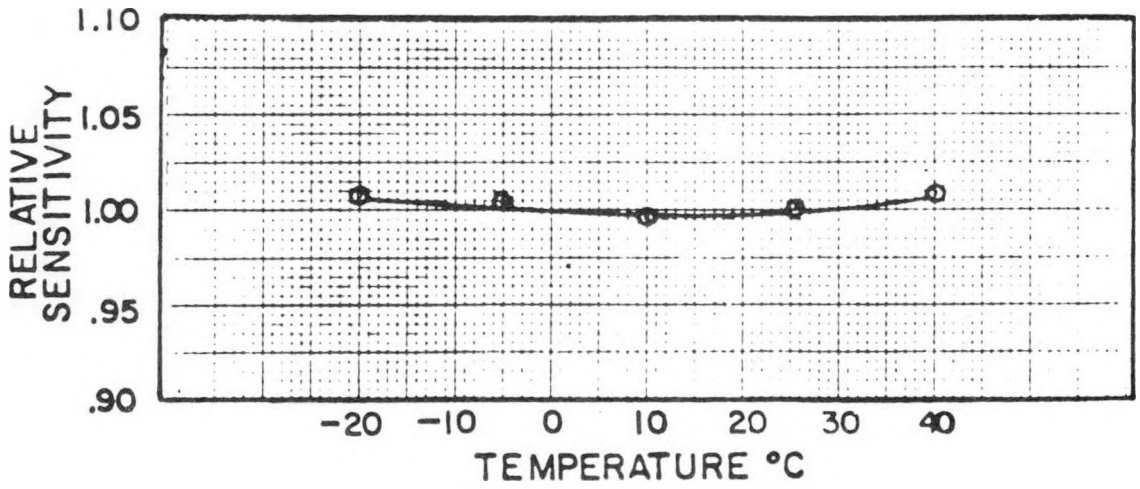

TESTED BY

DATE 10/17/77

Explanation of change in calibration traceability

As of April 1, 1977, the calibration traceability of Eppley solar radiation measuring instruments has been changed from the International Pyrheliometric Scale of 1956 (IPS 1956) to the Absolute Scale (SI). This change based on the results of IPC IV is such that instruments calibrated in SI units yield irradiance values which are 2.1% higher than values which would be obtained using Eppley instruments calibrated previously and referenced to IPS.

CERTIFICATE of CALIBRATION
LI-COR PYRANOMETER SENSOR

Model Number: LI-200SB Pyranometer

Serial Number: PY 2631 Date of Calibration: 12-29-80 By: DH

Output:* 79.5 microamps per 1000 watts m^{-2}

Calconnector resistance for SENSOR (in air) 4.96K ohms

Output:** 10.0 millivolts per 1000 watts m^{-2} when using millivolt adaptor.
3.15 millivolts per 100 BTU ft^{-2} h^{-1} when using millivolt adaptor.
Calconnector resistance for millivolt adaptor 125.8 ohms

The above sensor is supplied with a calibrated connector (calconnector) that has resistance values unique to that sensor. For that reason, the calconnector has a serial number that matches the serial number on the sensor. ALWAYS MAKE SURE THAT THE SENSOR IS USED WITH THE CALCONNECTOR THAT HAS THE SAME SERIAL NUMBER.

This feature allows the above sensor to be used with any LI-COR LI-185B, LI-188B, and LI-1776 without need for correction factors or recalibration of the readout instrument in order to obtain a direct readout.

**When using a sensor with a LI-COR LI-510B or LI-550B Integrator, the sensor's calibration constant as listed here must be used to determine the relationship between the sensor input and the counts recorded by the integrator. See sample calculations in the LI-510B, LI-550B manual for further instructions.*

***Each LI-COR sensor is provided with a millivolt adapter. There is also a resistance in the calconnector that is sensed when the millivolt adapter is connected to the sensor to allow for direct millivolt output.*

IMPORTANT: Read the appropriate sensor manual before using this sensor.

IMPORTANT: It is recommended that sensors be recalibrated every two years.

LI-COR, inc. / LI-COR, Ltd.
P.O. Box 4425 / 4421 Superior Street
Lincoln, Nebraska 68504 USA

INSTRUCTION MANUAL

LI-200SB PYRANOMETER SENSOR

TABLE OF CONTENTS

LIST OF FIGURES

APPENDIX

(The LI-200SB Instruction Manual contains sections used also within the LI-COR light meter and integrator manuals. When a sensor is ordered separately, only the pertinent instruction sections are included.)

SECTION III
COSINE RESPONSE

3-1. IMPORTANCE OF COSINE CORRECTION

3-1a. Measurements intended to approximate radiation impinging upon a flat surface (not necessarily level) from all angles of a hemisphere are most accurately obtained with a cosine corrected sensor.

3-1b. A sensor with a cosine response (follows Lambert's cosine law) allows measurement of flux densities through a plane surface. This allows the sensor to measure flux densities per unit area (m^2). A sensor without an accurate cosine correction can give a severe error under diffuse radiation conditions within a plant canopy, at low solar elevation angles, under fluorescent lighting, etc.

3-1c. The cosine relationship can be thought of in terms of radiant flux lines striking a flat surface. Lambert's Cosine Law is explained by illustrating radiant flux lines impinging upon a surface normal to the source (Figure 1A) and at an angle of 60° from normal (Figure 1B). Figure 1A shows 6 rays striking the unit area, but at a 60° angle, only 3 rays strike the same unit area. This is illustrated mathematically as

$$S = (I)\ (\text{cosine } 60°) \text{ per unit area} \qquad (3\text{-}1)$$
$$3 = (6)\ (0.5) \text{ per unit area}$$

where S = vertical component of solar radiation; I = solar radiation impinging perpendicular to a surface and cosine 60° = 0.5 .

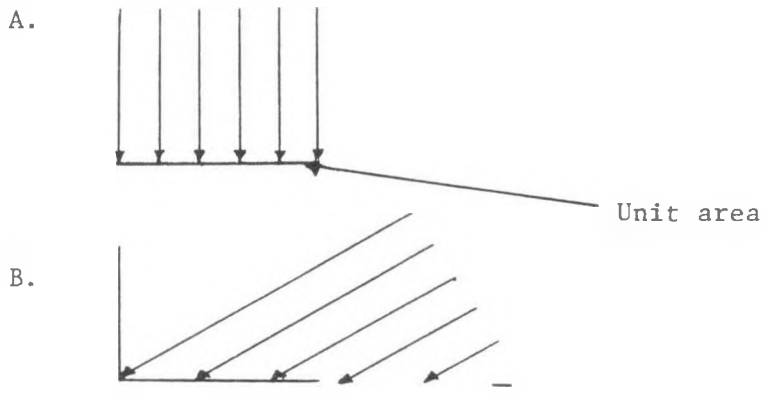

Figure 1. Lambert's Cosine Law.

2. COSINE CORRECTION PROPERTIES

3-2a. Cosine corrected LI-COR terrestrial type sensors are all designed for the same cosine response characteristics. The instruction manual included with underwater sensors contains information on cosine response for LI-COR underwater sensors.

3-2b. The percent of true cosine response is presented in Figure 2. The error is typically less than ±5% for angles less than 80° from the normal axis of the sensor. At 90° a perfect cosine collector response would be zero and at that angle any error is infinite. Some other cosine response reporting techniques provide more attractice data which can be deceiving. Careful data interpretation is necessary when those reporting techniques are encountered.

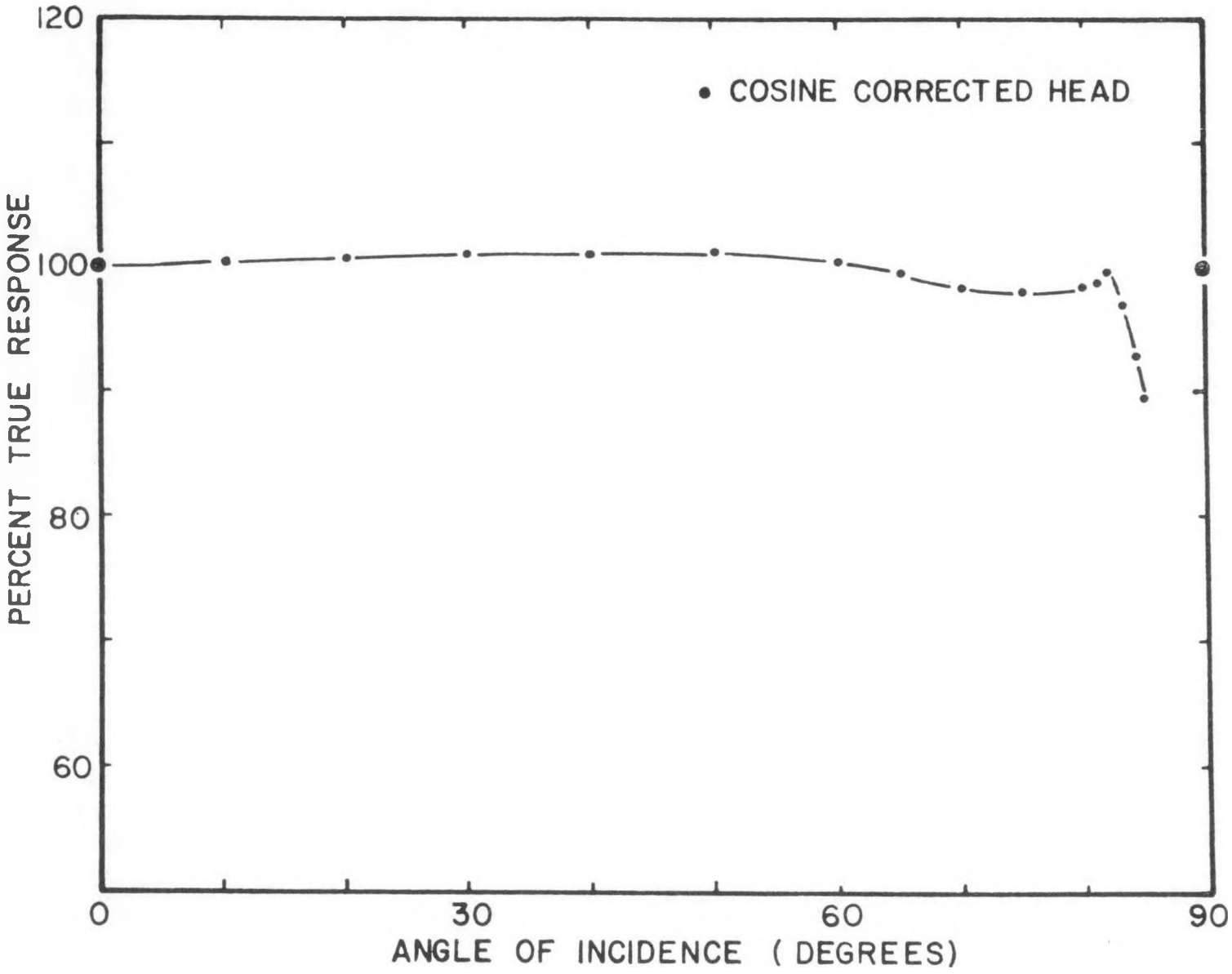

Figure 2. Cosine response of LI-COR Terrestrial Type Sensors.

SECTION VI
LI-200SB PYRANOMETER SENSOR

6-1. USE OF THE PYRANOMETER SENSOR

6-1a. A pyranometer is an instrument for measuring solar radiation received from a whole hemisphere. It is suitable for measuring global sun plus sky radiation.

6-1b. Solar radiation varies significantly among regions. Season and time of day are major considerations, but atmospheric conditions such as surrounding terrain elevation, man-made obstructions, and surrounding trees can also cause large variations in locations of a small area. Often, the most required measurement is the energy flux density of both direct beam and diffuse sky radiation passing through a horizontal plane of known unit area (i.e. global sun plus sky radiation).

6-1c. The silicon photodiode has made possible the construction of simple pyranometers of reasonable accuracy where the photodiode is stable. The response of the silicon photodiode sensor (Figure 6) does not cause serious error provided the photodiode is used only for solar radiation and not under conditions of altered spectral distribution. IMPORTANT: For this reason, we do not recommend its use under artificial lighting or within plant canopies. Also, reflected radiation can be erroneously measured.

6-1d. The LI-COR pyranometer may be handheld or mounted at any required angle, provided that reflected radiation is not a significant portion of the total. In its most frequent application, the pyranometer sensor is set on a level surface free from any obstruction to either direct or diffuse radiation. The sensor may be most conveniently leveled by using the 2003S Mounting and Leveling Fixture.

6-1e. Keep the sensor clean and treat it as a scientific instrument in order to maintain the accuracy of its calibration. The vertical edge of the diffuser must be kept clean in order to maintain appropriate cosine correction.

6-1f. The LI-COR pyranometer sensor is a miniaturized version of the pyranometer developed by Kerr, Thurtell and Tanner.[4]

6-2. CALCONNECTOR

6-2a. The LI-COR LI-200SB Pyranometer Sensor utilizes a LI-COR Calconnector which provides direct unit readout with LI-COR models LI-185B Quantum/Radiometer/Photometer, LI-188B Integrating Quantum/Radiometer/Photometer and LI-1776 Solar Monitor. If the Calconnector is detached from the sensor cable at the BNC connection, the sensor can be connected to the LI-510B Integrator or LI-550B Printing Integrator for readouts that are easily converted to the desired units. The LI-175 Solar Meter/Integrator uses this BNC connector also, and should be used only with the LI-COR pyranometer that is directly calibrated to it. This connection is also used with the 2222SB Extension Cable.

6-2b. The Calconnector contains the calibration resistances (potentiometer) for direct unit readout, and direct millivolt readout (if the millivolt adapter is used). Because of this standardized sensor output, radiation sensors can be used interchangeably with any LI-COR LI-185B, LI-188B or LI-1776 without calibrating the instrument to the sensor. This applies to LI-COR sensors of the same type, or different types of LI-COR radiation sensors. IMPORTANT: Each sensor is to be used only with the Calconnector that is supplied with it (i.e., the sensor serial number and the Calconnector serial number must be the same).

6-2c. The LI-200SB Pyranometer Sensor may be used with millivolt recorders if the Millivolt Adapter (included with each Calconnector) is connected to the Calconnector, and the wire leads are connected to the recorder. In this case, a LI-COR Light Meter or Integrator is not used. Cable length of 1000 feet (304 m) or more will not degrade the signal when high impedance recorders (>1 megohm, such as potentiometric types) are used. If extension cable is needed, use LI-COR extension cable, or coaxial (RG174) cable. Recorder range adjustment should be approximately 0-10 mV full scale. Sensor output in this configuration is given as 10.0 millivolts per 1000 watts m^{-2}. This millivolt adapter can be used with any LI-COR Calconnector. See Section 6-6 for further details.

6-3. COSINE RESPONSE

Information concerning cosine correction and the properties of a cosine corrected sensor are contained in Section III.

6-4. SPECTRAL RESPONSE

6-4a. The relative spectral response of the silicon photodiode does not extend uniformly over the full solar radiation range. A typical response curve is presented in Figure 6. The response is very low at 0.4 µm and increases nearly linear to a maximum at about 0.95 µm and then decreases nearly linear to a cutoff near 1.2 µm. Changes in the spectral distribution of the incident light, coupled with the non-uniform spectral response, can cause errors in the photodiode output. Hull[3] shows that in the 0.4 to 0.7 µm range, the spectral distribution of sun plus sky radiation on a horizontal surface is remarkably constant even when clear and overcast days are compared. However, Gates[2] indicates that the major change in spectral distribution of solar radiation occurs in the near infrared where water vapor absorption takes place on cloudy days. Data collected at low solar elevations can show significant error because of altered spectral distribution which changes in atmospheric transmission. This is a small part of the daily total so the possible observed error usually has an insignificant effect on daily integrations.

6-4b. The area under the spectral irradiance curve of the source is directly proportional to the energy received by a horizontal surface. Under specific but typical conditions, energy received on a completely overcase day has been estimated to be 11.3% of that received on a clear day. When both spectral distributions are weighted according to a typical response curve of a silicon photodiode, the response on this cloudy day is 12.6%. Therefore, errors incurred under different sky

conditions, due to the spectral response of the photodiode, will be small. The field tests of Federer and Tanner[1] and Kerr, Thurtell and Tanner[4] confirm this conclusion.

6-5. CALIBRATION

The LI-200SB Pyranometer has been calibrated against an Eppley Precision Pyranometer of which the calibration is periodically confirmed. The calibration was performed under full sun conditions at solar noon. The uncertainty of the calibration is ±5%.

6-6. IMPORTANT NOTICES

6-6a. The Calconnector and Millivolt Adapter are not weatherproof. If the Millivolt Adapter is attached to the Calconnector for connection to a datalogger or millivolt recorder, this connection should be made at the recorder end (indoors). This is done to protect the Calconnector, and to eliminate thermocouple effects that could be caused by exposing the Calconnector to rapidly-changing direct solar radiation. These effect are not noticeable when the Calconnector is used indoors out of direct radiation.

If extension cable is needed, the Calconnector should be attached to the end of the extension cable for connection to the recorder.

6-6b. If extension cable is used where the BNC termination will be exposed outdoors or on a conductive surface, the BNC connection should be insulated by wrapping it with tape. This is done to avoid ground loops.

6-6c. The shield of LI-COR light sensor coaxial cable is positive and the center conductor is negative. This is done because the trans-impedance amplifier used in LI-COR light meters requires a negative signal. For datalogger or millivolt applications where the Millivolt Adapter is used, the positive (red) lead should be connected to the low impedance (common terminal) when plus or minus signal capability is available on the datalogger or recorder. This will minimize noise.

If plus or minus capability is not available on the datalogger or recorder, the red lead should be connected to the positive input and the black lead to the negative input. If noise difficulties are encountered, consult LI-COR for special wiring instructions.

REFERENCES

1. Federer, C.A., and C.B. Tanner, 1965. A simple integrating pyranometer for measuring daily solar radiation. J. Geophys. Res. 70, 2301-2306.

2. Gates, D.M., 1965. Radiant energy, its receipt and disposal. Meteor. Monogr., 6, No. 28, 1-26.

3. Hull, J.N., 1954. Spectral distribution of radiation from sun and sky. Trans. Illum. Eng. Soc. (London), 19:21-28.

4. Kerr, J.P., G.W. Thurtell, and C.B. Tanner, 1967. An integrating pyranometer for climatological observer stations and mesoscale networks. Journal of Applied Meteorology, 6, 688-694.

LI-COR, inc. / LI-COR, Ltd.
P.O. Box 4425 / 4421 Superior Street
Lincoln, Nebraska 68504 USA

SENSOR TYPE LI-COR Pyranometer Sensor
SERIAL NUMBER Typical LI-COR Sensor
CALIBRATION DATE _____
PEAK ABSOLUTE SENSITIVITY _____ MICROAMP/WATT M^{-2} @_____NANOMETERS

Figure 6. LI-COR Pyranometer Sensor Spectral Response Curve

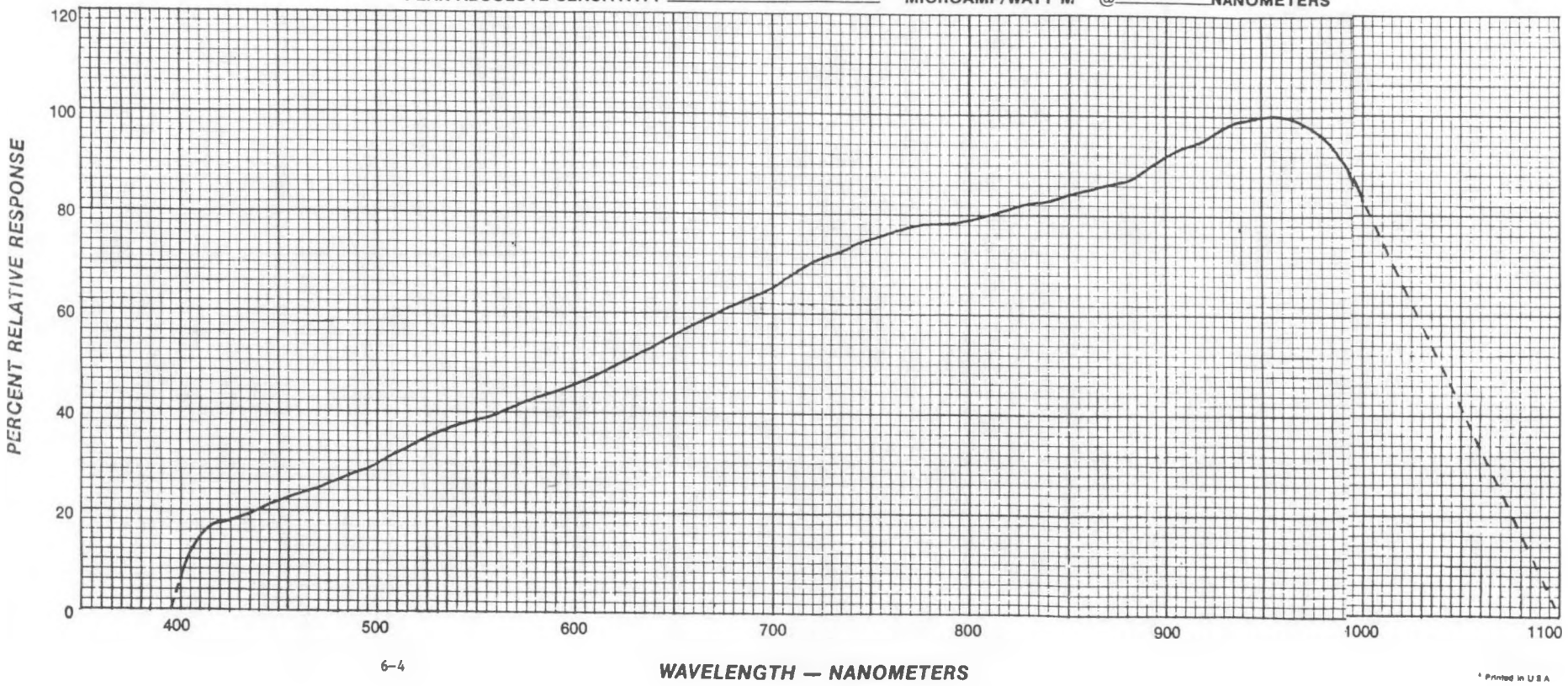

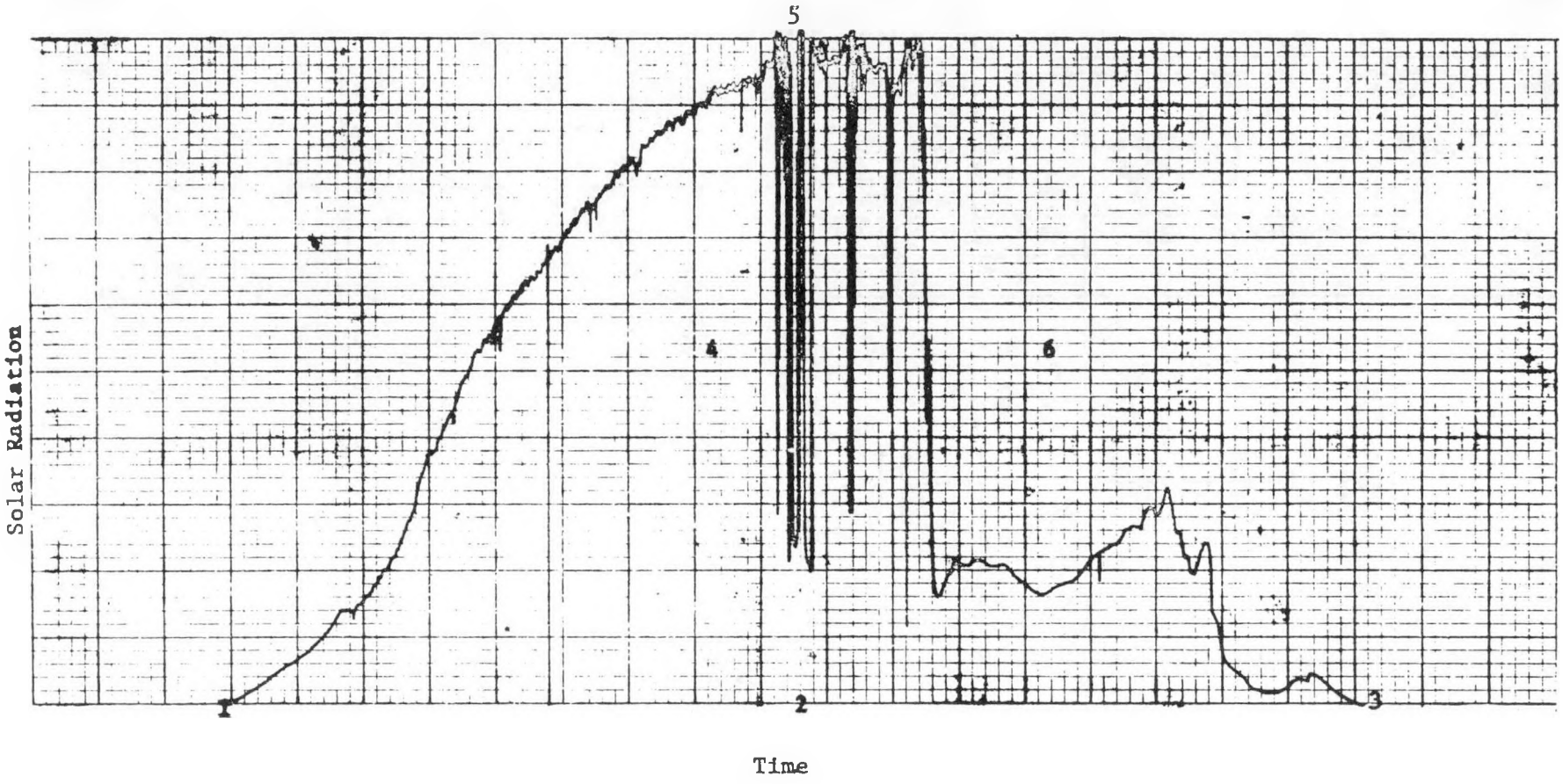

Strip Chart Recording of Instantaneous Solar Radiation recorded at LI-COR in May, 1980 using LI-200SB Pyranometer connected to LI-1776 Solar Monitor with output to strip chart recorder using 2228S Millivolt Recorder Leads.*

Point 1 is around sunrise, point 2 is solar noon, and point 3 is around sunset. The time span between 1 and 2 is ≃7 hours and ≃7 hours between 2 and 3. Before solar noon, the sky was clear, with relatively few variations in the expected smooth rising curve (4). Around solar noon, cloud cover caused variations in the radiation level, and lensing effects caused the level to rise to ≃1100 W m^{-2} (5). Later in the afternoon, a longer period of cloud cover (6) caused the radiation level to remain around 200 W m^{-2}.

The major divisions are 1 cm wide; chart speed was 1.2 cm/hr ; and the vertical axis is 100 W m^{-2}/cm.

*The LI-200SB can also be connected directly to a millivolt recorder by using the Millivolt Adapter.

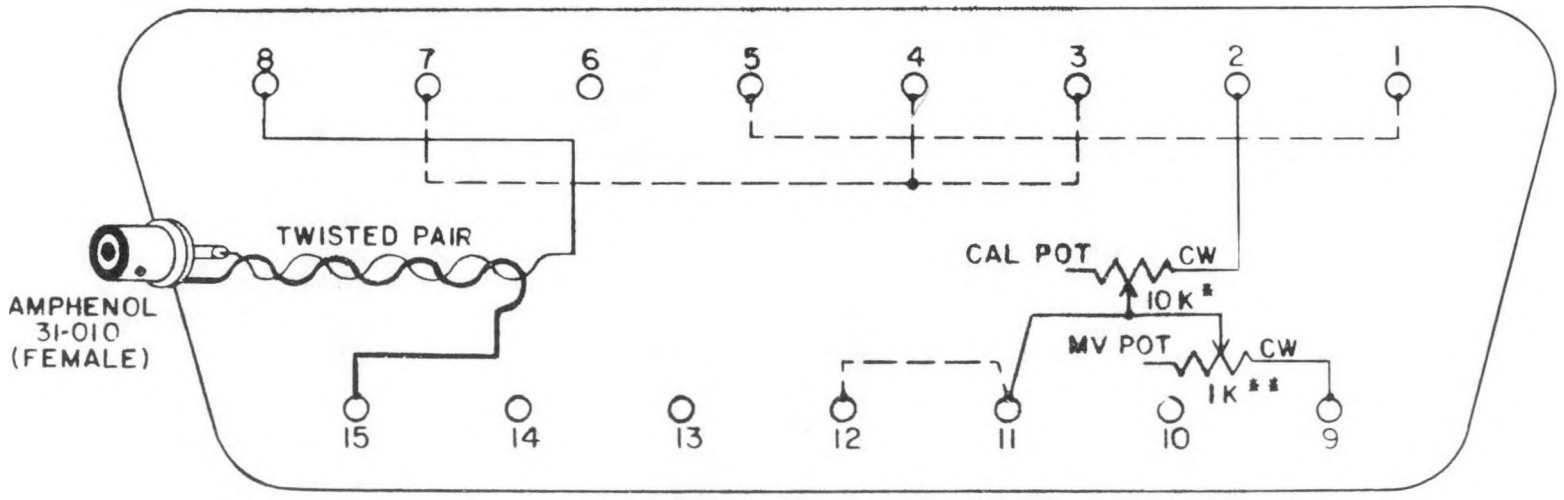

CONNECTOR: DA-15P

* 2K for LI-210SB

** 2K for LI-220SB
2K for LI-191SB

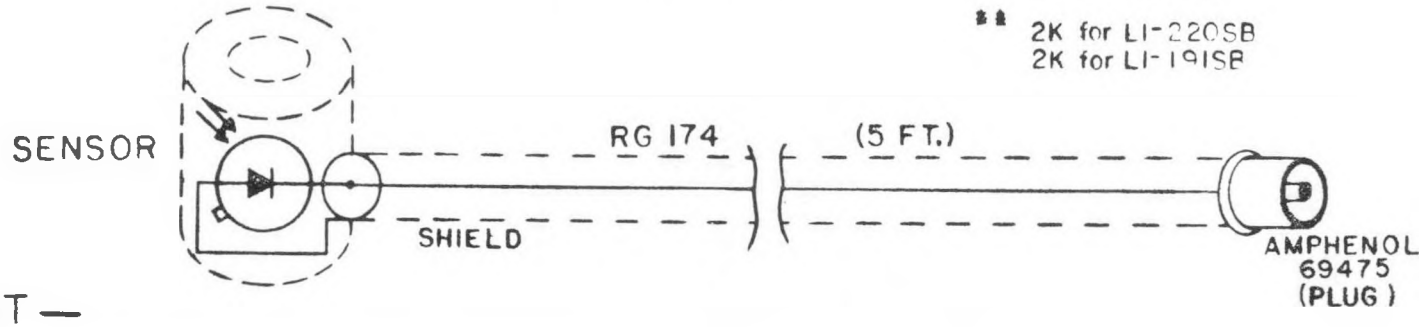

IMPORTANT —

THE FOLLOWING PINS ARE TO BE CONNECTED FOR EACH TYPE OF SENSOR
(LI-190SB & LI-191SB ARE ILLUSTRATED, BY DASHED LINES, AS AN EXAMPLE)

	LI-191SB LI-190SB	LI-220SB LI-200SB LI-190SEB	LI-210SB
CONNECT THESE PINS	1-5 3-4-7 11-12	1-4 3-5-7 11-13	1-3 4-5-7 11-13

REV #	DATE	BY	DESCRIPTION/REASON FOR CHANGE
1	8-1-80		

TOLERANCES UNLESS NOTED
FRACT. ± 1/64
X ± .015
XX ± .010
XXX ± .005
XXXX ± .0005
ANGLES ± 5°

LI-COR, Inc. / LI-COR, Ltd.
P.O. Box 4425 / 4421 Superior Street
Lincoln, Nebraska 68504 USA

SCALE N A	TITLE CALCONNECTOR & SENSOR	DRN BY DLG
DATE 6-13-80	DWG #	CKD. BY
	DO NOT SCALE	

TABLE I
CONVERSION FACTORS

1a. Photosynthetic Photon Flux Density (PPFD) (LI-190SB, LI-191SB, LI-192SB Quantum Sensors)

Photosynthetic Photon Flux Fluence Rate (PPFFR) (LI-193SB, LI-194SB Spherical Quantum Sensors.

UNITS (instantaneous):

$1\ \mu E\ s^{-1}\ m^{-2} \equiv 1.0\ \mu mol\ s^{-1}\ m^{-2}$
$\equiv 6.02 \cdot 10^{17}$ quanta $s^{-1}\ m^{-2}$
$\equiv 6.02 \cdot 10^{17}$ photon $s^{-1}\ m^{-2}$

Full Sunlight $\simeq$ 2000 $\mu E\ s^{-1}\ m^{-2}$ for the 400-700 nm waveband

1b. Photosynthetic Photon Exposure (LI-190SB, LI-191SB, LI-192SB, LI-193SB, LI-194SB)

UNITS (integrated):

$1\ \mu E\ s^{-1}\ m^{-2}\ h = 3600\ \mu E\ m^{-2}$
$= 3600\ \mu mol\ m^{-2}$
$= 2.17 \cdot 10^{21}$ quanta m^{-2}
$= 2.17 \cdot 10^{21}$ photon m^{-2}

One day's integration $\simeq$ 60 E m^{-2}

2a. Solar Irradiance (LI-200SB Pyranometer, LI-201SB Pyrheliometer)
Photosynthetic Irradiance (LI-190SEB, LI-192SEB Photosynthetic Irradiance sensors)
Near Infrared Irradiance (LI-220SB Near Infrared sensor)

UNITS (instantaneous):

$1\ W\ m^{-2} = 1.433 \cdot 10^{-3}$ cal $cm^{-2}\ min^{-1}$
$= 1.433 \cdot 10^{-3}$ langley min^{-1}
$= 0.100$ mW cm^{-2}
$= 1000$ erg $cm^{-2}\ s^{-1}$
$= 5.285 \cdot 10^{-3}$ BTU $ft^{-2}\ min^{-1}$
$= 0.317$ BTU $ft^{-2}\ h^{-1}$

Full Sunlight $\simeq$ 1000 W m^{-2} when using Pyranometer and Pyrheliometer sensors
$\simeq$ 500 W m^{-2} when using Photosynthetic Irradiance sensor
$\simeq$ 60 W m^{-2} when using Near Infrared Sensor

TABLE I (cont.)

2b. Energy Density (LI-200SB, LI-201SB)
Photosynthetic Energy Density (LI-190SEB, LI-192SEB)
Near Infrared Energy Density (LI-220SB)

UNITS (integrated):

1 Wh m^{-2}	=	0.0860 cal cm^{-2}
	=	0.0860 langley
	=	3600 joule m^{-2}
	=	$3.600 \cdot 10^{6}$ erg cm^{-2}
	=	0.317 BTU ft^{-2}

One day's integration ≃ 8000 Wh m^{-2} when using Pyranometer sensor (horizontal)
≃ 11,000 Wh m^{-2} when using normal incidence Pyrheliometer tracking the sun
≃ 4000 Wh m^{-2} when using Photosynthetic Irradiance sensor

≃ 500 Wh m^{-2} when using Near Infrared sensor

3a. Illumination (LI-210SB, LI-212SB Photometric sensors)

UNITS (instantaneous):

1 lux	=	1 lumen m^{-2}
	≒	0.0929 lumen ft^{-2}
	=	0.0929 footcandle
	=	$1.0 \cdot 10^{-4}$ photon
	=	0.001 klux

Full Sunlight ≃ 100 klux

3b. Luminous Exposure (LI-210SB, LI-212SB)

UNITS (integrated):

1 lux-h	=	3600 lux-s
	=	0.0929 footcandle-h
	=	0.001 klux-h

One day's integration ≃ 800 klux-h

The values shown for "Full Sun" and "One day's integration" are measurements taken in mid-summer in Lincoln, Nebraska. These values can vary greatly depending on location, time of year, and atmospheric conditions.

LI-COR Calconnector

Included as a part of all LI-COR radiation sensors is the *NEW Calconnector*, which provides the following Features:

- Direct Readout of "in air" measurements when any LI-COR terrestrial or underwater sensor is used with the LI-185B Quantum/Radiometer/Photometer, LI-188B Integrating Quantum/Radiometer/Photometer, and the LI-1776 Solar Monitor.
- Direct Readout of "in water" readings, including the immersion effect, when LI-COR Underwater sensors are used with the LI-185B or LI-188B.
- All LI-COR sensors can be used interchangeably with the LI-185B, LI-188B, or LI-1776 to provide direct readout, without calibrating the readout instrument to the sensor.

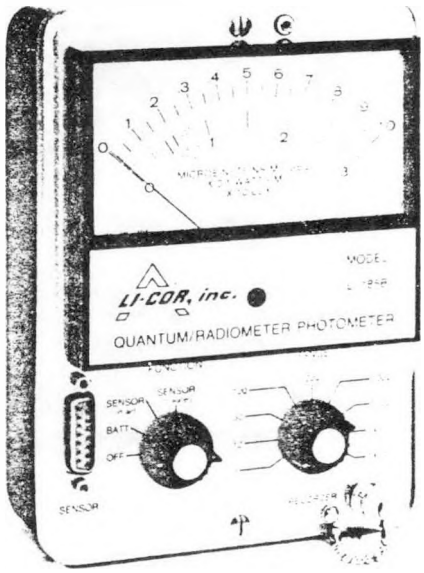

LI-185B Quantum/Radiometer/Photometer

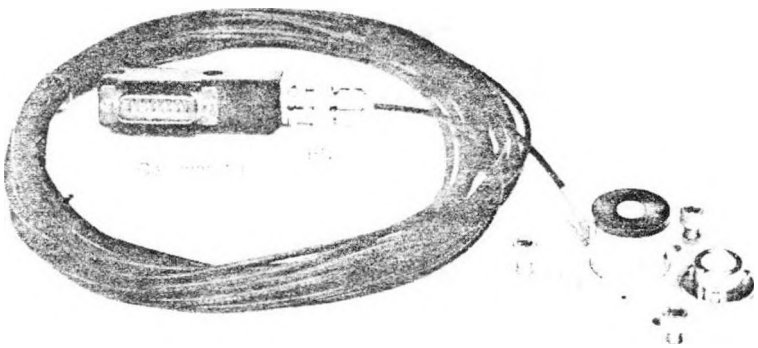

Shown above is a LI-COR terrestrial type sensor with the Calconnector attached to the end of the cable. For underwater sensors, a Calconnector is also included with each sensor, and underwater cable is ordered separately. The Calconnector included with each sensor is matched to that particular sensor.

Because of the Calconnector, several changes should be noted in Brochures RS1-279, RS2-279, RM1-779, RM2-279, and INT-579.

1. New model numbers reflecting this change are:
   Readout Instruments and Modules: LI-185B, LI-188B, LI-510B, LI-550B, 185MB, 900MB.

   Sensors: LI-190SB, LI-191SB, LI-192SB, LI-193SB; LI-190SEB, LI-192SEB; LI-200SB, LI-200SB-50; LI-210SB, LI-212SB; LI-220SB, LI-900STB.

   Cables and Leads: 2222SB, 2222UWB, 2224SB, 2225SB, 2226SB.

2. The LI-170, LI-500, 2190S, 2200S, 192DS, 2227S, LI-902ST, LI-191SE have been discontinued.

3. The SS-3 Sensor Selector replaces the 192DS deck-to-sea switch.

A special feature on the LI-185B and LI-188B Quantum/Radiometer/Photometers is the *"SENSOR (in air) – SENSOR (in water)" switch*. The "in air" position is used when LI-COR sensors are used in the atmosphere, and the "in water" position is used for underwater measurements using LI-COR underwater sensors.

To use a radiation sensor with either the LI-510B or LI-550B Integrators, the Calconnector is removed at the BNC termination, and the sensor is then connected to the integrator. For underwater sensors, the Calconnector is attached to the end of the 2222UWB Cable that is to be connected to the LI-185B or LI-188B. NOTE: Only sensors that have a Calconnector are compatible with the LI-185B, LI-188B, and LI-1776.

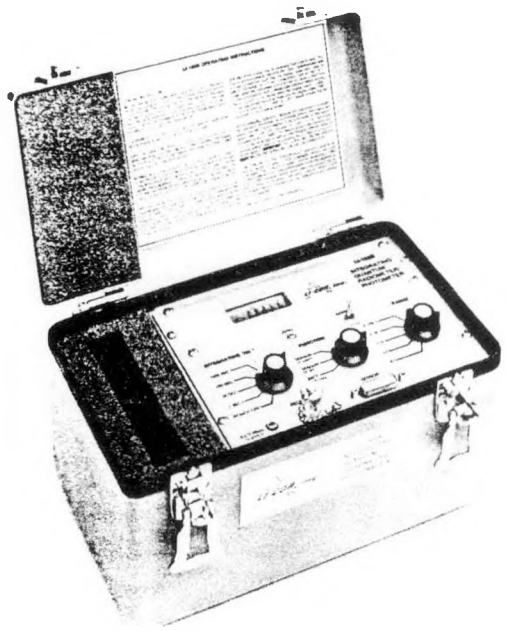

LI-188B Integrating Quantum/Radiometer/ Photometer.

The SS-3 Sensor Selector is used to compare instantaneous readings from up to three sensors, using either the LI-188B, LI-185B or LI-1776 as the readout instrument. The connection lead between the SS-3 and the readout instrument is included.

Included with each radiation sensor is a *Millivolt Adapter*. When connected to the Calconnector, the sensor will provide a millivolt output to a datalogger, strip chart recorder, or millivolt recorder. A standardized millivolt output is provided with all LI-COR terrestrial type sensors:

- 10.0 mV per 1000 Watts m^{-2} when using the LI-200SB Pyranometer, LI-190SEB Photosynthetic Irradiance Sensor.
- 5.0 mV per 1000 μE s^{-1} m^{-2} when using the LI-190SB or LI-191SB Quantum Sensors.
- 10.0 mV per 100 klux when using LI-210SB Photometric Sensor.

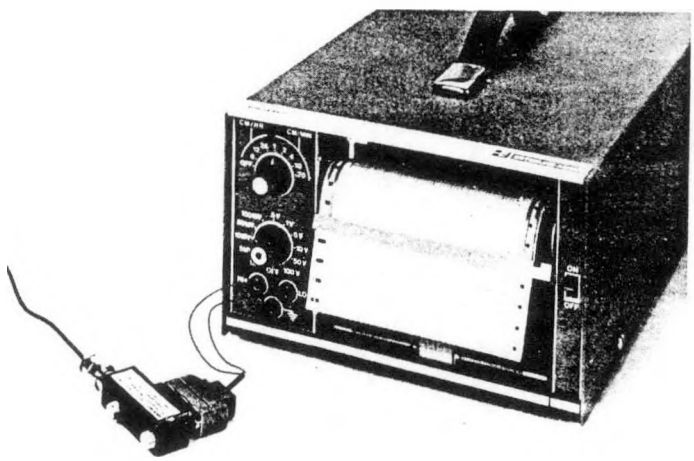

SPECIFICATIONS

LI-192SB UNDERWATER QUANTUM SENSOR

Absolute Calibration – ±5% in air traceable to N.B.S. Immersion effect data is included for underwater measurements.
Relative Error – Less than 5% under most conditions.
Sensitivity – Typically 5 microamp/1000 $\mu E\ s^{-1}m^{-2}$.*
Linearity – Maximum deviation of 1% up to 10 000 $\mu E\ s^{-1}m^{-2}$.
Stability – Less than 2% change over a 1 year period.
Response Time (10-90%) – 10 microseconds.
Temperature Dependence – ± .15%/degree C maximum.
Cosine Correction – Optimized for both underwater and atmospheric use.
Azimuth Error – Less than 1% over 360° at 45° elevation.
Sensor Case – Corrosion resistant metal for both seawater and freshwater applications. Waterproof to withstand 800 psi. Size 1¼" dia. x 1 13/16" height (3.18 x 4.62 cm). Three 6-32 mounting holes are tapped into the base.
Connector – Kintec HS2-2BPX.

*1 microeinstein (μE) = 6.02 X 10^{17} photons = 1 μmol
Daylight PPFD measured at solar noon is ≈ 2000 $\mu mol\ s^{-1}m^{-2}$ or 2000 $\mu E\ s^{-1}m^{-2}$. (3,5,7).

LI-190SB QUANTUM SENSOR

Absolute Calibration – ±5% traceable to N.B.S.
Relative Error – Less than 1% for plant canopies. Less than 5% for standard growth chamber lighting.
Sensitivity – Typically 5 microamp/1000 $\mu E\ s^{-1}m^{-2}$

Linearity – Maximum deviation of 1% up to 10 000 $\mu E\ s^{-1}m^{-2}$.
Stability – Less than 2% change over a 1 year period.
Response Time (10-90%) – 10 microseconds.
Temperature Dependence – ±.15%/degree C maximum.
Cosine Correction – Cosine corrected up to 80° angle of incidence.
Azimuth Error – Less than 1% over 360° at 45° elevation.
Sensor Case – Weatherproof anodized aluminum case with diffuser and stainless steel hardware. Size 15/16" dia. x 1.0" height (2.38 x 2.54 cm). 5 ft cable provided.

LI-200SB PYRANOMETER SENSOR

Calibration – Calibrated against an Eppley PSP Pyranometer under natural daylight clear conditions. Absolute accuracy under these conditions is ±5%.
Sensitivity – Typically 50 microamp/1000 watts m^{-2}

Linearity – Maximum deviation of 1% up to 3000 watts m^{-2}.
Stability – Less than 2% change over a 1 year period.
Response Time (10-90%) – 10 microseconds.
Temperature Dependence – ±.15%/degree C maximum.
Cosine Correction – Cosine corrected up to 80° angle of incidence.
Azimuth Error – less than 1% over 360° at 45° elevation.
Sensor Case – Weatherproof anodized aluminum case with diffuser and stainless steel hardware. Size 15/16" dia. x 1.0" height (2.38 x 2.54 cm). 5 ft cable provided.

Terms of Sale: *FOB Lincoln, Nebraska USA; net 30 days; workmanship and materials guaranteed one year. Prices and specifications subject to change without notice.*

LI-210SB PHOTOMETRIC SENSOR

Absolute Calibration – ±5% traceable to N.B.S. Sensors are calibrated to within 1% of each other.
Sensitivity – Typically 50 microamp/100 klux*

Linearity – Maximum deviation of 1% up to 100 klux.
Stability – Less than 2% change over a 1 year period.
Response Time (10-90%) – 10 microseconds.
Temperature Dependence – ±.15%/degree C maximum.
Cosine Correction – Cosine corrected up to 80° angle of incidence.
Azimuth Error – Less than 1% over 360° at 45° elevation.
Sensor Case – Weatherproof anodized aluminum case with diffuser and stainless steel hardware. Size 15/16" dia. x 1.0" height (2.38 x 2.54 cm). 5 ft cable provided.

LI-220SB NEAR INFRARED SENSOR

Specifications similar to other LI-COR atmospheric type sensors except:

Bandwith – 70 nm.
Center Wavelength – 780 nm.
Sensitivity – Typically 7 microamp/kw m^{-2} $micron^{-1}$.

LI-212SB UNDERWATER PHOTOMETRIC SENSOR

Specifications are similar to the LI-192S Underwater Quantum Sensor except as follows:
Sensitivity – 50 microamp/100 klux.*
Linearity – Maximum deviation of 1% up to 100 klux.

*10.764 lux = 1 footcandle.

REFERENCES

1. *Biggs, W. W., A. R. Edison, J. D. Eastin, K. W. Brown, J. W. Maranville and M. D. Clegg.* 1971. Photosynthesis light sensor and meter. Ecology 52:125-131.
2. *Federer, C. A. and C. B. Tanner.* 1966. Sensors for measuring light available for photosynthesis. Ecology 47:654-657.
3. *Incoll, L. D., S. P. Long and M. R. Ashmore.* 1977. SI units in publications in plant science. Commentaries in Plant Science (No. 28). Published in: Current Adv. Plant Science 9:331-343.
4. *Kerr, J. P., G. W. Thurtell and C. B. Tanner.* 1967. An integrating pyranometer for climatological observer stations and mesoscale networks. J. Appl. Meteorol. 6:688-694.
5. *McCree, K. J.* 1972. Test of current definitions of photosynthetically active radiation against leaf photosynthesis data. Agr. Meteorol.
6. *Rabinowitch, E. E.* 1951. Photosynthesis and related processes. Interscience, New York, N.Y. 2088 pages.
7. *Shibles, R.* 1976. Committee Report: Terminology pertaining to photosynthesis. Crop Sci. 16:437-439.

LI-COR, inc.

Instrumentation for biological and environmental sciences

4421 Superior Street / P.O. Box 4425 / Lincoln, Nebraska 68504 USA (402) **467-3576**

TWX: 910-621-8116

Dear Scientist,

We would like to take this opportunity to "enlighten" those involved with photosynthesis radiation measurement on the current state of "flux" concerning units and terminology, some often overlooked measurement errors, and some information on converting units. Also, we would like to inform you that we have changed our name from Lambda Instruments Corporation to LI-COR, inc. The change is in name only. All officers, stockholders and facilities remain the same.

UNITS AND TERMINOLOGY

There is disagreement concerning units and terminology used in radiation measurements in conjunction with the plant sciences. It will be LI-COR'S policy to adopt the recommendation of the international committees, such as the Commission Internationale de l'Eclairage (CIE), the International Bureau of Weights and Measures and the International Committee on Radiation Units.

UNITS

The einstein as a unit to designate Avogadro's number of photons is under controversy. It has been suggested that this quantity be expressed in units of moles (Incoll et al, 1977). The einstein has been used to represent both the quantity of radiant energy in Avogadro's number of photons and also Avogadro's number of photons. When the latter definition of einstein is used, the quantity of photons in a mole is equal to the quantity of photons in an einstein as shown in the equality: 1 einstein $\equiv$ 1 mole $\equiv$ 6.02×10^{23} photons

TERMINOLOGY

LI-COR is following the lead of the Crop Science Society of America, Committee on Terminology (Shibles, 1976) until international committees put forth recommendations. We have introduced the term PPFFR (Photosynthetic Photon Flux Fluence Rate). Oceanographers and limnologists have sometimes called this SCALAR QUANTUM IRRADIANCE. From our correspondence with the CIE, it seems more likely that the term photon flux fluence rate will be adopted.

.PAR (Photosynthetically Active Radiation) is defined as radiation in the 400 to 700 nm waveband. PAR is the general radiation term which covers both photon terms (preferred: McCree, 1972) and energy terms.

.PPFD (Photosynthetic Photon Flux Density) is defined as the photon flux density of PAR. This is the number of photons in the 400 to 700 nm waveband incident per unit time on a unit surface. The ideal PPFD sensor responds equally to all photons in the 400-700 nm waveband and has a cosine response. This physical quantity is measured by a cosine quantum sensor such as the LI-190S, LI-191S or LI-192S.
UNITS: 1μE $s^{-1}m^{-2}$ $\equiv$ 1μmol $s^{-1}m^{-2}$ $\equiv$ 6.02×10^{17} photons $s^{-1}m^{-2}$

.PPFFR (Photosynthetic Photon Flux Fluence Rate) is defined as the photon flux fluence rate of PAR. This is the integral of photon flux radiance at a point over all directions about the point. PPFFR is the same as PPFD for normal incident collimated radiation and it is 4 times that of PPFD in totally diffuse radiation. The ideal PPFFR sensor has a spherical collecting surface which exhibits the properties of a cosine receiver at every point on its surface and responds equally to all photons in the 400- 700 nm waveband. This physical quantity is measured by a spherical (4π collector) quantum sensor such as the LI-193S.
UNITS: 1μE $s^{-1}m^{-2}$ $\equiv$ 1μmol $s^{-1}m^{-2}$ $\equiv$ 6.02×10^{17} photons $s^{-1}m^{-2}$

.PI (Photosynthetic Irradiance) is defined as the radiant energy flux density of PAR. This is the radiant energy (400-700 nm) incident per unit time on a unit surface. The ideal PI sensor responds equally to energy in the 400-700 nm waveband and has a cosine response. This physical quantity is measured by a cosine PI sensor such as the LI-190SE, LI-191SE or LI-192SE.
UNITS: watts m^{-2}

MEASUREMENT ERRORS:

At a recent Controlled Environments Working Conference in Madison, Wisconsin, an official from NBS stated that one could not expect less than 10-25% error in radiation measurements made under non-ideal conditions. In order to shed some "light" on the subject, we have tabulated the sources of errors which the researcher must be aware of when making radiation measurements.

1) ABSOLUTE CALIBRATION ERROR:
Absolute calibration error depends on the source of the lamp standard and its estimated uncertainty at the time of calibration, accuracy of filament to sensor distance, alignment accuracy, stray light and the lamp current measurement accuracy. Where it is necessary to use a transfer sensor (such as for solar calibrations) additional error will be introduced. LI-COR quantum, photometric and PI sensors are calibrated against a working quartz halogen lamp (except for the line sensors). These working quartz halogen lamps have been calibrated against laboratory standards traceable to the NBS. Standard lamp current is metered to 0.035% accuracy. Microscope and laser alignment in the calibration setup reduce alignment errors to less than 0.1%. Stray light is reduced by black velvet to less than 0.1%. The absolute calibration accuracy is limited to the uncertainty of the NBS traceable standard lamp. The absolute calibration specification for LI-COR sensors is 5% traceable to the NBS. This accuracy is conservatively stated and the error is typically 3%. Absolute calibrations and spectral responses of LI-COR sensors have been checked by the National Research Council of Canada to insure accuracy and quality of LI-COR calibrations.

2) RELATIVE ERROR: (spectral response error)
This error is also called actinity error or spectral correction error. The error is due to the spectral response of the sensor not conforming to the ideal spectral response. This error occurs when measuring radiation from any source which is spectrally different than the calibration source.

The quantum, PI and photometric sensor spectral response conformity is checked by LI-COR with a monochromator with a 2.5 nm bandwidth and a blackened thermopile calibrated silicon photodiode. The spectral response of the sensor is achieved by the use of computer tailored filter glass. Relative errors for various sources due to a non-ideal spectral response are checked both by actual measurement and by a computer program which convolutes the source spectral irradiance with the sensor spectral response.

2.1 All LI-COR quantum and photometric sensors have relative errors <7% when used in growth chambers, daylight, greenhouses, plant canopies and aquatic conditions. When used with sources that have strong spectral lines such as gas lamps, or lasers, this error could be larger depending on the location of the lines.

2.2 The LI-COR pyranometer measures global radiation from sun plus sky. The LI-200S is not spectrally ideal (flat 280-2800 nm) and therefore should not be used except under natural, unobstructed daylight conditions. The LI-200S should not be used in spectrally different radiation such as in growth chambers and plant canopies. Under such artificial or shaded conditions, a thermopile type pyranometer should be used. NOAA states in a recent test report that for clear, unobstructed daylight conditions, the LI-200S compares favorably with first class thermopile type pyranometers. The cost of the LI-200S is 1/10 that of such thermopile pyranometers. See "Comparison of Solar

Radiation Sensors from Various Manufacturers" by Edwin Flowers, NOAA., Environmental Research Laboratories, Solar Radiation Facility, Boulder, CO.

3) SPATIAL ERROR
This error is caused by a sensor not responding according to its designed purpose to radiation at various incident angles.

3.1 COSINE ERROR
A sensor with a cosine response (follows Lambert's cosine law) allows measurement of flux densities through a given plane (flux densities per unit area). A sensor without an accurate cosine correction can give a severe error under diffuse radiation conditions within a plant canopy, at low solar elevation angles, under fluorescent lighting, etc.

Cosine response is measured by placing the sensor on a platform which can be adjusted to rotate the sensor about an axis placed across the center of the measuring surface. A collimated source is directed at normal incidence. The output of the sensor is measured as the angle of incidence is varied. The cosine error at angle θ is the percent difference of the ratio of the measured output at angle θ versus normal incidence (angle 0 deg.) as compared to the cosine of angle θ. This is repeated for various azimuth angles as necessary.

3.1.1 The LI-190S, the LI-190SE, the LI-200S, and the LI-210S are fully corrected cosine sensors. These sensors have a typical cosine error of less than 5% up to 80 deg. angle of incidence. Totally diffuse radiation introduces a cosine error of approximately 2.5%. For sun plus sky at sun elevation of 30 deg., the error is about 2%.

3.1.2 The LI-192S and the LI-212S sensors have a slightly greater error since these sensors have cosine errors optimized for both air and water.

3.1.3 The LI-191S and the LI-191SE sensors use uncorrected acrylic diffusers and have a greater error at high angles of incidence. For totally diffuse radiation, the error is about 8%. For conditions within canopies, the error is less.

3.2 SPHERICAL ANGLE ERROR
A spherical PPFFR sensor measures the total flux incident on its spherical surface divided by the cross-sectional area of the sphere. Spherical angle error is measured by directing a collimated source at normal incidence and rotating the sensor 360 deg. about an axis directly through the center of the sphere at 90 deg. from normal incidence. This is repeated for various azimuth angles as necessary to characterize the sensor.

3.2.1 The LI-193S spherical angle error is due to variations in density in the diffusion sphere and sphere area lost because of sensor base. This error is less than 10% for totally diffuse radiation, but is usually much less than 10% because the upwelling radiation is much smaller than downwelling.

3.3 AZIMUTH ERROR
This is a subcategory of both cosine and spherical angle error. We specify it separately at a particular angle of incidence. This error is the percent change of the sensor output as the sensor is rotated about the normal axis at a particular angle of incident radiation. This error is less than 1% at 45 deg. for the LI-190S, LI-190SE, LI-192S, LI-192SE, LI-200S, LI-210S and LI-212S sensors. The error is less than 3% for the LI-191S, LI-191SE and LI-193S sensors, (see brochures).

4) DISPLACEMENT ERROR
In highly turbid waters, the LI-193S spherical sensor will indicate high PPFFR values due to the displacement of water by the sensor sphere volume. This is because the point of measurement is taken to be at the center of the sphere but the attenuation which would have been provided by the water within the sphere is absent. This error is typically 5% for water with an attenuation coefficient of 3, (Combs, 1977).

5) TILT ERROR
Tilt error exists when a sensor is sensitive to orientation due to the effects of gravity. This exists primarily in thermopile type detectors. Silicon type detectors do not have this error. All LI-COR sensors are of the latter type and have no tilt error. This error in the LI-200S pyranometer is nonexistent and has an advantage over thermopile type detectors for solar insolation measurements. (Flowers, see para 2.2.)

6) LINEARITY ERROR
Linearity error exists when a sensor is not able to follow proportionate changes in radiation. The type of silicon detectors used in LI-COR sensors have a linearity error of less than 1% over seven decades of dynamic range.

7) FATIGUE ERROR
Fatigue error exists when a sensor exhibits hysteresis. This is common in selenium based illumination meters and can add a considerable error. For this reason, LI-COR sensors incorporate only silicon detectors which exhibit no fatigue error.

8) TEMPERATURE COEFFICIENT ERROR
Temperature coefficient error exists when the output of a sensor changes as the temperature changes with a constant input. This error is typically less than 0.1% per deg. C for the LI-190S, LI-190SE, LI-192S, LI-192SE, LI-193S, LI-210S and LI-212S sensors. This error is slightly higher for the LI-200S, (see brochures).

9) RESPONSE TIME ERROR
This error exists when the source being measured changes rapidly during the period of measurement.

.Averaging - Large errors can exist when measuring radiation under rapidly changing conditions such as changing cloud cover, wind, if measuring within a crop canopy and waves, if measuring underwater. The use of an integrating meter such as the LI-188 Integrating Quantum/Radiometer/Photometer to average the reading will eliminate this error.

. Instantaneous - When radiation measurements are desired over a period of time, much less than the response time of the system, large errors can exist. For example, if one were to measure the radiation from a pulsed source such as a gas discharge flash lamp with a typical system designed for environmental measurements, the reading would be meaningless. Such a measurement should not be made with our equipment without consultation with LI-COR.

10) LONG-TERM STABILITY ERROR
This error exists when the calibration of a sensor changes with time. This error is usually low for sensors using high qualtity silicon photovoltaic/photodiodes and glass filters (LI-COR uses only these high quality components). The use of Wratten filters and/or inexpensive silicon or selenium cells add significantly to long-term stability error. The stability error of LI-COR sensors is typically 2% per year. IMPORTANT: Customers should return their instruments to LI-COR for recalibration every two years.

11) IMMERSION EFFECT ERROR
A sensor with a diffuser for cosine correction will have an immersion effect when immersed in water. Radiation entering the diffuser scatters in all directions within the diffuser with more radiation lost through the water-diffuser interface than is the case when the sensor is in air. This is because the air-diffuser interface offers a greater ratio of indices of refraction than the water-diffuser interface. LI-COR provides a typical immersion effect correction factor for the LI-COR underwater sensors. Immersion effect error is the difference between this typical figure and the actual figure for a particular sensor in a particular environment. Since our test measurements are done in clear water, the error is also dependent on other variables such as salinity, turbidity, etc. Immersion effect error is typically 2% or less.

12) SURFACE VARIATION ERROR
In general, the absolute responsivity and the relative spectral responsivity are not constant over the radiation sensitive surface of sensors. This error has little effect in environmental measurements except for spatial averaging sensors (line sensors LI-191S and LI-191SE). This error is $\leq 7\%$ for the line sensor, (see brochures).

13) USER ERRORS

13.1 SPATIAL USER ERROR

This is different than sensor caused spatial error. Spatial user error can be introduced by using a single small sensor to characterize the radiation profile within a crop canopy or growth chamber. The flux density measured on a given plane can vary considerably due to shadows and sunflecks. To neglect this in measurements is to introduce errors of up to 1000%. Multiple sensors or sensors on track scanners can be used to minimize this error. If track scanners are used, the output of the sensors must be integrated with an instrument such as the LI-188 Integrating Quantum/Radiometer/Photometer. The LI-191S Line Sensor which spatially averages radiation over its one meter length minimizes the error and allows one person to easily make many measurements in a short period of time. Another method, although not as accurate, is the use of the LI-188 integrating meter and the LI-190S Quantum Sensor and physically scanning the sensor by hand within the canopy while integrating the output with the LI-188.

Another type of spatial user error can be caused by misapplication of a cosine corrected sensor where a spherical sensor would give a more accurate measurement. An example is in underwater photosynthesis radiation measurements when studying phytoplankton.

13.2 USER SET-UP/APPLICATION ERRORS

These errors include such causes as:

.Reflections or obstructions from clothing, buildings, boats, etc.
.Dust, fly specs, sea weeds, bird droppings.
.Shock causing permanent damage of optics within the sensor.
.Submersion of terrestrial sensors in water for an extended period (partial or total) - Rain is OK.
.Using sensors with serial numbers other than the one for which the meter was calibrated and not making the necessary correction.
.Incorrect interpolation of analog meters.
.Using the wrong meter function.
.Failure to have sensors recalibrated periodically.

14) READOUT ERROR

This error is due to the readout instrument as distinguished from the sensor. Zero drift, temperature, battery voltage, electronic stability, line voltage, humidity and shock are all factors which can contribute to readout error. The use of electronic circuitry, such as chopper stabalized amplifiers and voltage regulators largely eliminates in the LI-188 and the LI-185A Quantum/Radiometer/Photometer many of these problems: zero drift, temperature, battery voltage, electronic stability, line voltage. Below is a summary of readout error for LI-COR instruments over the temperature range 0-50 degrees C.

LI-170	meter	2% full scale *
LI-185A	meter	1% full scale *
LI-188	meter	1% full scale
LI-500	integrator	3% full scale
LI-510	integrator	2% full scale
LI-550	integrator	2% full scale

* Additional error is caused by non-linearity of the analog meter movements. It can add as much as 1.5% of the full scale reading to points less than full scale. Therefore, always use the most sensitive range possible.

15) TOTAL ERROR

The errors given are largely independent of each other and are random in polarity and magnitude. Therefore, they can be summed in quadrature (the square root of the sum of the squares). The total error is shown below for an LI-190S Quantum Sensor and LI-188 Integrating Quantum/Radiometer/Photometer when used for measuring lighting in a typical growth chamber or natural daylight over a temperature range of 15-35 deg. C.

	Typical
ABSOLUTE ERROR	5% max., 3% typ.
RELATIVE (SPECTRAL RESPONSE) ERROR	5%
SPATIAL (COSINE) ERROR	2%
DISPLACEMENT ERROR	0%
TILT ERROR	0%
LINEARITY ERROR	0% nil
FATIGUE ERROR	0%
TEMPERATURE COEFFICIENT ERROR, SENSOR	1% (0.1%/deg C)
RESPONSE TIME ERROR	0%
LONG-TERM STABILITY ERROR	2% (2%/year)
IMMERSION EFFECT ERROR	0%
SURFACE VARIATION ERROR	0%
USER ERROR	(0-1000%)
READOUT ERROR	1%

Total error = SQRT(5X5+5X5+2X2+1X1+2X2+1X1) = 7.6%
All the above errors are minimized by LI-COR through design and calibration. While the above error seems reasonably low, it must be remembered that we have added no user error and that statistically it is possible that all the errors could be of the same polarity. The sum of the errors (less user) could equal 16% worst case. The absolute error is conservatively stated and is more typically 3%. User error in vegatation canopies where shadows and sunflecks exist can be very large (1000%) and one of the methods described under SPATIAL USER ERRORS, paragraph 13.1, should be employed.

When purchasing a radiation measuring system, it is necessary to insure that the spatial (cosine, etc.) and relative (spectral response) errors are as low as possible. These two errors depend upon the skill and expertise of the designer and manufacturer. Some manufacturers deliberately do not give specifications for these errors and the user can expect large errors. The absolute error is largely dependent on the NBS lamp standards and minimization of this error can be achieved by the more experienced companies through the use of precise techniques and expensive capital equipment. In order to insure long-term stability, it is necessary that the manufacturer use the highest quality silicon photovoltaic/photodiodes and only the best glass filters. Electronic readout instruments are available that virtually eliminate readout error (such as the LI-188).

The user should be aware of all the types of errors that can occur and particularly the relative and spatial errors since these can add considerably to the total error. LI-COR has and continues to put forth a considerable effort to insure that the spectral and cosine response of our quantum, photometric and PI sensors are as nearly ideal as optically possible. This assures LI-COR customers of the best possible accuracy.

CONVERSION OF UNITS

CONVERSION OF PHOTON UNITS TO RADIOMETRIC UNITS

Conversion of quantum sensor output in $\mu E\ s^{-1}m^{-2}$, 400-700 nm, to radiometric units in watts m^{-2}, 400-700 nm, is complicated. The conversion factor will be different for each light source, and the spectral distribution curve of the radiant output of the source (W_λ, in watts $m^{-2}\ nm^{-1}$) must be known in order to make the conversion. The accurate measurement of W_λ is a difficult task, which should not be attempted without adequate equipment and calibration facilities. The radiometric quantity desired is the integral of W_λ over the 400-700 nm range, or:

$$W_T = \int_{400}^{700} W_\lambda \, d\lambda. \qquad \text{Eq. 1}$$

At a given wavelength (λ) the number of photons/sec is $W_\lambda/(hc/\lambda)$ where hc/λ is the energy of one photon. The total number of photons per second in the 400-700 nm range is:

$$\int_{400}^{700} W_\lambda \,/\, (hc/\lambda) \, d\lambda.$$

This is the integral which is measured by the sensor. If 'R' is the reading of the quantum sensor in $\mu E\ s^{-1}m^{-2}$ which is equal to: 6.02×10^{17} photons $s^{-1}m^{-2}$, then:

$$6.02 \times 10^{17}\ R = \int_{400}^{700} W_\lambda/(hc/\lambda) \ d\lambda. \qquad \text{Eq. 2}$$

Combining Eq. 1 and Eq. 2, one gets:

$$W_T = 6.02 \times 10^{17}\ Rhc \ \frac{\int_{400}^{700} W_\lambda \, d\lambda}{\int_{400}^{700} \lambda W_\lambda \, d\lambda}. \qquad \text{Eq. 3}$$

To achieve the two integrals, discrete summations are necessary. Also, since W_λ appears in both numerator and denominator, the normalized curve N_λ may be substituted for it. Then:

$$W_T = 6.02 \times 10^{17} \text{ Rhc} \frac{\sum_i N_{\lambda_i} \Delta\lambda}{\sum_i \lambda_i N_{\lambda_i} \Delta\lambda}, \qquad \text{Eq. 4}$$

where $\Delta\lambda$ is any desired wavelength interval, λ_i is the center wavelength of the interval and $N_{\lambda i}$ is the normalized radiant output of the source at the center wavelength. In final form this becomes:

$$W_T = 119.6R \frac{\sum_i N_{\lambda_i}}{\sum_i \lambda_i N_{\lambda_i}} \text{ watts m}^{-2} \qquad \text{Eq. 5}$$

where 'R' is the reading in $\mu E\ s^{-1}m^{-2}$, h = 6.63×10^{-34} joule-sec, c = 3.00×10^8 m s^{-1}, and λ is in nm.

The following procedure should be used in conjunction with the above formula:

1) Divide the 400-700 nm range in 'i' intervals of equal wavelength spacing $\Delta\lambda$.

2) Determine the center wavelength (λ_i) of each interval.

3) Determine the normalized radiant output of the source (N_{λ_i}) at each of the center wavelengths.

4) Sum the normalized radiant outputs as determined in step three to find $\sum_i N_{\lambda_i}$.

5) Multiply the center wavelength by the normalized radiant output at that wavelength for each interval.

6) Sum the products determined in step five to find $\sum_i \lambda_i N_{\lambda_i}$.

7) Use Equation 5 to find W_T in watts m^{-2} where 'R' is the quantum sensor output in $\mu E\ s^{-1}m^{-2}$.

The following approximation assumes a flat spectral distribution curve of the source over the 400-700 nm range.

i = 1
$\Delta\lambda$ = 300 nm
λ_i = 550 nm

$$W_T = 119.6\ R \frac{N(550)}{550 \times N(550)} = \frac{119.6R}{550} = 0.22R \text{ watts m}^{-2}$$

or:

1 watt m^{-2} = 4.6 $\mu E\ s^{-1}m^{-2}$.

This conversion factor is within ± 8.5% of the factors determined by McCree (1972), for the following sources:

SOURCE	$\mu E\ s^{-1}m^{-2}$ per watts m^{-2}
Sun + Sky	4.57
Blue Sky	4.24
Lucalox	4.98
Metalarc	4.59
Mercury	4.74
WW Fluorescent	4.67
CW Fluorescent	4.59
GL Fluorescent	4.69
Quartz-Iodine	5.02

CONVERSION OF PHOTON UNITS TO PHOTOMETRIC UNITS

To convert photon units ($\mu E\ s^{-1}\ m^{-2}$, 400-700 nm) to photometric units (lux, 400-700 nm), use the above procedure except:

Replace Eq. 1 with:

$$\text{Lux} = 683 \int_{400}^{700} y_\lambda W_\lambda\, d\lambda$$

where W_λ is the spectral irradiance (watts m^{-2} nm^{-1}) and y_λ is the luminosity coefficient of the standard C.I.E. curve with y_λ = 1 at 550 nm.

b) Replace Eq. 3 with:

$$\text{Lux} = (683)(6.02 \times 10^{17}\ \text{Rhc}) \frac{\int_{400}^{700} y_\lambda W_\lambda\, d\lambda}{\int_{400}^{700} \lambda W_\lambda\, d\lambda}$$

c) Replace Eq. 4 with:

$$\text{Lux} = (683)(6.02 \times 10^{17}\text{Rhc}) \frac{\sum_i y_{\lambda_i} N_{\lambda_i} \Delta\lambda}{\sum_i \lambda_i N_{\lambda_i} \Delta\lambda}$$

d) Replace Eq. 5 with:

$$\text{Lux} = 8.17 \times 10^4\ R \frac{\sum_i y_{\lambda_i} N_{\lambda_i}}{\sum_i \lambda N_{\lambda_i}}$$

e) Replace Step 4 with:

4a) Multiply the luminosity coefficient ($y\lambda$) of the center wavelength by the normalized radiant output (N_λ) at that wavelength for each interval.

4b) Sum the products determined in Step 4a to find $\sum_i y_{\lambda_i} N_{\lambda_i}$

The following approximation assumes a flat spectral irradiance curve of the source over the 400-700 nm range.

i = 1-31
$\Delta\lambda$ = 10 nm
λ_1 = 400, λ_2 = 410, λ_3 = 420..... λ_{31} = 700
N_λ = 1 for all wavelengths
y_{λ_1} = .0004 y_{λ_2} = .0012 y_{λ_3} = .004 ..... $y_{\lambda_{31}}$ = .0041

$$\text{Lux} = 8.17 \times 10^4\ R \frac{\sum_i y_{\lambda_i}}{\sum_i \lambda_i} = 8.17 \times 10^4\ R \frac{(10.682)}{17050}$$

Lux = 51.2 R where R is in $\mu E\ s^{-1}m^{-2}$

or:

1000 lux = 1Klux = 19.53 $\mu E\ s^{-1}m^{-2}$

Your comments on the subjects addressed in this letter or any other measurement problems are always welcome and will be treated as valuable inputs.

REFERENCES

Combs, W.S., Jr. 1977. The measurement and prediction of irradiances available for photosynthesis by phytoplankton in lakes. University of Minnesota Ph.D. Thesis, Limnology.

Incoll, L.D., S.P. Long and M.R. Ashmore. 1977. SI units in publications in plant science. Commentaries in Plant Science (No. 28). Published in: Current Adv. Plant Science 9: 331-343.

McCree, K.J., 1972. Test of current definitions of photosynthetically active radiation against leaf photosynthesis data. Agric. Meteorol. 10: 443-453.

Shibles, R. 1976. Committee Report: Terminology pertaining to photosynthesis. Crop Sci. 16: 437-439.

LI-COR, inc./Ltd.
Martin Hansen
Martin C. Hansen
Director of Marketing

LI-COR, inc./Ltd.
W. W Biggs
William W. Biggs
President

Appendix C

Pyrgeometer Adjustment

Standardization of Eppley Radiometer (Pyrgeometer)

Pyrgeometer Adjustment
(for battery output changes)

1. Remove Pyrgeometer from roof and place it in the data building.

2. Attach spare plug and leads (located in drawer marked "Pyrgeometer Leads").

3. Read resistance of thermistor in temperature compensation circuit. Use Simpson Ohmmeter across brown and yellow leads.

4. Allow Pyrgeometer temperature to stabilize ~ one hour. Check thermistor resistance periodically to assure stabilization.

5. Convert resistance to temperature, using attached table or table in Pyrgeometer literature. (YSI 44031)

6. Convert temperature from ^{o}C to ^{o}K ($^{o}K = {}^{o}C + 273$).

7. Attach the blue and green leads to connector #138 on the instrument board, which measures millivolts when ØTM 001 is called for (Press K3 - ØTM 001 - end line, when HP 85 is not reading other sensors).

8. Read the millivolts across the blue/green leads (mv).

9. Use the equation

$$mv = T^4(^{o}k^4) * 8.124 * 10^{11} \frac{cal}{cm^2 \text{ min } K^4} \times 2.66 \frac{mv}{\frac{cal}{cm^2 \text{ min}}}$$

T: Temp from step #6

2.66: Calibration factor from Eppley calibration document, valid until April, 1983

$$= T^4 * 21.61 * 10^{11}$$

to balance the mv reading and the temperature side of the equation.

To adjust the pyrgeometer to equalize the above equation,

a. Remove the bottom plate.

b. Adjust the potentiometer until the millivolt reading (step 8) equals the right side of the equation.

c. Recheck the thermistor temperature to be certain it hasn't changed, and the right side of the equation hasn't changed.

YSI Thermistor Resistance Versus Temperature

PART NO.	44001	44002	44003	44004 / 44033	44005 / 44030	44007 / 44034	44006 / 44031	44008 / 44032	44011	44014	44015
Ω @ 25°C	100	300	1000	2252	3000	5000	10,000	30,000	100,000	300,000	1 MEG.
BODY	BLACK	BLACK	BLACK	BLACK / ORANGE	BLACK / ORANGE	BLACK / ORANGE	BLACK / ORANGE	BLACK / ORANGE	BROWN	BROWN	BROWN
END	BROWN	RED	ORANGE	YELLOW / ORANGE	GREEN / BLACK	VIOLET / YELLOW	BLUE / BROWN	GRAY / RED	BROWN	YELLOW	GREEN
TEMP. °C	RESISTANCE Ω										
−80	11.73K	53.50K	229.0K	1660K	2211K	3685K	3558K				
79	10.97K	49.93K	213.1K	1518K	2022K	3371K	3296K				
78	10.30K	46.62K	198.5K	1390K	1851K	3086K	3055K				
77	9656	43.55K	184.9K	1273K	1696K	2827K	2833K				
76	9061	40.70K	172.4K	1167K	1555K	2592K	2629K				
75	8506	38.06K	160.8K	1071K	1426K	2378K	2440K				
74	7990	35.61K	150.0K	982.8K	1309K	2182K	2266K				
73	7509	33.33K	140.0K	902.7K	1202K	2005K	2106K				
72	7060	31.22K	130.8K	829.7K	1105K	1843K	1957K				
71	6642	29.25K	122.2K	763.1K	1016K	1695K	1821K				
−70	6251	27.42K	114.3K	702.3K	935.4K	1560K	1694K				
69	5886	25.71K	106.9K	646.7K	861.4K	1436K	1577K				
68	5545	24.12K	100.0K	595.9K	793.7K	1323K	1469K				
67	5227	22.65K	93.63K	549.4K	731.8K	1220K	1369K				
66	4929	21.27K	87.70K	506.9K	675.2K	1126K	1276K				
65	4650	19.98K	82.18K	467.9K	623.3K	1039K	1190K				
64	4389	18.78K	77.04K	432.2K	575.7K	959.9K	1111K				
63	4144	17.66K	72.25K	399.5K	532.1K	887.2K	1037K				
62	3915	16.62K	67.80K	369.4K	492.1K	820.5K	968.4K				
61	3700	15.64K	63.64K	341.8K	455.3K	759.2K	904.9K				
−60	3499	14.73K	59.77K	316.5K	421.5K	702.9K	845.9K				
59	3310	13.88K	56.16K	293.2K	390.5K	651.1K	791.1K				
58	3132	13.08K	52.78K	271.7K	361.9K	603.5K	740.2K				
57	2965	12.33K	49.63K	252.0K	335.7K	559.7K	692.8K				
56	2809	11.63K	46.69K	233.8K	311.5K	519.4K	648.8K				
55	2661	10.98K	43.94K	217.1K	289.2K	482.2K	607.8K				
54	2523	10.36K	41.37K	201.7K	268.6K	447.9K	569.6K				
53	2392	9785	38.97K	187.4K	249.7K	416.3K	534.1K				
52	2270	9245	36.72K	174.3K	232.2K	387.1K	501.0K				
51	2154	8738	34.62K	162.2K	216.0K	360.2K	470.1K				
−50	2045	8262	32.64K	151.0K	201.1K	335.3K	441.3K				
49	1942	7815	30.80K	140.6K	187.3K	312.3K	414.5K				
48	1846	7395	29.06K	131.0K	174.5K	291.0K	389.4K				
47	1754	7000	27.44K	122.1K	162.7K	271.3K	366.0K				
46	1668	6629	25.92K	113.9K	151.7K	253.0K	344.1K				
45	1587	6280	24.49K	106.3K	141.6K	236.2K	323.7K				
44	1510	5951	23.15K	99.26K	132.2K	220.5K	304.6K				
43	1438	5642	21.89K	92.72K	123.5K	205.9K	286.7K				
42	1369	5351	20.70K	86.65K	115.4K	192.5K	270.0K				
41	1304	5076	19.59K	81.02K	107.9K	180.0K	254.4K				
−40	1243	4818	18.55K	75.79K	101.0K	168.3K	239.8K	884.6K	3356K		
39	1185	4574	17.56K	70.93K	94.48K	157.5K	226.0K	830.9K	3147K		
38	1130	4344	16.64K	66.41K	88.46K	147.5K	213.2K	780.8K	2951K		
37	1078	4127	15.77K	62.21K	82.87K	138.2K	201.1K	733.9K	2769K		
36	1029	3922	14.94K	58.30K	77.66K	129.5K	189.8K	690.2K	2599K		
35	981.8	3729	14.17K	54.66K	72.81K	121.4K	179.2K	649.3K	2440K		
34	937.6	3546	13.44K	51.27K	68.30K	113.9K	169.3K	611.0K	2292K		
33	895.6	3374	12.76K	48.11K	64.09K	106.9K	160.0K	575.2K	2154K		
32	855.8	3211	12.11K	45.17K	60.17K	100.3K	151.2K	541.7K	2025K		
31	818.0	3057	11.50K	42.42K	56.51K	94.22K	143.0K	510.4K	1904K		
−30	782.1	2911	10.92K	39.86K	53.10K	88.53K	135.2K	481.0K	1791K		
29	748.1	2773	10.38K	37.47K	49.91K	83.22K	127.9K	453.5K	1685K		
28	715.7	2642	9866	35.24K	46.94K	78.26K	121.1K	427.7K	1586K		
27	685.0	2519	9381	33.15K	44.16K	73.62K	114.6K	403.5K	1494K		
26	655.7	2402	8922	31.20K	41.56K	69.29K	108.6K	380.9K	1407K		
25	627.9	2291	8489	29.38K	39.13K	65.24K	102.9K	359.6K	1326K		
24	601.5	2185	8079	27.67K	36.86K	61.45K	97.49K	339.6K	1250K		
23	576.4	2086	7692	26.07K	34.73K	57.90K	92.43K	320.9K	1178K		
22	552.4	1991	7325	24.58K	32.74K	54.58K	87.66K	303.3K	1111K		
21	529.6	1901	6978	23.18K	30.87K	51.47K	83.16K	286.7K	1049K		
−20	507.9	1816	6649	21.87K	29.13K	48.56K	78.91K	271.2K	989.8K		
19	487.3	1736	6338	20.64K	27.49K	45.83K	74.91K	256.5K	934.6K		
18	467.6	1659	6043	19.48K	25.95K	43.27K	71.13K	242.8K	882.7K		
17	448.8	1586	5764	18.40K	24.51K	40.86K	67.57K	229.8K	834.0K		
16	430.9	1517	5499	17.39K	23.16K	38.61K	64.20K	217.6K	788.2K		
15	413.8	1451	5248	16.43K	21.89K	36.49K	61.02K	206.2K	745.2K		
14	397.5	1388	5009	15.54K	20.70K	34.50K	58.01K	195.4K	704.7K		
13	382.0	1329	4783	14.70K	19.58K	32.63K	55.17K	185.2K	666.7K		
12	367.1	1272	4569	13.91K	18.52K	30.88K	52.48K	175.6K	630.9K		
11	352.9	1218	4365	13.16K	17.53K	29.23K	49.94K	166.6K	597.2K		
−10	339.4	1167	4172	12.46K	16.60K	27.67K	47.54K	158.0K	565.5K		
9	326.5	1118	3988	11.81K	15.72K	26.21K	45.27K	150.0K	535.6K		
8	314.1	1072	3813	11.19K	14.90K	24.83K	43.11K	142.4K	507.5K		
7	302.3	1028	3647	10.60K	14.12K	23.54K	41.07K	135.2K	481.0K		
6	291.0	985.5	3489	10.05K	13.39K	22.32K	39.14K	128.5K	456.0K		
5	280.2	945.3	3339	9534	12.70K	21.17K	37.31K	122.1K	432.4K		
4	269.8	907.0	3196	9046	12.05K	20.08K	35.57K	116.0K	410.2K		
3	259.9	870.4	3061	8586	11.44K	19.06K	33.93K	110.3K	389.2K		
2	250.5	835.5	2931	8151	10.86K	18.10K	32.37K	104.9K	369.4K		
−1	241.4	802.3	2808	7741	10.31K	17.19K	30.89K	99.80K	350.7K		
0	232.7	770.5	2691	7355	9796	16.33K	29.49K	94.98K	333.1K	1088K	3966K
+1	224.4	739.9	2579	6989	9310	15.52K	28.15K	90.41K	316.4K	1030K	3740K
2	216.4	710.7	2472	6644	8851	14.75K	26.89K	86.09K	300.6K	975.3K	3529K
3	208.7	682.8	2370	6319	8417	14.03K	25.69K	81.99K	285.7K	923.8K	3330K
4	201.4	656.2	2273	6011	8006	13.34K	24.55K	78.11K	271.6K	875.2K	3144K
5	194.3	630.8	2181	5719	7618	12.70K	23.46K	74.44K	258.3K	829.5K	2969K
6	187.6	606.4	2093	5444	7252	12.09K	22.43K	70.96K	245.7K	786.3K	2804K
7	181.1	583.2	2009	5183	6905	11.51K	21.45K	67.66K	233.8K	745.6K	2649K
8	174.9	561.0	1928	4937	6576	10.96K	20.52K	64.53K	222.5K	707.2K	2504K
9	169.0	539.8	1852	4703	6265	10.44K	19.63K	61.56K	211.9K	671.0K	2367K
+10	163.3	519.4	1779	4482	5971	9951	18.79K	58.75K	201.7K	636.8K	2238K
11	157.8	500.0	1709	4273	5692	9486	17.98K	56.07K	192.2K	604.5K	2117K
12	157.5	481.4	1642	4074	5427	9046	17.22K	53.54K	183.1K	574.0K	2003K
13	147.4	463.6	1578	3886	5177	8628	16.49K	51.13K	174.5K	545.2K	1896K
14	142.6	446.6	1518	3708	4939	8232	15.79K	48.84K	166.3K	518.0K	1795K
15	137.9	430.2	1459	3539	4714	7857	15.13K	46.67K	158.6K	492.3K	1700K
16	133.4	414.6	1404	3378	4500	7500	14.50K	44.60K	151.3K	468.0K	1610K
17	129.1	399.6	1351	3226	4297	7162	13.90K	42.64K	144.3K	444.9K	1525K
18	125.0	385.3	1300	3081	4105	6841	13.33K	40.77K	137.7K	423.2K	1446K
19	121.0	371.5	1251	2944	3922	6536	12.79K	38.99K	131.4K	402.6K	1370K
+20	117.1	358.3	1204	2814	3748	6247	12.26K	37.30K	125.5K	383.1K	1299K
21	113.4	345.6	1160	2690	3583	5972	11.77K	35.70K	119.8K	364.6K	1232K
22	109.9	333.5	1117	2572	3426	5710	11.29K	34.17K	114.5K	347.1K	1169K
23	106.4	321.9	1076	2460	3277	5462	10.84K	32.71K	109.4K	330.6K	1110K
24	103.1	310.7	1037	2354	3135	5225	10.41K	31.32K	104.5K	314.9K	1053K
25	100.0	300.0	1000	2252	3000	5000	10.00K	30.00K	100.0K	300.0K	1000K
26	96.9	289.7	963.4	2156	2872	4787	9605	28.74K	95.51K	285.9K	949.7K
27	94.0	279.8	928.9	2064	2750	4583	9227	27.54K	91.34K	272.5K	902.2K
28	91.1	270.3	895.9	1977	2633	4389	8867	26.40K	87.38K	259.8K	857.2K
29	88.4	261.1	864.1	1894	2523	4204	8523	25.31K	83.60K	247.8K	814.7K
+30	85.7	252.4	833.7	1815	2417	4029	8194	24.27K	80.00K	236.4K	774.5K
31	83.2	244.0	804.5	1739	2317	3861	7880	23.28K	76.58K	225.6K	736.5K
32	80.7	235.9	776.5	1667	2221	3702	7579	22.33K	73.32K	215.3K	700.5K
33	78.4	228.1	749.6	1599	2130	3549	7291	21.43K	70.22K	205.5K	666.4K
34	76.1	220.6	723.8	1533	2042	3404	7016	20.57K	67.26K	196.2K	634.1K
35	73.9	213.4	699.0	1471	1959	3766	6752	19.74K	64.44K	187.4K	603.6K
36	71.7	206.5	675.2	1412	1880	3134	6500	18.96K	61.75K	179.0K	574.6K
37	69.7	199.8	652.4	1355	1805	3008	6258	18.21K	59.19K	171.0K	547.2K
38	67.7	193.4	630.4	1301	1733	2888	6026	17.49K	56.75K	163.5K	521.2K
+39	65.8	187.2	609.3	1249	1664	2773	5805	16.80K	54.42K	156.3K	496.6K

PART NO.	44001	44002	44003	44004 / 44033	44005 / 44030	44007 / 44034	44006 / 44031	44008 / 44032	44011	44014	44015
Ω @25°C	100	300	1000	2252	3000	5000	10,000	30,000	100,000	300,000	1 MEG.
BODY	BLACK	BLACK	BLACK	BLACK ORANGE	BLACK ORANGE	BLACK ORANGE	BLACK ORANGE	BLACK ORANGE	BROWN	BROWN	BROWN
END	BROWN	RED	ORANGE	YELLOW ORANGE	GREEN BLACK	VIOLET YELLOW	BLUE BROWN	GRAY RED	BROWN	YELLOW	GREEN
TEMP. °C				RESISTANCE Ω							
+40	63.9	181.2	589.0	1200	1598	2663	5592	16.15K	52.19K	149.4K	473.2K
41	62.1	175.5	569.5	1152	1535	2559	5389	15.52K	50.07K	142.9K	451.0K
42	60.4	170.0	550.7	1107	1475	2459	5193	14.92K	48.04K	136.7K	430.0K
43	58.7	164.7	532.7	1064	1418	2363	5006	14.35K	46.11K	130.8K	410.0K
44	57.1	159.6	515.3	1023	1363	2272	4827	13.80K	44.26K	125.1K	391.1K
45	55.6	154.6	498.6	983.8	1310	2184	4655	13.28K	42.50K	119.8K	373.1K
46	54.1	149.9	482.5	946.2	1260	2101	4489	12.77K	40.81K	114.7K	356.1K
47	52.6	145.3	467.0	910.2	1212	2021	4331	12.29K	39.20K	109.8K	339.8K
48	51.2	140.9	452.1	875.8	1167	1944	4179	11.83K	37.66K	105.2K	324.4K
49	49.8	136.6	437.8	842.8	1123	1871	4033	11.39K	36.19K	100.8K	309.8K
+50	48.5	132.5	423.9	811.3	1081	1801	3893	10.97K	34.78K	96.54K	295.9K
51	47.2	128.5	410.6	781.1	1040	1734	3758	10.57K	33.44K	92.52K	282.7K
52	46.0	124.7	397.8	752.2	1002	1670	3629	10.18K	32.15K	88.69K	270.1K
53	44.8	121.0	385.4	724.5	965.0	1608	3504	9807	30.92K	85.04K	258.1K
54	43.6	117.4	373.5	697.9	929.6	1549	3385	9450	29.74K	81.55K	246.7K
55	42.5	114.0	362.0	672.5	895.8	1493	3270	9109	28.61K	78.22K	235.9K
56	41.4	110.7	351.0	648.1	863.3	1439	3160	8781	27.53K	75.04K	225.6K
57	40.3	107.5	340.3	624.8	832.2	1387	3054	8467	26.50K	72.01K	215.8K
58	39.3	104.4	330.0	602.4	802.3	1337	2952	8166	25.50K	69.11K	206.4K
59	38.3	101.4	320.1	580.9	773.7	1290	2854	7876	24.56K	66.34K	197.5K
+60	37.3	98.5	310.5	560.3	746.3	1244	2760	7599	23.65K	63.70K	189.1K
61	36.4	95.7	301.2	540.5	719.9	1200	2669	7332	22.77K	61.17K	181.0K
62	35.5	93.0	292.3	521.5	694.7	1158	2582	7076	21.94K	58.75K	173.3K
63	34.6	90.3	283.7	503.3	670.4	1117	2497	6830	21.14K	56.44K	166.0K
64	33.8	87.8	275.3	485.8	647.1	1079	2417	6594	20.37K	54.23K	159.0K
65	33.0	85.4	267.3	469.0	624.7	1041	2339	6367	19.63K	52.12K	152.3K
66	32.1	83.0	259.5	452.9	603.3	1006	2264	6149	18.93K	50.10K	146.0K
67	31.4	80.7	252.0	437.4	582.6	971.1	2191	5940	18.25K	48.17K	139.9K
68	30.6	78.5	244.8	422.5	562.8	938.0	2122	5738	17.60K	46.32K	134.1K
69	29.9	76.4	237.8	408.2	543.7	906.3	2055	5545	16.97K	44.54K	128.6K
+70	29.2	74.3	231.0	394.5	525.4	875.7	1990	5359	16.37K	42.85K	123.3K
71	28.5	72.3	224.5	381.2	507.8	846.4	1928	5180	15.80K	41.23K	118.3K
72	27.8	70.3	218.2	368.5	490.9	818.3	1868	5007	15.25K	39.67K	113.5K
73	27.2	68.5	212.0	356.2	474.7	791.2	1810	4842	14.72K	38.18K	108.9K
74	26.5	66.6	206.1	344.5	459.0	765.1	1754	4682	14.21K	36.75K	104.5K
75	25.9	64.9	200.4	333.1	444.0	740.0	1700	4529	13.72K	35.39K	100.3K
76	25.3	63.2	194.9	322.3	429.5	715.9	1648	4381	13.25K	34.08K	96.31K
77	24.7	61.5	189.5	311.8	415.6	692.7	1598	4239	12.79K	32.82K	92.48K
78	24.2	59.9	184.3	301.7	402.2	670.3	1549	4102	12.36K	31.62K	88.82K
79	23.6	58.4	179.3	292.0	389.3	648.8	1503	3970	11.94K	30.46K	85.32K
+80	23.1	56.8	174.5	282.7	376.9	628.1	1458	3843	11.54K	29.35K	81.98K
81	22.6	55.4	169.8	273.7	364.9	608.2	1414	3720	11.15K	28.29K	78.78K
82	22.1	54.0	165.2	265.0	353.4	588.9	1372	3602	10.78K	27.27K	75.71K
83	21.6	52.6	160.8	256.7	342.2	570.4	1332	3489	10.42K	26.29K	72.78K
84	21.1	51.3	156.6	248.6	331.5	552.6	1293	3379	10.08K	25.35K	69.98K
85	20.6	50.0	152.4	240.9	321.2	535.4	1255	3273	9744	24.45K	67.29K
86	20.2	48.7	148.4	233.4	311.3	518.8	1218	3172	9424	23.59K	64.72K
87	19.7	47.5	144.5	226.2	301.7	502.8	1183	3073	9117	22.76K	62.26K
88	19.3	46.3	140.8	219.3	292.4	487.4	1149	2979	8821	21.96K	59.91K
89	18.9	45.2	137.1	212.6	283.5	472.6	1116	2887	8536	21.19K	57.65K
+90	18.5	44.1	133.6	206.1	274.9	458.2	1084	2799	8261	20.45K	55.48K
91	18.1	43.0	130.2	199.9	266.6	444.4	1053	2714	7996	19.75K	53.41K
92	17.7	41.9	126.8	193.9	258.6	431.0	1023	2632	7741	19.07K	51.42K
93	17.3	40.9	123.6	188.1	250.9	418.2	994.2	2552	7496	18.41K	49.52K
94	17.0	39.9	120.5	182.5	243.4	405.7	966.3	2476	7259	17.78K	47.69K
95	16.6	39.0	117.5	177.1	236.2	393.7	939.3	2402	7030	17.18K	45.94K
96	16.3	38.1	114.5	171.9	229.3	382.1	913.2	2331	6810	16.60K	44.26K
97	15.9	37.2	111.7	166.9	222.6	370.9	887.9	2262	6598	16.04K	42.65K
98	15.6	36.3	108.9	162.0	216.1	360.1	863.4	2195	6393	15.50K	41.10K
99	15.3	35.4	106.2	157.3	209.8	349.7	839.7	2131	6195	14.98K	39.62K
+100	15.0	34.6	103.6	152.8	203.8	339.6	816.8	2069	6005	14.48K	38.20K
101	14.7	33.8	101.1	148.4	197.9	329.8	794.6	2009	5821	14.00K	36.84K
102	14.4	33.0	98.6	144.2	192.2	320.4	773.1	1950	5643	13.54K	35.53K
103	14.1	32.2	96.2	140.1	186.8	311.3	752.3	1894	5472	13.09K	34.27K
104	13.8	31.5	93.9	136.1	181.5	302.5	732.1	1840	5307	12.66K	33.06K
105	13.5	30.8	91.6	132.3	176.4	294.0	712.6	1788	5147	12.25K	31.91K
106	13.3	30.1	89.5	128.6	171.4	285.7	693.6	1737	4993	11.86K	30.79K
107	13.0	29.4	87.3	125.0	166.7	277.8	675.3	1688	4844	11.47K	29.72K
108	12.8	28.7	85.3	121.6	162.0	270.1	657.5	1640	4700	11.11K	28.69K
109	12.5	28.1	83.2	118.2	157.6	262.6	640.3	1594	4561	10.75K	27.71K
+110	12.3	27.5	81.3	115.0	153.2	255.4	623.5	1550	4427	10.41K	26.76K
111	12.0	26.8	79.4	111.8	149.0	248.4	607.3	1507	4297	10.08K	25.84K
112	11.8	26.2	77.6	108.8	145.0	241.6	591.6	1465	4172	9763	24.96K
113	11.6	25.7	75.8	105.8	141.1	235.1	576.4	1425	4051	9456	24.12K
114	11.4	25.1	74.0	103.0	137.2	228.7	561.6	1386	3933	9161	23.31K
115	11.1	24.6	72.3	100.2	133.6	222.6	547.3	1348	3820	8876	22.52K
116	10.9	24.0	70.7	97.6	130.0	216.7	533.4	1311	3711	8601	21.77K
117	10.7	23.5	69.1	95.0	126.5	210.9	519.9	1276	3605	8336	21.05K
118	10.5	23.0	67.5	92.5	123.2	205.3	506.8	1241	3502	8080	20.35K
119	10.3	22.5	66.0	90.0	119.9	199.9	494.1	1208	3403	7832	19.68K
+120	10.1	22.0	64.5	87.7	116.8	194.7	481.8	1176	3307	7594	19.03K
121		21.6	63.1	85.4	113.8	189.6	469.8	1145	3214	7364	18.41K
122		21.1	61.7	83.2	110.8	184.7	458.2	1114	3124	7142	17.81K
123		20.6	60.3	81.1	107.9	179.9	446.9	1085	3038	6927	17.23K
124		20.2	59.0	79.0	105.2	175.3	435.9	1057	2953	6720	16.68K
125		19.8	57.7	77.0	102.5	170.8	425.3	1029	2872	6519	16.14K
126		19.4	56.4	75.0	99.9	166.4	414.9	1002	2793	6326	15.62K
127		19.0	55.2	73.1	97.3	162.2	404.9	976.3	2717	6139	15.12K
128		18.6	54.0	71.3	94.9	158.1	395.1	951.1	2643	5958	14.64K
129		18.2	52.9	69.5	92.5	154.1	385.6	926.7	2571	5784	14.18K
+130		17.8	51.7	67.8	90.2	150.3	376.4	903.0	2501	5615	13.74K
131		17.5	50.6	66.1	87.9	146.5	367.4	880.0	2434	5452	13.31K
132		17.1	49.5	64.4	85.7	142.9	358.7	857.7	2369	5294	12.89K
133		16.8	48.5	62.9	83.6	139.4	350.3	836.1	2306	5141	12.49K
134		16.4	47.5	61.3	81.6	136.0	342.0	815.0	2244	4994	12.10K
135		16.1	46.5	59.8	79.6	132.6	334.0	794.6	2185	4851	11.73K
136		15.8	45.5	58.4	77.6	129.4	326.3	774.8	2128	4713	11.37K
137		15.5	44.6	57.0	75.8	126.3	318.7	755.6	2072	4580	11.02K
138		15.2	43.6	55.6	73.9	123.2	311.3	736.9	2018	4450	10.69K
139		14.9	42.7	54.3	72.2	120.3	304.2	718.8	1965	4325	10.36K
+140		14.6	41.9	53.0	70.4	117.4	297.2	701.2	1914	4204	10.05K
141			41.0	51.7	68.8	114.6	290.4	684.1	1865	4087	9746
142			40.2	50.5	67.1	111.9	283.8	667.5	1817	3974	9455
143			39.4	49.3	65.5	109.2	277.4	651.3	1770	3864	9173
144			38.6	48.2	64.0	106.7	271.2	635.6	1725	3757	8901
145			37.8	47.0	62.5	104.2	265.1	620.3	1681	3654	8637
146			37.0	45.9	61.1	101.8	259.2	605.5	1639	3555	8383
147			36.3	44.9	59.6	99.40	253.4	591.1	1598	3458	8137
148			35.6	43.8	58.3	97.10	247.8	577.1	1558	3364	7899
149			34.9	42.8	56.9	94.87	242.3	563.5	1519	3274	7669
+150			34.2	41.9	55.6	92.70	237.0	550.2	1481	3186	7447

Note: Data in black refer to thermistors with ±0.2°C interchangeability. Data in color refer to thermistors with ±0.1°C interchangeability. Temperature/resistance figures are the same for both types.

Note: Only thermistors with ±0.2°C interchangeability are available encased in Teflon as standard parts. For Part No. of Teflon encased thermistors add 100 to part No. of ±0.2°C interchangeable thermistors. Example: 44001 is a standard thermistor, 44101 is a Teflon encased thermistor with the same resistance values.

THE EPPLEY LABORATORY, INC.
12 Sheffield Ave., Newport, R. I. 02840, U.S.A. Telephone 401 847-1020

EPLAB
Scientific Instruments
for Precision Measurements
Since 1917

STANDARDIZATION

OF

EPPLEY RADIOMETER (PYRGEOMETER)

(horizontal surface receiver - coated silicon hemisphere, temperature compensated)

Infrared Radiometer Serial No.: 20480F3

Resistance 658 ohms at 21°C.

Temperature Compensation: -20 to +40°C

This radiometer has been compared with the Eppley group of reference standards, under radiation intensities of about 200 watts meter^{-2} and at an average ambient temperature of 23 °C. As a result of a series of comparisons, it has been found to develop an emf of:

3.92 x10^{-6} volts/watt meter^{-2}

2.73 millivolts/cal cm^{-2} min^{-1}

The calculation of this constant is based on the assumption that the relationship between radiation intensity and emf is rectilinear. The recommended orientation, when installed, is such that the circular level support faces North in the northern hemisphere, (in the southern hemisphere, the orientation should be opposite).

Date of Test: January 5, 1981

The Eppley Laboratory, Inc.

By: W. J. Scholes

Newport, Rhode Island

IN CHARGE OF TEST:

Richard H. Hatch

S. O. 40569

Shipped to: University of Arizona
Tucson, Arizona

Date January 9, 1981

THE EPPLEY LABORATORY, INC.
12 Sheffield Ave., Newport, R. I. 02840, U.S.A. Telephone 401 847-1020

Scientific Instruments
for Precision Measurements
Since 1917

STANDARDIZATION

OF

EPPLEY RADIOMETER (PYRGEOMETER)

horizontal surface receiver - coated silicon hemisphere, temperature compensated.

Infrared Radiometer Serial No.: 20480F3

Resistance 679 ohms at 24°C.

Temperature Compensation: -20 to +40°C

This radiometer has been compared with the Eppley group of reference standards, under radiation intensities of about 200 watts meter^{-2} and at an average ambient temperature of 23 °C. As a result of a series of comparisons, it has been found to develop an emf of:

3.82×10^{-6} volts/watt meter^{-2}

2.66 millivolts/cal cm^{-2} min^{-1}

The calculation of this constant is based on the assumption that the relationship between radiation intensity and emf is rectilinear. The recommended orientation, when installed, is such that the circular level support faces North in the northern hemisphere, (in the southern hemisphere, the orientation should be opposite).

Date of Test: April 12, 1982

The Eppley Laboratory, Inc.

By: W J Scholes

Newport, Rhode Island

IN CHARGE OF TEST:

Richard H. Hatch

S. O. 42388

Shipped to: University of Arizona
Tucson, Arizona

Date April 21, 1982

Appendix D

Gill Propeller Vane

GILL PROPELLER VANE

Designed and developed by Gerald C. Gill, Professor of Meteorology at the University of Michigan, the Propeller Vane provides, in a single moderately priced instrument, very sensitive measurements of horizontal wind direction and wind speed.

The Propeller Vane utilizes a fin molded of low density foamed polystyrene and achieves a delay distance (50% recovery) of 1.2 meters. Damping ratio is 0.49. The wind speed sensor is a molded polystyrene propeller which provides a distance constant (63% recovery) of 1.0 meter or less. Through considerable engineering effort a close match in dynamic response has been achieved between vane and propeller.

The vane assembly rotates on a vertical shaft which is supported on two sealed stainless steel ball bearings. The angular position of the vane is transmitted through a set of gears in the lower housing to the shaft of a precision conductive plastic potentiometer. With a constant voltage applied to the potentiometer, the signal output is an analog voltage directly proportional to the vane direction. A dual potentiometer 540° azimuth range option is also available.

The helicoid propeller wind speed sensor rotates on a stainless steel shaft which is supported on two precision instrument grade ball bearings. The propeller shaft is coupled to a miniature d.c. generator whose analog d.c. voltage output is directly proportional to rpm and is linear throughout the entire working range. The standard propeller is 23 cm diameter x 30 cm pitch. Smaller diameters are available to extend the working range (with some sacrifice in threshold sensitivity). The wind speed signal is connected by means of two small wires within the vertical shaft to a precision slip ring assembly in the lower housing. The signal is then transmitted along with the direction signal through a multiconductor cable to the Power Supply Translator at the central data station. Calibration of the wind speed sensor is accomplished by driving the propeller shaft at a known rpm by means of the synchronous motor Calibrating Unit and adjusting the signal output level from the Power Supply Translator.

The Power Supply Translator is available in several different models for bench top use or rack mounting. One model is expandable for operation of one to four instruments. An alternate model has panel meters to display the wind speed and direction signals. The Power Supply Translator contains a regulated power supply for the azimuth potentiometer and independent calibration adjustments for both wind speed and wind direction signals to provide simultaneous current outputs for operation of galvo recorders or panel meters and voltage outputs for operation of a magnetic tape recorder or data logger.

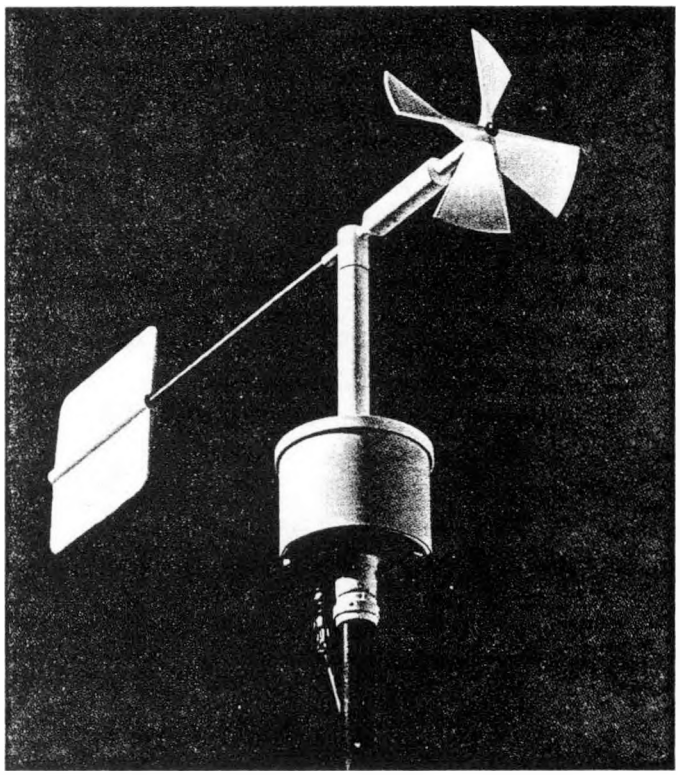

ORDERING INFORMATION

GILL PROPELLER VANE. Supplied with molded polystyrene vane (23 cm x 23 cm) and molded polystyrene propeller (23 cm dia. x 30 cm pitch). Instruction manual included.

GILL PROPELLER VANE WITH 360° AZIMUTH RANGE . . . . . **CAT. NO. 35003**

GILL PROPELLER VANE WITH 540° AZIMUTH RANGE . . . . . **CAT. NO. 35003C**

SPARE FIN. Molded polystyrene (23 cm x 23 cm) . . . . . **CAT. NO. 35090**

SPARE PROPELLER. Standard 23 cm x 30 cm pitch, molded polystyrene. Threshold 0.1-0.2 m/s; maximum speed 30 m/s **CAT. NO. 21281**

SPARE PROPELLER. Optional 19 cm dia. x 30 cm pitch, molded polystyrene. Threshold 0.2-0.3 m/s; maximum speed 40 m/s . . . . . **CAT. NO. 21282**

CABLE & WIRING DIAGRAM
GILL PROPELLER VANE MODEL 35003C
0-540° AZIMUTH RANGE OPTION C

YOUNG

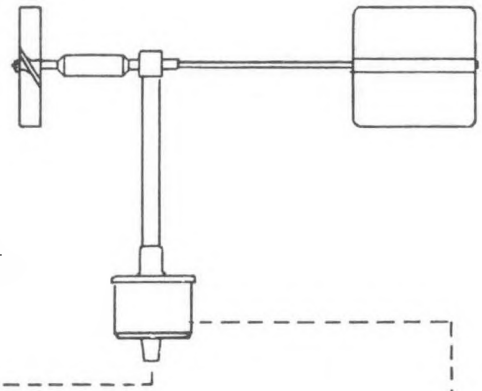

AZIMUTH POTENTIOMETERS:
CONDUCTIVE PLASTIC
1000 OHMS, 0.25% LINEARITY
1 WATT @ 40°C (DERATED TO 0 @ 125°C)
FUNCTION ANGLE 352° (7-9° DEADBAND)

TWO POTENTIOMETERS GEARED TOGETHER 1:1
ARMS PHASED 180° APART.
POTENTIOMETER NO 1 GEARED
TO VERTICAL SHAFT.

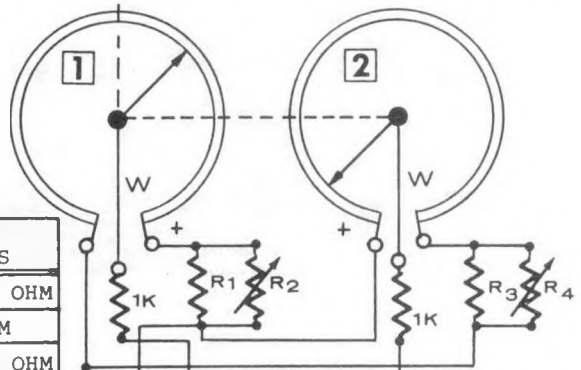

VOLTAGE DIVIDERS	
R1	680 OHM
R2	TRIM
R3	680 OHM
R4	TRIM

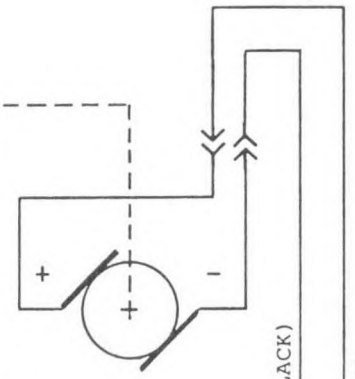

WIND SPEED GENERATOR:
2400 mV @ 1800 RPM
2000 mV @ 1500 RPM
LINEAR 0 TO 10,000 RPM
INT RES 71 OHMS NOM.

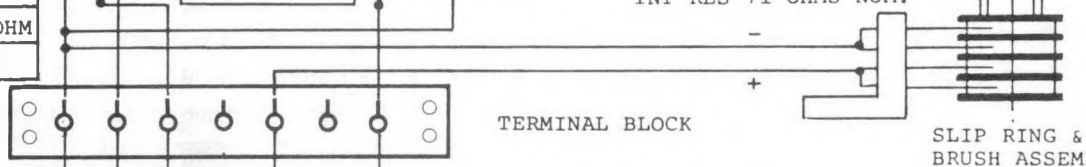

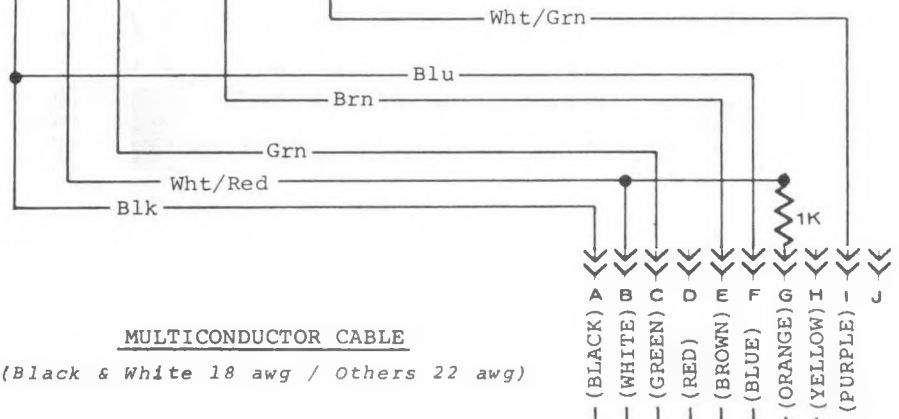

AMPHENOL
MS-3102A-18-1P
MS-3106A-18-1S

A	B	C	D	E	F	G	H	I	J
(BLACK)	(WHITE)	(GREEN)	(RED)	(BROWN)	(BLUE)	(ORANGE)	(YELLOW)	(PURPLE)	

MULTICONDUCTOR CABLE
(Black & White 18 awg / Others 22 awg)

D.C. GROUND & SIGNAL REFERENCE
POTENTIOMETER EXCITATION VOLTAGE
AZIMUTH SIGNAL 1
SPARE
WIND SPEED SIGNAL
CALIBRATION CHECK ZERO
CALIBRATION CHECK FULL SCALE
SPARE
AZIMUTH SIGNAL 2

AUG 77

SPECIFICATIONS GILL PROPELLER VANE MODEL NO. 35003

Range: Azimuth—360° mechanical, 352° electrical (7-9° open), continuous rotation. 540° azimuth range option available.

Threshold:* Wind speed—0-30 m/s (0-70 mph) with standard 23 x 30 cm polystyrene propeller.
Threshold sensitivity of vane 0.1-0.2 m/s (0.3-0.5 mph). Threshold sensitivity of standard 23 x 30 cm polystyrene propeller 0.1-0.2 m/s (0.3-0.5 mph).

Dynamic Response:* Delay distance (50% recovery) of vane 1.2 meters (3.9 feet). Distance constant of standard 23 x 30 cm polystyrene propeller 1.0 meters (3.1 feet).
Damped natural wavelength of vane 7.2 meters (24 feet). Theoretical undamped natural wavelength of vane 6.2 meters (20 feet). Damping ratio — h = 0.49. Maximum overshoot for sinusoidal fluctuations 8%.

Signal Output: Analog output signals for both wind speed and wind direction are suitable for recording on most galvo or millivolt chart recorders and magnetic tape recorders.
Azimuth signal-analog d.c. voltage from precision low torque conductive plastic potentiometer (requires regulated excitation voltage). Potentiometer resistance 1000 ohms. Linearity 0.25%. Life expectancy 50 million cycles (3-5 years normal operation).
Windspeed signal-analog d.c. voltage from miniature tachometer generator. Generator voltage output 2400 mV (into 10K load) at 1800 rpm which equals 9.0 m/s (20.1 mph). Generator armature resistance 71 ohms nominal. Life expectancy in excess of 750 million revolutions (2-4 years normal operation).
Power Supply Translator contains regulated power supply and proper damping and calibration circuits for vane potentiometer and tachometer generator to provide simultaneous current and voltage output signals.

Weight: Overall weight 2.7 kg (6 pounds). Shipping weight approximately 5.9 kg (13 pounds).

Dimensions: Overall height 53 cm (21 inches). Overall length of vane and propeller 86 cm (34 inches). Diameter of standard propeller 23 cm (9 inches). Diameter of base 16 cm (6¼ inches). Mounts on standard 1" iron pipe; orientation ring provided.

*Nominal values

DYNAMIC RESPONSE

Sensor response to sinusoidal wind speed and wind direction fluctuations of varying frequency (i.e. gust wavelength).

$$\text{Amplitude Ratio} = \frac{\text{Indicated Amplitude}}{\text{Actual Amplitude}}$$

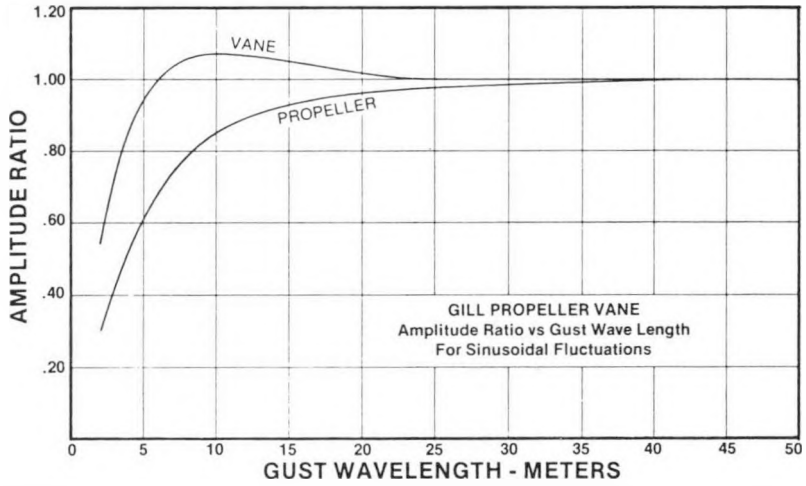

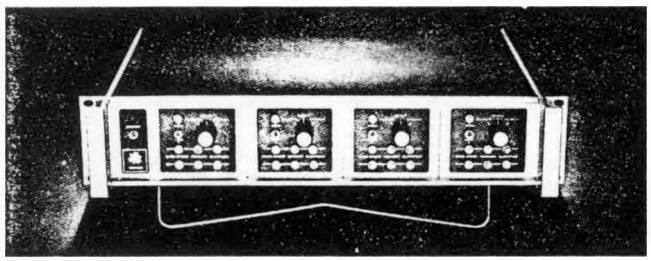

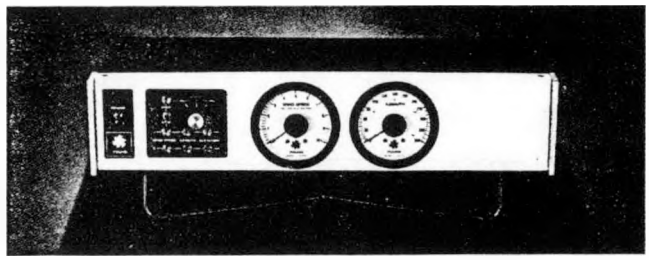

ORDERING INFORMATION

POWER SUPPLY TRANSLATOR. Modular unit supplies constant voltage for vane potentiometer and proper calibration and damping circuits for wind direction and wind speed signals. Available with one, two, three, or four control modules for operation of up to four Propeller Vanes (or combination of sensors). 15 meter (50 foot) multiconductor sensor cable included.* 115 V/50-60 Hz.**

POWER SUPPLY TRANSLATOR-ONE CONTROL MODULE	CAT. NO. 23401
POWER SUPPLY TRANSLATOR-TWO CONTROL MODULES	CAT. NO. 23402
POWER SUPPLY TRANSLATOR-THREE CONTROL MODULES	CAT. NO. 23403
POWER SUPPLY TRANSLATOR-FOUR CONTROL MODULES	CAT. NO. 23404

POWER SUPPLY INDICATOR-TRANSLATOR. In addition to power supply and controls, two meters indicate wind direction, 0-360°, and wind speed 0-10/0-50 m/s. Used to monitor signals when recorder is not required or when using magnetic tape recorder or data logger. Includes 15 meter sensor cable.* 115 V/50-60 Hz or 12 Vd.c**

POWER SUPPLY INDICATOR-TRANSLATOR	CAT. NO. 35403

*Longer cable available at additional cost.
**230 V/50 Hz available on special order.

See Technical Information bulletin for more complete description and specifications on these power supply units.

MAXIMUM RESPONSE PROPELLER

These extremely lightweight propellers are made of expanded polystyrene beads to achieve maximum sensitivity and fast response. The foamed polystyrene is molded in the form of a helicoid to provide one revolution for 30 centimeters of passing wind. The standard propeller is 23 cm diameter x 30 cm pitch. Smaller diameters are available to extend the working range (with some sacrifice in threshold sensitivity). Propellers 19 cm and 15 cm diameter are made from 23 cm diameter moldings by cutting with a hot wire. Bead size and weight are carefully controlled during the molding process to maintain proper response characteristics. After molding propellers are sprayed and balanced using a special acrylic paint. All propellers have four blades and are symmetrical radially and front to back.

Distance constant of the standard 23 cm diameter propeller is 1.0 meter (3.1 feet); the 19 cm diameter propeller is 0.8 meter (2.7 feet) and the 15 cm diameter propeller is approximately 1.1 meter (3.7 feet). Distance constant equals the wind passage required for 63% recovery from a step change in wind speed.

Threshold is measured with the propeller mounted on a standard sensor with the propeller shaft supported on precision instrument grade ball bearings and driving a miniature tachometer generator. Use of the optional photo-chopper type sensors reduces threshold slightly.

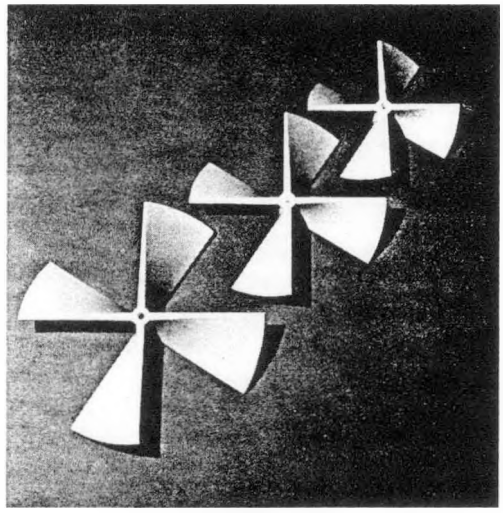

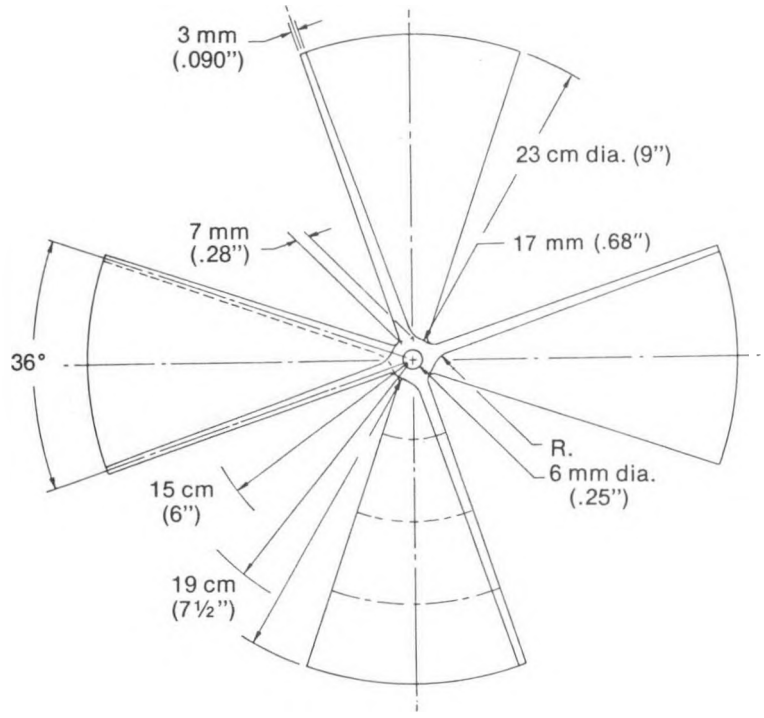

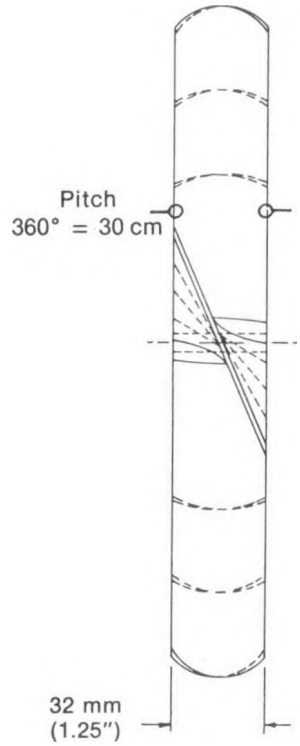

ORDERING INFORMATION

~70 mph ~50 mph

PROPELLER — 23 cm dia. x 30 cm pitch (molded polystyrene). Threshold 0.1-0.2 m/s; maximum speed 30 m/s (axial flow), 22 m/s (all angle flow) ..... **CAT. NO. 21281**

PROPELLER — 19 cm dia. x 30 cm pitch (molded polystyrene). Threshold 0.2-0.3 m/s; maximum speed 40 m/s (axial flow), 30 m/s (all angle flow) ..... **CAT. NO. 21282**

PROPELLER — 15 cm dia. x 30 cm pitch (molded polystyrene). Threshold 0.3-0.4 m/s; maximum speed 50 m/s (axial flow), 40 m/s (all angle flow) ..... **CAT. NO. 21283**

MAXIMUM RESPONSE PROPELLER

Calibration and Response Curves

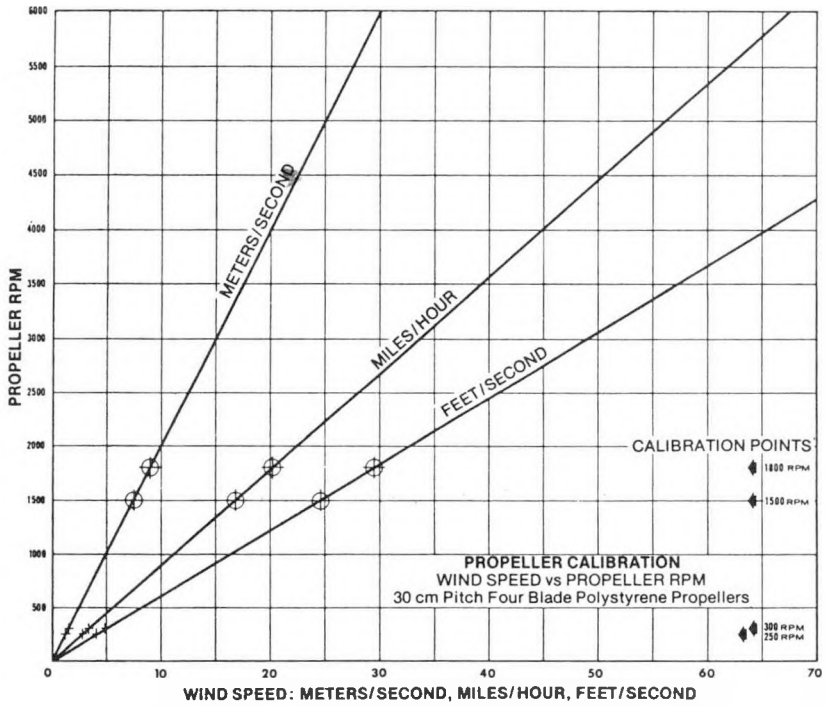

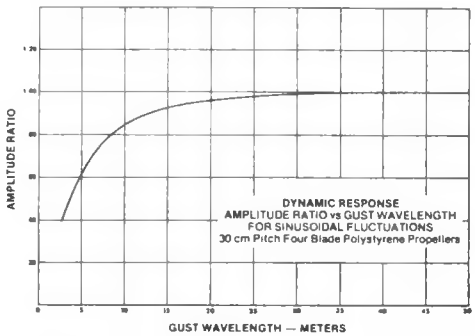

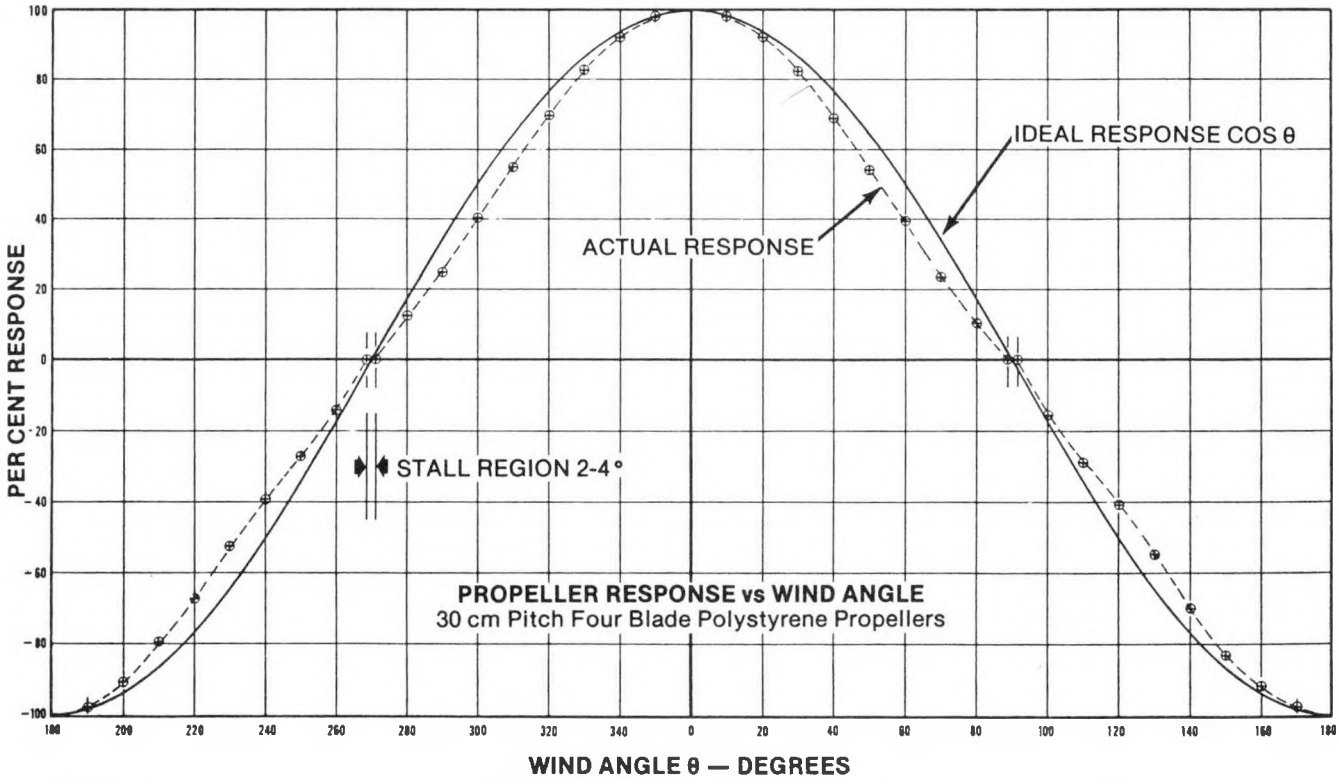

R.M. YOUNG COMPANY
2801 Aero-Park Drive, Traverse City, Michigan 49684, U.S.A.
Phone: (616) 946-3980
TWX: 810-291-3366

POWER SUPPLY TRANSLATORS

A Power Supply Translator is needed to interface the wind sensors with the data recording or display device. The Power Supply Translator contains a source of regulated d.c. power which provides constant excitation voltage for the azimuth and elevation potentiometers. It also provides proper calibration and damping circuits for the wind direction and wind speed signals produced by the sensors. Simultaneous voltage and current outputs are available for operation of standard galvo type chart recorders or panel meters as well as most millivolt chart recorders, magnetic tape recorders, or data loggers. Separate calibration adjustments are provided for both current and voltage output signals for azimuth, elevation (when required), and wind speed. The wind speed current signal is fed through a high-low range switch which allows expansion of the signal to record greater detail at the lower wind speeds.

Output signal levels are normally calibrated to system requirements as ordered or specified. If no ranges are specified voltage output signals are adjusted to 10 mV per azimuth degree, 50 mV per elevation degree, and 100 mV per m/s of wind speed. Maximum available output level is 7.5 V. Current output signals are normally adjusted to 0-1 ma (into 1.4 k) for azimuth and elevation and 0-5 ma (into 65 ohms) for wind speed unless other ranges are specified.

The regulated d.c. power supply and 540° logic circuitry are contained on 7.6x10 cm (3x4 inch) plug-in printed circuit cards for

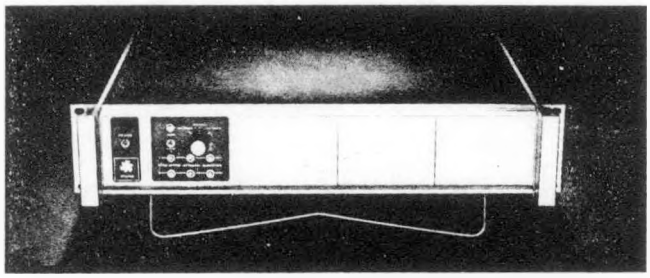

standardization and ease of maintenance. The 540° logic circuitry is required for operation of sensors with 540° azimuth range. This option eliminates the chart "painting" which results from gusty winds causing the vane to oscillate across the potentiometer open section or "dead band". With the 540° system a dual potentiometer is used in the sensor with open sections oriented 180° apart. When the azimuth signal, or wiper, nears either end of the potentiometer element the logic circuit causes a relay to switch to the other potentiometer. This results in only one signal shift for each 180° wind shift, therefore the continuous 0° to 360° shifting which can occur with 360° range is eliminated. The only disadvantage of the 540° system is a 3:2 reduction in signal resolution due to the increased chart range from 360° to 540°.

ORDERING INFORMATION

MODULAR POWER SUPPLY TRANSLATOR. Modular unit supplies constant voltage for wind direction potentiometers and proper calibration and damping circuits for wind direction and wind speed signals. Available with one, two, three, or four control modules for operation of up to four sets of sensors. 15 meter (50 foot) multiconductor sensor cable included for each module.* 115 V/50-60 Hz.**

POWER SUPPLY TRANSLATOR—ONE CONTROL MODULE ..... **CAT. NO. 23401**
POWER SUPPLY TRANSLATOR—TWO CONTROL MODULES ..... **CAT. NO. 23402**
POWER SUPPLY TRANSLATOR—THREE CONTROL MODULES ..... **CAT. NO. 23403**
POWER SUPPLY TRANSLATOR—FOUR CONTROL MODULES ..... **CAT. NO. 23404**

540° AZIMUTH RANGE. For operation of sensors with 540° azimuth range specify with order and add suffix "C" to above catalog numbers.

RACK MOUNTING. For mounting above units in standard 19" relay rack separate rack mounting brackets are required. Specify with order and add suffix "R" to catalog number.

*Longer cable available at additional cost. **Also available for 12 Vd.c. operation or 230 V/50 Hz on special order.

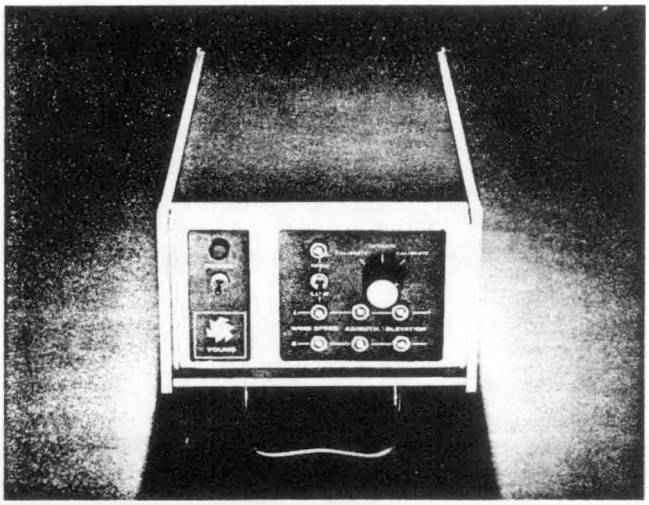

The Modular Power Supply Translator is a multiple unit which is available with one, two, three or four control modules for operation of up to four sets of wind sensors. All calibration controls and adjustments are located on the front panel of each module with the sensor cable connector and signal output terminals located in the back. A 15 meter (50 foot) multiconductor sensor cable is included for each module. Longer cables can be supplied at additional cost. For cable length greater than 300 meters (1000 feet) please contact us for quotation. The chassis measures 8.9 cm H x 43cm W x 33cm D (3.5x17x13 inches) and is designed to fit a standard 19" relay rack with the use of optional rack mounting handles. When rack mounting is desired the tilt up bail, normally supplied, must be removed from the bottom of the chassis.

The Single Unit Power Supply Translator contains one control module and associated circuitry, as described above, however the unit is intended for field use for operation of one set of sensors. The chassis is smaller for portability, measuring 8.9cm H x 14.5cm W x 33cm D (3.5x5.7x13 inches) and the unit can be operated from either 115 Va.c. line power (5 watts) or from a 12 Vd.c. storage battery drawing about 15 ma current (25 ma with 540° circuits). A 15 meter (50 foot) sensor cable is included.

ORDERING INFORMATION

POWER SUPPLY TRANSLATOR - SINGLE UNIT. Same power supply and controls as modular unit except smaller chassis for portability and a.c.-d.c. power. Operates one set of sensors. Includes 15 meter sensor cable* 115 V/50-60 Hz or 12 Vd.c.** ..... **CAT. NO. 23201**

POWER SUPPLY TRANSLATOR - SINGLE UNIT. Same as above except with 540° azimuth range circuitry **CAT. NO. 23201C**

*Longer cable available at additional cost. **230 V/50 Hz available on special order.

PROPVANE

The Model 8002 Propvane is a ruggedized and lower cost version of the Gill Propeller Vane. The polystyrene fin used on the Propeller Vane has been replaced with an aluminum fin of reduced area and with a shortened vane shaft. An extended range molded ABS thermoplastic 3 blade propeller has been substituted for the polystyrene propeller. This propeller has a working range from 0 to 120 mph yet still has a threshold well below 1 mph. Distance constant of the propeller is approximately 8 ft. (2.4 meters). The propeller and vane combination exhibits a damping ratio of approximately 0.34 making the instrument suitable for most air pollution studies as well as many other routine wind measurements.

The vane assembly is mounted on a vertical shaft, supported on stainless steel ball bearings, which transmits the angular position of the vane through a pair of gears to a conductive plastic potentiometer in the lower housing of the instrument. The potentiometer requires a regulated excitation voltage from a battery or power supply located external to the instrument. With constant voltage applied to the potentiometer the analog voltage signal output is directly proportional to wind direction.

The 3 blade propeller is molded in the form of a helicoid with 50 cm pitch. The propeller shaft is supported on two stainless steel ball bearings and coupled to a miniature d.c. tachometer generator in the anemometer head. The self generated analog voltage output is directly proportional to wind speed and is linear throughout the working range.

The instrument mounts on vertical 1" standard iron pipe and weighs approximately 5½ pounds.

SPECIFICATIONS:

Range: Azimuth—360° mechanical, 342° electrical (5% open), continuous rotation, 540° azimuth range available on special order.
Wind speed—0-120 mph (0-54 m/s). Threshold less than 0.9 mph (0.4 m/s). Damping ratio of vane approximately 0.34. Distance constant of three blade propeller approximately 8 ft. (2.4m).

Signals: Analog signals for both wind speed and wind direction suitable for recording on most chart recorders or data loggers. Azimuth signal from precision conductive plastic potentiometer (requires excitation voltage). With constant voltage applied output signal is linearly proportional to azimuth degrees. Potentiometer resistance 1000 ohms; linearity 1%; power rating 1 watt. Life expectancy 50 million cycles (3-5 yrs). Wind speed signal from miniature d.c. tachometer generator. Voltage output linearly proportional to wind speed. Output 2400 mV (nominal) at 1800 rpm which equals 34.2 mph (15.3 m/s). Generator armature resistance 71 ohms. Life expectancy 750 million revolutions (1-3 yrs).

Physical: Principally aluminum alloy; stainless steel vertical shaft and propeller shaft. Vertical shaft has double sealed stainless steel instrument grade ball bearings; propeller shaft has stainless instrument grade ball bearings with double shields. Fin is .016" (0.4mm) aluminum 8" x 9" (20 x 23 cm). Propeller is injection molded ABS thermoplastic 8" (20 cm) diameter with 50 cm pitch. Overall length of vane and anemometer assembly 28" (71 cm). Overall height 23" (58 cm). Weight 5½ lbs. (2.5 kg). Mounts on 1" standard iron pipe; orientation ring provided.

ORDERING INFORMATION

PROPVANE with 360° azimuth range ..... **CAT. NO. 8002**
PROPVANE with 540° azimuth range ..... **CAT. NO. 8002C**
SPARE PROPELLER 20 cm diameter x 50 cm pitch, 3 blade ..... **CAT. NO. 8253**

R.M. YOUNG COMPANY
2801 Aero-Park Drive, Traverse City, Michigan 49684, U.S.A.
Phone: (616) 946-3980
TWX: 810-291-3366

Appendix E

Triple Range Air Flow Sensor
300 Series Model 310S

EII ENVIRONMENTAL INSTRUMENTS, INC.
7 ERIE DRIVE – NATICK, MASS. 01760 – (617) 235-2525 TELEX NO. 948343

DESCRIPTION

TRIPLE RANGE AIR FLOW SENSOR

300 SERIES MODEL 310S

OPERATION

Operation of this instrument is quite straight forward and simple. Make all the connections, probe to probe cable, to electronics pack and make the connections to the power source (see paragraph Power Source).

Turn the instrument on. There will be a settling time of several seconds following an initial signal surge when the power is turned on. This surge and settling time will also occur if the probe is accidently unplugged and replugged into the power supply while the power is on. The instrument can not be damaged if it is operated without the probe, or if the probe is unplugged while the instrument power is on.

PROBE

The probe is effectively a solid tubular member containing the temperature and velocity sensor, with protective basket, at one end and a quick connect connector on the other. Both the velocity sensor and the temperature sensor are platinum units with tracking adjustments being made internally.

The probe should be allowed to thermally stabilize to its intended environment of operation.

If mounting brackets are to be used they should be located near the connector end of the probe or the cable connector itself may be gripped.

Probe disengagement is by a push-pull action rather than by twisting. This type of connector is also used on the cable for attaching to the front panel of the electronics pack.

POWER SOURCES

This instrument has been designed to use three different power sources. It is equipped to utilize 120 V.A.C., 60 Hz, 240 VAC, 50/60 Hz or 12 Volts D.C. Access for these connections are on the front panel of the electronics pack.

12 V.D.C. OPERATION

Connections for using this source are made using the dual binding posts on the front panel and should be wired as indicated. Red is +, Black is -. MOve the A.C./D.C. toggle switch on the front panel to the D.C. mode which is in the DOWN position from the central off position and the instrument is on.

A.C. OPERATION

Connections for 120 V.A.C. are made using the line cord supplied with the instrument. This plugs into the fused connector located on the front panel. To change to 240 V operation, remove the fuse and change the P.C. board to read 240 V. Move the A.C./D.C.toggle switch on the front panel to the A.C. mode which is the UP position and the instrument will be operating.

OUTPUTS

Access to the outputs are provided by a binding post on the front panel and byturning the selector switch, you will engage the output jack to the desired range of interest. This also applies to the recorder output.

RANGE

This instrument is set up for use over three seperate ranges. The first range is for velocities from 0-1 meters/ seconds. This section is set up and calibrated for this particular range. If the instrument is overpowered while on the low range setting (approx 1.2 m/s= 6.2 V) no harm will be incurred but the instrument will not read properly above these values.

The second range is for velocities from 0-10 m/s and the third range is for velocities from 0-50 m/s and all three ranges have been individually set up to the particular range requested. Calibration data from all the ranges are supplied with the instrument.

The front panel meter reads in direct engineering units of 0-50 m/s, 0-10 m/s and 0-1.0 m/s respectively.

The output jack reads 0 to 5 V on all ranges. The recorder outfit is set up for a 0-1 MA current source on all ranges respectively.

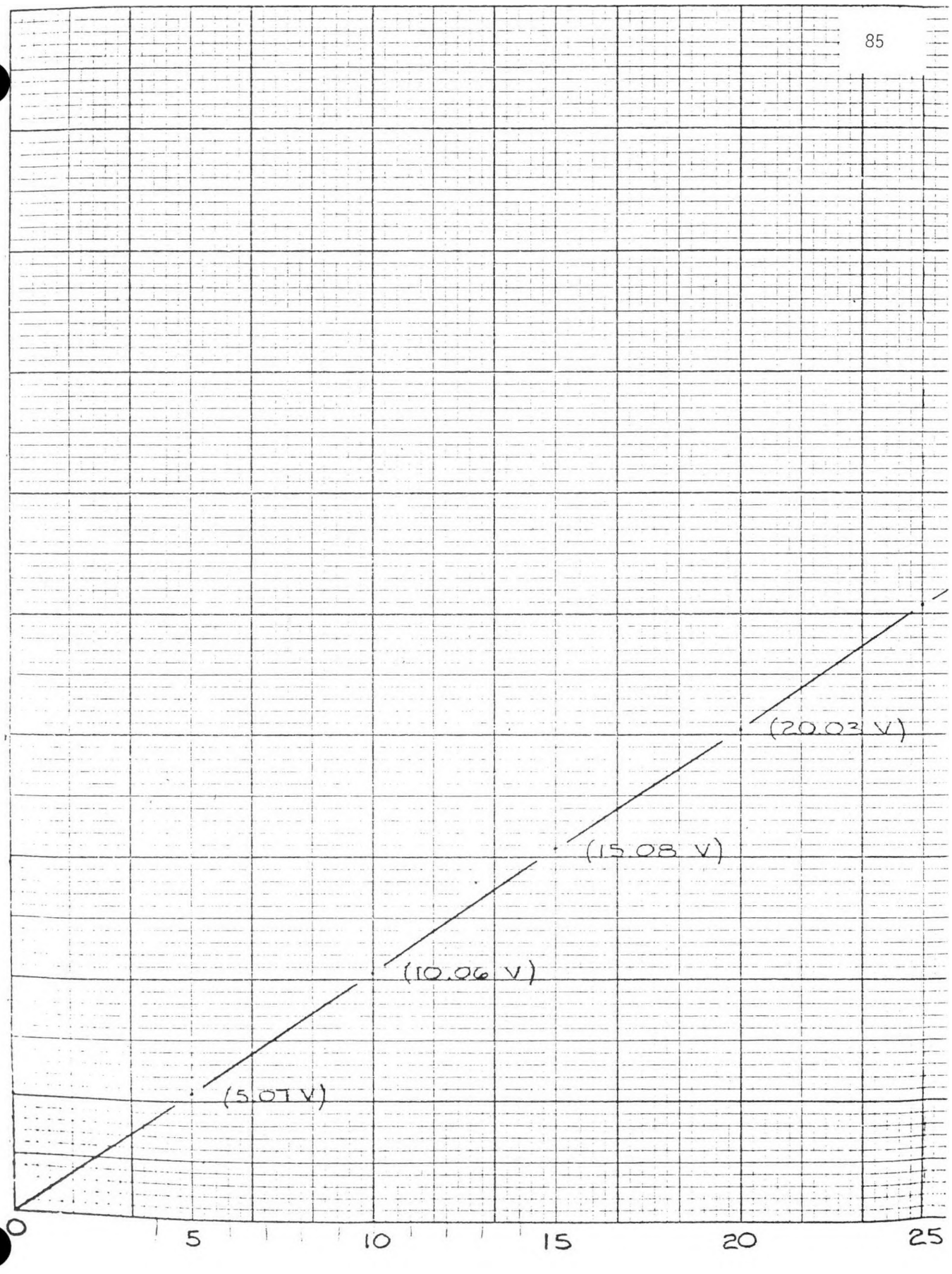
(20.03 V)
(15.08 V)
(10.06 V)
(5.07 V)
0
5
10
15
20
25

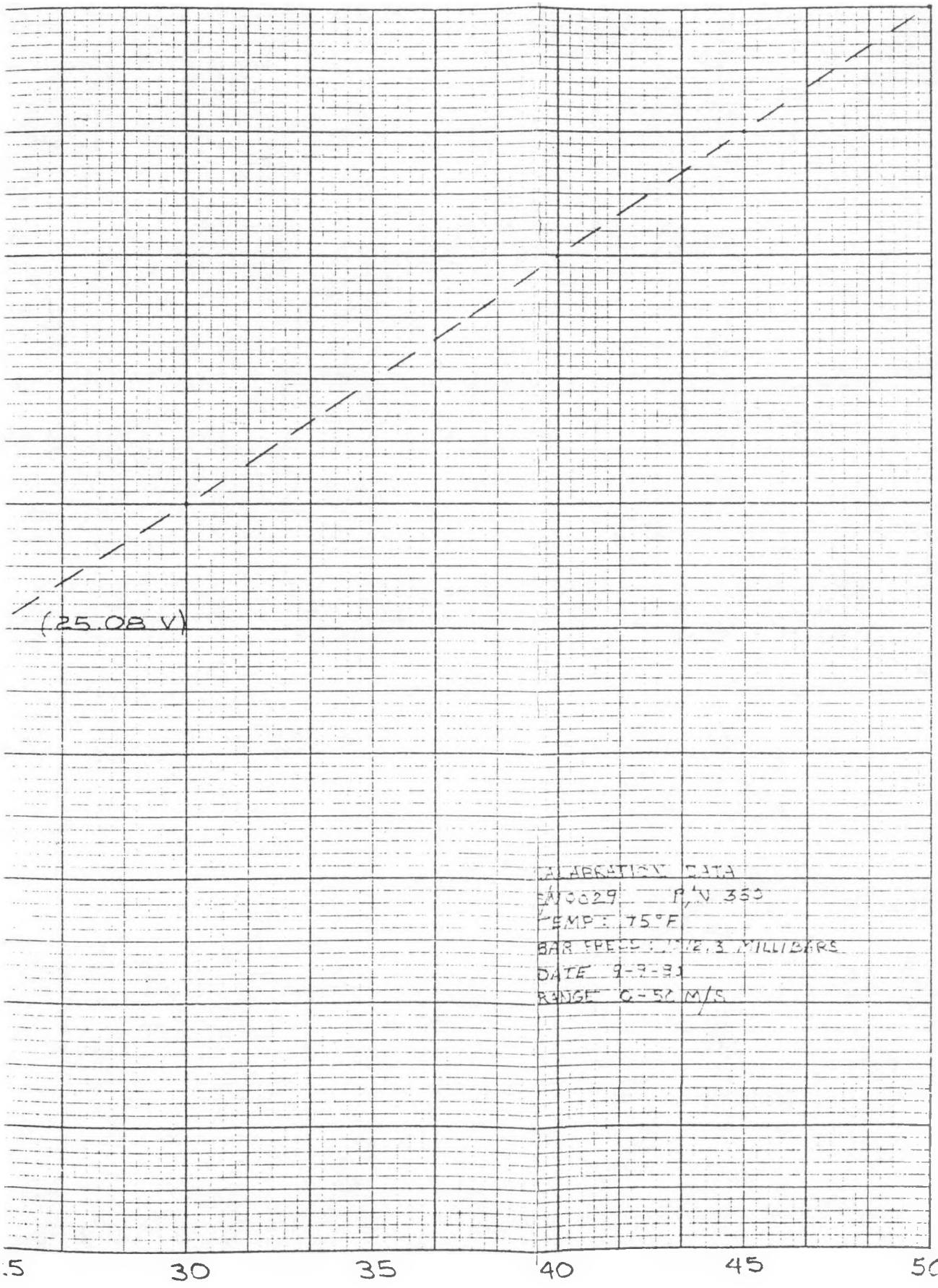
(25.08 V)
CALIBRATION DATA
SAT 0029 P/N 350
TEMP: 75°F
BAR PRESS: 1012.3 MILLIBARS
DATE 9-9-91
RANGE 0-50 M/S
.5
30
35
40
45
50

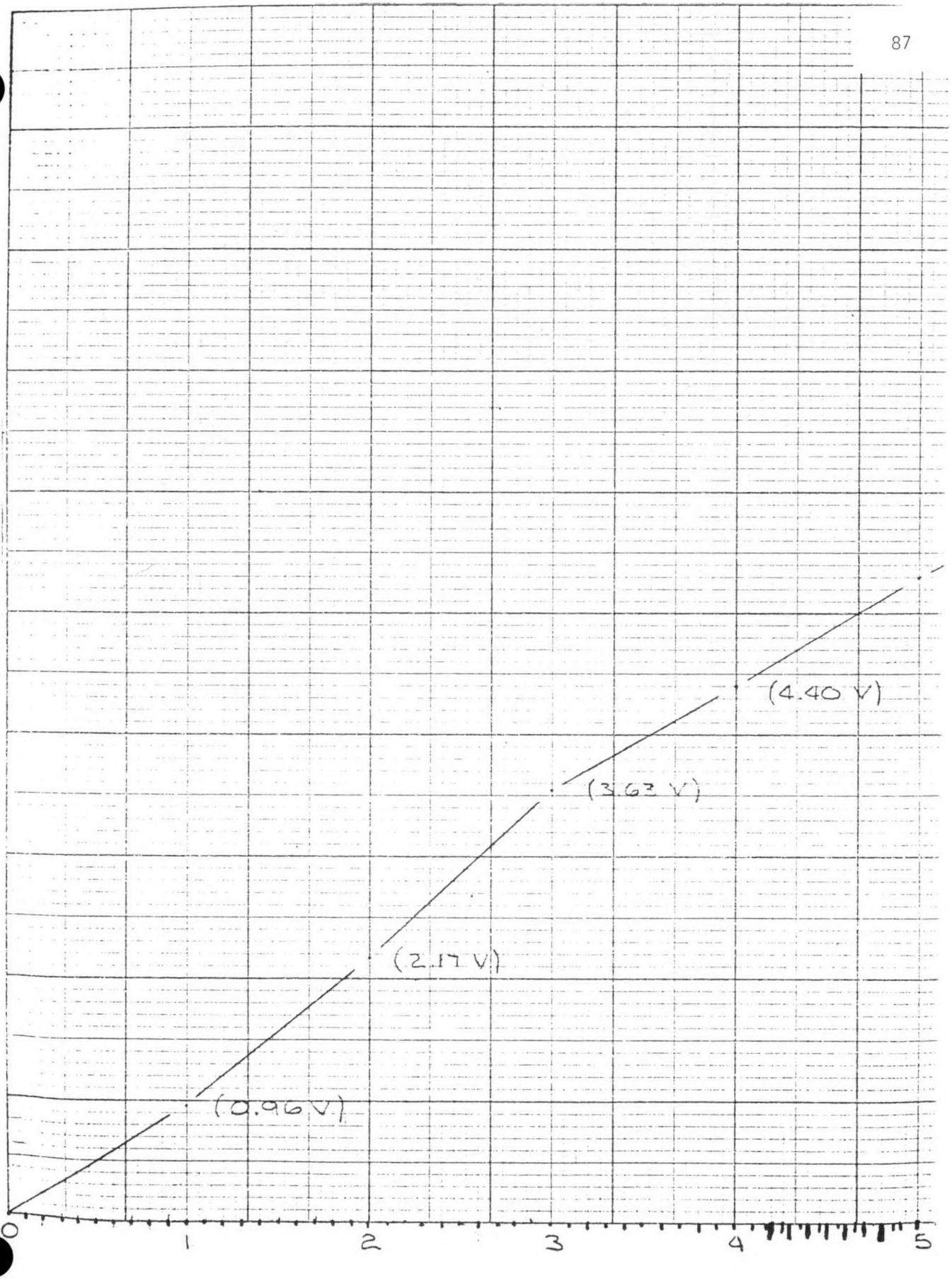
(4.40 V)
(3.63 V)
(2.17 V)
(0.96 V)
0
1
2
3
4
5

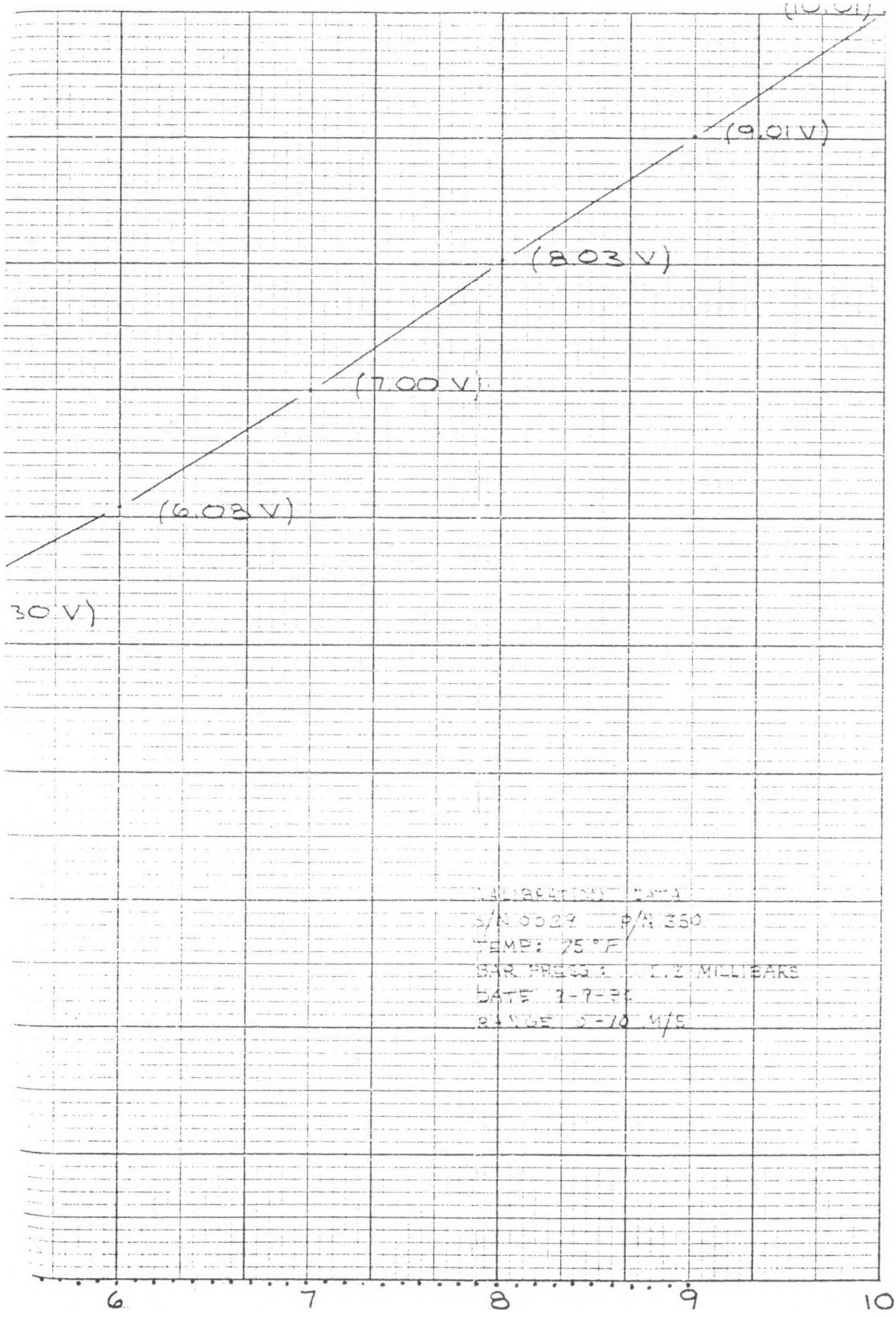
(10.01 V)
(9.01 V)
(8.03 V)
(7.00 V)
(6.08 V)
30 V)
CALIBRATION DATA
S/N 0029 P/N 350
TEMP: 75 °F
BAR PRESS: 1 [illegible] MILLIBARS
DATE 1-7-[illegible]
RANGE 5-10 M/S
6
7
8
9
10

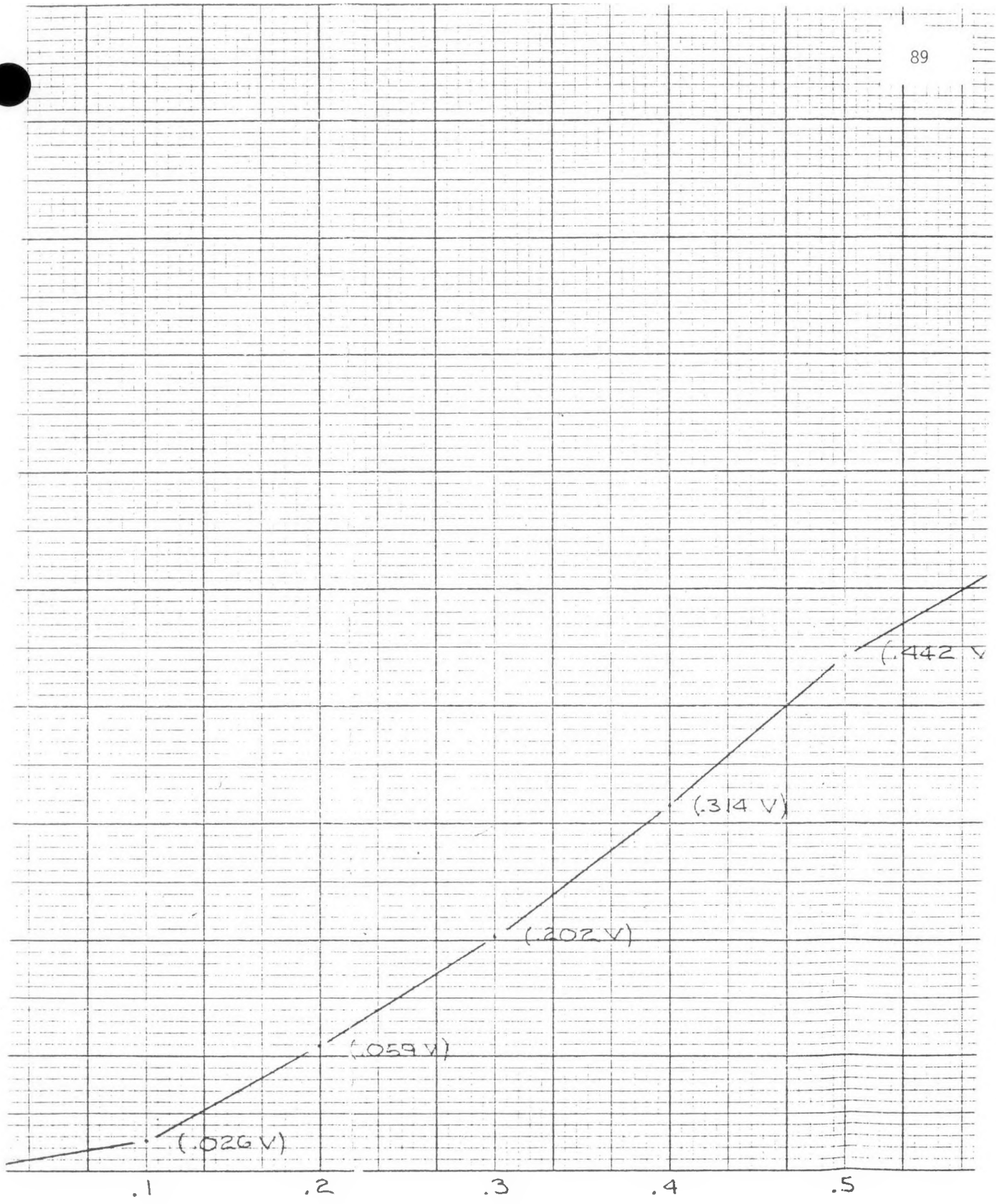
(.442 V
(.314 V)
(.202 V)
(.059 V)
(.026 V)
.1
.2
.3
.4
.5

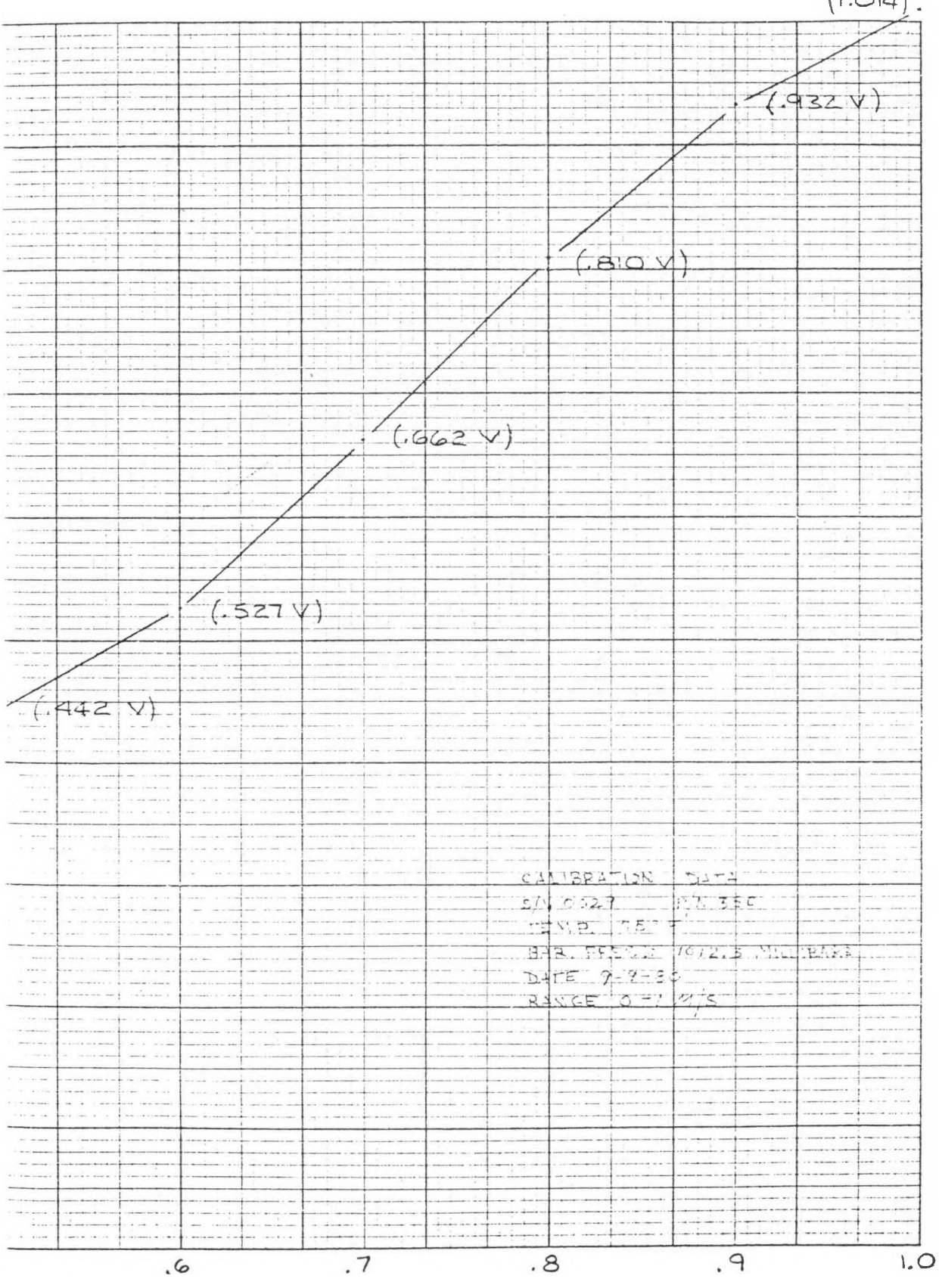
(1.014)
(.932 V)
(.810 V)
(.662 V)
(.527 V)
(.442 V)
CALIBRATION DATA
S/N 0527
BAR. PRESS. 1012.3 MILLIBARS
DATE 9-2-80
RANGE 0-1 PSIG
.6
.7
.8
.9
1.0

Appendix F

Soil Moisture - Temperature Meter


MC-300 Series
SOIL
MOISTURE-
TEMPERATURE
METER
And Soil Cells
SOILTEST INC.
SOILTEST
Subsidiary of GENCO INCORPORATED
Telephone Area Code 312/869-950

Soiltest's Advanced Soil Moisture-Temperature Meter And Cells

MC-300 Series
Description and Instructions

USED FOR Agricultural Studies • Education And Research • Routine and Control Testing

Special Applications in Construction:
Soil Moisture-Temperature Studies in Roads • Building Foundations • Levees Dams • Reservoirs • Airstrips • Canals

USED BY Agricultural Departments Soil Scientists • Engineers • Growers Universities • Agronomists • Researchers Schools • Ranchers • Environmentalists

This instruction manual (Revised 1975) explains the use of the electrical Soil Moisture-Temperature Meter, developed originally by the California Forest and Range Experiment Station. The present Soiltest instrument is the result of years of development. It has been subjected to considerable laboratory study and has been tested in field installations for many years.

Portions of the text of this booklet are based on the technical paper prepared originally by E. A. Colman, California Forest and Range Experiment Station.

SOILTEST, INC.
2205 LEE STREET
EVANSTON, ILL. 60202, U.S.A.
Subsidiary of CENCO INCORPORATED
Telephone: Area Code 312/869-5500
Cable: SOILTEST-EVANSTON • Telex 72-4496

BULLETIN C172-75
Printed In U.S.A.

Soiltest MC-300 Series

Widely Used for Measuring Soil Moisture and Temperature

MC-300B *Fahrenheit* MC-302 *Celsius*

Wherever soil is used as a material in engineering, agriculture, construction, or research the Soiltest MC-300 Series Soil Moisture-Temperature Meter is an important working tool.

The MC-300 Series instruments are used on the building site and on the farm; for research and education; and in many other soil-related applications such as measuring freezing and thawing in soil and snow and monitoring temperature and moisture conditions in and around pavements of roads, streets, and airports.

Wherever Soil Is An Important Factor

Soil moisture and temperature are detected and measured by burying thermistor soil cells in the test soils, permanently or semi-permanently, and taking both temperature and resistance readings directly from the MC-300 Series dial. One meter can be used for monitoring many cells.

All the standard Soiltest soil moisture-temperature cells and soil moisture cells connect to the MC-300 Series Meter and read out on its dial.

The MC-300 Series has many applications in research, contracting, agriculture, transportation, education; around farms, dams, levees, airports, building foundations, highways, reservoirs, canals, and other structures of all kinds.

Fahrenheit and Celsius

Weighing only 3 pounds and powered by just 6 penlight batteries, the MC-300 Series meter is completely portable. Its electronic circuitry is all solid-state.

A rugged hinged case with neoprene gasket gives the MC-300 Series water resistance for operation in the field even during severe weather. And its operation is not affected by either partial battery drain or temperature variations.

First temperature readings can be taken from the meter about 3 hours after the cells are placed in the soil. Since the dial is direct-reading for temperature, no computations nor special calibration graphs are needed.

Dial temperature ranges are 0° to 120° F on the MC-300B Fahrenheit model and −10° to 44° C on the MC-302 Celsius (centigrade) model. On both models, electrical resistance ranges for moisture readings are 0 ohms to 20 million ohms. Moisture percentage is determined by relating resistance readings to a calibration curve (resistance vs moisture %) for each type of soil tested.

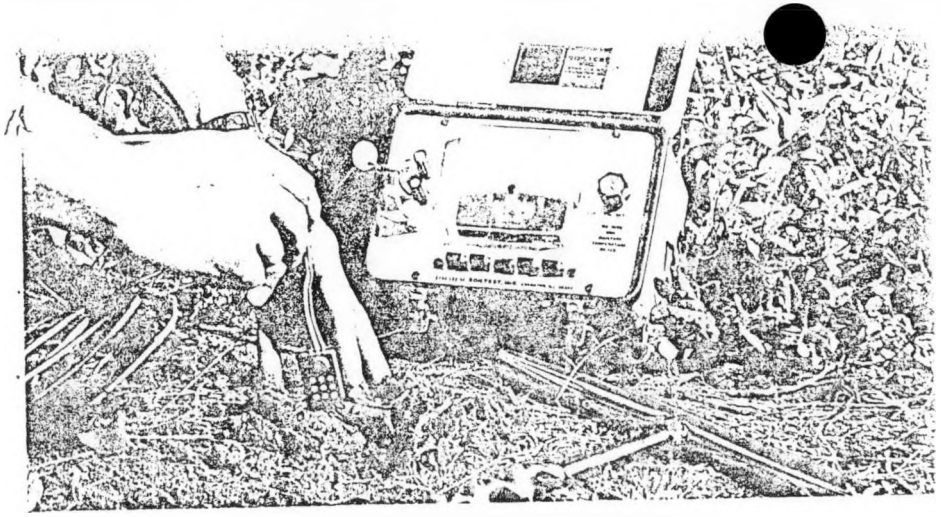

MC-300 Series soil cell is set in hole drilled with A-1 kit auger.

Now, Extended Metering Range

The resistance metering range of the MC-300 Series has been extended, compared to earlier models, to allow use of the meter and cells for a variety of applications in addition to the more common uses in testing for construction and agriculture. For example:

- The meter and cells can be used to measure soil-moisture tension.
- They are used in irrigation control and may be adapted for automatic irrigation.
- The MC-300 Series and cells will determine the depth of frost penetration in various layers.
- They will monitor temperature and moisture conditions in sanitary land fills.

(See Models available, next page)

New direct-reading, easier-to-use MC-300 Series was developed through field studies at Soiltest Environmental Research Center, Baraboo, Wis.

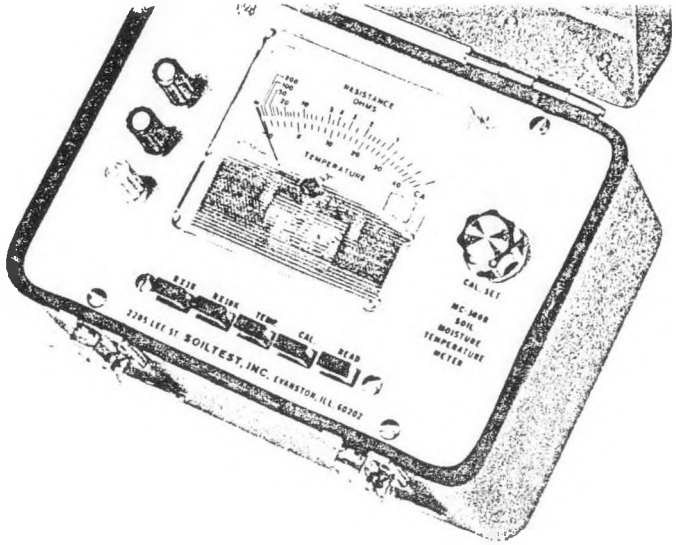

Moisture-Temperature Meter and Cells

Meters and Meter Sets Available

MC-300B Moisture-Temperature Meter Direct-reading 93-cycle AC-type ohmmeter with Fahrenheit temperature scale, 0° to 120°F. It is housed in a compact case with latches and handy carrying grip. Circuitry is all solid-state. Batteries and instructions are included. Case dimensions are 6⅞ inches long by 5 inches wide by 5 inches high. Purchase soil cells separately.

~~$250~~ 209.25

Shipping weight: 4 pounds (1.82 kilograms).
Net weight: 3 pounds (1.46 kilograms).

MC-302 Moisture-Temperature Meter Same as MC-300B but with a Celsius (centigrade) temperature scale −10° to 44°C. ~~$240~~

Shipping weight: 4 pounds (1.82 kilograms).
Net weight: 3 pounds (1.46 kilograms).

MC-312 Moisture-Temperature Meter Set Includes one MC-300B Moisture-Temperature Meter and 25 MC-310A Standard Soil Moisture-Temperature Cells.

Shipping weight: 7 pounds (3.15 kilograms).
Net weight: 5 pounds (2.26 kilograms).

MC-315 Moisture-Temperature Meter Set Same as MC-312 but includes the MC-302 Moisture-Temperature Meter with Celsius (centigrade) Temperature scale.

Shipping weight: 7 pounds (3.15 kilograms).
Net weight: 5 pounds (2.26 kilograms).

(See Cells available, page 6)

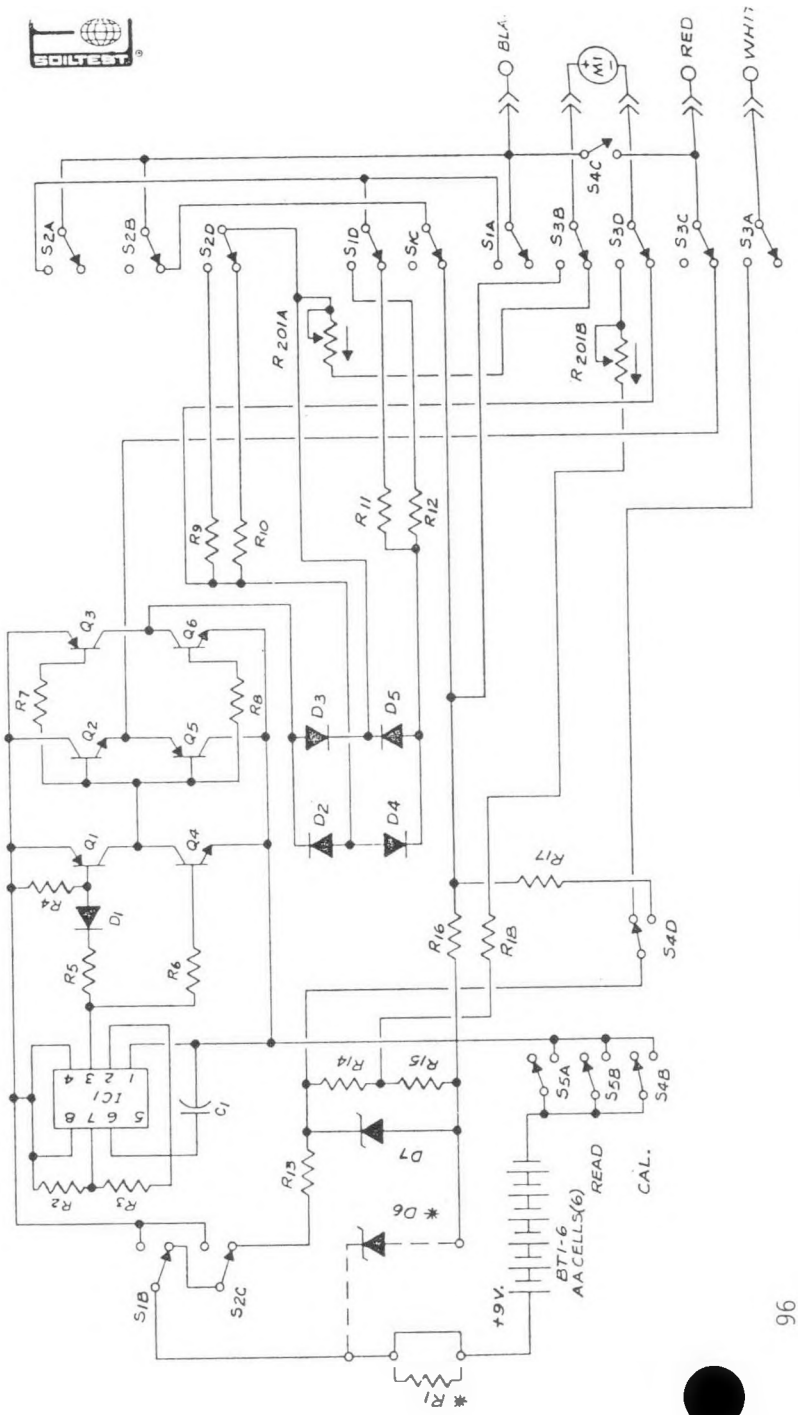

Fig. 1. MC-300 Series Moisture-Temperature Meter Circuit Diagram

Soil Cells and Calibration Equipment Available

Corrosion-resistant cells made up of two metal plates separated by a fiberglass binding which provides a coupling that varies with soil moisture content. The cell is approximately 1 inch by 1½ inches by ⅛ inch thick. A small thermistor completes this two-circuit, three-wire unit.

MC-310A Standard Soil Moisture-Temperature Cell for moisture and temperature measurements. Leads, 6′ long (1.83 m.).

MC-314 Soil Moisture Cell. Similar to MC-310A but for moisture measurement only.

Shipping weight: 1 pound (.45 kilogram).
Net weight: 1 ounce (28.3 grams).

MC-313 Soil Cell Calibration Box 2 inches high by 1.6 inches wide by 1.6 inches deep. Bottom and sides are stainless steel mesh (20 x 200 mesh).

Shipping weight: 1 pound (.45 kilogram).
Net weight: ½ pound (.225 kilogram).

Soil Moisture-Temperature Cells With Long Wire Leads

These cells may be used with the MC-300 Series Moisture-Temperature Meters, both Fahrenheit and Celsius (centigrade) models. The construction of these cells is similar to the MC-310A, which has 6-foot-long leads (1.83 meters).

MC-360	10′ (3.05 m.) Lead Cell	**MC-364**	30′ (9.14 m.) Lead Cell
MC-361	15′ (4.57 m.) Lead Cell	**MC-365**	40′ (12.2 m.) Lead Cell
MC-362	20′ (6.1 m.) Lead Cell	**MC-366**	50′ (15.2 m.) Lead Cell
MC-363	25′ (7.6 m.) Lead Cell	**MC-367**	60′ (18.3 m.) Lead Cell

"Lead" refers to length of cell's wires.

Soil Moisture Cells

Corrosion-resistant cells made up of two metal plates separated by a fiberglass binding which provides a coupling that varies with soil moisture content. The cell is approximately 1 inch by 1½ inches by ⅛ inch thick. *These cells are similar to the soil moisture-temperature cells in construction but without the thermistor.* Available in various lead lengths for moisture measurement only.

MC-314	6′ (1.83 m.) Lead Cell	**MC-374**	30′ (9.14 m.) Lead Cell
MC-370	10′ (3.05 m.) Lead Cell	**MC-375**	40′ (12.2 m.) Lead Cell
MC-371	15′ (4.57 m.) Lead Cell	**MC-376**	50′ (15.2 m.) Lead Cell
MC-372	20′ (6.1 m.) Lead Cell	**MC-377**	60′ (18.3 m.) Lead Cell
MC-373	25′ (7.6 m.) Lead Cell		

"Lead" refers to length of cell's wires.

Soil Cell
Typical Construction Details

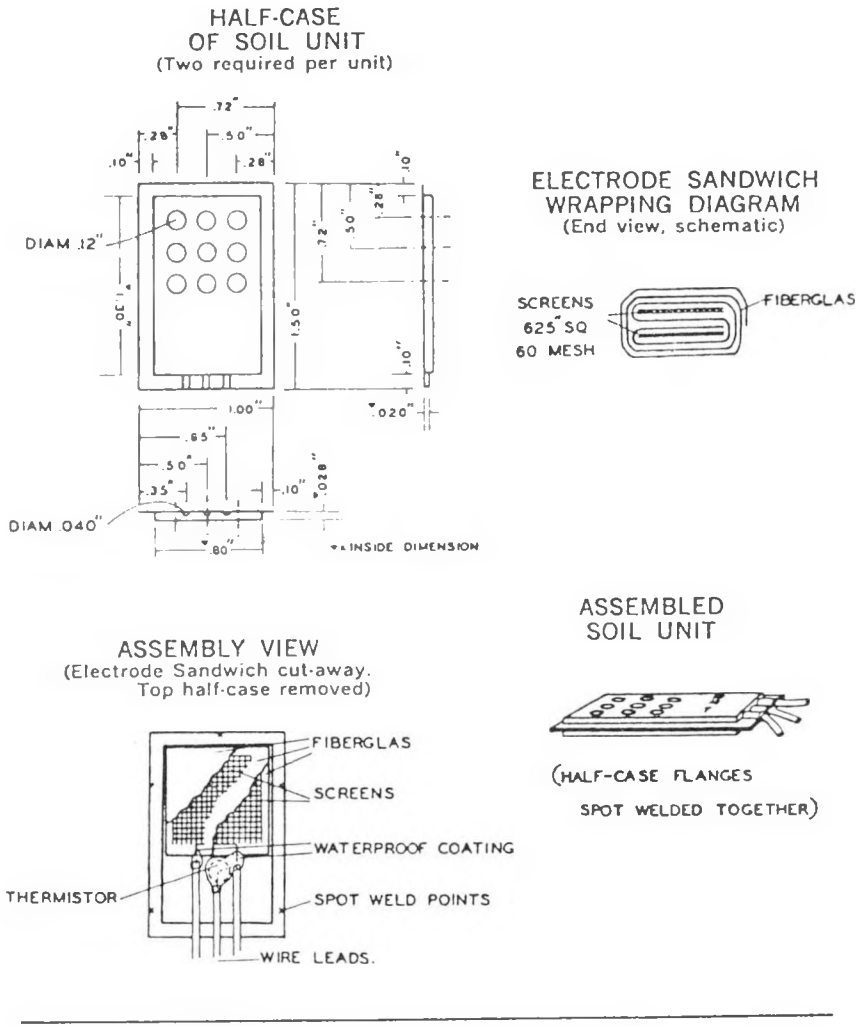

Fig. 2. Drawing of MC-310A soil cell for use with the Soiltest MC-300 Series Moisture-Temperature Meters.

Design of the MC-300 Series

The meter is an alternating-current ohmmeter, entirely self-powered. Alternating current of 93 hertz is generated in the solid-state circuitry, passed through the soil cell or the thermistor, and rectified for indication on a d.c. microammeter. The thermometer portion supplies direct current to the thermistor and indicates temperature on the meter. Fig. 1 shows the meter circuitry.

Background and Working Details

The basic design and uses of the Soiltest Soil Moisture-Temperature Meter have been documented in a research paper, "The Place of Electrical Soil Moisture Meters in Hydrologic Research," by E. A. Colman, *American Geophysical Union Transactions* 27(6): 847-853, December, 1946. Other improvements and results of testing were reported in 1949 in "The Fiberglas Electrical Soil-Moisture Instrument," by E. A. Colman and T. M. Hendrix, *Soil Science* (67)6: 425-438, June, 1949.

The soil cell is shown in Figure 2. The two half-cases of the soil cell are spot-welded together. They are held together in this way to insure uniform spacing between the screens of the electrode sandwich.

Soil cell cases should not be opened. Once sprung out of shape, the cells are difficult and sometimes impossible to re-form properly.

Soil cell leads are colored as follows: White for the thermistor, red for the electrode switch, and black for the lead common to the first two. Each soil cell carries a tag indicating the thermistor coefficient.

Testing soil with the MC-300 Series Fahrenheit-scale model, MC-300B.

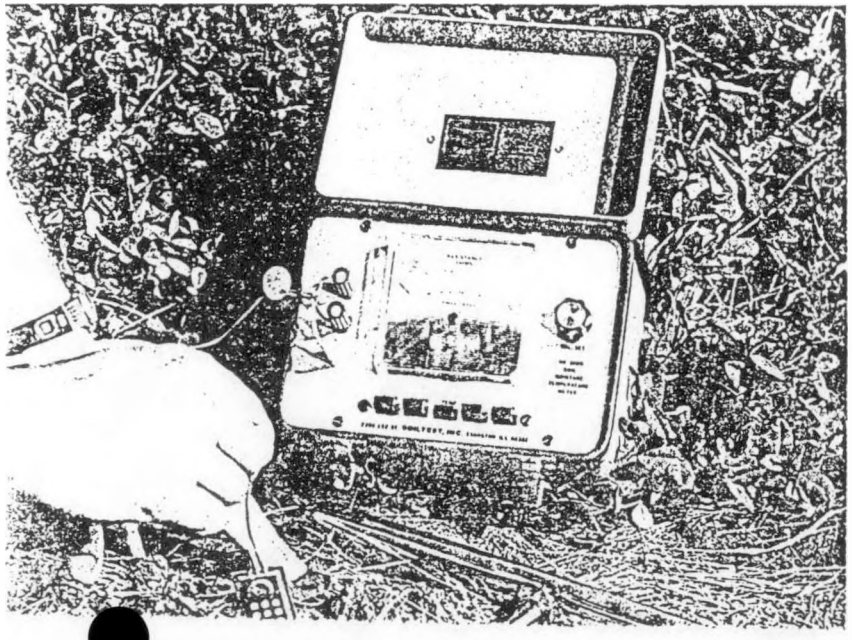

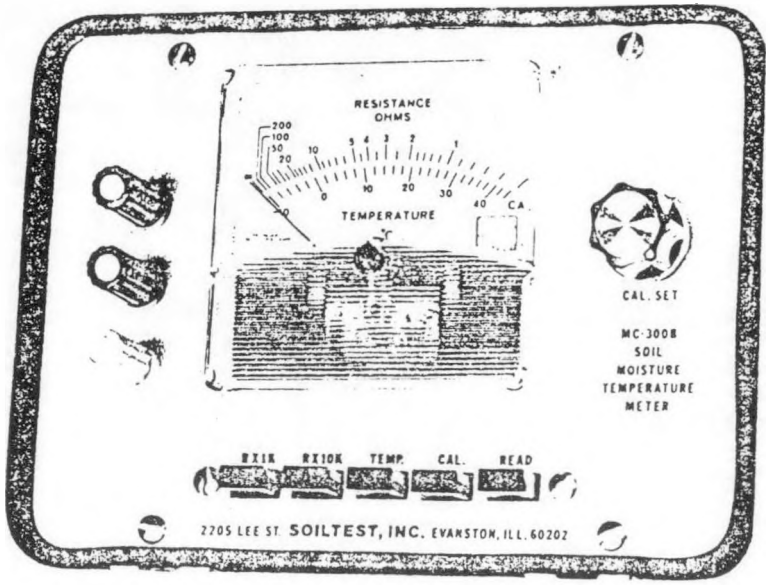

Using the Instrument

NOTE: Refer to photos at left and above.

1. Open the cover and connect the soil cell leads to the corresponding binding posts.

2. Press the button labeled for the range of the measurement wanted.

3. Press the CAL (calibration) button and use the CAL knob to adjust the reading to the CAL mark on the meter face.

4. Press the READ button, and read the value from the scale. Use the scale labeled OHMS for resistance readings (moisture) and the TEMP scale for temperature readings.

5. Each time the range is switched, the instrument must be calibrated for the new range.

6. The scale multiplier for the resistance range is combined with the meter reading as follows: If the meter reads 15 on the OHMS scale, and the multiplier is x 10K, the resistance is 15 times 10K or 150,000 ohms resistance.

Standardization

It would be advantageous if a large number of soil cells, all set in a single mass of soil, under uniform moisture and temperature conditions, all had the same resistance. This would mean that all the cells were closely similar in construction and that differences noted between units set in different soils would be due to soil, and not cell, differences. It would also simplify calibration of the soil cells and would make possible the development of standard relationships between cell resistance and temperature, soil moisture, or soil-moisture tension.

Cell Uniformity

Preliminary studies made with the present type of soil cell have, in fact, shown that there is very little difference between the moisture-resistance relations of duplicate cells, chosen at random, when placed in the same soil. This is encouraging, but, since these studies were conducted on a small scale, they cannot be considered conclusive.

To date, no method has been developed for standardizing the electrode sandwich resistance. Every effort has been made to insure the most uniform materials, construction, and assembly.

Thermistor Coefficient

The resistance of the thermistor in the soil cell is accurate to 1%. The thermistor coefficients of individual cells are tagged on each cell. Thermistor coefficient is the ratio of the nominal resistance of the thermistor to the measured resistance at that temperature. The value of the thermistor coefficient is supplied for the convenience of some users who may want to use more accurate readout meters with the soil cells. Thermistor coefficient is not required for measuring soil temperature using MC-310A cells and MC-300B meter. The temperature is read directly on the meter.

Soil Thermometers

The Soiltest G-225 Maximum-Minimum Thermometer is used in making records of high and low temperatures at a given point over a protracted period. The dial range is −40°F to +120°F in 1-degree increments. The G-225 is designed for remote reading. Its 13-inch-long bulb is connected to the dial by a 5-foot-long, ¼-inch-diameter cable sheathed in stainless steel. The Soiltest G-190 Thermometer is a convenient 16-inch size for taking soil temperatures both indoors and outdoors. Its temperature range is +20°F to 180°F.

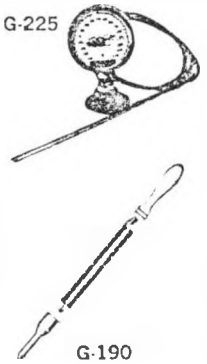

Installing Cells To Measure Both Moisture and Temperature

Preparation of Soil Units

The standard soil cell is supplied with color-coded 6-foot leads (1.83 meters). Cells with longer leads are available. For field installations it may be necessary to connect the leads to a waterproof cable long enough to reach some convenient measurement location. At the working site waterproof connections should be made to the meter. Where more than a single soil cell is used within a small area, it may be desirable to make use of a multiple pole switch at the meter connection.

Identifying, Waterproofing

Vinyl-covered 3-conductor cable can be used between the soil-unit and meter connection. Usually the individual wires in such a cable are color-coded. Confusion of wires at the meter connection can be avoided if a color is assigned for each cell lead. Identifying each lead by color coding or tagging is important because, once a cell is buried, it may be difficult to distinguish the individual cables.

All wire connections must be made waterproof and resistant to weathering. If this is not done, high-resistance short circuits may develop between leads, resulting in erroneous measurements. Soldering connections between soil cell leads and cable wires, using non-corrosive flux, is a good practice. The solder connections then should be coated with a waterproof insulating coating and wrapped tightly with a pressure-sensitive insulating tape made of vinylite or other weather-resistant plastic. Scotch electrical tape is suitable for this purpose.

At the meter location the cable must have a waterproof terminal. Here, some kind of weatherproof shelter must also be provided so that shorts will not develop during wet weather. Soldered connections used here should be coated with waterproof insulating coating.

A triple-leaf, multiple-pole switch can be used at a meter location designed to handle more than one soil cell. In this kind of installation the meter would be connected across the switch and a different cell brought into the meter circuit at each switch position. This type of installation greatly simplifies the measurements of temperature and resistance of a group of soil cells.

Placing Soil Cells in the Ground

Soil cells can be placed in holes drilled with an auger such as Soiltest Models A-4 and DR-2. The cells can be pressed directly into moist or yielding soil from the edge of a pit. It is important that good contact be

maintained between the outside of the fiberglass sandwich and the soil. This insures prompt response of the electrode sandwich to changes in soil moisture.

For single installations drop the cell on the end of its cable to the bottom of an auger hole and tamp the removed soil back in around and above it. For multiple installations (cells, at several depths) drop cells into the hole as the replaced soil rises to each desired depth. In such an installation, the hole must be large enough to accommodate the cables as well as the soil cells.

Preventing Water Problems

Set the cells in place either flat or on edge. There may be some advantage in orienting them parallel to the most usual direction of water movement, so that they will not impede this movement. In most field studies this means placing them on edge. The final choice of orientation, however, will depend upon the type of information needed from each installation.

To insure against the possibility of water flow down along the cell cables, these cables should not pass vertically from the cells up through the soil surface. Instead, they should be buried about 3 inches below the surface, run underground horizontally for about a foot, and then extend upward and out of the ground.

Adequate tamping is essential in placing these cells and leads. When refilling an auger hole in which soil cells have been placed, it is important that the soil be tamped tightly enough to prevent the auger hole from becoming an abnormal water passage. This means packing the soil in the auger hole at least to the density of the soil around it.

Correction for Apparent Resistance of Three-Conductor Cable

The alternating current ohmmeters (MC-300B and MC-302) are calibrated in ohms resistance, but because of the use of alternating current in the circuit the indicated resistance is influenced by the amount of capacitance as well as resistance in the measured circuit. This introduces no complications in the use of the Soil Moisture Meter when lead-wires are short. But when lead-wires are long, correction must be made for the capacitance of the cable, which permits a small current to flow from wire to wire. This can be done by measuring the resistance between the wires.

The apparent resistance between any pair of wires in the three-conductor cable can be considered to be in parallel with the combined reactance and resistance of the soil cell. The following equation for parallel resistances can be used, therefore, to calculate the soil cell resistance:

$$\frac{1}{R\ (\text{soil unit})} = \frac{1}{R\ (\text{measured})} - \frac{1}{R\ (\text{cable})}$$

R (measured) is the resistance shown by the ohmmeter, and R (cable) is the meter-read resistance between the cable wires when the far ends of these wires are disconnected and fully insulated from each other. R (cable) will remain constant for any particular soil cell once that unit is installed. It can be measured, therefore, before the soil cell is connected to the cable which will lead from its point of installation to the point of measurement.

Converting to Soil Cell Resistance

Figure 6 presents a chart that can be used for converting from measured resistance to soil cell resistance. If less than 30 feet of three-conductor cable is used, the cable resistance will probably exceed 1 megohm. In that case, no significant corrections need to be made at measured resistances of less than 50,000 ohms. Shorter cables show higher values of cable resistance, and raise the minimum measured resistance at which corrections need be made. When three-conductor cables less than 10 feet long are used, it is unlikely that a correction will ever be needed.

Calibration of Soil Cells

The relation between soil moisture content and soil cell resistance must be determined for each soil in which the soil cell is to be used. The relation can be determined either in the field where the soil cell is buried or in the laboratory. Three methods can be used:

1 Field Calibration

This method involves repeated soil-moisture sampling in the immediate vicinity of each soil cell. In locations where soil moisture goes through only one or two drying cycles each year, field calibration is likely to be a lengthy affair. But in some cases, such calibration may be more feasible than calibration in the laboratory.

The important considerations in field calibration are these:

1. Sample as close to the soil cell as possible, and at the same depth, so that the sampled soil moisture is representative of the moisture at the soil cell. But do not sample less than 6 inches from the cell.

2. Take as small a sample as possible so that repeated samplings will not invalidate the area being studied.

3. Take duplicate soil moisture samples, if possible.

4. Re-pack sample holes with soil of the same kind, packed to the same density, as that removed.

5. Sample frequently enough to insure adequate coverage of the soil-moisture range, and to minimize the experimental error of the sampling.

6. Continue sampling through several drying cycles.

II Laboratory Calibration — First Method

For Sandy Soils With No Structural Development

This method is based upon that described by O. J. Kelley in *Soil Science* 58: 433-440: 1944.

1. Use a box 2 inches high, 1 9/16 inches wide and 1 9/16 inches thick with a cover. The four sides and bottom are to be made of 20 x 200-mesh stainless steel screen. (Stainless is used because of its resistance to corrosion.) There is a notch in the top rim of the box to pass the lead wires. These calibration boxes are available on order from Soiltest, Inc.*

2. Weigh the box plus cover plus soil cell.

3. Place the soil cell vertically in the center of the box and pack air-dry soil around the cell to fill the box to within ¼-inch of the top. The soil is to come from the location the soil cell is to occupy in the field, and should be packed uniformly in the box to its apparent field density. This will require some practice.

4. Weigh the filled box plus cover. The oven-dry weight of the soil is calculated by determining the air-dry moisture content of a duplicate sample of the same soil. The total weight of the box, including cover, soil cell, and oven-dry soil, now becomes the tare. The oven-dry weight becomes the basis for soil-moisture determinations.

*MC-313 Soil Cell Calibration Box

A-4 Screw-Type Auger

This is a spiral-type auger, 1½ inches in diameter, with a 6-inch-long flight section. For those working with soil materials it is a useful tool for manual boring. The A-4 comes with an extension 36 inches long and a handle. The assembled total length is 48 inches.

DR-2 Post Hole Auger

The design of the DR-2 allows easy, rapid advancement of the sampling hole. It is manufactured with carbon steel blades and furnished complete with a 3-foot extension upright and hardwood cross handle.

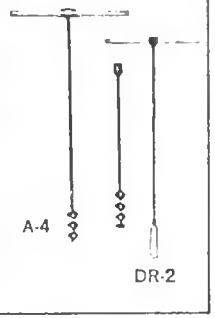

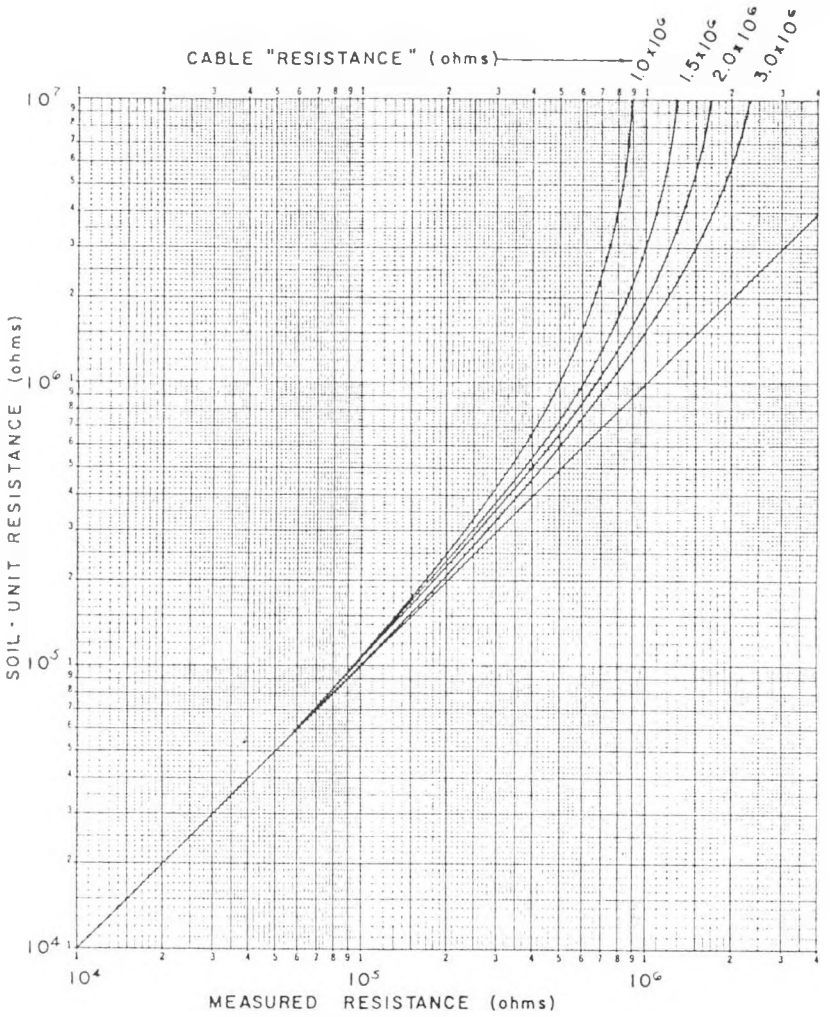

Fig. 3. Chart for determining soil cell resistance when cable and measured resistances are known.

SOIL MOISTURE-TEMPERATURE CELLS

The cells are made up of two plates separated by a processed fiberglass binding which provides a coupling which varies with the moisture content of the surrounding medium. A small thermistor completes this two-circuit, three-wire unit. Cells are approximately 1" by 1½" by ⅛" thick. The leads are 6 feet long. Other lengths available on order.

See specifications, page 6.

5. Half-submerge the filled box in distilled water until the soil is saturated. Then dry the outside of the box, cover it, and place it in a tightly closed chamber. This chamber can be made of a bell-jar resting on a flat plate. Wick-equipped beakers inside are filled with a saturated solution of $Pb(NO_3)_2$, to maintain the air there at 98 per cent relative humidity. The soil boxes can rest on a wire rack in the chamber. Insulated wires leading from the chamber make it possible to measure soil resistances while the soil boxes are inside.

6. Leave the box in the chamber overnight; then measure the soil-cell resistance, remove it from the chamber, and weigh it for moisture determination.

7. Expose the box to evaporation in the laboratory until its moisture content has dropped several per cent; then replace it in the humidity chamber and leave it there overnight. Measure resistance and weigh it in the morning. This cycle of drying, resting in the chamber, and measurement is repeated until the soil is dry. Resistances must be corrected to 60°F.

It is a good practice to wet and dry the soil in the box once or twice before taking resistance measurements. This permits a stable structure to develop in the soil. It is also advantageous to run the soil through more than one series of drying cycles because the characteristic moisture-log resistance curve is double-S shaped (see Figure 7), and in the first drying some important points along the curve may be missed.

III Laboratory Calibration — Second Method

For Soils of Sandy Loam and Finer Texture

The preceding Laboratory Calibration procedure (II) will provide an erroneous calibration curve for soils with any degree of structural development. Although it is possible to pack granulated soil to natural field density, field structure cannot be duplicated by packing. Pore space ar-

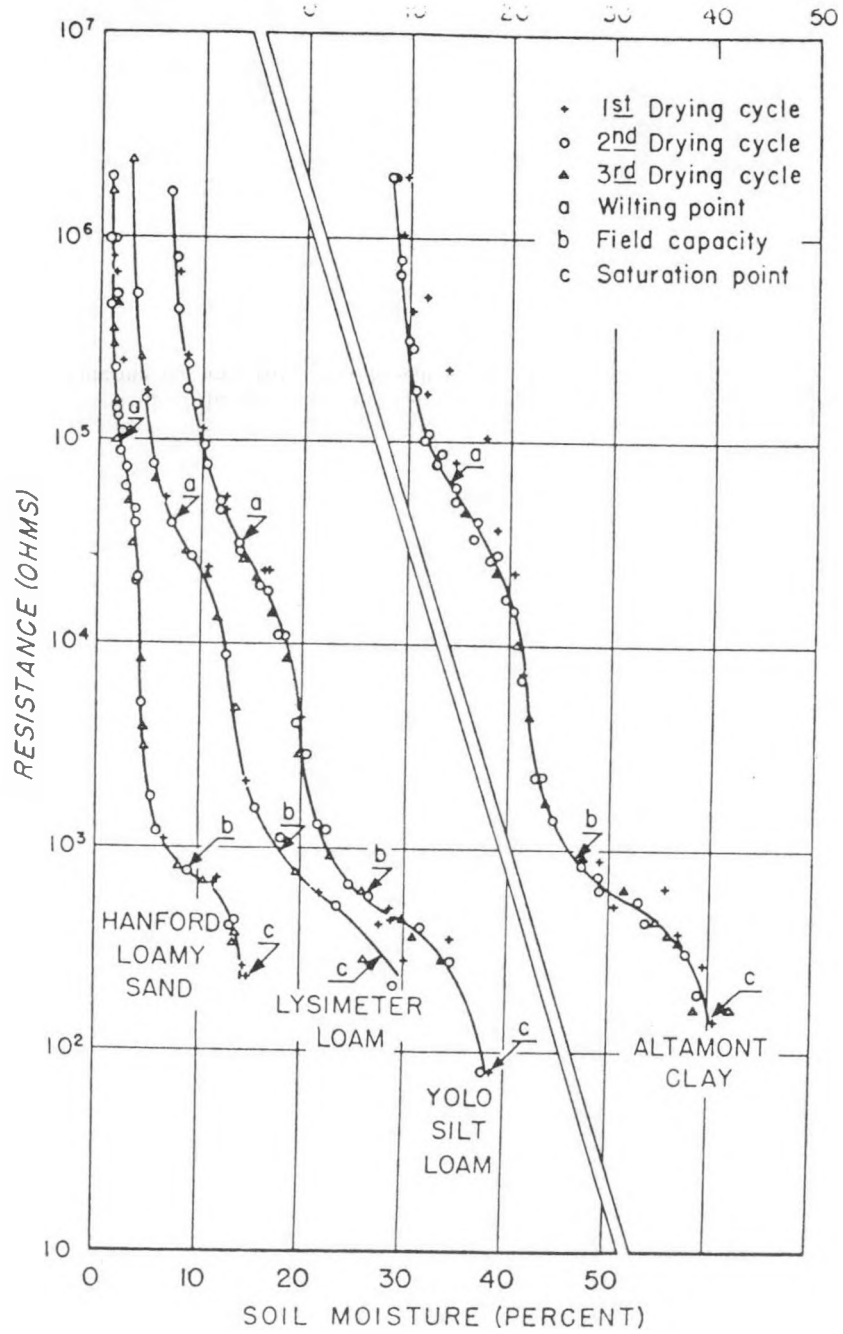

Fig. 4. Sample calibration curves for three California soils. Soil moisture for the Altamount clay is read on the top abscissa.

rangement as well as total pore space determine the shape of the calibration curve, and there is no way of duplicating field pore space arrangement in the laboratory.

The following procedure is designed to preserve field structure (pore space arrangement) by making the calibration on a soil core cut from the location that the soil cell is to occupy.

1. Obtain the soil for calibration as an undisturbed core, using a type of core-cutting cylinder in which the soil can be left during calibration. Any diameter of core greater than 2 inches can be used. The core length should be about 3 inches. Soiltest samplers CN-990, CN-1025 or CN-1030 may be used.

2. It is best to press the soil cell end-down into the soil *before* the core is cut. The cell can be inserted readily and the core cut easily if the soil is wet, naturally or artificially, to about field capacity. If the cell is inserted before cutting the core, compaction of the core is minimized and stones can be detected.

3. After obtaining the soil core the soil should be trimmed off flush. Then rigid screens should be attached closely to both ends of the soil in the core-cutter to hold the soil core in shape and prevent swelling. A fine screen or cheesecloth laid between soil and screen may be needed to prevent the loss of soil. Metal caps can be made to fit over the screens at the ends of the core-cutter.

4. The saturation and progressive drying can be carried on as described in the section on Laboratory Calibration (II). Because the dry weight of the soil core is not known, it is not possible to construct the calibration curve as drying proceeds. At the end of the calibration period, however, the soil can be removed from the core-cutter, weighed, oven-dried, and re-weighed to provide the necessary measurements. No soil should be lost in this process. The soil cell, core-cutter, and screens also should be weighed so that moist weights can be corrected and moisture contents calculated.

5. Moisture contents can be calculated on the basis of either dry weight or volume. The dry weight basis is described above. For the volume basis the core-cutter volume must be determined, as well as the water content of the soil prior to oven-drying.

Special Installation for Testing Soil Cells

The following instructions are for soil cell installations that are designed specifically to test the long-duration field performance or educational experimental use of soil cells.

• The installation must be made in uniform soil that has as little profile development as it is possible to find. The latter precaution is important, for soil horizon differences can cause inconsistencies in moisture sampling that may be serious.

• Install at least three sets of soil cells in a single study area. This means at least three soil cells at each depth studied. This is necessary because of random soil or moisture variations that occur even within supposedly uniform areas. The magnitude of these differences can be detected by replicated soil cells and replicated sampling, as follows:

1. Place cells in the soil so that (a) they are below the surface horizon, which varies most in organic content and density, (b) they are within the horizon of most uniform soil and, (c) they are within the horizon which is subject to relatively rapid drying by evaporation and transpiration. These three conditions cannot always be met to complete satisfaction in any one soil horizon, but the best compromise usually can be found if the soil cells are placed 6 inches to 18 inches deep. A "stack" of several cells usually can be placed vertically within this layer.

2. To insure uniform evapo-transpiration losses throughout the test section, establish a uniform vegetation cover on the area. Heavy water-using vegetation is best for this purpose because it will make possible the greatest number of soil-drying cycles within the period of study. If desired, the soil may be kept bare and evaporation alone relied upon to dry the soil. If this is done, the study area should be surrounded by a trench dug deeper than the maximum soil cell depth. This is necessary so that roots entering the area from outside will be cut. The trench should be refilled after digging, and opened occasionally during the course of the study.

3. Periodically determine soil-moisture content at the depths of the soil cells. Sampling can be done at fixed intervals or when resistance measurements made on the soil cells indicate that the soil moisture has changed. If possible the soil at all depths sampled should be allowed to dry to the wilting point between irrigations. Irrigation should be uniform over the entire area and sufficient to wet the soil well below the greatest depth of sampling.

Soil-moisture samples should be taken at least in triplicate at the depth of each soil cell. An auger or soil tube, such as the Soiltest A-1 or A-2,

CN-940 Eley Volumeter

For anyone using soil — the engineer, agriculturalist, environmentalist, or others — the Eley Volumeter is valuable for making fast measurements of field density in undisturbed soils. The CN-940 is used as a tube sampler, with the piston fully retracted. The cylinder can be retrieved full of soil by pushing the cylinder into the soil. The operator screws in the threaded stem to extrude a specific volume, as indicated on the stem scale which is marked *0-30 cubic centimeters*. The sample is weighed, and the value for this weight is divided by the stem reading to get the soil density in grams per cubic centimeter.

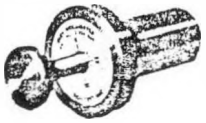

can be used. Samples should not be taken less than 6 inches from a stack of soil cells so that the sampling hole will not affect the cells. The sampling holes should be re-filled with well-tamped soil like that removed. Each hole should be marked to avoid sampling there again.

If the stacks of soil cells are placed in a triangular pattern, sampling can be done in the same pattern, so that the triangles, in effect, interlock. Repeated samplings in this pattern eventually will form a circle.

4. It is desirable to continue records on the study area for a period of time, to learn whether any change develops in the relation of soil cell resistance to soil moisture content.

NIC-5 Series Nuclear Moisture-Density Meters

Soiltest's NIC-5 Nuclear Moisture-Density Meters are innovative instruments used in non-destructive testing of the density and moisture of soils, stabilized soils, and aggregates. They also are used to test the density of asphalt mixtures. The depth of moisture measurement is about 3 to 6 inches (76.2 to 152.4 millimeters), inversely proportional to moisture. Measurement volume is approximately 55 to 450 cubic inches (about 900 to 7375 cubic centimeters). Both English-measure and metric gauges are available. A single direct-reading dial displays *density* readings in a range of 70 to 170 pounds-per-cubic-foot (1.100 to 2.700 grams-per-cubic centimeter) and *moisture* readings of 0 to 40 pcf (0 to 0.640 gms/cc).

Among the various NIC-5 Series instruments are models that combine direct transmission and backscatter capability and some that are backscatter-type only. The battery-powered, 23-pound NIC-5 Series instruments are easily carried to the test site and quickly put into operation by setting directly on the test surface. No air gap stand is needed, as with other nuclear test devices, because the NIC-5 *dual-gauge* principle offsets the effect of test material chemical composition on density measurements. Just one minute after proper seating on the test material, the instrument is giving readings on the single panel dial when the pushbuttons for Moisture and Density are depressed.

SOILTEST Equipment for Agricultural Testing

Soil Testing Kits A complete variety ranging from large sets that test for everything to small kits for specific soil components.

A-8

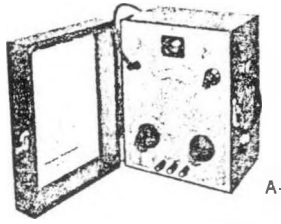

A-109

Conductivity Equipment Meters, kits, and other equipment for field and laboratory tests of water conductivity and resistivity; salt content of soils and water; fertilizer content of water; and soil moisture.

Soil Samplers and Augers Soil sampling kits, augers, and sampling tubes that are used to take samples of various types of soils for agricultural purposes. Some are manual, some powered.

A-1

A-35

Salinity Equipment Various instruments for determining salt and fertilizer content in soils and measuring the moisture content of soil.

Moisture Extraction Apparatus Equipment for removing soil moisture in the laboratory so that field conditions are duplicated. Includes porous plate, pressure membrane, and filter funnel apparatus.

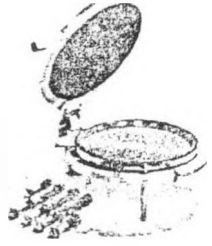

A-79

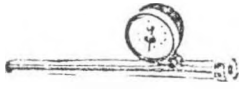

A-164

Tensiometers, Water Samplers A selection of tensiometers for measuring soil suction and a broad variety of other instruments and devices for sampling, detecting, measuring, and gauging soil water and moisture.

Appendix G

Instrumentation for the Measurement of the Components of Solar and Terrestrial Radiation

THE EPPLEY LABORATORY, INC.
12 Sheffield Ave., Newport, R. I. 02840 U.S.A. Telephone 401 847-1020

Scientific Instruments
for Precision Measurements
Since 1917

INSTRUMENTATION FOR THE MEASUREMENT OF THE COMPONENTS OF SOLAR AND TERRESTRIAL RADIATION

1. General

Short-wave solar radiation is comprised of the direct component of sunlight and the diffuse component of skylight. When measured together, as the total short-wave flux on a horizontal surface, this integral is referred to as the global radiation. The other short-wave component of the radiation budget is that reflected from natural surfaces. The wavelength range of these components is usually taken to be 0.3-5 um but about 0.3-3 um in practice.

Long-wave terrestrial radiation is comprised of the incoming atmospheric component (i.e. downward emission by the gases of the atmosphere, especially water vapor and carbon dioxide) and the outgoing terrestrial component (i.e. upward emission and reflection by natural surfaces and atmospheric gases). The wavelength range of these components is usually taken to be 3-100 um ideally but about 4-50 in practice.

When the two long-wave components (there are strictly three, but it is impracticable to attempt to separate long-wave emission and reflection) are measured together, differentially, this flux is termed the net long-wave radiation. When the four components (global and reflected short-wave radiation and incoming and outgoing long-wave radiation) are combined, as a single measurement of the difference between long and short-wave incoming and similarly outgoing, this flux is termed the net total radiation. However, there is presently strong support for separate measurement of each of these four components, as a more accurate approach to the determination of the radiation budget. Eppley Laboratory policy is, therefore, along these lines.

2. Short-wave Radiation Sensing

Two improved Eppley pyranometers are available.

(a) The Precision Spectral Pyranometer - which is believed to be the most accurate radiometer produced commercially for the measurement of global sun and sky radiation, totally or in defined wavelength bands. It is equally suitable for the measurement of reflected short-wave radiation (albedo) or, with the incorporation of a shading arrangement to screen off the sun, the diffuse sky component separately. Such a special stand is available from the Eppley Laboratory.

This radiometer (pyranometer) is an improved smaller model of the earlier Eppley instrument introduced in 1957. It comprises a circular multi-junction Eppley thermopile of the plated (copper-constantan), wirewound type which, when necessary, is temperature compensated to render the response essentially independent of ambient temperature. The thermopile has the added advantage of withstanding severe mechanical vibration and shock. Its receiver is coated with Parsons' black lacquer (nonwavelength-selective absorption). This instrument is supplied with a pair of removable precision ground and polished concentric hemispheres of Schott optical glass (the inner of clear WG7 glass and the outer of WG7 glass or yellow GG14, orange OG1, red RG2 or dark red RG8 filter glass, as preferred). Also supplied is a desiccator which can readily be inspected. The instrument has a painted cast bronze stand carrying a white enameled guard disc. It is shown in Fig. 1.

The WG7 clear glass is transparent from a wavelength of about 285 to 2800 nm. The centers of lower sharp cutoff of the hemispherical filters are as follows: GG14, approzimately, 500 nm; OG1, 530 nm; RG2, 630 nm; and RG8, 700 nm. For solar ultraviolet measurements, hemispheres of quartz are available.

(b) The Black and White Pyranometer - also for the measurement of global, reflected and diffuse short-wave radiation is a more economic development of the well-known Eppley 10- and 50- junction 180° pyrheliometer originally introduced by Kimball and Hobbs in 1923. The detector is a differential electroplated (copper-constantan) thermopile with the hot-junction receivers blackened and the cold-junction receivers whitened.

The innovations are:

(a) replacement of the two concentric-ring detector, of gold-palladium: platinum-rhodium alloys, by one of radial wirewound-plated construction;

(b) use of a more stable 3M Velvet Black coating and of barium sulfate as the whitening agent (non-hydroscopic as compared with the previous hygroscopic magnesium oxide deposit);

(c) precision-ground, optical glass envelope instead of the former blown-glass bulb;

(d) built-in temperature compensation for instrument sensitivity dependence upon ambient temperature.

The spectral response of this new model is similar to that of the later 10- and 50-junction type pyranometers since the reflectance of $BaSo_4$ is essentially identical to that of MgO over the solar range of wavelengths. The Schott WG7 glass used is usefully transparent from about 280 to 2800 nm. This hemispherical envelope has a weather-proof seal but is readily removable for instrument repair. Fig. 2 is a photograph of the pyranometer.

3. Long-wave Radiation Sensing

All pyrgeometers (long-wave radiometers) inherently measure the exchange of radiation between a horizontal blackened surface (i.e., the detector) and the target viewed (i.e. sky or ground, etc.). In the case of a net radiometer, the instrument can be so designed to eliminate (by differential means) the radiation emitted, both upwards and downwards, by the detector. The instrument described below is believed to be the first of its type where the detector flux is automatically compensated, allowing isolation of the radiation from the target impinging on the detector.

The Precision Infrared Radiometer is, therefore, a new Eppley development intended for the measurement of (unidirectional) incoming or outgoing long-wave terrestrial radiation. It is a modification of the Eppley Precision Spectral Pyranometer.

For the measurement of long-wave radiation in general, and for the isolation of this flux from the solar short-wave radiation in daytime, the glass hemisphere system has been replaced by a (30-mm diameter) hemisphere of silicon, which is cemented into a removable collar (with an O-ring seal) on the instrument case. On the inner surface of this envelope is a vacuum-deposited interference filter. The composite envelope transmission exhibits a sharp transition between about 3

and 4 μm. from complete opaqueness to maximum transparency, and (apart from the normal waviness associated with such interference patterns) a general transmittance of about 0.50 decreasing, with increasing wavelength, to 0.30-0.40 around 50 μm. Tests have demonstrated that this coated hemisphere does not exhibit significant transmission of sunlight; absorption and re-emission effects are small and have been determined. The pyrgeometer is shown in Fig. 3.

A thermistor-battery-resistance circuit (in addition to that employed for temperature compensation of radiometer response) is incorporated to precisely compensate for detector temperature. The basis of this innovation is that since the signal out of the pyranometer (when used for the measurement of infrared radiation) is representative of net radiation flux at the receiver surface,

$$R_{net} = (R_{in}-R_{out}),$$

then R_{in} can be directly measured if the portion of the signal due to R_{out} can be removed. And because

$$R_{in} = R_{net} + R_{out}$$

(and R_{out} is essentially dependent on the temperature of the receiver) a voltage, controlled by a thermistor which senses receiver temperature continuously, can be introduced (added) between the thermopile output and the measuring device. The circuit is simple, although choice of the correct thermistor is essential. It consists of the thermistor, a shunt resistor, a series resistor, a variable resistor (across which the equivalent R_{out} voltage is sensed) and a 1.35V battery. The variable resistor is used to match thermopile sensitivity. The electrical circuit arrangements are shown in Fig. 4 (which also indicates the means for checking thermopile and battery outputs).

4. Calibration of Radiation Sensors

The radiometeric references and techniques are different for the two types of radiometer. At Newport, calibration of short-wave pyranometers is with respect to the World Radiation Reference (WRR) while long-wave pyrgeometers are basically referred to blackbody sources. As of April 1, 1977, the calibration traceability of Eppley pyranometer and pyrheliometer instruments has been changed from the International Pyrheliometric Scale of 1956 (IPS 1956) to the Absolute Scale (SI). This change based on the results of IPC IV is such that instruments calibrated in SI units yield irradiance values which are 2.1% higher than values which would be obtained using Eppley instruments calibrated previously and referenced to IPS.

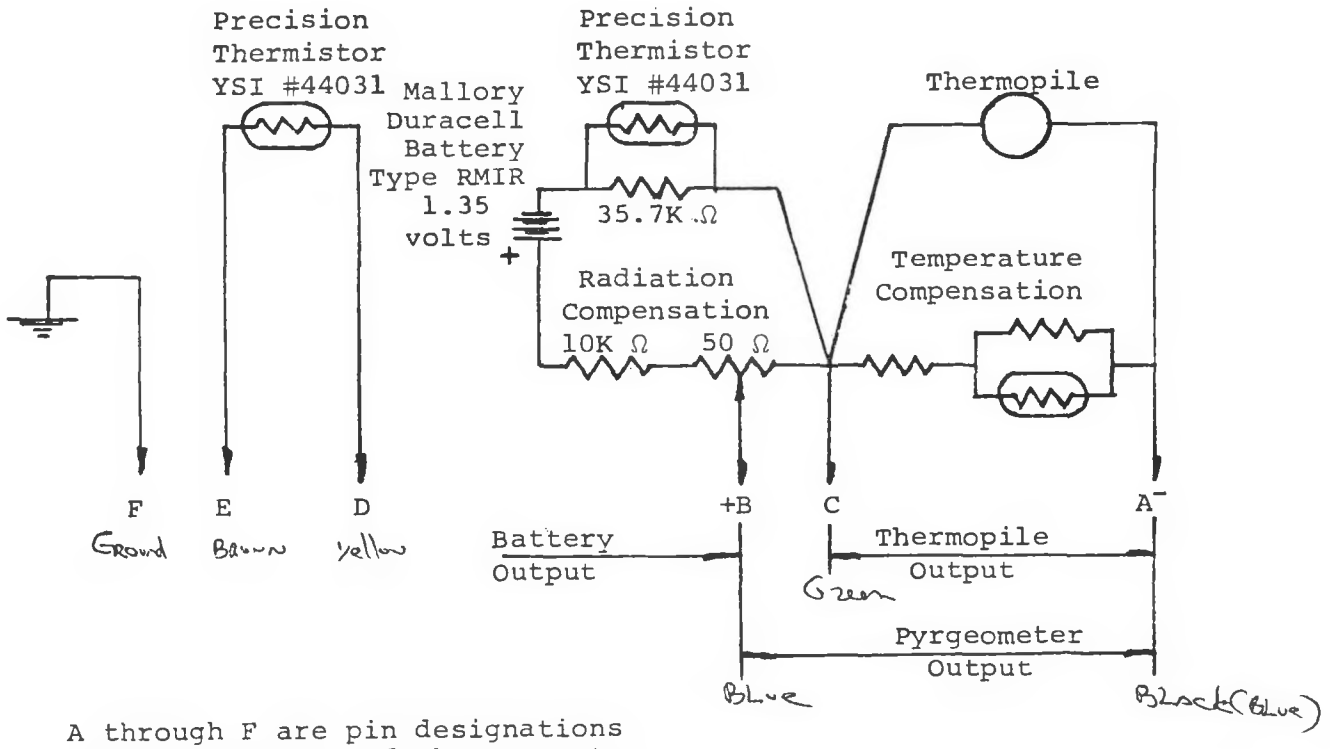

A through F are pin designations on both portions of the connector.

Fig. 4. Schematic for elimination the effect of detector temperature on the measurement of infrared radiation fluxes (including temperature compensation circuit and connections for checking thermopile and battery outputs)

BLACK(BLUE) - A
BLUE - B
GREEN - C
YELLOW - D
BROWN - E
GROUND - F

(a) Short-wave Pyranometers

These are normally calibrated by exposure in an integrating hemisphere (artificial sky) where the diffuse radiation, at a flux level of approximately 1.0 cal cm^{-2} min^{-1}, is produced by a series of tungsten-filament lamps totalling about 5 KVA in power. By means of water cooling the walls of the chamber and refrigerating the air inside, the ambient temperature is maintained close to +25°C. For a description of the system and the calibrating techniques, reference should be made to Eppley Reprint No. 30. The comparison reference is a working standard pyranometer calibrated, in sunlight, against the Eppley group of primary electrical compensation pyrheliometers which, in collaboration with similar standards in the National Weather Service (NOAA), maintain and reproduce the World Radiation Reference (WRR) for the United States. The calibration of the above-mentioned working standard pyranometer comprises a comparison between the difference in pyranometer voltage output, when alternately exposed to the global sun and sky radiation and (by shading the sun) the diffuse sky radiation alone, and one of the standard pyrheliometers sensing, simultaneously, only the direct solar radiation. In this condition, the comparison is represented through the relationship $T - D = I \sin h$, where T and D are, respectively, the voltage equivalents of the total sun and sky (global) and the diffuse sky radiations, I is the direct solar radiation measured, in energy units, at normal incidence and h is the mean solar height. Essentially, the comparison is one of the vertical component of direct solar radiation.

In routine operation, in the field, there are two ways whereby short-wave global pyranometers can be checked for constancy of instrument sensitivity. The first is to preserve a similar (calibrated) pyranometer for this purpose and occasionally (e.g. once per year) compare it with the field instruments, side by side in sunlight, ideally on cloudless occasions. The second is to repeat the basic pyranometer type radiometric calibration using either a pyrheliometer or a thermopile-type derived standard (e.g. the Eppley normal incidence pyrheliometer.

Newport calibrations of the Precision Spectral Pyranometer reproduce the WRR to within ±1 per cent in general. The corresponding figure for the Black and White Pyranometer is ±2 per cent.

Whenever the radiometer is employed as a spectral pyranometer, the instrument sensitivity indicated in the relevant calibration

certificate and engraved on the name plate can be adopted for all practical purposes. This value is established by exposure of the pyranometer with both clear glass hemispheres in position during the calibration operation. However, there can be small differences in the general transmission characteristics of the several glasses (as shown by the relevant factors supplied with the filter hemispheres). Typical values are given in Table 1. If it is desired to apply such correction, the procedure is straightforward, viz. pyranometer sensitivity (for RG2 filter in position) = calibration value x 1.10/1.11.

(b) Long-wave Pyrgeometers

The fundamental calibration of detectors intended for the measurement of terrestrial long-wave radiation is based upon their exposure to an ideal blackbody radiator. However, in practice, the alternate method of comparison against a (blackbody) calibrated working standard pyrgeometer, preferably of similar type, may be employed solely or as a check on the more difficult direct blackbody calibration. In this instance, a good source of steady long-wave radiance, for pyrgeometer exposure, is a cloudless night sky. In the Eppley Laboratory, both approaches are adopted. The reference blackbody is a low-temperature (50 to 80°C) source which has a circular opening of about 10 cm in diameter and is temperature stabilized by circulating oil. Temperature is measured with a series of strategically located calibrated thermocouples. The reference detectors are (a) Eppley pyrgeometer (new thermopile model, as described in Section 3 above), (b) Ångström electrical compensation pyrgeometer (without filtering window); this working standard (a) is first calibrated basically against Eppley Laboratory blackbodies and against the Ångström pyrgeometer using either artificial or natural sources. The production model is then compared to working standard (a).

5. Installation, Operation and Maintenance of Radiation Sensors

(a) Installation

The site for an upward-looking pyranometer or pyrgeometer should be free from any significant obstructions above the plane of the sensing element and, at the same time, should be readily accessible. If it is impracticable to obtain such an exposure, the site selected must be as free from obstructions (artificial as well as natural) as possible, especially (in the N. Hemisphere) from east-northeast, through south, to west-northwest and (in the S. Hemisphere) from east-southeast, through north, to west-southwest. If

THE EPPLEY LABORATORY, INC.

Representative values for the transmittance of Schott filter glass (2.0 mm thickness, +25°C)

λ nm	New Old	WG295 WG7	GG395 GG22	GG400 ___	GG495 GG14	OG530 OG1	OG570 OG2	RG610 RG1	RG630 RG2	RG695 RG8	RG715 RG10	RG805+ ___
270		0.22	0.00	0.00	0.00	0.00	0.00	0.00	0.00	0.00	0.00	0.00
80		.41										
90		.60										
300		.74										
20		.83										
40		.90	.00									
60		.91	.01	.00								
80		.91	.31	.01								
400		.91	.68	.52								
20		.91	.82	.78								
40		.91	.87	.83	.00							
60		.92	.88	.87	.01							
80		.92	.88	.89	.27							
500		.92	.89	.90	.80	.00						
20		.92	.90	.90	.88	.05						
40		.92	.90	.90	.90	.76	.00					
60		.92	.90	.90	.90	.88	.38					
80		.92	.90	.90	.91	.90	.83	.00				
600		.92	.90	.90	.91	.91	.89	.33	.00			
20		.92	.90	.90	.91	.91	.91	.83	.26			
40		.92	.90	.90	.91	.91	.91	.89	.85			
60		.92	.90	.91	.91	.91	.91	.90	.91	.00	.00	
80		.92	.90	.91	.91	.91	.91	.91	.91	.27	.01	
700		0.92	0.90	0.91	0.91	0.91	0.91	0.91	0.91	0.84	0.25	0.00

+RG805 standard thickness is 4.0 mm.

λ nm	New / Old	WG295 WG7	GG395 GG22	GG400 ——	GG495 GG14	OG530 OG1	OG570 OG2	RG610 RG1	RG630 RG2	RG695 RG8	RG715 RG10	RG805+ ——
720		0.92	0.90	0.91	0.91	0.91	0.91	0.91	0.91	0.91	0.74	0.00
40		.92	.90	.91	.91	.91	.91	.91	.92	.92	.89	.00
60		.92	.90	.91	.91	.92	.91	.91	.92	.92	.91	.02
80		.92	.90	.91	.91	.92	.91	.91	.92	.92	.92	.09
800		.92	.90	.91	.91	.92	.91	.91	.92	.92	.92	.34
20		.92	.90	.91	.91	.92	.91	.91	.92	.92	.92	.68
40		.92	.90	.91	.91	.92	.91	.91	.92	.92	.92	.84
60		.92	.90	.91	.91	.92	.91	.91	.92	.92	.92	.88
80		.92	.90	.91	.91	.92	.91	.91	.92	.92	.92	.89
900		.92	.90	.91	.91	.92	.91	.91	.92	.92	.92	.89
1000		.92	.90	.91	.91	.92	.91	.91	.92	.92	.92	.90
1200		.92	.90	.91	.91	.92	.91	.91	.92	.92	.92	.90
1500		.92	.90	.91	.91	.92	.91	.91	.92	.92	.92	.90
2000		.91	.89	.90	.90	.90	.90	.91	.91	.91	.91	.88
2500		0.85	0.86	0.85	0.85	0.87	0.86	0.87	0.87	0.87	0.87	0.82
Center of cutoff (nm)		281	385	397	485	529	562	603	623	686	707	807
Filter factor		1.09	1.11	1.10_5	1.10	1.09_5	1.09_5	1.10_5	1.09_5	1.09	1.09	1.11

N.B. Variation from these values of transmittance of up to +0.01 and of center of cutoff of up to +2 nm can occur within the glass melt.

practicable, the instrument should be so located that (a) a shadow will not be cast on it at any time (e.g. by radio masts, etc.); (b) it is not close to light-colored walls or other objects likely to reflect sunlight onto it; and (c) it is not exposed to artificial radiation sources.

At most places, a flat roof provides the best location for mounting the instrument; if such a site cannot be obtained, a rigid stand with a horizontal upper surface some distance from building structures or other obstructions should be used.

On the initial installation of the instrument, or whenever its location is changed or if a significant change occurs in regard to any surrounding obstructions, the angular elevation above the plane of the receiving surface of the pyranometer (or upward-looking pyrgeometer) and the angular range in azimuth of all obstructions throughout the full 360° around it should be observed. If it is at all possible, the site should be so chosen that any obstruction over the azimuth range between earliest sunrise and latest sunset should have an elevation not exceeding 5°. It is also useful, for reference purposes, to note the altitude above M.S.L. of the detector and its geographical co-ordinates.

In the case of a downward-looking pyranometer or pyrgeometer, for the measurement of outgoing radiation fluxes, the principal requirement is similar, viz. that the lower hemisphere be viewed as fully as possible. This may entail mounting the instrument at the end of a long boom, so that the vertical support causes minimum obstruction to the instrument receiver.

The pyranometer or pyrgeometer should be securely attached to whatever mounting stand is decided upon, using the holes provided in the instrument baseplate and, at the same time, levelling it with the adjustable feet. Precautions should be taken to avoid subjecting the instrument to shocks or vibration during installation. The stand should be sufficiently rigid that severe shocks to the instrument do not occur or, throughout operation, the horizontal position of the receiving surface does not change, especially during high winds.

The cable employed to connect the pyranometer or pyrgeometer with the respective readout should be twin conductor (No. 20 wire is generally used at the Eppley Laboratory) and waterproofed. If there is the possibility of electrical interference (e.g. from power lines or radio transmissions), the cable should also be screened. It

should be firmly secured to the mounting stand to minimize breakage and intermittent contacts in windy weather. Wherever possible, the cable should be run either along or under the surface to the readout, especially if the latter is to be located at some distance. High overhead connections should be avoided, particularly in areas of severe thunderstorm activity. When potentiometric recorders are employed cable lengths of 1000 feet or more may be used without impairing the quality of the records. As with other types of thermoelectric radiometer, care must be exercised to obtain a permanent (soldered) copper-to-copper junction between instrument connector and cable. All junctions exposed out of doors must be weatherproofed. On all standard Eppley instruments, Pin B is positive and Pin A negative.

(b) Operation

In the case of the pyranometer, there are two main requirements: viz. (a) periodic verification of pyranometer calibration, and (b) application of corrections, where judged necessary, to take account of instrument obstruction to a free horizon.

Calibration constancy should be checked at least once per year, if the highest measurement accuracy is desired.

With regard to significant correction (see below) for general horizon obstruction (as distinct from the simpler and obvious correction for obstruction to the solar beam), the procedure is to separate out the diffuse radiation (by measurement or estimation), correct it and then adjust the total short-wave (global) radiation accordingly. In this connection, however, it must be pointed out that it is the fraction of the vertical component of the short-wave flux from the sky, lost by obstruction, which is to be computed and not the fraction of sky so obscured. It will hence be apparent that radiation incident at angles less than 5° to the horizon has only an extremely small contribution to make to the total. For example, it may be demonstrated (see below) that a horizon limited by a continuous circular obstruction with an average elevation of 5° diminishes the diffuse (vertical) flux by only about 1 per cent, and such an effect can normally be neglected. Strictly, in determining corrections of this nature, account should be taken of the variation in intensity of the diffuse radiation over the hemisphere of sky which, of course, depends upon the sky conditions at the time. The only

practical procedure is to assume isotropy. For determining these corrections for objects of finite size, the following expression is applicable.

$$\frac{1}{2\pi}\int_{\theta}\int_{\psi}\sin 2\theta \, d\theta \, d\psi$$

Here, θ and ψ are the elevation and azimuth of the object, respectively; an elementary area with these co-ordinates will contribute a fraction $\sin\theta\cos\theta \, d\theta \, d\psi/\pi$ to the vertical flux. The outlines of the obscuring objects should be mapped out on a $\theta - \psi$ diagram and these projections then divided into suitable component areas over which a mean value of $\sin 2\theta$ may be assigned, and the fractional correction obtained by summation. Since the formula is exactly valid only for obstructions with a completely black surface, the effect of the albedo of lighter colored objects will be to reduce the magnitude of the correction, through inwards reflection (and may even yield a correction of opposite sign).

In the case of the pyrgeometer, there are two main requirements, viz. (a) periodic verification of pyrgeometer calibration, it is suggested this be done yearly against a blackbody or returned to Eppley, (b) periodic testing of compensation circuit (battery) stability.

To check calibration of compensation circuit, measure across pins E & D to obtain the temperature of the instruments, express it in absolute terms (T_1). Measure millivolt output across pins B & C (mv). S equals sensitivity of instrument expressed in mv/cal, cm^{-2} $min.^{-1}$ Stefan-Boltzmann Constant = 8.124×10^{-11} cal cm^{-2} deg^{-4} min^{-1}. Then $T_1^4 \ (8.124 \times 10^{-11}) = \frac{mv}{S}$. The millivolt output can be adjusted with the small pot inside the instrument (take bottom off, the battery life, in this operation, is believed to be at least one year).

With regard to correcting for obstructions, this is much simplier than for the pyranometer since the radiation measured is essentially diffuse. The same error limitation and corrective computational procedure, detailed above, is theoretically applicable. But, it is not possible to separate long-wave emission from long-wave reflection by pyrgeometer obscuring objects and, therefore, it is recommended that, in general, such correction here should either be ignored or only attempted on the basis of specific experimental investigation (e.g. comparison of simultaneous results at different locations).

The aforegoing also applies to both pyranometer and pyrgeometer, when they are exposed in the inverted position.

c) Maintenance

Pyranometers and pyrgeometers in continuous operation should be inspected, ideally, at least once per day. At these inspections, the (outer) hemisphere should be wiped clean and dry with a lint-free soft cloth. In desert or arid regions, the hemisphere should be cleaned very gently in order to prevent scratching of the surface. Such abrasive action can alter appreciably the original transmission properties of the material and, hence, the radiometer calibration. If frozen snow, glazed ice, hoar frost or rime is present, an attempt should be made to remove, at least temporarily, the deposit carefully with warmed cloths.

With regard to the two models of pyranometer, should the internal surface of the (outer) hemisphere become coated with moisture, it can be cleaned by careful removal on a dry day, allowing the air to evaporate the moisture and then firmly re-securing the hemisphere. The inside of the hemisphere should not be wiped unless smears are visible. Precautions should be taken to avoid scratching the undersurface of the collar carrying this hemisphere. In the case of the precision spectral pyranometer, the external surface of the inner hemisphere can also be cleaned, if necessary, when the large one is removed. Should moisture be deposited on the inside of the small hemisphere, this can similarly be removed. However, in this instance, and also with removal of the single hemispherical envelope of the black and white model, extreme care must be exercised since the thermopile element is now unprotected and could be seriously damaged.

Occasionally, the desiccator installed in the pyranometer case should be inspected. Whenever the silica gel drying agent is pinkish or white in color, it should be replaced (N.B. silica gel can be rejuvenated by drying in an oven at about 135°C for a few hours, until the original dark blue color reappears).

The circular spirit level of the pyranometer or pyrgeometer should be inspected at regular intervals.

With regard to the pyrgeometer, the same maintenance procedures are applicable. The hemisphere should only be removed when calibration verification indicates that the results are suspect; in this instance, the interference filter (vacuum) deposited on the internal surface of the hemisphere must never be touched.

EPPLEY PRECISION INFARED RADIOMETER (PYRGEOMETER)

Model PIR

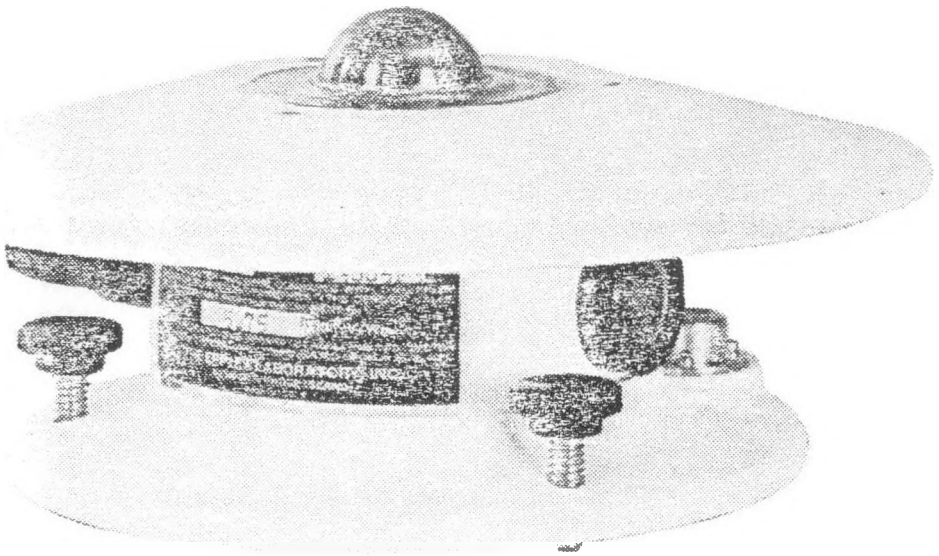

INSTRUMENT CHARACTERISTICS

Sensitivity	6 microvolts/watt meter^{-2} approx.
Impedance	700 ohms approx.
Temperature dependance	±2 per cent, -20 to 40°C (nominal):
Linearity	± 1 per cent, 0 to 700 watts m^{-2}
Response time	2 seconds (i/e signal);
Cosine response	better than 5 per cent from normalization, insignificant for a diffuse source;
Orientation	no effect on instrument performance;
Mechanical vibration	capable of withstanding up to 20 g's;
Calibration	blackbody reference.

Fig. 3

EPPLEY BLACK AND WHITE PYRANOMETER

Model 8-48

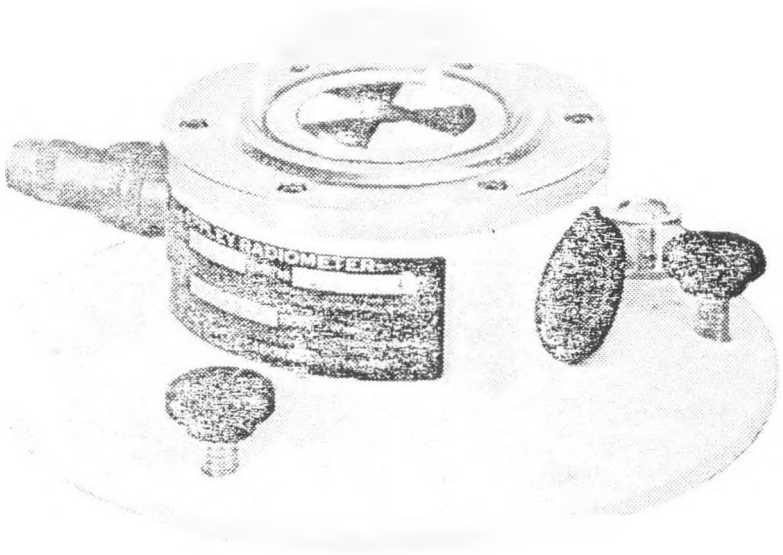

INSTRUMENT CHARACTERISTICS

Sensitivity	11 microvolts/watt meter^{-2} approx.
Impedance	350 ohms approx.
Temperature dependance	± 1.5 per cent constancy from -20 to +40° C
Linearity	± 1 per cent from 0 to 1400 watts meter^{-2}
Response time	3 to 4 seconds (i/e signal)
Cosine response	± 2 per cent from normalization 0-70° zenith angle, ± 5 per cent 70-80° zenith angle
Orientation	no effect on instrument performance
Mechanical vibration	capable of withstanding up to 20 g's
Calibration	integrationg hemisphere (approx. 1 cal cm^{-2} min^{-1}, ambient temperature +25° C): calibration reference Eppley primary standard group of Angstrom Pyrheliometers reproducing the International Pyrheliometric Scale
Readout	potentiometric in preference to microammeter devices

Fig. 2

EPPLEY PRECISION PYRANOMETER

Model PSP

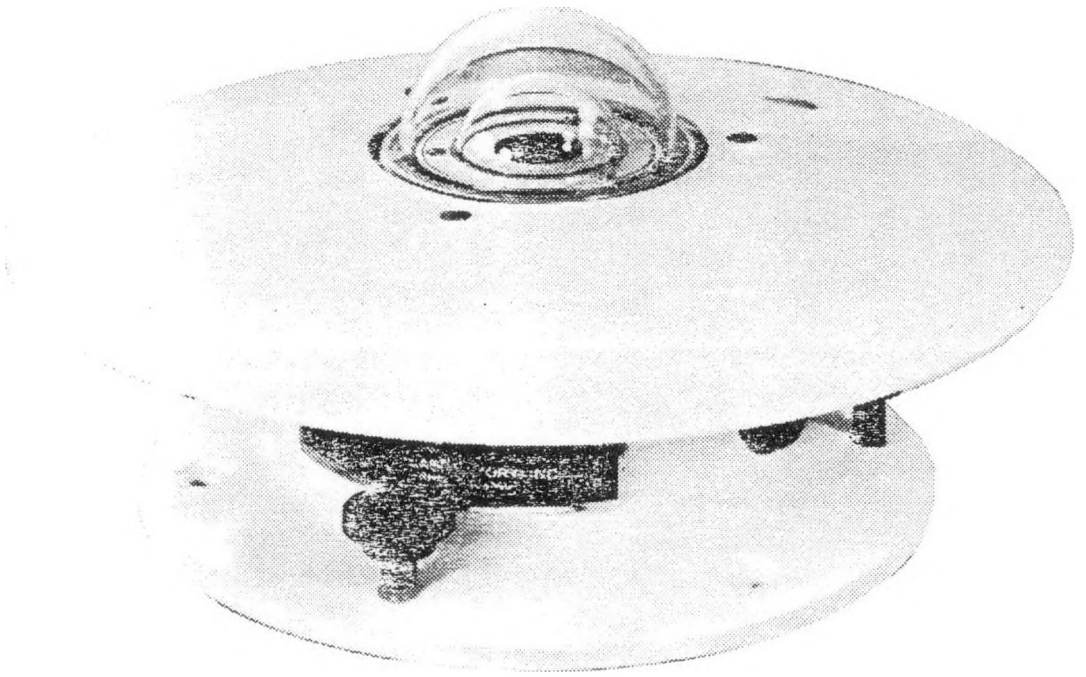

INSTRUMENT CHARACTERISTICS

Sensitivity	9 microvolts per watt meter^{-2} approx.
Impedance	650 ohms approx.
Receiver	circular 1 cm^{-2}, coated with Parsons' black optical lacquer
Temperature dependance	± 1 per cent over ambient temperature range -20 to +40°C (temperature compensation of sensitivity can be supplied over other ranges at additional charge
Linearity	± 0.5 per cent from 0 to 2800 watts m^{-2}
Response time	1 second (1/e signal)
Cosine	± 1 per cent from normalization 0-70° zenith angle ± 3 per cent 70-80° zenith angle
Orientation	no effect on instrument performance
Mechanical vibration	tested up to 20g's without damage
Calibration	integrating hemisphere (approx. 1 cal cm^{-2} min^{-1}, ambient temperature +25°C): calibration reference Eppley primary standard group of Angstrom pyrheliometers reproducing the International Pyrheliometric Scale
Readout	potentiometric in preference to microammeter devices

Fig. 1

Appendix H

Measuring Air Infiltration Using Tracer Dilution Method

Task VI
Appendix B

Measuring Air Infiltration in ERL Test Structures Using Tracer Dilution Method

Helen J. Kessler

A procedure for measuring air infiltration in the ERL Passive Cooling Experimental Facility test structures using Sulfur Hexaflouride (SF_6) tracer gas is discussed. The following sources have been used:

a. "Measuring Air Leakage by the Tracer Dilution Method," ASTM Standard E741, 1980.

b. Grot, R.A., "A Low-Cost Method for Measuring Air Infiltration Rates in a Large Sample of Dwellings," Building Air Change Rate and Infiltration Measurements, ASTM STP 719, C.M. Hunt, J.C. King and H.R. Trechsel, Eds., American Society for Testing and Materials, 1980, pp. 50-59.

c. David Harrje, Center for Environmental Studies, Princeton University.

A. Introduction of Gas into Test Structures

1. Before injecting the tracer gas into the space, the air should be well-mixed and a sample should be taken in order to measure the background level of SF_6 (if any).

2. Tracer gas SF_6 should be injected into each test structure, beginning with a concentration of 100-150 parts per billion (~100-150 ml of SF_6 per 1000 cu.m. of living space).

   Structure 1 - 24'x38'x10' = 9000 cu.ft. = 255 cu.m., use 38 ml SF_6
   Structure 2 - 18'x18'x8'x3 = 8000 cu.ft. = 227 cu.m., use 34 ml SF_6
   Structure 3 - 20'x48'x9' = 8640 cu.ft. = 245 cu.m., use 37 ml SF_6
   Data Acq. Bldg. - 15'x20'x10' = 3000 cu.ft. = 85 cu.m., use 11.3 ml SF_6

   Disposable 50.0 ml graduated syringes can be used. They should be filled far away from the test structures in case any SF_6 accidently leaks out. The syringe can be filled using tygon tubing fitted with a rubber septa. Caution must be taken not to apply too much pressure to the connections.

   To introduce the gas into the structures, slowly walk through the building, injecting amounts approximately proportional to the size of the rooms.

3. Thirty minutes to one hour should be allowed to establish equilibrium.

B. Structure Configurations to be Tested

1. Structure one should be tested in the following modes:

   a. outside vents in roof duct taped, door to solar/screen porch closed, recirculating fan off (summer and winter)

   b. same as above, but with recirculating fan on (nighttime test using radiating roof in summer)

   c. solar/screen porch by itself (winter)

   An oscillating fan should be used at opposite ends of the structure to mix the air (one in the large south room and one in the northeast room).

2. Structure two should be tested in the following modes:

   a. with the de-stratification fan on (winter and summer)

   b. with the de-stratification fan off (summer)

   An oscillating fan should be used on all three levels during both winter and summer testing. It also would be useful to test structure two before and after the windows have been insulated and taped.

3. Structure three should be tested in the following modes:

   a. attic fan circulation system on

   b. attic fan system off, house totally sealed from attic (including Up-Dux)

   An oscillating fan should be used at opposite ends of the structure to mix the air (one in the area in front of the solar collector and one in the northeast "room").

4. The Data Acquisition Building should be tested in the following modes:

   a. with just an oscillating fan to mix the air

   b. with the air conditioner to mix the air. This may help determine any absorption or adsorption of SF_6 by the air conditioner.

All interior doors, cabinets, closets, etc. should be opened inside all the buildings to allow for free movement of air. (All tests will need to be repeated at various wind speeds.)

C. Sampling Locations and Methods, Analysis of Samples

1. After the tracer gas has been well mixed, initial samples are taken. Suggested locations include:

   Structure 1 - living room, northeast bedroom (14-samples)
   Structure 2 - center of each floor (21-samples)
   Structure 3 - northeast corner and in area adjacent to Clearview Solar Collector (14-samples)
   Data Acquisition Building - center of room (7-samples)

   Samples can be taken in the following ways. (We will use method a.)

   a. Five (5.0) ml polypropylene syringes can be used to take samples at the locations enumerated above in each building. This method has been used by Subrato Chandra at the Florida Solar Energy Center. Plastic valves may be used to seal the syringes.

   b. 500 ml "squeeze bottles" can be filled either by squeezing enough times to almost fill the bottle or by pumping air from the structure into the bottle with a small hand-held battery operated pump. One bottle can be used in each general location. The use of the squeeze bottle was suggested by David Harrje at Princeton University. He also suggests that the cap be modified with a rubber gasket for a better seal. Several samples may be taken from the bottle for testing and once testing is completed, the bottle may be re-used.

   c. Approximately 10 litre air sample bags can be filled by walking through the house and pumping air into the bag. Since this should provide a well-integrated sample, only one sample bag per floor is needed. Structure 2 may only need one bag per collection time as well, but for the first tests, it would be preferable to test each floor. This method has been used by the National Bureau of Standards as a low cost, essentially one shot sampling system.

   (It was recommended by suppliers of SF_6 that we not use chlorinated or fluorinated plastics.)

2. The amount of gas in the air is then allowed to decay over a period of one to two hours. Samples should be taken over a period of at least one hour. (It is assumed that the person taking the samples will remain in the building and no doors or windows will be opened during the test period).

3. Samples will be taken with the syringes at each location every 20 minutes over a period of two hours. Thus a total of seven syringes for each location will be needed. For the large sample bag, only one additional sample, about 1-2 hours after the initial sample, needs to be taken.

4. Concentrations of SF_6 in the air sample will be analyzed by gas chromatography using an electron capture detector. According to the ASTM Standard, the gas analyzer needs to be calibrated--either by the manufacturer or by using standard mixtures of at least two different concentrations in the range anticipated in the actual test. Standards (calibrated gas) are available from Scott Marin, 2001 3rd St., Riverside, CA 93656 (714) 784-1241.

D. Calculation of Infiltration Rates

1. Air infiltration is then calculated from the results of the above analysis. The calculation methods depend in part on the sampling system used. The following assumptions have to be made in order to simplify the calculations:

   a. that mixing throughout the area tested is uniform and

   b. that the outdoor concentration of tracer gas and the rate per unit volume of production (or absorption) of the tracer gas inside the building is negligible.

2. Several calculation methods are described in the enclosed method ASTM E741. Since we are using the 5.0 ml syringes for taking samples every 20 minutes, the graphical method would be an appropriate calculation method.

   a. Graphical Method (from ASTM E741) Plot the natural logarithm of concentration on a linear scale against time in hours on a linear scale. The measurements should fall on a straight line with time, provided the air change rate remains fairly constant. Some scatter of points is expected and a straight line may have to be determined by the method of least squares, or other appropriate methods. A minimum of three points over one hour should be used to determine this straight line.

   On the straight line determined above, pick two points with coordinates (C_1, t_1) and (C_2, t_2) where C_i is the concentration in parts per billion at time i in hours. Calculate I, the air change rate, as follows:

$$I \quad \frac{\text{air changes}}{\text{hour}} = \frac{\ln C_1 - \ln C_2}{t_2 - t_1}$$

   This technique is illustrated in Fig. 3 of the ASTM Standard.

   This method lends itself quite nicely to field study of the data, since one can easily plot the log of concentration as a function of time. It is less sensitive to errors in concentration than other methods. It has the further advantage that a graph provides a visual display of any departures from

the exponential decay law. As long as the data fall on a reasonably straight line, one has confidence that the data obtained are valid within the assumptions necessary for the validity of the tracer dilution method. One caveat that should be observed during any measurement interval is that the data points used in determining the air leakage rate should encompass the mean winds observed during the course of the measurement.

b. The basic equation for determining air infiltration is as follows and would be used directly if we were taking only two measurements and using the sample bag method:

$$I = \frac{1}{\Delta t} \ln (C_1/C_2)$$

where C_1 and C_2 are the initial and final tracer gas concentration, respectively and Δt is the interval between filling the sample bags.

Wind speed and indoor and outdoor temperatures will be measured at the same time samples are being taken since air infiltration and wind speed are closely related. In order to take wind into account, the procedure will be completed during at least two different days with different wind speed factors.

E. Major Items That Will Need to be Purchased (or Have Been Purchased)

1. 50.0 ml syringes - for injecting SF_6 into building
2. 5.0 ml syringes - for taking samples
3. plastic valves to seal syringes
4. oscillating fans
5. column for gas chromagraph
6. SF_6 gas

Designation: E 741 – 80

Standard Practice for MEASURING AIR LEAKAGE RATE BY THE TRACER DILUTION METHOD[1]

This standard is issued under the fixed designation E 741, the number immediately following the designation indicates the year of original adoption or, in the case of revision, the year of last revision. A number in parentheses indicates the year of last reapproval.

1. Scope

1.1 This practice describes a standardized technique for measuring air change rate in buildings under natural meteorological conditions by tracer gas dilution.

1.2 This practice shall not be used to determine the individual contribution of various building components to the air change rates of a building.

1.3 This is a practice that requires a knowledge of the principles of gas analysis and instrumentation.

1.4 The current state of the art does not possess analytical techniques to extrapolate precisely measured air change rates to meteorological conditions different from those prevailing during measurement.

2. Summary of Practice

2.1 A small amount of tracer gas is introduced into a structure, thoroughly mixed, and the rate of change (decay) in tracer concentration is measured. The air change rate can be determined from the decay rate of tracer concentration with respect to time. On-site meteorological conditions are measured concurrently.

3. Significance

3.1 Air leakage accounts for a significant portion of the thermal space conditioning load; it can introduce outdoor air contaminants in conditioned indoor air, and it can dilute indoor-generated contaminants, thus detracting from or providing for occupant comfort.

3.2 Air leakage rates are difficult to predict analytically because they are functions of building tightness and configuration, inside-outside temperature differences, wind speed and direction, quality of workmanship in construction, and numerous other factors.

3.3 This practice allows measurements of air leakage rates. In applying the results of this practice to the design of buildings, it should be borne in mind that the air leakage characteristics of a structure are affected by building operation, maintenance, and the resistance of the building components to deterioration.

3.4 The air leakage rate of a building is hard to quantify, as it depends on so many variables. The most direct way is to measure it under the field conditions. The tracer dilution method has been proven to be an effective way of measuring the air leakage rate. The fan pressurization method provides an indirect way to relate the air leakage rate or air tightness to the leakage area of a structure.

3.5 The fan pressurization method has several differences from the tracer dilution method. It can be used to compare the relative air tightness of several buildings. It can be used to identify the leakage source and rate of leakage from different components of the same building envelope. It can be used to determine the air leakage reduction for individual retrofit measures applied incrementally to an existing building.

3.6 When the absolute air leakage rate is needed, the tracer dilution method should be used over a wide range of wind velocities and indoor and outdoor temperature differences. However, the measuring equipment and techniques are relatively complicated for the tracer dilution method, and the data analysis and correlation are more involved. It is best to use the fan pressurization method for diagnostic purposes and resolve the absolute air leakage rate with the tracer dilution method.

4. Descriptions of Terms

4.1 *air leakage rate*—the volume of air movement per unit time, in this specific sense, across the boundary of the building envelope. This movement includes flow through joints, cracks, and porous surfaces, or both.

4.2 *infiltration*—air leakage rate into a building space.

4.3 *exfiltration*—air leakage rate from a building space.

4.4 *air change rate*—air leakage rate in volume units per hour divided by the building space volume with identical volume units (normally expressed in air changes per hour, ACH or ACPH).

4.5 *tracer gas*—a gas that can be mixed with air and measured in very small concentrations, making it possible to detect air movements and measure air change rates.

4.6 *building space*—the volume of a building that exchanges air with outside ambient air. In most cases, this volume is the deliberately conditioned space within a building, generally not including the attic space, basement space, and attached structures, unless such spaces are connected to the heating and air conditioning system, as a crawl space plenum.

4.7 *building envelope*—the exterior shell enclosing the interior space.

5. Apparatus

5.1 The description of apparatus in this section is general in nature and any equipment capable of performing the test measurements within the allowable tolerances is permitted. An appendix is provided which documents both tracer gases and their measurement instrumentation which have been used in tracer dilution studies.

5.2 *Major Components:*

5.2.1 *Tracer Gas Monitor*—A device to measure whichever tracer gas is used in the study.

5.2.2 *Sampling Network*—A network consisting of tubing, tubing junctions, a pump, and possibly an aspirator. This network is used to draw samples from remote locations within a structure, blend them, and bring the blended sample to a convenient place for analysis. In general, it is best to avoid plasticized tubing such as vinyl and use copper, stainless steel, or possibly polypropylene or nylon. The experimenter should be aware that surface absorption within the sampling network can be a major source of confusion in any concentration decay measurement.

5.2.3 *Syringes*—Usually disposable syringes are used to inject gas samples when the trace gas monitor is a gas chromatograph.

5.2.4 *Circulating Fans*—Fans are used to circulate air within a structure. They should be capable of circulating air over 360°. Oscillating or hassock fans are preferred.

5.2.5 *Meteorology Stations*—A portable meteorology station that records wind speed and direction, outside temperature, and, if available, relative humidity, is used to obtain on-site meteorological data.

5.2.6 *Barometer*—A device to measure local barometric pressure is required. If one is not available, barometric pressure from the nearest weather station is obtained for the time during which measurements are performed. These data are corrected for any elevation difference between the weather station and the test structure.

5.2.7 *Tracer Gas*—A cylinder or container of gas chosen from among those listed in the appendix is necessary as a source of the trace gas used in the test.

6. Safety Precautions

6.1 The maximum allowable concentration in air for each of the tracer gases that have been used for tracer dilution air leakage measurements is provided in the appendix. Under no circumstances should this concentration be exceeded. Good experimental practice is to ensure that the maximum allowable concentration of the particular tracer is less than this maximum by at least a factor of four. *Under no circumstances should the initial tracer gas concentration exceed the OSHA time-weighted average for substances included in the latest OSHA-controlled gases list.*

[1] This practice is under the jurisdiction of ASTM Committee E-6 on Performance of Building Constructions and is the direct responsibility of Subcommittee E 06.41 on Infiltration Performances.

Current edition approved August 29, 1980. Published October 1980.

7. Procedure

7.1 The assumption underlying the tracer gas measurement of air change rate is that for perfect mixing with steady air flow, the loss rate of tracer gas concentration conforms to the exponential dilution law, that is, the loss rate on dilution of an escaping gas is proportional to its concentration. Mathematically, this assumption leads to Eq 1. A detailed derivation and discussion of this equation are contained in Footnotes D and G to Table A1.1.

$$C = C_0 e^{-It} \quad (1)$$

where:

C = tracer gas concentration at time t,
C_0 = tracer gas concentration at time = 0,
I = air change rate, and
t = time.

7.2 *Injection and Mixing of Tracer Gas*—At one or more points in the test structure, release an amount of tracer gas sufficient to produce an easily discernible response in the gas-measuring instrument. The location of release is governed by the location of air handling system(s) or mixing fans in a structure with no air-handling system. This release can be done with a disposable syringe filled with tracer gas.

7.3 In a building with central heating and air conditioning system(s), the main fan(s) is operated continuously. Introduce tracer gas into the main supply or return duct(s) preferably in the vicinity of the main fan(s).

7.4 Leaks in the ductwork system may produce an incremental increase in the air leakage rate. There are two methods to assess this leakage. (See 7.4.1 and 7.4.2 below.)

7.4.1 After beginning a test, as in 7.3, operate the main fan(s) only for initial mixing and shortly before sampling.

7.4.2 Use portable fans for mixing after initiating a test as in 7.3. Perform the remainder of the test as in 7.5.

7.4.3 Comparison of the air leakage determined by 7.4.1 or 7.4.2 and 7.3 indicates the leakage due to ductwork.

7.5 In a building without central heating and air conditioning system(s), release tracer gas at one or more points within the structure. Use fans to circulate the air and mix the gas. Take care not to affect the pressure distribution within the structure. Open all doors connecting contiguous living spaces.

8. Sampling

8.1 Before taking gas samples, allow at least 30 min for mixing.

8.2 To test for homogeneity in tracer gas concentration, take samples from a number of building spaces. When concentrations differ by less than 5 % of the average concentration measured within the structure, begin monitoring the decay of tracer concentration. In a residential structure, two or more samples from widely separated locations are required. In multistory structures, two widely separated samples per floor are required.

8.3 Tracer samples may be measured at a single central location by taking individual samples (grab samples) at a number of distinct locations, or by drawing samples from a number of locations through a common network (multipoint sampling).

8.3.1 When multipoint sampling is used, place sensors at strategic points within the test structure and feed to a central measuring terminal. For methods that analyze air with a single measurement device, use a sampling network to bring blended air samples to the analyzer. A diagram of a sampling network and a sampling junction is given in Figs. 1 and 2. Note that if the dilution rate in different rooms or floors is different, samples drawn by this method yield air leakage rates slightly less than the true average rate. For example, if one of the rooms or floors is leaking air at twice the rate of the other (1 ACPH and 0.5 ACPH), analysis of the blended samples of the two will lead to an air leakage rate estimate about 4 % lower than the true average rate.

9. Calibration

9.1 State the method of calibration of the gas analyzer. If the analyzer is not provided with a manufacturer's calibration, perform an on-site calibration. Use standard mixtures of at least two different concentrations in the range anticipated in an actual test.

10. Calculation

10.1 Rearrange Eq 1 as follows:

$$I = \frac{1}{t} \ln \frac{C_0}{C} \quad (2)$$

where:

C = measured time-dependent concentration,
C_0 = concentration at $t = 0$,
I = air change rate, and
t = time.

Equation 2 is the starting point for several means of calculating air change rate from concentration and time measurements.

10.2 *Graphical Method*—Plot the natural logarithm of concentration on a linear scale against time in hours on a linear scale. The measurements should fall on a straight line with time, provided the air change rate remains constant. Scatter of points is expected and a straight line may have to be faired in the "best fit" sense. A minimum of three points over 1 h should be used to determine this straight line.

10.2.1 On the straight line determined in 10.2, pick two points with coordinates (C_1, t_1) and (C_2, t_2) where C_i is the concentration at time i. Calculate I, the air change rate, as follows:

$$I = \frac{\ln C_2 - \ln C_1}{t_2 - t_1} \quad (3)$$

This technique is illustrated in Fig. 3.

10.2.2 This method lends itself quite nicely to field study of the data, since one can easily plot the log of concentration as a function of time. It is less sensitive to errors in concentration than other methods. It has the further advantage that a graph provides a visual display of any departures in the exponential decay law. So long as the data fall on a reasonably straight line, one has confidence that the data obtained are valid within the assumptions necessary for the validity of the tracer dilution method. One *caveat* that should be observed during any measurement interval is that the data points used in determining in air leakage rate should encompass the mean winds observed during the course of the measurement.

10.2.3 When many data points are obtained, a least-square computer program is used to calculate a best fit to the straight line.

10.3 *Finite Difference Method*—Calculate the air change rate after each sampling using the finite difference form of Eq 2, as follows:

$$I = \frac{L}{V} = \frac{1}{(t_{i+1} - t_i)} \ln \frac{C_i}{C_{i+1}} \quad (4)$$

where:

L = leakage rate,
V = room volume,
t_i = time at ith interval, and
C_i = tracer concentration at ith sample interval.

For measurement over N sampling intervals one may form a mean and standard deviation as follows:

$$\text{Mean } I = \bar{I} = \frac{1}{N} \Sigma I$$

$$\text{Standard deviation} = S_I = \sqrt{\frac{\Sigma I^2 - (\Sigma I)^2/N}{N - 1}}$$

The air change rate, $I = L/V$, is "best fit" the sample values of this parameter. The best fit for I is the mean, and is determined from the test data in accordance with Eq 5. This method has the advantage of simplicity, but is very sensitive to errors in concentration and the effects of poor mixing, especially when short sampling intervals are used.

10.4 *Decay Time Method*—Concentration decay usually occurs quickly. This fact allows for a rapid means of estimating I. For example, with time measured in minutes, the time for one half of the initial concentration to decay is noted as $t_{1/2}$ and the I estimate is given by $41.59/t_{1/2}$. Similar ratios are given for other decay fractions and are shown in Table 1. These ratios are simply computed for C/C_0 ratios of ¾, ⅔, ½, etc. The measurer has to record the time that a desired ratio is encountered.

11. Report

11.1 The report should include the information listed. As much of this information as possible should be included to facilitate comparison with other data at a later time.

11.1.1 *Measurement Characterization:*

- Air Mixing: Method of initial mixing and method of maintaining mixing during the measurement if one is used
- Air Sampling: Location of sampling site, sample interval, initial sample time, method of sampling
- Tracer Gas: Type, initial concentration, method of introduction
- Detector: Type and method of calibration
- Type of Calculation: Finite difference, decay time, graphical, least square

11.1.2 *Meteorological Conditions:*

- Location and height of meteorological measurement

Wind speed and direction (both maximum and average)
Temperature and measurement technique.
Barometric pressure and measurement technique.
Relative humidity or wet bulb temperature and measurement technique.

11.1.3 *Test Space Characterization:*

Structure Type: Residential, commercial, industrial, other
Location of Structure Relative to: Proximity to other structures (give type) and roadways
Description of surrounding terrain (give type, that is, gullies, mountain, mounds, cliffs, etc.)
Structure orientation and elevation relative to items above
Windows: Type, dimensions, number, location in test space
Doors: Type, dimensions, number, location in test space.
Walls: Interior and exterior
Noticeable areas of leakage
Location of chimneys, vents, and other such specified opening
Type and capacity of heating, ventilation, and air-conditioning systems

11.1.4 *Test Space Operating Characteristics:*

- Doors: Open or closed
- Windows: Open or closed
- HVAC System: On or off
- Vent Fans: On or off
- Special Circumstances or Characteristics: Occupied, unoccupied
- Indoor temperature and measurement technique
- Barometric pressure and measurement technique
- Relative humidity and measurement technique

12. Precision and Accuracy

12.1 At present, insufficient data exist for purposes of precision and accuracy determination. A reasonable estimate of the *uncertainty* in a given air change rate determination is of the order of 10 % or less.

12.2 Note that the air change rate is a strong function of indoor-outdoor temperature difference and wind speed and direction. When interpreting or comparing air change rate data, the fact that a pressure and temperature dependence does exist should be borne in mind. It can have a strong effect on the results.

TABLE 1 Decay Ratios to Compute ACPH

Concentration Ratio	Decay Time, minutes	*I*, ACPH
¾	$t_{3/4}$	$17.26/t_{3/4}$
⅔	$t_{2/3}$	$24.33/t_{2/3}$
½	$t_{1/2}$	$41.59/t_{1/2}$
⅓	$t_{1/3}$	$65.92/t_{1/3}$
¼	$t_{1/4}$	$83.18/t_{1/4}$
⅛	$t_{1/8}$	$124.77/t_{1/8}$

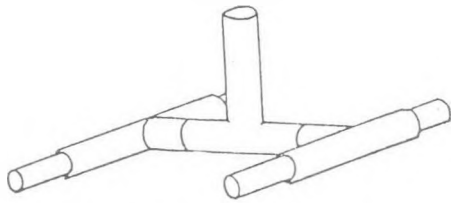

FIG. 1 Four-Point Sampling Junction

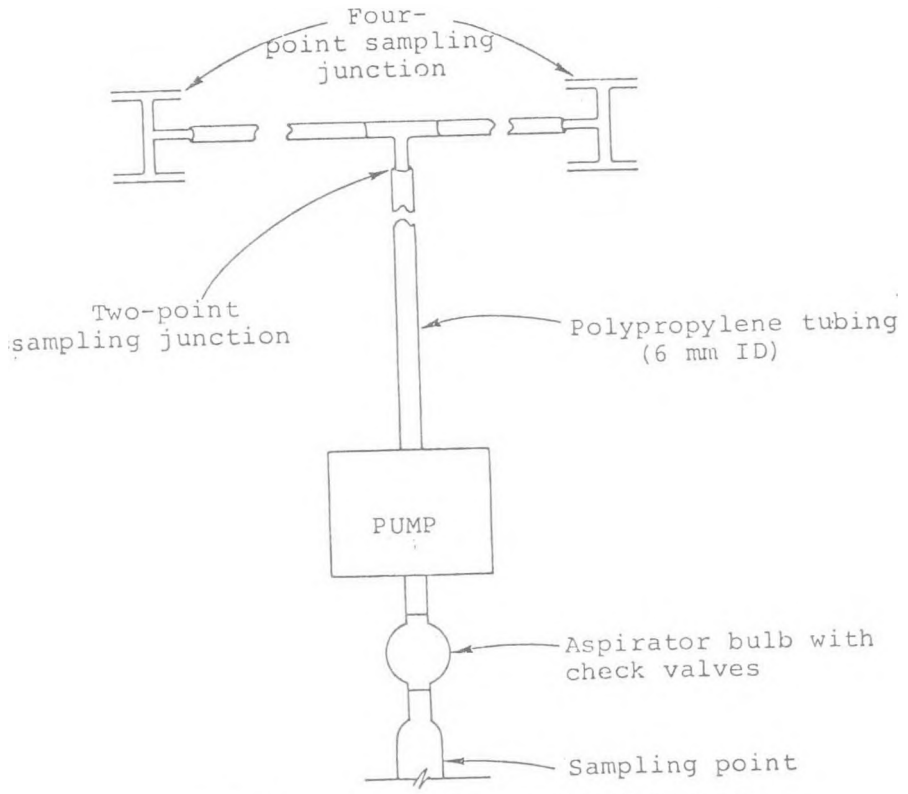

FIG. 2 Diagrammatic Representation of Symmetrical Eight-Point Sampling System

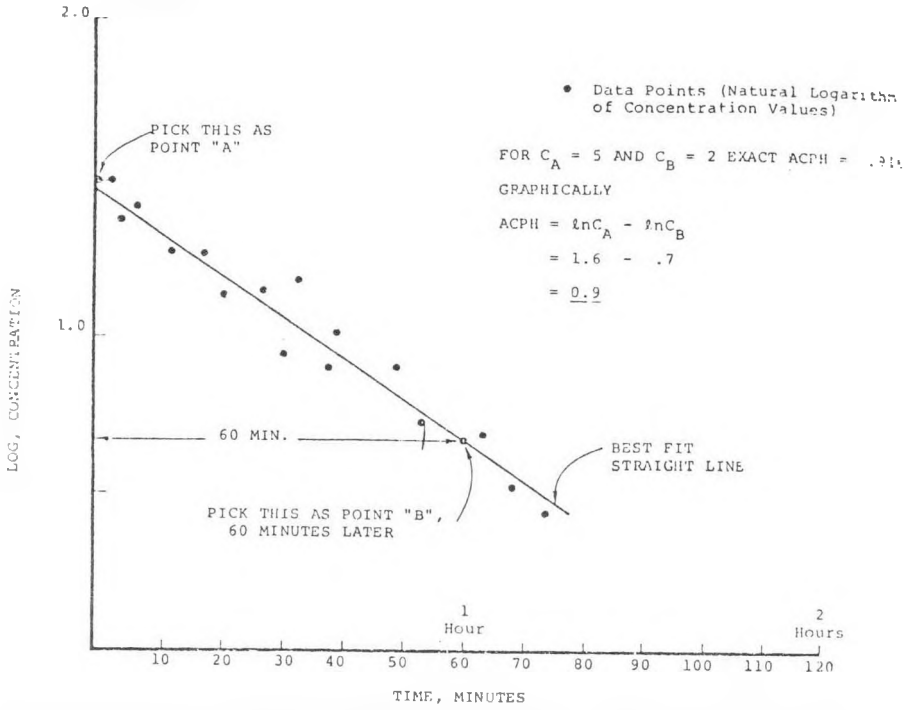

NOTE—Shorter test times may be employed provided that correct time interval is used in calculating air change rate.

FIG. 3 Graphical Determination of Air Change Rate

APPENDIX

A1. SUMMARY OF TRACER GASES USED IN AIR LEAKAGE MEASUREMENTS

A1.1 This appendix presents a compilation of gases and associated instrumental techniques that have been used to perform air leakage measurements as well as a table of typical background levels of these gases. Note that some of these gases may not be suitable for use under present-day guidelines for health and safety. Nevertheless, these gases are presented for historical completeness.

A1.2 In general, the desirable characteristics of a tracer gas are:

Measurable at very low concentrations

- Inert, nonpolar, and not absorbed
- Nontoxic, nonallergenic
- Nonflammable and nonexplosive
- Easily and inexpensively measurable
- Not a normal constituent of air
- Measurable by a technique that is free of interference by substances normally in air.

No single gas fulfills all these conditions.

A1.3 It should be emphasized that the measurement of air change rate by the tracer dilution method is independent of which tracer is selected.

TABLE A1.1 Gases and Techniques for Tracer Dilution Method

Tracer	Measuring Apparatus	Maximum Allowable Concentration in Air (vol/vol)	Minimum Detectable Concentration, ppm	Toxicology[A]	Chemical Inertness	Comments[A]
Hydrogen	Katharometer[A,B]	4 % (lower explosive limit)	200	nontoxic	extremely reactive in presence of oxygen and heat or flame	flammable or explosive in presence of oxygen and heat or flame
Helium	Katharometer[A,B]		300	nontoxic	nonreactive	nonreactive
Carbon monoxide	infrared absorption; heat of absorption measurement[B];	50 ppm	5	combines with hemoglobin to produce asphyxia	can be dangerous when exposed to open flame	can also react with oxygen in air in sufficient concentration, may explode when exposed to open flame
	gas chromatograph followed by reduction to methane and measurement with flame ionization detector[I]	0.4				
Carbon dioxide	infrared absorption;[B]	5000 ppm	1	nontoxic	very soluble in water	
	gas chromatograph with thermal conductivity detector		70			
Sulfur hexafluoride	electron capture[E,F,G]; gas chromatograph	1000 ppm	0.000002	nontoxic	chemically inert when pure	When heated to decomposition (550°C), toxic byproducts may be formed
Nitrous oxide	infrared absorption[J,K]	25 ppm[M]	1	nontoxic	very soluble in water	can form explosive mixtures in air
Ethane	flame ionization detector;[I] gas chromatograph with flame ionization detector	3 % (lower explosive limit)	5	nontoxic	will burn when exposed to flame	may explode in presence of oxygen and heat or flame

TABLE A1.1 *Continued*

Tracer	Measuring Apparatus	Maximum Allowable Concentration in Air (vol/vol)	Minimum Detectable Concentration, ppm	Toxicology[L]	Chemical Inertness	Comments[I]
Methane	infrared absorption[N]	5 % (lower explosive limit)	5	nontoxic	will burn when exposed to flame	may explode in presence of oxygen and heat or flame

[A] Dick, J. B., "Measurements of Ventilation Using Tracer Gas Technique," *Heating, Piping, and Air Conditioning Journal*, HPHOAM, Vol 23, No. 5, May 1950, pp. 131 - 137.

[B] Coblentz, C. W., and Achenbach, P. R., "Design and Performance of a Portable Infiltration Meter," *ASHRAE Transactions* ASHTAG, Vol 69, 1963, pp. 358 - 365.

[C] Elins, H. R., and Wensman, C. W., "Natural Ventilation of Modern Tightly Constructed Homes," Paper presented at American Gas Association-Institute of Gas Technology Conference on Natural Gas Research and Technology, Chicago, Ill., F[illegible]8 - March 3, 1971.

[D] [illegible]ill, J. E., and Kusuda, T., "Dynamic Characteristics of Air Infiltration," *ASHRAE Transactions*, ASHTAG, Vol 81, Part I, 1975, pp. 168 - 185.

[E] Drivas, P. J., Simmonds, P. G., and Shair, F. H., "Experimental Characterization of Ventilation Systems in Buildings," *Environmental Science and Technology*, ESTHAG, Vol 6, No. 7, 1972, pp. 577 - 666.

[F] Harrje, D. T., et al, "Automated Instrumentation for Air Infiltration in Buildings," Center for Environmental Studies Engineering Quadrangle, Princeton University, Princeton, N.J., Report No. 13.

[G] Hunt, C. M., and Treado, S. J., "A Prototype Semi-Automated System for Measuring Air Infiltration in Buildings Using Sulfur Hexafluoride as a Tracer Gas," *National Bureau of Standards Technical Note 898*, March 1976.

[H] Prado, R., Leonard, R. G., and Goldschmidt, V., "Measurement of Infiltration in a Mobile Home," Purdue University Report.

[I] Porter, K., and Volman, D. F., "Flame Ionization Detection of Carbon Monoxide for Gas Chromatographic Analysis," *Analytical Chemistry*, ANCHAM, Vol 34, No. 7, June 1962, pp. 748 - 749.

[J] Lidwell, O. M., "The Evaluation of Ventilation," *Journal of Hygiene*, JOHYAY, Vol 58, 1960, pp. 297 - 305.

[K] Howard, J. S., "Ventilation Measurements in Houses and the Influence of Wall Ventilators," Commonwealth of Australia, DBR Report No. 347, *Building Science*, BUSCBE, Vol 1, 1966, pp. 251 - 257.

[L] Sax, N. I., *Dangerous Properties of Industrial Materials*, Third Edition, Van Nostrand, New York, 1968.

[M] *Occupational Exposure to Anesthetic Gases and Vapors* Department of Health, Education and Welfare (NIOSH), U. S. Government Printing Office, Washington, D. C., 1977.

[N] Janssen, J. E., Torborg, R. H., and Bonne, V., "Measurement of Heating System Dynamics for Computation of Sensoral Efficiency," *ASHRAE Transactions*, ASHTAG, Vol 83, 1977.

TABLE A1.2 Atmospheric Constituents

Compound	Average Tropospheric Background Concentrations, ppm	Typical Indoor and Urban Ambient Concentrations, ppm	Anthropogenic Sources	References
H_2	0.5	0.5	...	A
He	5.2	5.2	...	A
CO	0.1	5–50	combustion	A
CO_2	320	30–5000	combustion	A
N_2O	0.3	0.3–several ppm	combustion	B, C, D
Ethane	1.5×10^{-3}	0.1	incomplete combustion	E, F
Methane	1.5	2–5	incomplete combustion	E, F
SF_6	10^{-8}	10^{-5}	telephone switching stations	G, H

[A] Williamson, S. F., *Fundamentals of Air Pollution*, Addison-Wesley, Reading, Mass., 1973.

[B] Pierotti, D., and Rasmussen, R. A., "Combustion as a Source of Nitrous Oxide in the Atmosphere," *Geophysical Research Letter*, GPRLAJ, Vol 4 No. 5, 1976, pp. 615 - 618.

[C] Rasmussen, R. A., Drasnec, J., and Pierotti, D., "N_2O Analysis in the Atmosphere via Electron Capture-Gas Chromatography," *Geophysical Research Letter*, GPRLAJ, Vol 3, No. 10, October 1976, pp. 615 - 618.

[D] Weiss, R. F., and Craig, H., "Production of Atmospheric Nitrous Oxide by Combustion," *Geophysical Research Letter*, GPRLAJ, Vol 3, No. 12, December 1976, pp. 751 - 753.

[E] *Air Quality Criteria for Hydrocarbons*, National Air Pollution Control Association Publication No. AP-64, U. S. Department of Health, Education and Welfare, Washington, D. C., 1970.

[F] Rasmussen, K. H., Taheri, M., and Kabel, R. L., "Global Emissions and Natural Processes for Removal of Gaseous Pollutants," *Water, Air, and Soil Pollution*, WAPLAC, Vol 4, March 1975, pp. 33 - 64.

[G] Lillian, D., Singh, H. B., Appleby, A., Lobban, L., Arnts, R., Gumpert, R., Hague, R., Toomly, J., Kazazis, J., Antell, M., Hansen, D., Scott, B., "Atmospheric Fates of Halogenated Compounds," *Environmental Science and Technology*, ESTHAG, Vol 9, November 1975, p. 1042.

[H] Simmonds, P. G., Shoemake, G. R., Loveluck, J. E., Lord, H. C., "Improvements in the Determination of Sulfur Hexafluoride for Use as a Meteorological Tracer," *Analytical Chemistry*, ANCHAM, Vol 44, No. 4, April 1972, p. 860.

Appendix I

Infiltration Pressurization Correlation: Simplified Physical Model

Infiltration-Pressurization Correlation: Simplified Physical Modeling

M.H. Sherman, D.T. Grimsrud

Energy and Environment Division
Lawrence Berkeley Laboratory
University of California
Berkeley, Ca. 94720

ABSTRACT

In this paper we present a model for predicting air infiltration that eliminates many site-specific parameters normally required. The only information necessary is the geometry and leakage of the structure. The leakage quantities, expressed in terms of effective areas, are total leakage area and the leakage areas of the floor and ceiling. Weather parameters are mean wind speed, terrain class, and average temperature difference. The model separates the infiltration problem into two distinct parts: stack and wind regimes. Each regime is treated independently; the transition between them is sharp. The model has been tested with data from several sites, differing in climate and construction methods.

INTRODUCTION

Understanding the infiltration process is critical to any residential conservation program inasmuch as infiltration is a primary source of energy loss in residences. Yet we are far more capable of calculating conduction losses than losses due to infiltration. Several explanations for this disparity can be cited. First, conduction losses are more easily calculated because the heat transfer is proportional to the temperature difference and does not depend strongly on any other driving force. Infiltration, on the other hand, depends on the interior-exterior pressure difference but is not simply proportional to it. Furthermore, the driving pressure is caused by uncorrelated

---

The work described in this report was funded by the Office of Buildings and Community Systems, Assistant Secretary for Conservation and Solar Applications of the U.S. Department of Energy under contract No. W-7405-Eng-48.

Infiltration-Pressurization Correlation: Simplified Physical Modeling

M.H. Sherman, D.T. Grimsrud

Energy and Environment Division
Lawrence Berkeley Laboratory
University of California
Berkeley, Ca. 94720

In this paper we present a model for predicting air infiltration that eliminates many site-specific parameters normally required. The only information necessary is the geometry and leakage of the structure. The leakage quantities, expressed in terms of effective areas, are total leakage area and the leakage areas of the floor and ceiling. Weather parameters are mean wind speed, terrain class, and average temperature difference. The model separates the infiltration problem into two distinct parts: stack and wind regimes. Each regime is treated independently; the transition between them is sharp. The model has been tested with data from several sites, differing in climate and construction methods.

Keywords: Infiltration, Pressurization, Leakage, Modeling, Correlation, Weather

---

This paper was prepared for the semi-annual ASHRAE meeting in Denver Colorado, June 1980.

physical effects (wind speed and temperature difference). Second, conduction losses can be characterized by means of one parameter, the thermal resistance; infiltration, until now, has had no equivalent quantity. We propose in this paper that an appropriate parameter for characterizing the infiltration loss is the effective leakage area.

It is because of these problems that infiltration has been a difficult quantity to model. Previous attempts at modeling infiltration have used statistical fitting[1-3] or have involved measurements or calculations that are too difficult to make on a large scale.[4] This paper introduces a model that sacrifices accuracy for versatility and simplicity. Rather than predicting accurately the weather induced infiltration of a particular structure, the model is designed to calculate the infiltration of a general structure. Furthermore, the model predicts the impact of retrofits or other changes in the building envelope generally on the basis of performance changes effected in a few measurable parameters.

The parameters used in the model are:

1) The leakage area(s) of the structure.
   The leakage area is the parameter that describes the tightness of the structure (obtained by pressurization). Most retrofits will affect the leakage area or the leakage distribution.

2) The height of the structure.
   The height and other geometric quantities are usually known or can be directly measured.

3) The inside-outside temperature difference.
   The temperature difference gives the magnitude of the stack effect. It is also necessary for the calculation of the energy load due to infiltration.

4) The terrain class of the structure.
   The terrain class of the structure is a description of the density of other buildings and obstructions which influence the dependence of wind speed on height near the structure. Knowing the terrain class of the structure allows the use of off-site weather data for the calculation of wind induced pressures.

5) The wind speed.
   The wind speed is required to calculate the wind induced infiltration for comparison with the stack effect.

The wind speed used by the model can be calculated from a wind speed measured on any weather tower in the area. Using standard wind formulas (cf. Table A1) the wind speed in any terrain class and at any height can be converted to the wind speed at the site. Thus, on-site weather collection is not necessary in our model. We must emphasize, however, that the measured wind data must be for the "same wind", i.e. there can be no mountain ranges or other major terrain disturbances between the site and the wind tower.

AIR LEAKAGE

Air leakage is the simple process of air passing through normal openings or cracks in the structure. These openings range in size from those of undampered vents (about 0.2m) to tiny cracks around windows (about 0.2mm).

As we know from hydrodynamics, the character of the air flow through a leakage opening changes as the pressure across the opening changes. At very low pressures, the flow is dominated by viscous forces; at high pressures, by inertial forces. Therefore, at low pressures we expect the flow to be proportional to the applied pressure and at high pressures we expect the flow to be proportional to the square root of the applied pressure. At intermediate pressures the behavior will be a mixture of these effects.

The pressure range in which the flow behaviour changes depends on the geometry of the individual crack. While good data[5] exist describing the functional form for an individual crack, the leakage characteristic of the entire structure is much harder to model. The flow vs. pressure curve of the structure will be the summation of all of the individual crack curves. Since it is impossible to know the geometry of each crack, calculating the flow vs. pressure curve of a real structure cannot be done from first principles.

Field measurements[6-9] have shown that the behavior of the actual leakage curve more closely resembles that expected for turbulent flow than for viscous flow in the pressure region typical of the pressures which drive infiltration. These findings indicate that the transition pressure (where the flow changes from viscous to turbulent) is below the experimental range. Therefore, in our model, we assume flow to be proportional to the square root of the applied pressure.

$$Q = A \sqrt{\frac{2}{\rho} \Delta P} \qquad (1)$$

where:

Q is air flow (m^3/sec), $\frac{m^3}{hr}$?

A is the effective leakage area (m^2),

ρ is the density of air (1.2 kg/m^3) and

ΔP is the applied pressure (Pa.).

It is the effective leakage area that characterizes the air leakage. In subsequent discussion we refer to this simply as the leakage area.

In an actual structure there are many leakage sites, each having a leakage area. In this model we combine the leakage sites into three areas: A_o is the total leakage area of the structure (the sum of the leakage areas of the floor, walls and ceiling), A_f is the leakage area of the floor, and A_c is the leakage area of the ceiling.

As will be shown in the Appendices, it is necessary to differentiate the floor and ceiling leakages from the total leakage area because the stack and wind pressures influence these locations differently.

Leakage Measurement

Air leakage is usually measured by fan pressurization.[4] This technique uses a large capacity fan to push air either into or out of the structure. Flow continuity requires that all the air that flows through the fan must flow out through the building shell. The flow measured as a function of the pressure drop across the envelope is called the leakage curve of the building.

In general, leakage curves obtained by this method will not be proportional to the square root of the pressure drop across the envelope. Our model assumes that it is, however, and so we extrapolate the leakage curve (if necessary) down into the pressure range of natural weather effects (0-10 Pa.). We then fit the leakage curve to a square root in that region. The fitting procedure gives us the total leakage area of the structure.

Example: Assume that through fan pressurization tests the following flow vs. pressure data have been measured:

ΔP (Pa.)	10	20	30	40	50
Q (m^3/hr)	800	1220	1560	1850	2110

A two-parameter fit of these data (cf. Eq A1) gives us a flow coefficient of 202 and a pressure exponent of 0.6. Thus the data are

$\left(\frac{lb}{in^2}\right) \times 6.894757^3 = pascals$

$(in\ H_2O) \times 2.488403^2 = pascals$

described by this equation:

$$Q = 202\ \Delta P^{(0.6)}$$

$$\left(\frac{m^3}{hr}\right) \qquad (Pa)$$

We use this equation to find the flow at our reference pressure. We have chosen 4 Pa. as our reference pressure because it is the representative pressure for square root flow in the 0-10 Pa range.

$$Q(\ 4Pa.\ ) = 464\ \frac{m^3}{hr}$$

Using this 4 Pa. flow in Eq. 1 the leakage area is

$$A_o = 500\ cm^2$$

One can estimate the floor and ceiling leakage areas by measurement, by inspection, or by assumption. Direct measurement of the leakage curve for the floor and ceiling is the most accurate method; however, it is difficult and time-consuming. It requires isolating the floor and ceiling from the rest of the structure and a separate fan pressurization test. Accordingly, unless very detailed results are desired, direct measurement is not usually warranted.

Unlike walls floor and ceiling surfaces have few penetrations. Once they are located and their physical dimensions measured, the leakage area (usually smaller than the physical area of the opening) can easily be calculated by estimating the discharge coefficient from the dimensions of the leak. Various references including the ASHRAE Handbook of Fundamentals contain tables or formulas for discharge coefficients. In cases where a floor or ceiling is made of materials that cannot leak (e.g., a slab floor), its leakage area may be assumed to be zero.

Finally, it is possible to assume a value for leakage not accounted for by measurement or calculation. For example, this can be done by assuming that the amount of leakage per unit shell area is the same for all surfaces.

INFILTRATION MODEL

In Appendix A we derive a general theory of infiltration. This derivation includes numerous physical parameters and is useful mainly for large computer programs (e.g., DOE-2). We have reduced the complexity of the model and the number of on-site measurements by introducing a set of simplifying assumptions, which are described in Appendix B.

In this model, we assume that the structure is a single well-mixed zone; we use typical shielding values for a simple rectangular structure; we neglect terms that depend on the sign of the temperature difference. Most importantly, we split the problem into two distinct parts: the wind regime where the dynamic wind pressure dominates the infiltration; and the stack regime, where the temperature difference dominates the infiltration. Infiltration in the two regimes is expressed as follows:

$$Q_{wind} = f_w A_o v \tag{2.1}$$

$$Q_{stack} = f_s A_o \sqrt{2gH \frac{\Delta T}{T}} \tag{2.2}$$

where:

Q_{wind} is the infiltration in the wind regime (m^3/sec),
Q_{stack} is the infiltration in the stack regime (m^3/sec),
v is the wind speed at ceiling height (m/sec),
ΔT is the inside-outside temperature difference (^oK),
g is the acceleration of gravity (9.8 m/sec^2),
H is the height of the ceiling above grade (m) and
T is the inside temperature (^oK).

Definitions for f_w and f_s are presented in Appendix B.

$$f_w = \frac{3 - R}{9} \tag{3.1}$$

$$f_s = \frac{2 + R}{9} \tag{3.2}$$

R is the fraction of the effective leakage that is horizontal (i.e. the sum of the floor and ceiling leakage divided by the total leakage).

$$R = \frac{A_c + A_f}{A_o} \tag{4}$$

The wind speed used in the equations above is the effective wind speed at ceiling height -- that is, the wind speed that would exist at the height of the ceiling if the building and its immediate surroundings were not there. The ceiling height is defined as the height (above grade) of the attic floor. In the case of raised foundations the total height of the living space may be different from the height of the attic floor above grade; however, we ignore this difference in our derivation. This wind speed can be calculated from any

measurement of the same wind using the following formula,

$$v = v' \left[\frac{\alpha \left[\frac{H}{10}\right]^{\gamma}}{\alpha' \left[\frac{H'}{10}\right]^{\gamma'}} \right] \tag{5}$$

where:

v' is the measured wind speed (e.g. from a weather tower)

H is the height of the ceiling,

H' is the height of the wind measurement,

α, γ are empirical constants given in Table A1.

The unprimed quantities refer to the structure site and the primed quantities refer to the wind-measurement site.

We have treated the intermediate regime (between stack and wind) by extrapolating the stack- and wind-regime formulae until they cross; thus, the predicted infiltration will be the larger of the two.

$$Q(\Delta T, v) = \text{MAX}(Q_{wind}, Q_{stack}) \tag{6.1}$$

$$= A_o \, \text{MAX}(v^*, v_s^*) \tag{6.2}$$

Where the starred (reduced) quantities are defined as,

$$v^* = f_w \, v = v' \, f_w^* \tag{7.1}$$

$$f_w^* = \frac{3 - R}{9} \left[\frac{\alpha \left[\frac{H}{10}\right]^{\gamma}}{\alpha' \left[\frac{H'}{10}\right]^{\gamma'}} \right] \tag{7.2}$$

reduced stack + wind parameters

$$v_s^* = f_s \, v_s = \sqrt{\Delta T} \, f_s^* \tag{8.1}$$

$$f_s^* = \frac{2 + R}{9} \sqrt{\frac{2gH}{T}} \tag{8.2}$$

Because the reduced stack and wind parameters (starred f's) in the above equations are weather independent, they need be calculated only once for a given structure. We have calculated the reduced parameters for a special case — i.e., when the terrain class of the structure is the same as that for the wind measurement, and when the height of the wind measurement is 10 meters.

This is the most common case, principally because most wind measurements are made with a 10-meter weather station on-site. Table 1 contains values of the reduced stack parameter as a function of the height of the structure and the fraction of leakage in the floor and ceiling. Tables 2.1 to 2.5 contain the values of the reduced wind parameter as a function of the height of the structure and the fraction of the leakage in the floor and ceiling for the five terrain classes.

Having completely separated the weather-dependent parts from the weather-independent parts, we were able to devise a single graph that allows the infiltration of any structure to be calculated in any weather condition (see Figures 1 and 2).

Description of Figures 1 and 2.

Either Figure 1 or Figure 2 can be used to predict the infiltration of a particular site under any given weather condition using a few simple steps. Refer to the symbol table and list of defining relations that precede the figures for the terms used below.

1) From leakage measurements, determine A_o, A_c, and A_f. These, in turn, determine the fraction of leakage in the floor and ceiling, R. R is then used to calculate f_w and f_s.

2) The height of the structure, H, and the internal temperature, T, are combined with the stack parameter, f_s, to give the reduced stack parameter, f_s^*. Table 1 can be used to give the reduced stack parameter for the special case of on-site weather collection at 10m.

3) The ceiling height of the structure and the height of the weather tower are combined with the terrain classes of the two sites and the wind parameter, f_w, to give the reduced wind parameter, f_w^*. For the special case of on-site weather collection at 10m, Table 2 can be used to give the reduced wind parameter.

4) The wind speed, v', can be combined with f_w^* to give v^* and the inside-outside temperature difference, ΔT, can be combined with f_s^* to give v_s^*.

The combination of v^* and v_s^* define a point on the graph. That point falls on one of the constant infiltration lines. The axes of the graphs are in metric units; the number read from the constant infiltration lines has units of $m^3/hr/cm^2$. To find the actual infiltration in cubic meters per hour, that number should be multiplied by the total leakage area in centimeters squared

(cm^2).

Steps 1-3 need be done only once per structure unless the leakage area of the structure is changed. Step 4 is necessary only if Figure 2 is used, because Figure 1 uses the reduced and weather parameters directly.

RESULTS

Fifteen different sites were extracted from the literature to represent a large spread in climate type, house construction type and measured infiltration rates.[10-12] In all cases, leakage data obtained by fan pressurization were available, permitting us to calculate the effective leakage area. (Note that the effective leakage area varies over a factor of 16 from tightest to loosest.) The fraction of leakage in the floor and ceiling and the terrain parameters were estimated from the qualitative description of each site. In Table 3, the effective leakage area, the reduced parameters, and the house volumes are presented for each site.

For most of the sites, the data consist of several short-term infiltration measurements made on a single day. Most infiltration measurements were made by using a tracer decay technique[4] which finds the average infiltration over a period of about an hour with a 5%-10% accuracy. For each measured infiltration point, a predicted infiltration was calculated from the weather variables and house parameters. Figures 3 and 4 contain the plots of predicted vs measured infiltration.

Since the set of data for each site was taken on the same day, we have combined the sets to find an average measured infiltration and an average predicted infiltration for each site. Table 2 contains these average infiltrations as well as the average weather variables from which the predicted infiltration was calculated, together with their associated standard errors.

DISCUSSION

Considering the simplicity of the model and the fact that there are no adjustable parameters, the agreement is good. However, there are a few sites that do not have particularly good agreement; some over-predict and some under-predict. In order to explain some of these discrepancies, we examined other factors that may affect the infiltration.

Site 15 (Southampton) was the leakiest of all the sites and proved to be an under-predictor. At the time we were measuring infiltration in this house, the furnace fan was on. Because the ducts run through unconditioned spaces, any leakage in the ducts means that part of the air circulated by the furnace fan will exfiltrate causing an increase in infiltration. This increase is not accounted for by our model.

Site 10 (Neilson), also one of the leakiest houses measured, showed significant under-prediction as well. Because this house had no chimney damper, the wind blowing over the chimney caused a net suction on the house. If there were a damper or glass doors on the fireplace, the effect of this suction would have been minimal; with no obstruction to the flow, however, exfiltration increased and could not be accounted for by our model.

One of the crudest assumptions we have made is that the shielding coefficients can be assumed to be those of an exposed rectangular structure. For structures that have significant local shielding, we might expect the measured infiltration to be lower than the predicted infiltration. Without precisely quantifying the degree of shielding at each site, we examined the description of all the structures and found three sites (9, 13 and 14) that were heavily shielded and two sites (2 and 8) that were very heavily shielded.

For the very heavily shielded sites the data clearly show that the model over-predicts the infiltration by a factor that approaches two. Of the heavily shielded sites, Site 13 (Fels) over-predicts by an average of 50%, Site 9 (Purdue) over-predicts by an average of 25%, and Site 14 (San Carlos) under-predicts by an average of 15%.

The case of site 14 is unique in that it was the only site to be heavily shielded and also have an undampered chimney. These two effects tend to counterbalance each other; however, in any given situation (depending on wind speed and direction) one could easily outweigh the other. The data from this site reflect this variability. In one case, the predicted infiltration is well below the measured infiltration, suggesting that the chimney has a substantial effect. In the other three cases, the predicted infiltration is slightly above the measured infiltration, suggesting that the excess shielding is playing an important role.

While the accuracy of the model is sufficient for a wide variety of applications, the shortcomings described above suggest ways in which accuracy can be improved. Not only can we include new parameters to account for local shielding, but we can extend the model to account for stack flows through vents and flues and for active systems (e.g. furnace fans) all of which may interact with natural ventilation.

Retrofit Evaluation

Infiltration depends on the leakage area in two different ways: (1) it scales linearly with the total leakage area and (2) the f's depend weakly on the fraction of the leakage in the floor and ceiling. In general a single retrofit will make only a small change in the leakage area of the structure; hence, we can ignore the effect that a particular retrofit will have on the f's. The impact of a retrofit in changing infiltration is proportional to the change it effects in the total leakage area. (It should be noted that the model is more accurate in predicting changes in infiltration due to changes in the leakage area than in predicting absolute infiltration. Accordingly, to evaluate the effect of a retrofit on infiltration requires simply an evaluation of its effect on the leakage area. We suggest that a list of leakage areas be compiled for various architectural components to aid in predicting infiltration savings. The effective leakage area of each component becomes a powerful tool for predicting energy losses due to infiltration.

CONCLUSION

We have introduced the concept of leakage area as the characteristic quantity associated with infiltration, just as conductivity is the characteristic quantity associated with conduction. Using this concept we have devised a model for predicting the infiltration based on a few easily determined physical parameters. Houses of widely different construction types and located in varying climate conditions can be measured and compared by means of this model, inasmuch as all of the parameters used (i.e. leakage areas, terrain classes etc.) have physical reality outside of our model and are therefore independently measurable.

In future studies, we will explore long-term average infiltration data from a number of dissimilar sites to test the overall scale of the model. In addition, we will measure infiltration before and after retrofit, comparing the predicted infiltration reduction using our model with the actual infiltration reduction measured using a tracer gas.

APPENDIX A

Derivation of basic model

In this appendix the basic physical model of infiltration will be derived. This model is similar to a previously presented model[13] with one exception: in the prior model we assumed linear (viscous) flow through cracks as the dominant leakage mechanism, while in this appendix we generalize the concept to allow the flow through a crack to be proportional to the applied pressure raised to an arbitrary power.

First, we separate out the effects of the driving force of the structure (air leakage), by using the intermediary of surface pressures; knowledge of the terrain and weather allows surface pressures to be calculated. Second, we combine the surface pressures with the leakage function (and geometry) to calculate infiltration. In the following sections, we will combine these two operations into a complete description of weather driven infiltration.

General Leakage Model

Air leakage is the natural flow of air through cracks, holes, etc. across the building envelope. There are two physically well-defined types of air flow: viscous and turbulent. In the viscous regime, the flow is proportional to the applied pressure; in turbulent flow, the flow is proportional to the square root of the applied pressure. The type of flow is determined by the applied pressure and the crack geometry. In most houses there will be air flows in both regimes as well as in transition between regimes. A popular way of expressing this fact is to assume that the air flow is proportional to the applied pressure raised to some power between 1/2 and 1, and then to find the parameters experimentally.

$$Q(\Delta P) = L\,\Delta P^{n} \qquad \text{(A1)}$$

where:

- Q is the air flow due to an applied pressure, (m^3/sec)
- ΔP is the applied pressure, (Pa.)
- L,n are semi-empirical constants.

In an actual structure, the leakage may depend on the sign of the applied pressure and will also be different on different faces of the structure. To

account for these possibilities, we further generalize the above expression to

$$Q_j^+ = L_j^+ \ (\Delta P_j^+)^{n_j^+} \tag{A2.1}$$

$$Q_j^- = L_j^- \ (\Delta P_j^-)^{n_j^-} \tag{A2.2}$$

where:

- j is the index to denote each face of the structure,
- + indicates depressurization
- - indicates pressurization.

Surface Pressures

Differential pressures on a structure are caused by the stack effect and the wind effect. The stack effect is the change in pressure due to a change in the density of two bodies of air which, in turn, is caused by a temperature difference between the two air masses. The size of this effect is given by the stack pressure,

$$P_s = \rho \ g \ H \frac{\Delta T}{T} \tag{A3}$$

where:

- P_s is the stack pressure,
- ρ is the density of air, (1.2 kg/m^3)
- g is the acceleration of gravity (9.8 m/sec^2)
- H is the height of the structure (m)
- ΔT is the inside-outside temperature difference (^oK) and
- T is the inside temperature ($\simeq$295 ^oK).

The change in pressure with respect to height can be calculated by the following equation

$$\frac{d\Delta P}{dh} = - \frac{P_s}{H} \tag{A4}$$

where:

- ΔP is the outside-inside pressure drop and
- h is the height from floor level

The minus sign comes from our definition of the relative signs of ΔT and ΔP.

The wind effect is an exterior pressure caused by a stream of air impinging upon a stationary object. The dynamic pressure caused by a wind striking a fixed object is called the stagnation pressure.

$$P_{st} = \frac{1}{2} \rho v^2 \quad \text{(A5)}$$

where:

P_{st} is the stagnation pressure and
v is the wind speed.

We can define a dimensionless measure of the wind strength relative to the stack pressure.

$$\sigma = \frac{P_{st}}{P_s} = \frac{v^2}{2gH} \frac{T}{\Delta T} \quad \text{(A6)}$$

where:

σ is the wind strength*

Wind Speed

The definition of wind speed is important in determining infiltration. We define the wind speed, v, to be the wind speed at the height of the ceiling of the structure if the structure and immediate surroundings were not there. Thus, we are excluding any effects of the local environment from the definition of wind speed. However, because of the nature of wind dynamics, the wind speed measured at one height in one type of terrain will not be the same as the wind speed measured at another height or in another type of terrain.

To account for this variability, we use a standard formula[14] to calculate the wind speed at any height and terrain class from the wind speed at any other height and terrain class.

---

*Our wind strength parameter is similar to other dimensionless quantities such as the Archimedes number. Specifically the wind strength, σ, is equal to the reciprocal of twice the square of the Archimedes number.

$$v = v_o \alpha \left[\frac{H}{10}\right]^{\gamma} \tag{A7}$$

where:

v is the actual wind speed

v_o is the wind speed at standard conditions

α, γ are constants that depend on terrain class

To calculate the wind speed at one site from measured data at another site, we first use the above formula is used to calculate the standard wind speed for the measurement site. Then the standard wind speed is used to calculate the wind speed at the desired site. Values for the two terrain class-dependent parameters are shown in Table A1.

We must take into account the effect of the local terrain on the wind pressures felt by the structure. We do this by introducing shielding coefficients* that convert the stagnation pressure into the actual pressure felt by the exterior of the structure. Full-scale studies[15] have shown that the pressure distribution on flat faces can be adequately described by using the average pressure on the face. Accordingly, there is one shielding coefficient for every face of the structure.

$$\Delta P_j^w = C_j \, 1/2 \, \rho v^2 = C_j \, \bar{\sigma} \, P_s \tag{A8}$$

where:

ΔP_j^w is the exterior pressure rise due to the wind and

C_j is the shielding coefficient for the jth face.

The shielding coefficients must be functions of the angle between the incident wind and the orientation of the structure. Since we will eventually average the shielding coefficients over angle, we have suppressed their explicit dependence of them on angle.

---

* The term shielding coefficient is equivalent to the more standard term of exterior pressure coefficient; the only difference lies in the interpretation. We use the term shielding coefficient to mean the ratio of the average exterior wind pressure to the stagnation pressure at the ceiling height.

Combining Stack and Wind Effects

Now that we have expressions for both the stack and wind effects, we can combine them to find the total pressure drop across each face of the structure.

$$\Delta P_j = \Delta P_o - P_s \frac{h}{H} + C_j \ 1/2 \ \rho \ v^2 \qquad (A9)$$

where:

ΔP_j is the pressure drop across the jth face and
ΔP_o is the internal pressure change

The internal pressure change is the shift in internal pressure due to weather. It is determined by the condition that the air flow into the structure must balance the air flow out of the structure. To simplify this expression we make the following definitions:

$$\beta = \frac{h}{H} \qquad (A10.1)$$

$$\Delta P_o = P_s \ \beta^o - C^o \ 1/2 \rho v^2 \qquad (A10.2)$$

$$\beta_j = \beta^o + \sigma \ (\ C_j - C^o \ ) \qquad (A10.3)$$

where:

β is a dimensionless height,
β^o is called the neutral level,
β_j is called the effective neutral level of the jth face and
C^o is called the internal pressure coefficient

At this point the neutral level and internal pressure coefficients must be regarded as arbitrary functions of weather but, as will be demonstrated in Appendix B, for most purposes they may be treated as constants. Note also that when there is no wind (σ=0) the effective neutral levels are equal to the neutral level.

Combining all this together, we get a deceptively simple expression for the pressure drop across the envelope:

$$\Delta P_j = P_s \ (\ \beta_j - \beta \ ) \qquad (A11)$$

COMBINING SURFACE PRESSURES AND AIR LEAKAGE

Now that we have expressions both for the surface pressures acting on the structure and the response of the structure to these pressures, we can derive an expression for the infiltration. We must be careful, however, to separate exfiltration (which is driven by negative differential surface pressures) and infiltration (which is driven by positive differential surface pressures). We must integrate the leakage expression over the entire surface and sum the infiltration and exfiltration separately. The results of these calculations are presented in Table A2, below.

There are three different types of structure faces to be considered: floor, walls and ceiling. Because the floor and ceiling are both at a constant height, the integration over height is trivial; there can only be infiltration or exfiltration through one of them but not both. The walls, being vertical, may have both infiltration and exfiltration if the effective neutral level is between the floor and the ceiling. We split the problem up into three cases, depending on the value of the effective neutral level:

1) The effective neutral level is above the ceiling.
   ($1 < \beta_j$)

2) The effective neutral level is between the floor and the ceiling.
   ($0 < \beta_j < 1$)

3) The effective neutral level is below the floor.
   ($\beta_j < 0$)

The combination of three faces, three neutral level positions and two air flow directions yields 18 entries for Table A2.

This analysis assumes knowing a host of structural site-specific parameters (L's, n's, C's). Additionally, the calculation of infiltration changes form depending on the value of the effective neutral level. These factors would make the calculation of infiltration very tedious and hence impractical for a large number of sites. In Appendix B, we show how the model can be simplified by making certain reasonable physical assumptions.

APPENDIX B

Simplified analysis

The purpose of this section is to present a simplified expression for the infiltration rate of a structure. We will make reference to the general theory of air infiltration, and apply many approximations. Along the way, the approximations will be explicitly stated as they are made.

APPROXIMATION 1: The flow is dominated by simple orifice flow

Recent evidence[7] indicates that even at low pressures the flow through a structure is dominated by turbulent flow. That is, viscous forces do not appear to dominate the air leakage at typical weather-induced pressures. The turbulent case is equivalent to restricting the values of the L's and n's used in the general model.

$$L_j^+ = L_j^- = A_j \sqrt{\frac{2}{\rho}} \tag{B1.1}$$

$$n_j^+ = n_j^- = 1/2 \tag{B1.2}$$

where:

A_j is called the effective leakage area of the jth face (m^2).

In terms of the air flow through a structure face,

$$Q_j = A_j \sqrt{\frac{2}{\rho} \Delta P_j} \tag{B2}$$

where:

Q_j is the flow through the jth leakage site,
ΔP_j is the pressure drop across the jth site.

APPROXIMATION 2: The floor and ceiling are well shielded

In most circumstances the wind pressure felt by the floor and ceiling is much smaller than that felt by the walls; therefore, we will set the shielding coefficients of the floor and ceiling arbitrarily to zero.

We are now in a position to rewrite Table A2 using our approximations. Before doing so, we will change nomenclature slightly. The subscript j refers to any of the structural faces; we introduce the subscript w which is restricted to the walls of the structure only. We also define the critical velocity, v_s, to be the velocity of the wind when the stack pressure equals the stagnation pressure.

$$v_s = \sqrt{2gH\frac{\Delta T}{T}} = \frac{v}{\sqrt{\sigma}} \qquad \text{(B3)}$$

where:

v_s is the critical velocity.

Table B1 presents the expressions relating the infiltration to the weather parameters under these assumptions.

APPROXIMATION 3: The infiltration can be split into two regimes.

Even though we have simplified the problem, we cannot yet calculate infiltration directly. To calculate the infiltration we split the problem into two halves: wind-dominated and stack-dominated regimes. We assume that either all of the effective neutral levels are between the floor and the ceiling or none of them are. If all of the effective neutral levels are between the floor and the ceiling ($0<\beta_j<1$) then infiltration is stack-dominated; if all of them are above the ceiling ($1<\beta_j$) or below the floor ($\beta_j<0$) then it is wind-dominated. The derivation for both cases is shown below.

Stack Regime

In the stack regime we require the effective neutral level to be between the floor and the ceiling ($0<\beta_j<1$). Extracting these lines from Table B1 and summing the infiltration and exfiltration, we have:

$$Q^+ = v_s\left[A_f\sqrt{\beta^o - \sigma C^o} + \frac{2}{3}\sum_w A_w(\beta^o + \sigma(C_w - C^o))^{3/2}\right] \qquad \text{(B4.1)}$$

$$Q^- = v_s\left[A_c\sqrt{1 - \beta^o + \sigma C^o} + \frac{2}{3}\sum_w A_w\left[-\beta^o - \sigma(C_w - C^o)\right]^{3/2}\right] \qquad \text{(B4.2)}$$

where:

Q^+ is the infiltration and

Q^- is the exfiltration.

APPROXIMATION 4: The neutral level is about half way up the structure.

The neutral level, β^o, represents the level at which the indoor-outdoor pressure difference is zero when there is no wind. Above the neutral level, the indoor pressure is larger, causing exfiltration; below, the indoor is smaller than the outdoor pressure and infiltration occurs. The height of the neutral level in a structure will be about half the height of the structure. To examine the dependence of the infiltration on position of the neutral level, we expand expressions which contain the height of the neutral level about the point $1/2$ (times the structure height). We define a quantity, μ, to be the deviation from that point ($\beta^o = 1/2$).

$$\mu = \beta^o - 1/2 \tag{B5}$$

We then rewrite the equations for the infiltration and exfiltration sums as:

$$Q^+ = v_s\left[A_f(1/2 + \mu - \sigma C^o)^{1/2} + \frac{2}{3}\sum_w A_w(1/2 + \mu + \sigma(C_w - C^o))^{3/2}\right] \tag{B6.1}$$

$$Q^- = v_s\left[A_c(1/2 - \mu + \sigma C^o)^{1/2} + \frac{2}{3}\sum_w A_w(1/2 - \mu - \sigma(C_w - C^o))^{3/2}\right] \tag{B6.2}$$

Since we are in the stack-dominated regime, the effective wind strength, $(C_w - C^o)\,\sigma$, must be small compared to unity to guarantee that the effective neutral level will be between the floor and the ceiling. Therefore, we can expand the terms containing σ and μ, assuming them to be small.

$$Q^+ = \sqrt{1/2}\; v_s\left[A_f(1 + \mu - \sigma C^0) + \sum_w A_w(\tfrac{1}{3} + \mu + \sigma(C_w - C^0))\right] \tag{B7.1}$$

$$Q^- = \sqrt{1/2}\; v_s\left[A_c(1 - \mu + \sigma C^0) + \sum_w A_w(\tfrac{1}{3} - \mu - \sigma(C_w - C^0))\right] \tag{B7.2}$$

We have replaced the quantity C^o by C^0 to indicate that we are evaluating the internal pressure coefficient at low wind strengths.

Flow continuity requires that the infiltration and exfiltration be equal; applying this restriction to Eq. B7.1 and B7.2 gives:

$$A_f(1 + \mu) + \frac{1}{3} \sum_w A_w(1 + 3\mu) = A_c(1 - \mu) + \frac{1}{3} \sum_w A_w(1 - 3\mu) \qquad (B8.1)$$

$$\sum_w A_w \ (C_w - C^0) = 1/2\, C^0 \ (A_c + A_f) \qquad (B8.2)$$

Solving these two equations leads to expressions for μ and C^0.

$$\mu = \frac{A_c - A_f}{A_c + A_f + 2 \sum_w A_w} \qquad (B9.1)$$

$$C^0 = \frac{\sum_w A_w \ C_w}{\sum_w A_w + \frac{A_c + A_f}{2}} \qquad (B9.2)$$

We have found that these two parameters to assure flow continuity and, thus, that infiltration and exfiltration will be equal. To calculate the actual infiltration (in the stack regime) it does not matter which we use. Therefore, we will use the average.

$$Q = 8^{-1/2} \ v_s \left[A_f(1+\mu) + A_c(1-\mu) + \frac{2}{3} \ (A_o - A_f - A_c) + \sigma C^0 A_o \mu \right] \qquad (B10)$$

Neglecting terms of order μ^2 we get,

$$Q = 72^{-1/2} \ v_s \left[2 \ A_o + A_f + A_c + 3 \ \sigma \ C^0 \ A_o \ (A_c - A_f) \right] \qquad (B11)$$

where:

A_o is the total leakage area ($\sum_w A_w + A_f + A_c$)

Wind Regime

In the wind regime we assume that none of the effective neutral levels are between the floor and the ceiling ($1<\beta_j$ or $\beta_j<0$). In the stack regime we assumed the effective wind strength was small compared to unity; here we will assume the opposite. Extracting the wind-regime data from Table B1 and making the indicated replacements, we form Table B2, simplified wind regime infiltration.

We can find the internal pressure coefficient in the same manner as we did the stack effect (i.e. by requiring infiltration and exfiltration to balance). However, in the wind regime the equations are non-linear and can only be solved numerically once values for shielding coefficients and leakage areas are known. Having found the internal pressure coefficient, we can find the infiltration by averaging the air flow out of the structure and the air flow into the structure.

$$Q = \frac{v}{2}\left[\sqrt{|C^{\infty}|}(A_c+A_f+\frac{\mu}{4\sigma C^{\infty}}(A_o+2A_f+2A_c))\right] \qquad \text{(B12.1)}$$

$$+\frac{v}{2}\left[\sum_w A_w\sqrt{|(C_w - C^o)|}\,(1+\frac{\mu}{\sigma(C_w - C^{\infty})})\right]$$

$$= \frac{v}{2}\left[\sqrt{|C^{\infty}|}\,(A_c + A_f) + \sum_w A_w\sqrt{(C_w - C^{\infty})}\right] \qquad \text{(B12.2)}$$

$$+\frac{v\,\mu}{2\sigma}\left[\sum_w \frac{A_w}{\sqrt{|(C_w - C^{\infty})|}} - \frac{(2A_o + A_f + A_c)}{2\sqrt{|C^{\infty}|}}\right]$$

where:

C^{∞} is the internal shielding coefficient at high wind strength,

Now that we have expressions for the infiltration in the stack and wind regimes, we must be able to reduce them to a level of simplicity commensurate with the results obtained from pressurization. To this purpose, we must make a few more approximations.

APPROXIMATION 5: Directional wind effects are unimportant

In any real structure, there are directional effects due to leakage distribution and shielding distribution. We are going to neglect such effects or, equivalently, assume that the wind direction changes enough in the time frame under consideration to average out any such effects.

If directional effects are unimportant, then we can simplify the various sums over shielding coefficients.

$$\sum_w A_w\, q_w = (A_o - A_c - A_f\ )\ \langle q_w \rangle \qquad \text{(B13)}$$

where:

q_w is any quantity that must be summed over the walls,
$\langle q_w \rangle$ is the average value of that quantity and

$$\sum_w A_w = A_o - A_f - A_c$$

APPROXIMATION 6: The structure is typically shielded.

We will use numerical values for the external shielding parameters for a typical house of rectangular floor plan. This assumption combined with the previous one allows us to average over wind directions as well. If a particular structure is has highly non-uniform shielding, then the dimensionless constants will retain their angular dependence.

We have chosen to use wind-tunnel values for a house of rectangular floor plan.[1]

APPROXIMATION 7: The internal pressure coefficient is constant

We have solved explicitly for the internal pressure coefficient at low wind strengths and we can solve numerically for the internal pressure coefficient at high wind strengths. If we do so, we find that they are roughly equal for any reasonable choice of C's and A's. We can then replace all of the internal pressure coefficients by a single value.

$$C^{\infty} = C^{0} = C^{o} \tag{B14}$$

We can now rewrite the stack-regime and wind-regime equations by making a new definition to eliminate A_c and A_f.

$$R = \frac{A_c + A_f}{A_o} \tag{B15}$$

Rewriting the two infiltration equations, we have:

$$Q_{stack} = 72^{-1/2} A_o v_s (2 + R) + 288^{-1/2} A_o \frac{v^2}{v_s} \mu C^{o} \tag{B16}$$

$$Q_{wind} = \frac{1}{2} A_o v \sqrt{|C^o|} \left(R + (1-R) \left\langle \sqrt{|(C_w - C^o)|} \right\rangle \right) + \tag{B17}$$

$$A_o \frac{v_s^2}{v} \mu \left[\frac{(1 - R)}{\left\langle \sqrt{|(C_w - C^o)|} \right\rangle} - \frac{(1 + \frac{R}{2})}{\sqrt{|C^o|}} \right]$$

APPROXIMATION 8: The infiltration is independent of the sign of ΔT

In the preceding derivation we assumed that the stack pressure was positive (i.e., that inside is greater than outside temperature) . If the reverse is true, the only change in these equations is a sign reversal of μ; for cooling loads μ should be replaced by $-\mu$ in all the above equations. In both equations this asymmetric term is quite small; therefore, we will set these terms to zero.

$$Q_{stack} = 72^{-1/2} A_o v_s (2 + R) \tag{B18.1}$$

$$Q_{wind} = 1/2 A_o v \left[\sqrt{|C^o|} R + (1-R) \left\langle \sqrt{|(C_w - C^o)|} \right\rangle \right] \tag{B18.2}$$

From the wind-tunnel data we can calculate the terms involving the shielding parameters.

$$C^o = -.21 \tag{B19.1}$$

$$\left\langle \sqrt{|(C_w - C^o)|} \right\rangle = 0.68 \tag{B19.2}$$

We now insert the numerical values into the equations and define two dimensionless parameters f_s and f_s.

$$f_s = \frac{2 + R}{9} \tag{B20.1}$$

$$f_w = \frac{3 - R}{9} \tag{B20.2}$$

These expressions are accurate to two significant figures.

Combining these terms yields expressions for the stack and wind infiltration.

$$Q_{stack} = f_s A_o v_s \quad \text{(B21.1)}$$

$$Q_{wind} = f_w A_o v \quad \text{(B21.2)}$$

COMBINING WIND AND STACK REGIMES

We have an expression for the infiltration in the stack regime and an expression for infiltration in the wind regime, but we have no adequate expression for the intermediate case. Although the intermediate case will no doubt be very complicated and site- specific, we will assume that one of the two equations will adequately describe the situation. We shall use the larger of the two infiltration values at all times.

$$Q(\Delta T , v) = A_o \, MAX(f_s v_s , f_w v) \quad \text{(B22)}$$

where:

$Q(\Delta T, v)$ is the instantaneous infiltration.

There is a wind speed at which the stack effect and wind effect become equal. Above that wind speed, the wind effect dominates while below, the stack effect dominates. At the equilibrium wind speed,

$$f_w v = f_s v_s = f_s \sqrt{2gH \frac{\Delta T}{T}} \quad \text{(B23)}$$

Depending on the value of R, the equilibrium wind speed may be anywhere from 2/3 v_s to v_s.

REFERENCES

1. D.R. Bahnfleth, D.T. Moseley, and W.S. Harris, "Measurement of Infiltration in Two Residences," ASHRAE TRANSACTIONS, 63, 439-452, 1957.

2. J.B. Dick, and D.A. Thomas, "Ventilation Research in Occupied Houses," J. Inst. Heat. Vent. Eng., 19, 306-332, 1951.

3. N. Malik, "Filed Studies of Dependence of Air Infiltration on Outside Temperature and Wind," Energy and Buildings, 1, 281-292, 1978.

4. D.T. Grimsrud, M.H. Sherman, R.C. Diamond, P.E. Condon, and A.H. Rosenfeld, "Infiltration-pressurization Correlations: Detailed Measurements on a California House," ASHRAE TRANSACTIONS, 85, 1:851-865, 1979. LBL Report No. 7824 (1978) → Tracer decay method

5. D.W Etheridge, "Crack Flow Equations and Scale Effect," Building & Environment, 12, 181-189, 1977.

6. M.H. Sherman, D.T. Grimsrud, and R.C. Sonderegger, "Low Pressure Leakage Function of a Building," Proc. ASHRAE-DOE Conference on the Thermal Performance of the Exterior Envelopes of Buildings, Orlando, Florida, December 1979. LBL Report No. 9162 (1979)

7. A.K Blomsterberg, and D.T. Harrje, "Approaches to Evaluation of Air Infiltration Energy Losses in Buildings," ASHRAE TRANSACTIONS, 85, 1:797-815, 1979.

8. D.T. Grimsrud, M.H. Sherman, R.C. Diamond, and R.C. Sonderegger, "Air Leakage, Surface Pressures and Infiltration Rates in Houses," Proc. of the Second International CIB Symposium, Copenhagen, Denmark, May 1979, LBL Report No. 8828 (1979)

9. D.T. Harrje, A.K. Blomsterberg, and A Persily, "Reduction of Air Infiltration due to Window and Door Retrofits in an Older Home," Princeton University/Center for Environmental Studies Report No. 85, 1979.

10. D.T. Grimsrud, M.H. Sherman, A.K. Blomsterberg, and A.H. Rosenfeld, "Infiltration and Air Leakage Comparisons: Conventional and Energy Efficient Housing Designs," Presented at the International Conference on Energy Use Management, Los Angeles, October 1979. LBL Report No. 9157 (1979)

11. Johns-Manville Research and Development Center, "Demonstration of Energy Conservation through Reduction of Air Infiltration in Electrically Heated Houses," RP 1351-1, 1979.

12. G.T. Tamura, "The Calculation of House Infiltration Rates," ASHRAE TRANSACTIONS, 85, 1:58-71, 1979.

13. M.H. Sherman, D.T. Grimsrud, and R.C. Diamond, "Infiltration-Pressurization Correlation: Surface Pressures and terrain Effects," ASHRAE TRANSACTIONS, 85, 2:458-479, 1979. LBL Report No.8785 (1979)

14. European Convention for Constructional Steelwork, "Recommendations for the Calculation of Wind Effects on Buildings and Structures", Technical General Secretariat, Brussels, Belgium September 1978.

15. S. Kim, K.C. Mehta, "Full Scale Measurements on a Flat Roof Area," Proceedings of the Fifth Int. Conf. Wind Engineering, Boulder, Colorado, July 1979.

16. R.E. Akins, J.A. Peterka, and J.E. Cermak, "Average Pressure Coefficients for Rectangular Buildings," Proceedings of the Fifth Int. Conf. Wind Engineering Boulder, Colorado, July 1979.

ACKNOWLEDGEMENT

The authors would like to thank Fannie Walkin for her invaluable guidance in simplifying this derivation.

Table 1: Reduced stack parameter(f_s^*)

H	R									
	.05	.10	.15	.20	.25	.30	.35	.40	.45	.50
0.5	.042	.043	.044	.045	.046	.047	.048	.049	.050	.051
1.0	.059	.060	.062	.063	.064	.066	.067	.069	.070	.072
1.5	.072	.074	.075	.077	.079	.081	.082	.084	.086	.088
2.0	.083	.085	.087	.089	.091	.093	.095	.097	.099	.101
2.5	.093	.095	.097	.100	.102	.104	.106	.109	.111	.113
3.0	.102	.104	.107	.109	.112	.114	.117	.119	.122	.124
3.5	.110	.113	.115	.118	.121	.123	.126	.129	.131	.134
4.0	.117	.120	.123	.126	.129	.132	.135	.137	.140	.143
4.5	.125	.128	.131	.134	.137	.140	.143	.146	.149	.152
5.0	.131	.134	.138	.141	.144	.147	.150	.154	.157	.160
5.5	.138	.141	.144	.148	.151	.154	.158	.161	.165	.168
6.0	.144	.147	.151	.154	.158	.161	.165	.168	.172	.175
6.5	.150	.153	.157	.161	.164	.168	.172	.175	.179	.183
7.0	.155	.159	.163	.167	.170	.174	.178	.182	.186	.189
7.5	.161	.165	.169	.173	.176	.180	.184	.188	.192	.196
8.0	.166	.170	.174	.178	.182	.186	.190	.194	.198	.203
8.5	.171	.175	.180	.184	.188	.192	.196	.200	.205	.209
9.0	.176	.180	.185	.189	.193	.198	.202	.206	.211	.215
9.5	.181	.185	.190	.194	.199	.203	.207	.212	.216	.221
10.0	.186	.190	.195	.199	.204	.208	.213	.217	.222	.226

Table 2.1: Reduced wind parameter (f_w^*) for terrain class 1

H	R									
	.05	.10	.15	.20	.25	.30	.35	.40	.45	.50
0.5	.243	.239	.235	.231	.226	.222	.218	.214	.210	.206
1.0	.260	.256	.252	.247	.243	.238	.234	.229	.225	.221
1.5	.271	.267	.262	.257	.253	.248	.244	.239	.234	.230
2.0	.279	.274	.270	.265	.260	.255	.251	.246	.241	.236
2.5	.285	.281	.276	.271	.266	.261	.256	.251	.247	.242
3.0	.291	.286	.281	.276	.271	.266	.261	.256	.251	.246
3.5	.295	.290	.285	.280	.275	.270	.265	.260	.255	.250
4.0	.299	.294	.289	.284	.279	.274	.269	.264	.259	.253
4.5	.303	.297	.292	.287	.282	.277	.272	.267	.262	.256
5.0	.306	.301	.295	.290	.285	.280	.275	.270	.264	.259
5.5	.309	.304	.298	.293	.288	.283	.277	.272	.267	.262
6.0	.311	.306	.301	.296	.290	.285	.280	.275	.269	.264
6.5	.314	.309	.303	.298	.293	.287	.282	.277	.271	.266
7.0	.316	.311	.306	.300	.295	.289	.284	.279	.273	.268
7.5	.318	.313	.308	.302	.297	.291	.286	.281	.275	.270
8.0	.321	.315	.310	.304	.299	.293	.288	.283	.277	.272
8.5	.322	.317	.312	.306	.301	.295	.290	.284	.279	.273
9.0	.324	.319	.313	.308	.302	.297	.291	.286	.280	.275
9.5	.326	.321	.315	.310	.304	.298	.293	.287	.282	.276
10.0	.328	.322	.317	.311	.306	.300	.294	.289	.283	.278

Table 2.2: Reduced wind parameter (f_w^*) for terrain class 2

H	R									
	.05	.10	.15	.20	.25	.30	.35	.40	.45	.50
0.5	.209	.206	.202	.199	.195	.191	.188	.184	.181	.177
1.0	.232	.228	.224	.220	.216	.212	.208	.205	.201	.197
1.5	.247	.242	.238	.234	.230	.226	.222	.217	.213	.209
2.0	.257	.253	.249	.244	.240	.236	.231	.227	.223	.218
2.5	.266	.262	.257	.253	.248	.244	.239	.235	.230	.226
3.0	.274	.269	.264	.260	.255	.250	.246	.241	.237	.232
3.5	.280	.275	.271	.266	.261	.256	.252	.247	.242	.237
4.0	.286	.281	.276	.271	.266	.261	.257	.252	.247	.242
4.5	.291	.286	.281	.276	.271	.266	.261	.256	.251	.246
5.0	.295	.290	.285	.280	.275	.270	.265	.260	.255	.250
5.5	.300	.295	.290	.284	.279	.274	.269	.264	.259	.254
6.0	.304	.298	.293	.288	.283	.278	.273	.268	.262	.257
6.5	.307	.302	.297	.292	.286	.281	.276	.271	.266	.260
7.0	.311	.305	.300	.295	.290	.284	.279	.274	.269	.263
7.5	.314	.309	.303	.298	.293	.287	.282	.277	.271	.266
8.0	.317	.312	.306	.301	.295	.290	.285	.279	.274	.269
8.5	.320	.314	.309	.304	.298	.293	.287	.282	.277	.271
9.0	.323	.317	.312	.306	.301	.295	.290	.284	.279	.273
9.5	.325	.320	.314	.309	.303	.298	.292	.287	.281	.276
10.0	.328	.322	.317	.311	.306	.300	.294	.289	.283	.278

Table 2.3: Reduced wind parameter (f_w^*) for terrain class 3

H	R									
	.05	.10	.15	.20	.25	.30	.35	.40	.45	.50
0.5	.180	.177	.174	.171	.168	.165	.162	.159	.156	.153
1.0	.207	.203	.200	.196	.193	.189	.186	.182	.179	.175
1.5	.224	.220	.217	.213	.209	.205	.201	.198	.194	.190
2.0	.238	.234	.230	.225	.221	.217	.213	.209	.205	.201
2.5	.248	.244	.240	.236	.232	.227	.223	.219	.215	.211
3.0	.258	.253	.249	.245	.240	.236	.231	.227	.223	.218
3.5	.266	.261	.257	.252	.248	.243	.239	.234	.230	.225
4.0	.273	.268	.264	.259	.254	.250	.245	.241	.236	.231
4.5	.279	.275	.270	.265	.260	.256	.251	.246	.242	.237
5.0	.285	.281	.276	.271	.266	.261	.256	.251	.247	.242
5.5	.291	.286	.281	.276	.271	.266	.261	.256	.251	.246
6.0	.296	.291	.286	.281	.276	.271	.266	.261	.256	.251
6.5	.301	.296	.291	.285	.280	.275	.270	.265	.260	.255
7.0	.305	.300	.295	.290	.285	.279	.274	.269	.264	.259
7.5	.309	.304	.299	.294	.288	.283	.278	.273	.267	.262
8.0	.313	.308	.303	.298	.292	.287	.282	.276	.271	.266
8.5	.317	.312	.307	.301	.296	.290	.285	.280	.274	.269
9.0	.321	.316	.310	.305	.299	.294	.288	.283	.277	.272
9.5	.324	.319	.313	.308	.302	.297	.291	.286	.280	.275
10.0	.328	.322	.317	.311	.306	.300	.294	.289	.283	.278

Table 2.4: Reduced wind parameter (f_w^*) for terrain class 4

H	R									
	.05	.10	.15	.20	.25	.30	.35	.40	.45	.50
0.5	.155	.152	.150	.147	.144	.142	.139	.137	.134	.131
1.0	.184	.181	.178	.175	.172	.169	.166	.162	.159	.156
1.5	.204	.201	.197	.194	.190	.187	.183	.180	.176	.173
2.0	.219	.215	.212	.208	.204	.201	.197	.193	.189	.186
2.5	.232	.228	.224	.220	.216	.212	.208	.204	.200	.196
3.0	.243	.238	.234	.230	.226	.222	.218	.214	.210	.206
3.5	.252	.248	.244	.239	.235	.231	.226	.222	.218	.214
4.0	.261	.256	.252	.247	.243	.239	.234	.230	.225	.221
4.5	.268	.264	.259	.255	.250	.246	.241	.237	.232	.228
5.0	.276	.271	.266	.262	.257	.252	.248	.243	.238	.234
5.5	.282	.277	.273	.268	.263	.258	.254	.249	.244	.239
6.0	.288	.284	.279	.274	.269	.264	.259	.254	.249	.244
6.5	.294	.289	.284	.279	.274	.269	.264	.259	.254	.249
7.0	.300	.295	.290	.285	.279	.274	.269	.264	.259	.254
7.5	.305	.300	.295	.290	.284	.279	.274	.269	.264	.259
8.0	.310	.305	.299	.294	.289	.284	.278	.273	.268	.263
8.5	.315	.309	.304	.299	.293	.288	.283	.277	.272	.267
9.0	.319	.314	.308	.303	.298	.292	.287	.281	.276	.271
9.5	.324	.318	.313	.307	.302	.296	.291	.285	.280	.274
10.0	.328	.322	.317	.311	.306	.300	.294	.289	.283	.278

Table 2.5: Reduced wind parameter (f_w^*) for terrain class 5

H	R									
	.05	.10	.15	.20	.25	.30	.35	.40	.45	.50
0.5	.133	.131	.129	.127	.124	.122	.120	.118	.115	.113
1.0	.164	.161	.159	.156	.153	.150	.148	.145	.142	.139
1.5	.186	.182	.179	.176	.173	.170	.167	.164	.160	.157
2.0	.202	.199	.195	.192	.189	.185	.182	.178	.175	.171
2.5	.216	.213	.209	.205	.202	.198	.194	.191	.187	.183
3.0	.228	.225	.221	.217	.213	.209	.205	.201	.197	.194
3.5	.239	.235	.231	.227	.223	.219	.215	.211	.207	.203
4.0	.249	.245	.241	.236	.232	.228	.224	.219	.215	.211
4.5	.258	.254	.249	.245	.240	.236	.232	.227	.223	.219
5.0	.266	.262	.257	.253	.248	.244	.239	.235	.230	.226
5.5	.274	.269	.265	.260	.255	.251	.246	.241	.237	.232
6.0	.281	.276	.272	.267	.262	.257	.253	.248	.243	.238
6.5	.288	.283	.278	.273	.269	.264	.259	.254	.249	.244
7.0	.295	.290	.285	.280	.275	.270	.265	.260	.255	.250
7.5	.301	.296	.290	.285	.280	.275	.270	.265	.260	.255
8.0	.307	.301	.296	.291	.286	.281	.275	.270	.265	.260
8.5	.312	.307	.302	.296	.291	.286	.280	.275	.270	.265
9.0	.318	.312	.307	.301	.296	.291	.285	.280	.275	.269
9.5	.323	.317	.312	.306	.301	.295	.290	.284	.279	.274
10.0	.328	.322	.317	.311	.306	.300	.294	.289	.283	.278

TABLE 3: Test Site Parameters

HOUSE ID	Ref No.	A_o cm^2	f_w^*	f_s^* $m/s/^oC^{1/2}$	Vol m^3
Ivanhoe	10	100	.26	.12	480
Nogal	10	960	.21	.10	290
Telemark	10	140	.26	.12	480
Torey Pines	10	200	.30	.14	480
R-10	11	330	.20	.09	233
T1	12	330	.18	.13	337
T2	12	680	.22	.11	433
Haven	10	770	.21	.11	230
Purdue	10	855	.21	.11	240
Neilson	10	1275	.20	.13	250
V1	10	560	.20	.12	270
V2	10	630	.19	.12	270
Fels	9	1480	.26	.15	470
San Carlos	10	845	.18	.11	145
Southampton	10	1640	.22	.16	1000

TABLE 4: Predicted Infiltration vs Measured Infiltration

HOUSE ID	v'	$\delta v'$	ΔT	δT	Q_p	δQ_p	Q_m	δQ_m
Ivanhoe	6.0	1.0	26	0	79	13	53	4
Nogal	1.7	0.1	3	1	114	4	123	12
Telemark	4.0	1.0	25	1	52	7	50	12
Torey Pines	7.2	1.0	19	1	156	10	180	23
R-10	2.0	0.1	28	1	72	2	77	7
T1	2.7	1.3	16	15	76	15	69	13
T2	2.7	2.0	15	15	149	110	139	80
Haven	3.0	2.0	8	4	175	60	68	42
Purdue	2.7	1.2	9	1	164	73	133	19
Neilson	1.7	0.3	5	1	156	28	173	13
V1	2.1	0.1	6	1	87	10	86	3
V2	3.3	1.1	7	2	142	44	125	48
Fels	4.0	2.0	16	4	554	140	355	175
San Carlos	1.7	0.2	0	1	93	11	114	26
Southampton	1.0	0.1	0	1	130	7	250	60

TABLE A1: Terrain Parameters for Standard Terrain Classes

Class	y	α	Description
I	0.10	1.30	ocean or other body of water with at least 5km of unrestricted expanse
II	0.15	1.00	flat terrain with some isolated obstacles (e.g. buildings or trees well separated from each other
III	0.20	0.85	rural areas with low buildings, trees, etc.
IV	0.25	0.67	urban, industrial or forest areas
V	0.35	0.47	center of large city (e.g. Manhattan)

TABLE A2: Infiltration through each Face

Direction	Condition	Location	Expression
infiltration	$\beta_j < 0$	floor	0
		wall	0
		ceiling	0
	$0 < \beta_j < 1$	floor	$L\ P_s^n\ \beta_j^n$
		wall	$\frac{L\ P_s^n}{n+1}\ \beta_j^{n+1}$
		ceiling	0
	$1 < \beta_j$	floor	$L\ P_s^n\ (\beta_j - 1)^n$
		wall	$\frac{L\ P_s^n}{n+1}\left[\beta_j^{n+1} - (\beta_j - 1)^{n+1}\right]$
		ceiling	$L\ P_s^n\ \beta_j^n$
exfiltration	$\beta_j < 0$	floor	$L\ P_s^n\ (-\beta_j)^n$
		wall	$\frac{L\ P_s^n}{n+1}\left[(1-\beta_j)^{n+1} - (-\beta_j)^{n+1}\right]$
		ceiling	$L\ P_s^n\ (1-\beta_j)^n$
	$0 < \beta_j < 1$	floor	0
		wall	$\frac{L\ P_s^n}{n+1}\ (1-\beta_j)^{n+1}$
		ceiling	$L\ P_s^n\ (1-\beta_j)^n$
	$1 < \beta_j$	floor	0
		wall	0
		ceiling	0

Table B1: Infiltration through each face

Direction	Condition	Location	Expression
infiltration	$\beta_j < 0$	floor	0
		wall	0
		ceiling	0
	$0 < \beta_j < 1$	floor	$A_f v_s \sqrt{\beta_f}$
		wall	$\frac{2}{3} A_w v_s \beta_w^{3/2}$
		ceiling	0
	$1 < \beta_j$	floor	$A_f v_s \sqrt{\beta_f - 1}$
		wall	$\frac{2}{3} A_w v_s \left[\beta_w^{3/2} - (\beta_w - 1)^{3/2}\right]$
		ceiling	$A_c v_s \sqrt{\beta_c}$
exfiltration	$\beta_j < 0$	floor	$A_f v_s \sqrt{-\beta_f}$
		wall	$\frac{2}{3} A_w v_s \left[(1-\beta_w)^{3/2} - (-\beta_w)^{3/2}\right]$
		ceiling	$A_c v_s \sqrt{1-\beta_c}$
	$0 < \beta_j < 1$	floor	0
		wall	$\frac{2}{3} A_w v_s (1-\beta_w)^{3/2}$
		ceiling	$A_c v_s \sqrt{1-\beta_c}$
	$1 < \beta_j$	floor	0
		wall	0
		ceiling	0

Table B2: Wind regime infiltration values	
Face	Infiltration/Exfiltration
floor	$v\, A_f \sqrt{\lvert C^o \rvert}\ \left(1 - \frac{2\mu - 1}{4\sigma C^o}\right)$
wall	$v \sum_w A_w \sqrt{\lvert (C_w - C^o) \rvert}\ \left(1 + \frac{\mu}{\sigma (C_w - C^o)}\right)$
ceiling	$v\, A_c \sqrt{\lvert C^o \rvert}\ \left(1 - \frac{2\mu + 1}{4\sigma C^o}\right)$

SYMBOL TABLE	
A	is the effective leakage area [m^2]
A_o	is the total leakage area ($\sum_w A_w + A_f + A_c$)
c	is the subscript indicating the ceiling
C	is a (wind pressure) shielding coefficient
C^o	is the internal (wind) pressure coefficient
C^∞	is the internal pressure coefficient at high wind strength
f_s	is the stack-effect factor
f_s^*	is the reduced-stack effect factor [$m/s/\sqrt{^oK}$]
f_w	is the wind-effect factor
f_w^*	is the reduced wind-effect factor
g	is the acceleration of gravity [9.8 m/sec^2]
h	is a height variable [m]
H	is the height of the ceiling above grade [m]
H'	is the height of the wind measurement
j	is an index to denote each face of the structure
L	is a semi-empirical constant used in empirical fits to leakage data
n	is a semi-empirical constant used in empirical fits to leakage data
P_{st}	is the stagnation pressure ($\frac{1}{2}\rho v^2$) [Pa.]
P_s	is the stack pressure ($\rho g H \frac{\Delta T}{T}$)
ΔP	is an applied pressure difference.

SYMBOL TABLE	
ΔP_j^w	is the exterior pressure rise due to the wind
ΔP_o	is the internal pressure change
Q	is air flow [m^3/sec]
$Q(\Delta T, v)$	is the instantaneous infiltration
Q_{stack}	is the infiltration in the stack regime
Q_{wind}	is the infiltration in the wind regime
R	fraction of leakage area combined in floor and ceiling
T	is the inside temperature [^oK]
ΔT	is the inside-outside temperature difference
v	is the wind speed at ceiling height [m/sec]
v^*	is the reduced wind speed
v_o	is the wind speed at standard (terrain) conditions
v_s	critical wind speed
v_s^*	reduced critical wind speed
v'	is the measured wind speed
w	is an index to denote the walls of the structure
α	is a constant that depends on terrain class (See tables above)
β	is a normalized height
β_j	is the effective neutral level of the jth face
β^o	is the neutral level
γ	is a constant that depend on terrain class (See tables above)
μ	is the fraction shift in the neutral level from the mid-point
ρ	is the density of air [1.2 kg/m^3]
σ	is the wind strength
$\pm$	indicates depressurization/pressurization or infiltration/exfiltration respectively

Defining Relations for Figures

$$R = \frac{A_c + A_f}{A_o}$$

$$f_w = \frac{3 - R}{9}$$

$$f_s = \frac{2 + R}{9}$$

$$v = v' \left[\frac{\alpha \left[\frac{H}{10} \right]^{\gamma}}{\alpha' \left[\frac{H'}{10} \right]^{\gamma'}} \right]$$

$$v^* = f_w \, v = v' \, f_w^*$$

$$f_w^* = \frac{3 - R}{9} \left[\frac{\alpha \left[\frac{H}{10} \right]^{\gamma}}{\alpha' \left[\frac{H'}{10} \right]^{\gamma'}} \right]$$

$$v_s^* = f_s \, v_s = \sqrt{\Delta T} \, f_s^*$$

$$f_s^* = \frac{2 + R}{9} \sqrt{\frac{2 \, g \, H}{T}}$$

Figure Captions

1) Figure 1 shows lines of constant infiltration as a function of the two reduced velocities. The dashed line separates the stack-dominated and wind-dominated regimes. Refer to "Symbol Table" and "Defining Relations" preceding the figures.

2) Figure 2 shows lines of constant infiltration as a function of wind speed and temperature difference. The dashed line separates the stack-dominated and wind- dominated regimes. Refer to "Symbol Table" and "Defining Relations" preceding the figures. This figure contains essentially the same information as Fig. 1, but expresses it in different variables.

3) Figure 3 is a graph of the predicted versus measured infiltration points for all data points that had both predicted and measured infiltration values of less than 150 m^3/hr. The solid line is the locus of points that represents perfect agreement. The dashed lines define an area of acceptable agreement based on the measurement uncertainties only.

4) Figure 4 is a graph of the predicted versus measured infiltration points not included on the previous graph. The box in the lower left hand corner is the range of the previous graph. The solid line is the locus of points that represents perfect agreement. The dashed lines define an area of acceptable agreement based on the measurement uncertainties only.

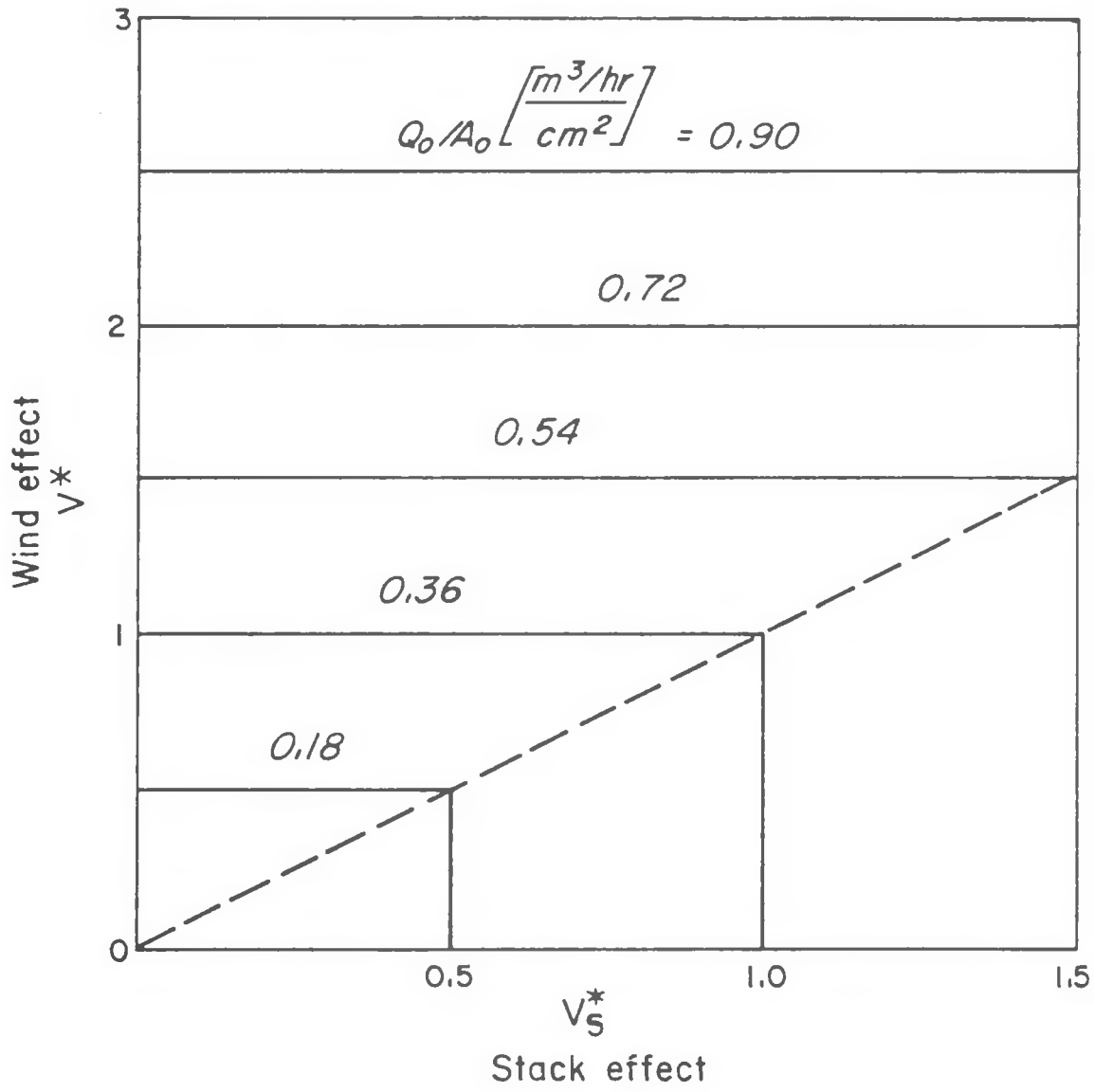

Predicted infiltration per unit leakage area

XBL 802-4044

FIG 1

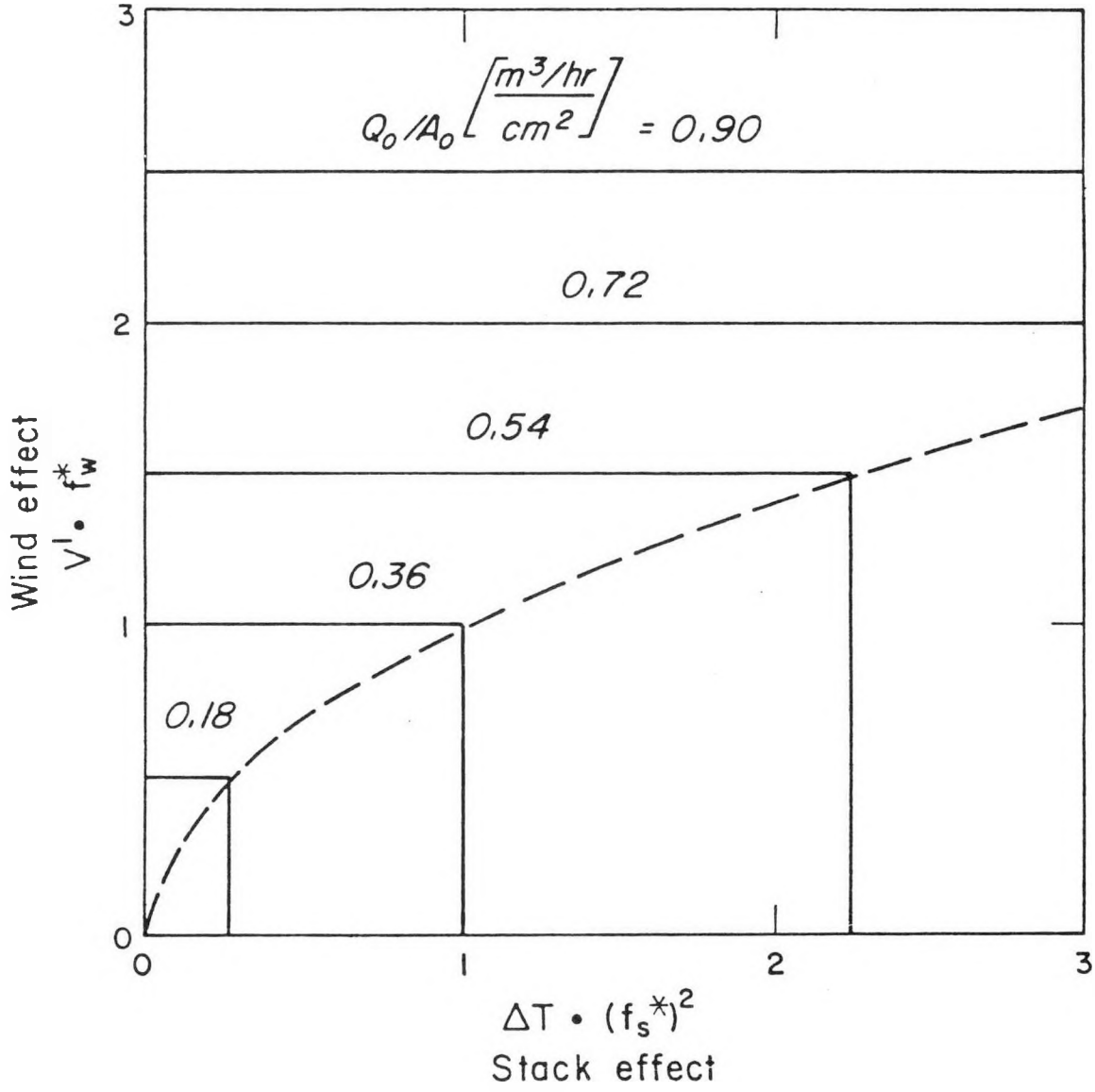

Predicted infiltration per unit leakage area

XBL 802-4045

FIG 2

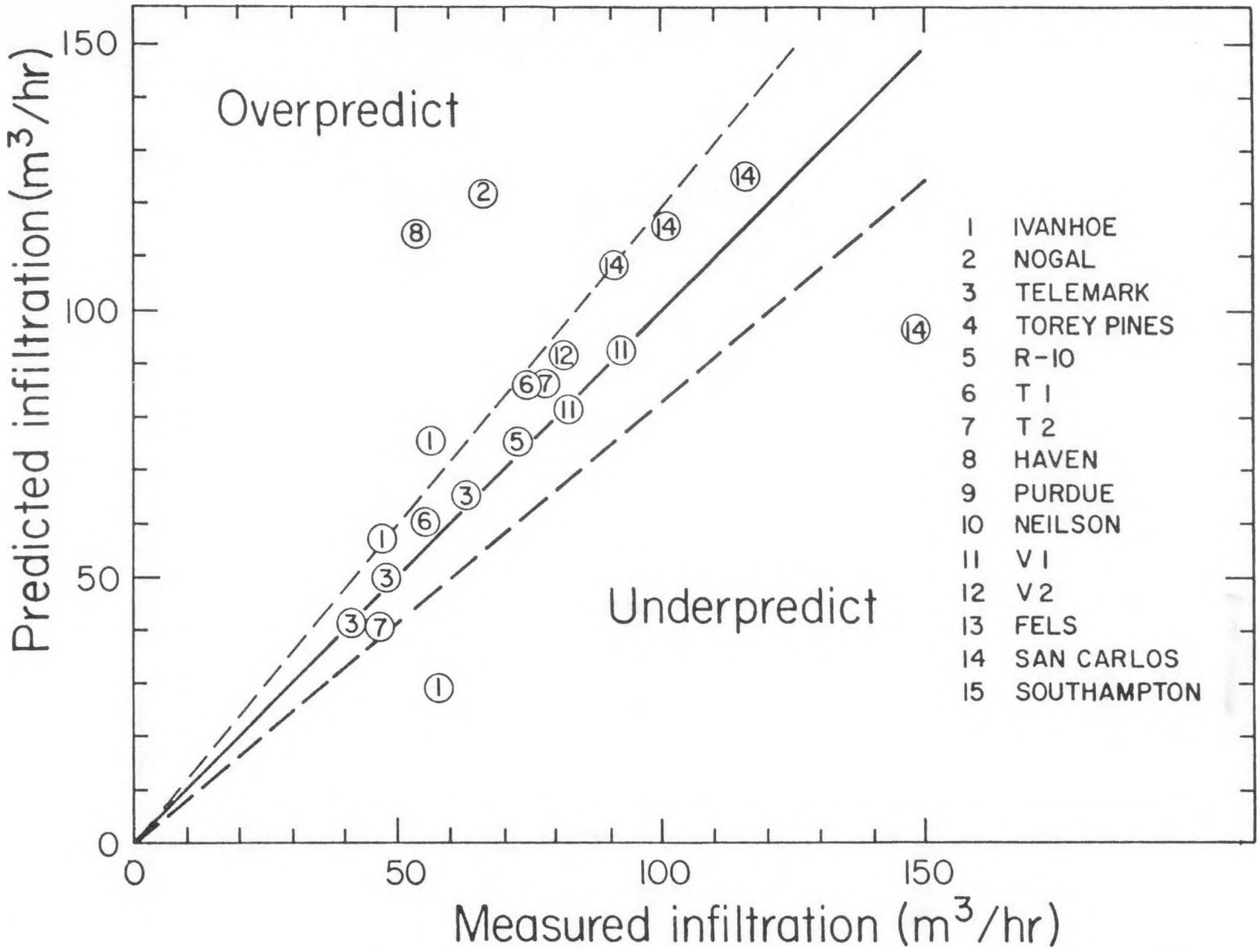

XBL 802-4043

FIG 3

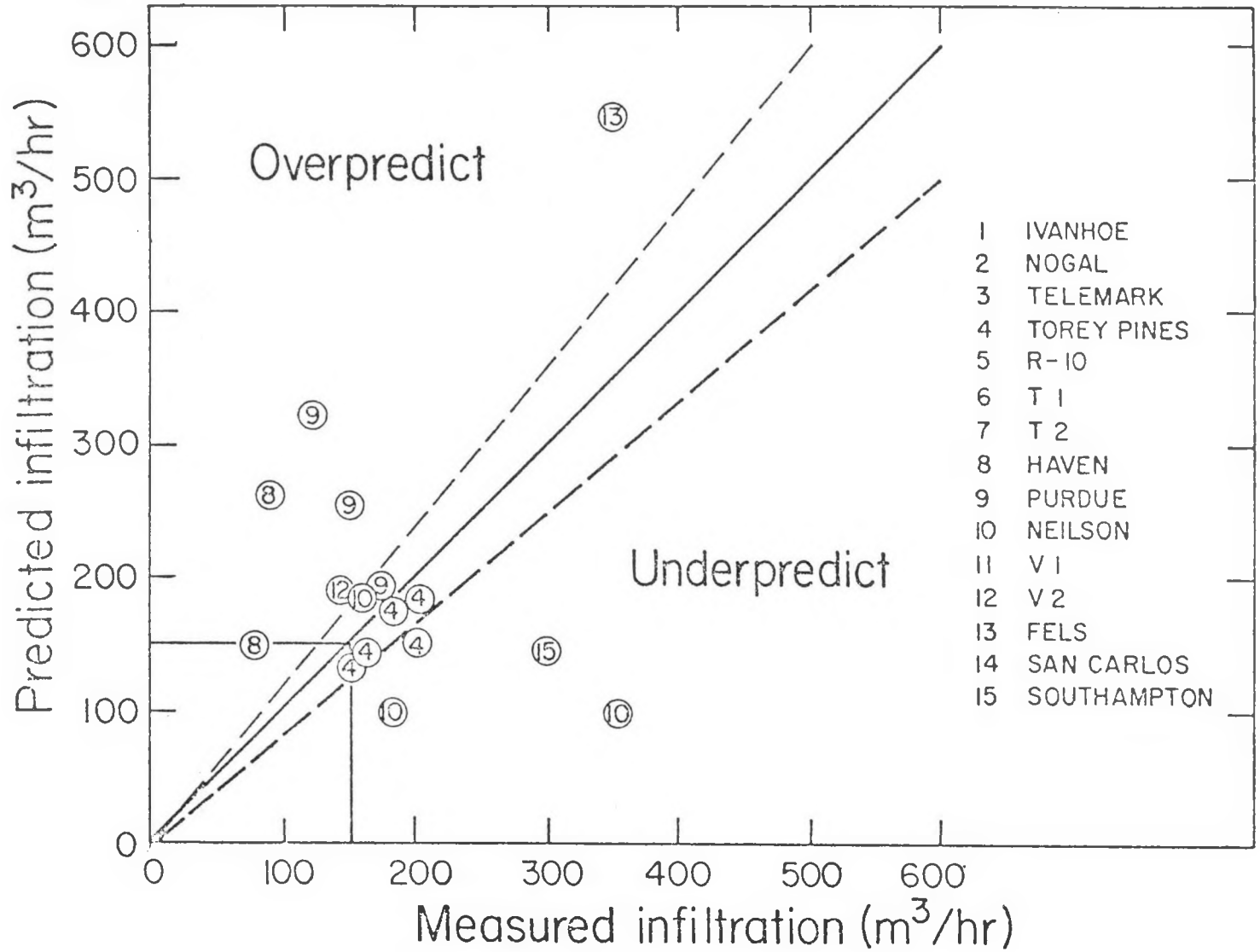

XBL 802-4042

FIG 4